Epidermal Sensors for Monitoring Skin Physiology

A thesis submitted to Dublin City University in fulfilment of the requirements for the award of the degree of Doctor of Philosophy

by

Keana Erika A. De Guzman BSc

School of Chemical Sciences

Dublin City University

Supervisor:

Dr. Aoife Morrin

January 2020

Declaration:

I hereby certify that this material, which I now submit for assessment on the programme of study leading to the award of PhD, is entirely my own work, that I have exercised reasonable care to ensure that the work is original, and does not to the best of my knowledge breach any law of copyright, and has not been taken from the work of others save and to the extent that such work has been cited and acknowledged within the text of my work.

Signed: _____

(Candidate) ID No.: _____

Date: _____

Table of Contents

Chapter 4

Porous Tattoo Platform for Skin Physiology Monitoring

Chapter 5

Towards Using Chemically Responsive Hydrogels in Epidermal Sensing

Chapter 6

Conclusions and Future Work

List of Abbreviations

AA	ascorbic acid
AD	atopic dermatitis
Ag/AgCl	silver/silver chloride
AOx	alcohol oxidase
BA	boronic acid
BSA	bovine serum albumin
CA	conducting adhesive
CAC	conducting adhesive contact
CF	cystic fibrosis
CNT	carbon nanotube
CPE	constant phase element
CS	chitosan
DC	direct contact
DI	deionised water
ECG	electrocardiogram
EEG	electroencephalography
FLG	filaggrin
GC-MS	gas chromatography - mass spectroscopy
GNP	gold nanoparticle
GOx	glucose oxidase
HA	hyaluronic acid
HEC	hydroxyethyl cellulose
HPLC	high performance liquid chromatography
HRP	horseradish peroxidase
HS	head space
HSE	human skin equivalent
HS-SPME	head space-solid phase microextraction
ICP-MS	inductively coupled plasma – mass spectrometry
ILTG	isoliquiritigenin
ISE	ion-selective electrode
ISF	interstitial fluid
LOx	lactate oxidase

MAE	microneedle array electrode
NMF	natural moisturising factor
PBA	phenyl boronic acid
PBS	phosphate buffer saline
PDA	polydopamine
PDA-PAM	polydopamine–polyacrylamide
PDMS	polydimethylsiloxane
PEDOT:PSS	poly(3,4-ethylenedioxythiopene) polystyrene sulfonate
PolyHEMA	polyhydroxyethylmethacrylate
PPDPS-TF	(4-phenoxyphenyl)diphenylsulfonium triflate
PSBMA	poly[2- (methacryloyloxy)ethyl]dimethyl-(3-sulfopropyl)
PU	polyurethane
$R_{elec/skin}$	electrode-skin resistance
RGB	red, green and blue
R_{gel}	bulk hydrogel resistance
R_{vt}	viable tissue resistance
SC	stratum corneum
SLS	sodium lauryl sulfate
SPE	screen printed electrodes
SPME	solid phase microextraction
SSB	sweat sensor belt
SWNT	single-walled carbon nanotubes
TDC	tissue dielectric constant
TEWL	transepidermal water loss
TPTZ	2,4,6-tris(2-pyridyl)-s-triazine
TTF	tetrathiafulvalene
UV	ultraviolet
VOC	volatile organic compound
Z	total impedance

List of Figures

List of Tables

List of Publications and Presentations

Publications

- K. De Guzman, G. Al-Kharusi, T. Levingstone and A. Morrin, *Robust Epidermal Tattoo Electrode Platform for Skin Physiology Monitoring*, Analytical Methods, 2019, 11,1460-1468.
- E. Duffy, K. De Guzman, R. Wallace, R. Murphy and A. Morrin, *Non-Invasive Assessment of Skin Barrier Properties: Investigating Emerging Tools for In Vitro and In Vivo Applications*, Cosmetics, 2017, 4(4), 44.
- K. De Guzman and A. Morrin, *Screen-printed Tattoo Sensor Towards the Non-Invasive Assessment of the Skin Barrier*, Electroanalysis, 2017, 29, 1, 188-196.
- A. Murphy, B. Gorey, K. De Guzman, Neil Kelly, Ekaterina P. Nesterenko and Aoife Morrin, *Microfluidic Paper Analytical Device for the Chromatographic Separation of Ascorbic Acid and Dopamine*, RSC Advances, 2015, 5, 93162-93169.

Oral presentations

- *Smart Tattoos for the Non-Invasive Assessment of the Skin Barrier Function*, 4th Insight Student Conference, University College Cork, Ireland, 2017.
- *Smart Tattoos for the Non-Invasive Assessment of the Skin Barrier Function*, Cosmetic Measurement and Testing, University of Cergy-Pontoise, France, 2017.
- *Fabrication and Characterisation of Flexible Smart Tattoos towards Epidermal Sensing*, 69th Irish Universities Chemistry Research Colloquium, Dublin City University, 2017
- *Non-Invasive Skin Diagnostics using Smart Tattoos***,** Chemistry Day, Dublin City University, Ireland, 2017.

Poster presentations

- *Characterisation of Stretchable Temporary Tattoo Platforms for Monitoring Skin Barrier Hydration*, 69th Annual Meeting of the International Society of Electrochemistry, Bologna, Italy, 2018.
- *Characterisation of Stretchable Temporary Tattoo Platforms for Monitoring Skin Barrier Hydration*, 70th Irish Universities Chemistry Research Colloquium, Queen's University Belfast, Ireland, (Poster and Flash presentation), 2018.

- *Smart Tattoos for the Non-Invasive Assessment of the Skin Barrier Function*, Insight Student Conference, University College Cork, Ireland, 2017.
- *Smart Tattoo for Monitoring Skin Hydration using AC Impedance*, 16th International Conference on Electroanalysis, Bath, UK, 2016.
- *Physical Characterisation of Silver Screen-printed Tattoo Sensor for Skin Hydration Monitoring*, 8th Conference on Analytical Sciences Ireland, The Helix, Dublin City University, Ireland, (Poster and Flash presentation), 2016.
- *Conformable Conducting Materials for Epidermal Sensing***,** 67th Irish Universities Chemistry Research Colloquium, NUI Maynooth, Kildare, Ireland, 2015.

Acknowledgements

First and foremost, I would like to thank my supervisor Dr. Aoife Morrin for her constant support, guidance and encouragement throughout the last few years. Thank you for being a great mentor, I am grateful for all the advice you have given me and all the opportunities you afforded me.

I am very grateful to the technical staff of the chemistry department and the NRF in DCU. I could always count on them for their help. I would like to thank Dr. Tanya Levingstone, her students and the School of Mechanical and Manufacturing Engineering for all their advice and help with mechanical testing. I would also like to thank Prof. Dermot Diamond and his research group, especially Colm and Larissa for helping me with some of the work in the final chapter. I was also lucky to spend some time in the University of Wollongong in Australia and wish to thank everyone that made this a possibility.

Thank you to all my postgraduate friends in DCU. Jess, Asmita, Jack and Sara. Thank you for all the support and all the good times. I would also like to thank Emer, Loanda, Donna and Declan for passing on your knowledge and experience. I am grateful for all the advice you have given me.

A huge thanks to Saorla and Steve, thank you for putting up with me in the lab. Thanks for being there throughout the highs and lows.

A special thanks to Aoife and Sinead, thank you for always being there for me and for always listening to me, I must have sounded like a broken record.

Finally, I would like to thank my family for their support, encouragement and love. I am grateful for everything they've done for me throughout my many years in college.

Abstract

Keana Erika A. De Guzman

Epidermal Sensors for Monitoring Skin Physiology

Wearable sensors are revolutionizing personalised healthcare and have continuously progressed over the years in both research and commercialization. However, most efforts on wearable sensors have been focused on tracking movement, spatial position and continuous monitoring of vital signs such as heart rate or respiration rate. Recently, there is a demand to obtain biochemical information from the body using wearables. This demand stems from an individuals' desire for improved personal health awareness as well as the drive for doctors to continuously obtain medical information for a patients' disease management. Epidermal sensors are a sub-class of wearable sensors that can intimately integrate with skin and have the potential for monitoring physical changes as well as detecting biomarkers within skin that can be related to human health. The holy grail for these types of sensors is to achieve continuous real-time monitoring of the state of an individual and the development of these sensors are paving the way towards personalised healthcare. However, skin is highly anisotropic which makes it challenging to keep epidermal sensors in consistent contact with skin. It is important that these sensors remain in contact with skin in order to measure its electrical properties and acquire high fidelity signals.

The key objective of this thesis is to develop thin conformable, stretchable epidermal sensors for tracking changes in skin physiology. The initial iteration of the screen printed epidermal sensor comprised of a flexible silver film. Impedance spectroscopy was used to understand the electrical signals generated on skin and it was used to measure relative changes due to varying water content. However, this iteration was more suited for single use. The next chapters explore different ink formulations and adherence methodologies to enhance the epidermal sensors adherence to skin. Impedance spectroscopy was used to characterise the electrical signals from these different epidermal sensor iterations, while tensile testing and on-body assessment was used to characterise its mechanical properties. The final chapter focused on investigating the use of phenyl boronic acid (PBA) functionalized hydrogels to modify the epidermal sensor with responsive hydrogel materials to enable chemical sensing of analytes relevant to skin physiology. Impedance spectroscopy was used to characterise and understand the electrical signals generated by the binding interaction of the PBA and analytes using the sensor. Overall, the work demonstrates the challenges of developing these epidermal sensors as well as presenting their potential for continuous monitoring of human skin in the future.

Chapter 1

Recent Developments in Epidermal Sensing

1.1 Wearable devices

Wearable sensing technology has recently and rapidly moved towards the development of a wide array of consumer and medical products. This growth of wearable sensors can be attributed to several factors, such as affordability and ergonomics provided by advances in miniaturized electronics, the proliferation of smart-phones and connected devices, and the growing interest for personalised healthcare [1].

Currently most wearable sensing devices focus on physical measurements such as heart rate, respiration rate or quality of sleep and are geared towards monitoring an individual's physical fitness [1]. A popular wearable physical activity monitor available in the consumer market is the Fitbit®, a wireless activity tracker that helps individuals obtain information such as amount of steps taken and distance travelled [2], [3]. This type of wearable technology helps promote the importance of physical activity with the aim of reducing or preventing conditions such as obesity by allowing individuals to track their progress and establish physical activity goals [4], [5]. However, these physical activity measurements give a limited insight into an individuals' health status. Therefore there has been increasing efforts towards developing wearable sensors that can monitor additional physiological parameters. The development of these types of wearable sensors can reduce the need for invasive blood sampling through non-invasive analysis of more accessible diagnostic fluids such as saliva [6], [7], tears [8], [9], and sweat [10].

An interesting sub-class of wearable devices are epidermal sensors, which directly adhere onto skin. This has clear advantages in terms of close proximity for direct access to the skin organ [11]–[13]. The skin has become a commonly targeted area for wearable sensing given its important role in human physiology and epidermal sensors have been used to monitor physiological parameters such skin barrier integrity via electrical measurements [14]–[16], measure temperature [17], and track electrical activity, such as electromyography (EMG) [18]. Epidermal sensors that measure these types of physiological activity require intimate contact and robust adherence to skin. However, the human skin composition is complex, highly anisotropic [19] and its mechanical properties can change depending on the age, hydration state and location on the body [20], [21]. Therefore designing suitable robust skin-electrode interfaces are required to acquire reproducible signals from skin. This can be achieved by using thin, soft, flexible, stretchable conducting materials and clever electrode geometries. These type of parameters are typically considered for interfacing epidermal sensors to skin, where the aim would be to broadly match the stiffness and elasticity of the epidermal sensor closely to that of skin.

The stratum corneum (SC) of the epidermis is a region of high metabolic activity, rich with a variety of biomarkers and its biochemistry offers valuable insight into health as it can reflect both localized and systemic skin conditions [22]. Detecting and analysing the levels of biomarkers in skin matrices such as sweat [23] can also provide insights into human health. Diagnostic opportunities from the skin gives rise to the fabrication and development fo epidermal sensors. For example, a UV skin patch (Fig. 1.1a) which is a commercially deployed epidermal sensor was recently developed by Rogers along with L'Oreal (La Roche-Posay) [24]. This epidermal sensor monitors the external environment to track UV exposure of skin over time. It contains UV sensitive dyes that change colour upon exposure to UV radiation and uses optical detection to quantify the colour change before and after skin UV exposure [24]. Another recent example of an epidermal sensor is the My Skin Track pH, a prototype wearable pH sensor developed by the same research group (Fig. 1.1b). This skin pH patch is a thin flexible epidermal sensor that uses intricate microfluidic channels to collect sweat from skin and also uses optical detection via image capturing software to measure the pH of skin.

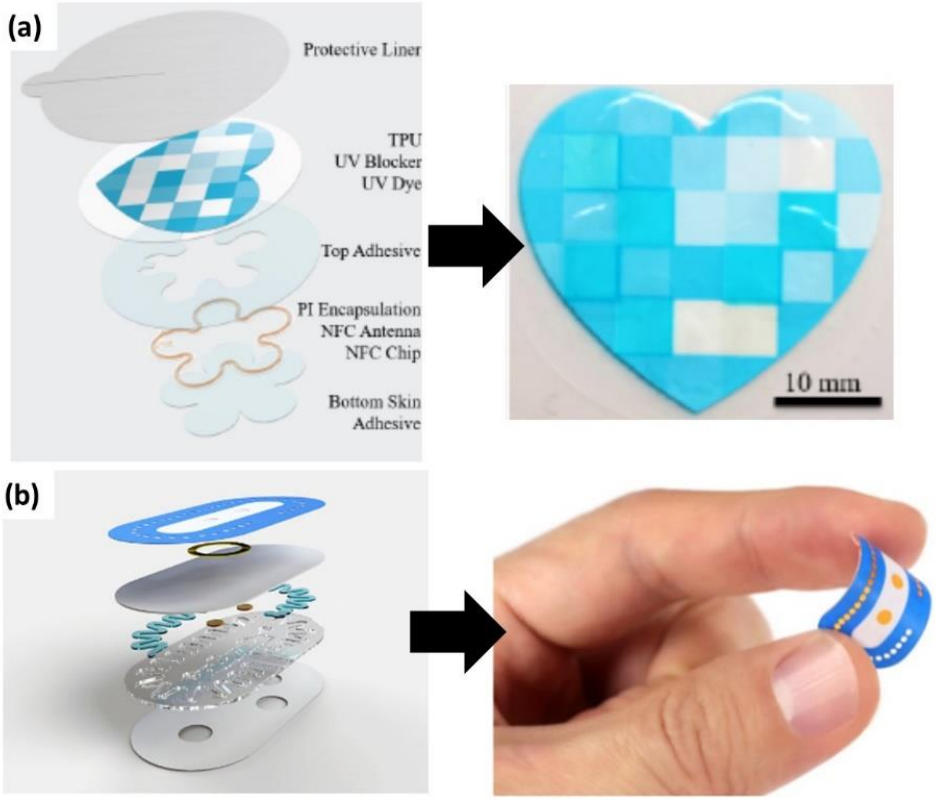

Figure 1.1 Images of the (a) Skin UV patch showing its sensor components for each layer, reproduced from [24] *and (b) My Skin Track pH and its individual sensor layers, reproduced from* [25].

Depending on the mode of epidermal sensor being developed, there are many challenges that need to be overcome. In the case of targeting biomarkers in skin matrices such as sweat or ISF, the sensor must be able to target analytes selectively and with short response times [1]. One of the biggest challenges for wearable sensors that analyse sweat or ISF is the reproducible extraction of fluid from skin in a facile and robust manner. Another factor to consider is how representative these fluids are with respect to blood, which is the gold standard diagnostic fluid. Current epidermal sensors require a defined sampling interval to allow ample time to pre-concentrate or extract a sufficient volume of fluid. There is also a requirement for the epidermal sensor to be highly sensitive as concentration ranges found in the skin and sweat tend to be lower than blood. Despite these challenges, epidermal sensors are beginning to show great potential towards providing comprehensive continuous monitoring of an individuals' health status.

1.2 The skin organ

The human skin is a complex organ that is composed of three main layers: epidermis, dermis and subcutaneous tissue (Fig. 1.2) and its functions include the protection of the body from the external environment, thermoregulation, and sensation [26]–[28]. The epidermis is the outermost layer of skin and it can be divided into four main layers depending on the state of keratinocyte differentiation and its main function is to act as a protective barrier from the external environment [26]. The dermis is the layer found between the epidermis and subcutaneous tissue and is composed of interstitial components such as collagen fibres and cellular components such as fibroblasts as well as blood vessels [26]. Due to the presence of collagen fibres, the dermis' role is to give the skin its flexibility. The subcutaneous layer is the inner most layer of skin and is primarily composed of lipocytes (fatty tissue) [26]. This is the insulation layer which helps regulate body temperature and act as a protective layer for muscles and bones.

The human skin has different properties and conditions which can be influenced by numerous body dependent factors such as age, skin type, gender and lifestyle [29]. These body dependent factors can influence human skin characteristics such as thickness, elasticity or hydration which also have an effect on the penetration of microbes and active cosmetic or topical treatments [29]. It also contains a plethora of biomarkers such as lipids, structural proteins and

inflammatory mediators that can serve as a "window" into the metabolic processes within the body [30].

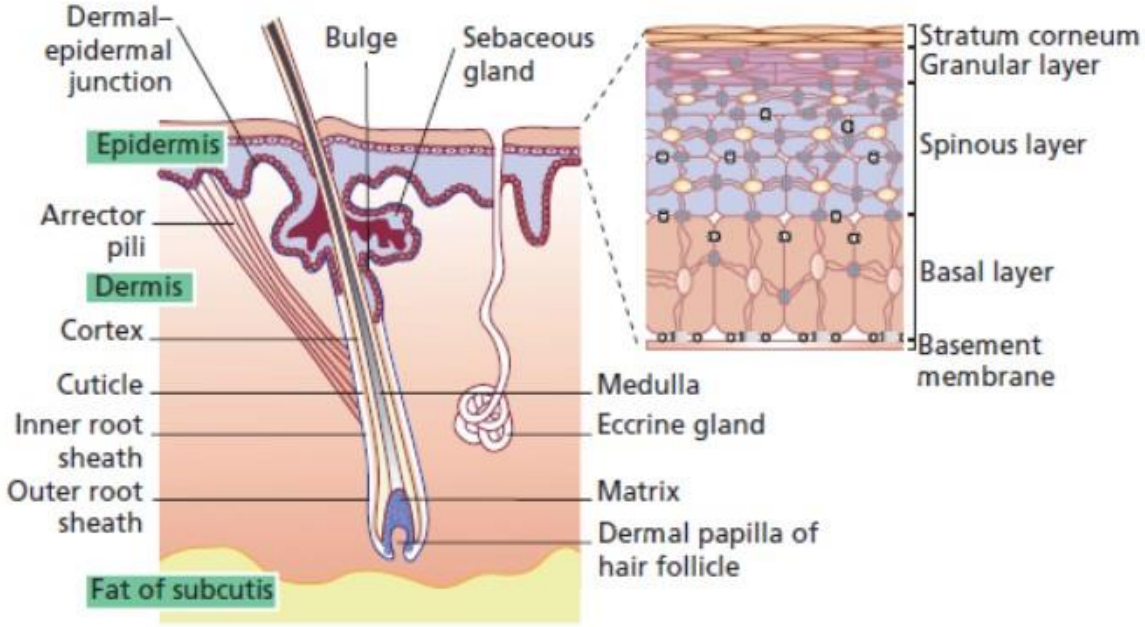

Figure 1.2 Diagram of the skin showing the three main layers: epidermis, dermis and subcutis. Magnification (top right) shows the different layers of the epidermis from the stratum corneum to the basement membrane, reproduced from [31].

Disease pathologies are also known to alter the molecular composition of skin and manifest itself as either a localised disease (i.e. atopic dermatitis, melanoma) or a systemic disease (i.e. diabetes) [30]. Such alterations in skin chemistry can offer valuable insight towards understanding human health. Researchers have gained interest in monitoring and understanding skin chemistry by using minimally or non-invasive approaches to sample and analyse skin, for example via its electrical properties or via matrices within the skin.

1.2.1 The Stratum Corneum (SC)

The stratum corneum (SC), the outermost layer of the epidermis is the first line of defence and is a region of high metabolic activity that is easily accessible for sampling. Both exogenous (i.e. environmental) and endogenous (i.e. genetic or hormonal) factors can compromise the protective nature of this skin barrier and cause both physical and chemical alterations in skin. These alterations in skin chemistry can have an impact on the structure and function of the skin

organ. The next sections will discuss the importance of skin barrier function and the different parameters that can be used to monitor skin barrier integrity.

The SC layer is composed of layers of corneocytes in a lipid matrix and is commonly described as the 'brick and mortar' layer of skin. The corneocytes are flattened layers or 'brick' layers filled with keratin while the 'mortar' layer is a complex mixture of extracellular lipids such as ceramides, cholesterol and free fatty acids that provide permeability to the barrier [27]. Depending on the anatomical site, the depth of the SC in human skin can vary between 8-40 µm [32].

Proper development and maintenance of the SC is key to defending the body against chemical and microbiological attack as well as maintaining skin hydration [33]. Skin barrier impairment is the breakdown of the SC barrier allowing the penetration of irritants, allergens and microbes into the skin (Fig. 1.3).

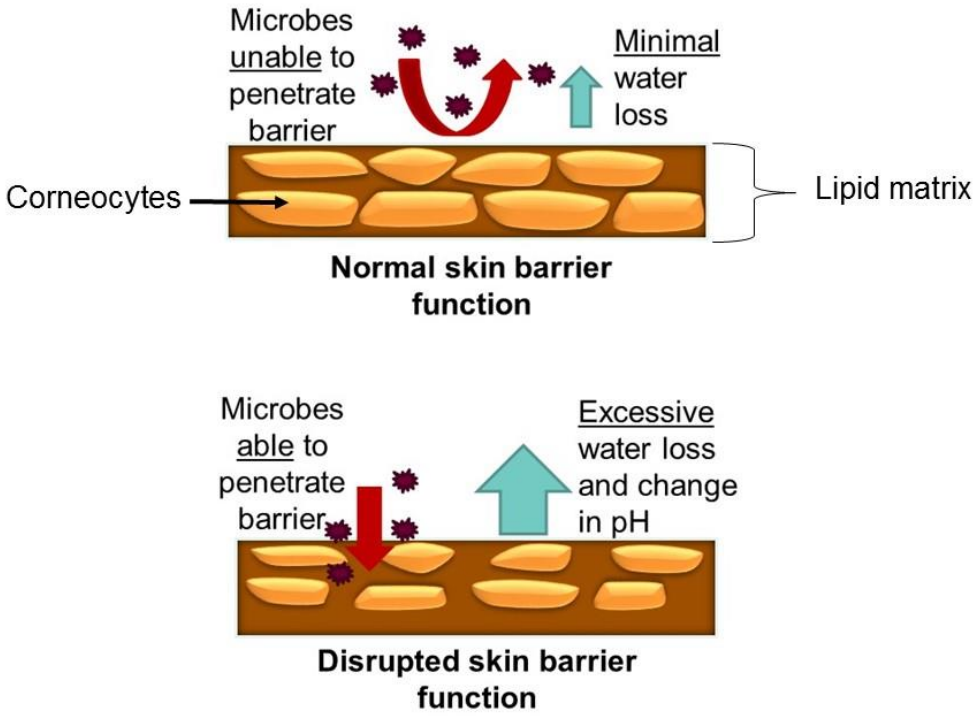

Figure 1.3 Schematic diagram of normal skin barrier function versus disrupted skin barrier function of the stratum corneum.

Skin conditions such as atopic dermatitis (AD), manifests itself as a skin barrier impairment and is one of the most prevalent skin conditions that affect adults and children [34]–[36]. It exhibits itself as a highly pruritic skin condition that commonly affects the face and flexural areas of the body and its histology has been described as a decrease in cornification and lipids [37]. This particular form of dermatitis has been related to different factors such as gene regulation and mutations [38] such as mutations in the filaggrin (FLG) gene [39], [40]. An individual with AD, has a damaged skin barrier that can easily allow for irritants or microbes to penetrate, which further induces dryness and inflammation or in worse cases infection in skin. Topical treatments such as moisturisers and emollients have been used specifically as a way of treating irritation and impairment of the skin barrier (Fig. 1.4) [41]. However, the most common treatment for AD would be the use of topical corticosteroids in order to manage flare-ups [42] which only provides temporary relief to patients. Therefore, monitoring the skin for early warning signs would be advantageous to individuals who suffer from these skin conditions. This has led to a significant interest in studying the skin barrier and different research groups have used commercial skin probes to monitor the water content and pH of the skin of patients with AD with the goal of deepening the understanding of the skin condition.

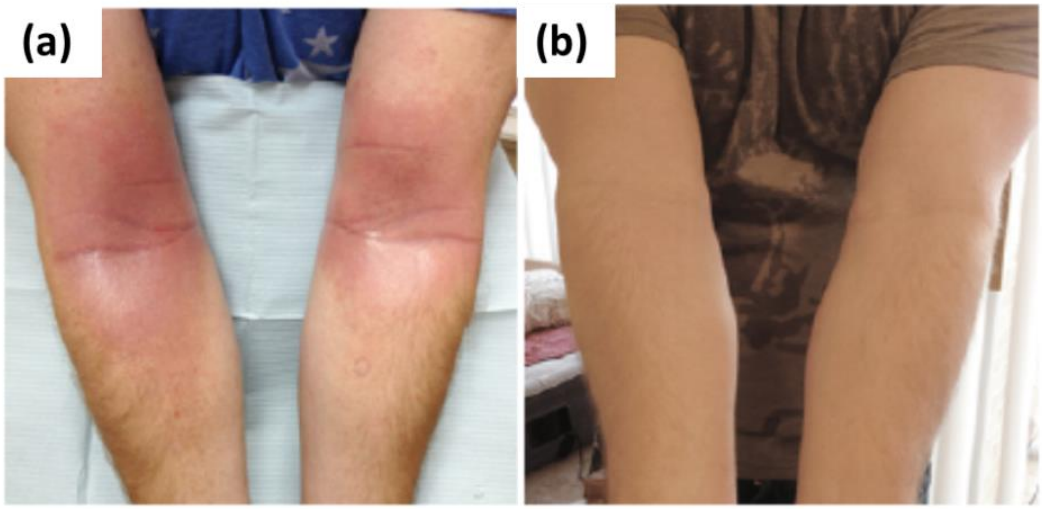

Figure 1.4 Example of (a) dermatitis on the inner forearm due to lanolin before treatment and (b) after treatment, reproduced from [43].

1.2.1.1 Skin impedance

As discussed previously, the SC is the first line of defence and serves as a protective barrier against water loss. The effectiveness of this barrier and its permeability has been extensively tested using a approaches such as skin biopsies [44]–[46] and tape-stripping [47]–[49]. One of the most common methods used to characterise skin is through the use of impedance. Impedance is the measure of a materials opposition to the flow of alternating electric currents over a frequency range. Impedance is a complex number, which consists of a real and an imaginary part:

$$\mathrm{Z} = R + jX \qquad \text{Equation 1.1}$$

where Z is the complex impedance and the real part (R) represents resistance, while the imaginary part (X) represents reactance and j is the imaginary number. In impedance spectrscopy, Nyquist and Bode plots are the two most common methods of displaying the generated data. The Nyquist plot shows the data as real ($Z^{'}$) versus imaginary ($Z^{''}$), with every point providing the characteristics of the complex impedance per frequency. However, the primary disadvantage with this plot is that the frequency is not explicitly shown. In comparison, the Bode plot shows the phase and total impedance over the frequency range analysed. Resistance in a circuit dissipates power as heat, while reactance stores energy in the form of an electric or magnetic field. The impedance of skin can be modelled using circuit elements that consist of parallel and series combinations of resistors, capacitors and constant phase elements [1]. The skin is typically modelled by either making a distinction between the different microanatomical structures of skin, for example lipids would be modelled as capacitors and electrolytes as resistors, while another way of modelling skin would focus on structures of the skin that make the largest contributions to the electrical properties [50]. However, producing an electrical model of skin to fully mimic all the electrical processes in tissue using only simple circuit elements can be quite challenging. A commonly used circuit model for skin typically uses a resistor and capacitor or constant phase element (CPE) in parallel to represent the SC or the epidermis, while the underlying viable tissue or dermis is considered to be more conductive than the epidermis and is then typically modelled as a resistor in series [1]. Another consideration in modelling would be the mode of electrode contact because the impedance measured from skin depends on the contact or adherence quality of the electrodes on skin. Another consideration would be the frequency range used to measure the skin. The frequency range measured represents a mixture of different skin layers and different dispersion mechanisms. These dispersion mechanisms reflect the various components of biological tissue

and have been divided into three regions: alpha (α), beta (β) and gamma (γ) dispersions. Schwan was the first to identify these dispersions, indicating that the α-dispersion is found in the frequency region between mHz up to a few kHz which reflects the surface admittance of the membrane surface [51]. The β-dispersion is found in the frequency region between a few kHz to a few MHz and was related to the polarization effects and structural changes of the cell membranes while the γ-dispersions is found in the frequency region of a few hundred MHz to GHz and was related to the polarization of water molecules [51]–[53]. In order to fully under these dispersion mechanisms parameters such as electrode materials (contact and adherence), electrode configuration, frequency range used and depth of measurement penetration into skin should be considered and related back to these mechanisms as these parameters would have an effect on the skin impedance measured.

The use of electrical impedance as a means to interrogate skin is a powerful technique to characterise the different layers of skin as well as detecting tissue alterations. Birgersson postulated that normal and abnormal tissue differ in electrical properties due to their cell structures, size and orientation and through the use and understanding of electrical skin impedance, different tissues can potentially be distinguished from each other [54]. It has been proven to be a technique of interest to monitor tissue water content [14], [15], [55], [56], investigate skin barrier integrity before and after chemical and mechanical damage [57], [58] as well as characterise and differentiate skin lesions [16], [59]–[61]. For example, the Nevisense (SciBase) is a diagnostic tool used to collect impedance data on skin lesions in order to differentiate between benign and malignant skin lesions [16], [59]. This device uses microneedle pins covered in gold to penetrate through the SC and adhere onto skin [16]. It uses a high frequency (1.0 kHz to 2.5 MHz) to propagate the electrical impedance signal through tissue [59]. Helen *at el.*, have demonstrated the development of a hypodermic needle integrated with an impedance sensor on the needle tip to detect changes in phantom tissue substances [61]. The performance of the needle was analysed by penetrating different tissue mimic layers (lard and conducting gel) while recording impedance at real time using a single frequency (10 kHz). A lag in the measured impedance was observed as the needle passed through the boundary between the layer, the research group has attributed this to the impedance analyser [61]. However, their results show that this impedance sensor is capable of differentiating between fatty tissue mimic (lard) and conductive gel tissue mimic, where high impedances were recorded in the lipid layers and low impedances for the conductive gel tissue due to the present of ions in the gel mimic. This group demonstrates a minimally invasive approach for

detecting changes in internal tissue during clinical procedures in the future. Further investigation using the needle tip impedance sensor should consider testing on real skin tissue, which would give more valuable information as these layers are much more complex compared to simplified skin-tissue models. Overall, this group has shown that impedance is a promising technique that can be used to detect alterations in tissue which can potentially be used to differentiate normal and cancerous tissue using a minimally invasive method. Impedance has also been used for early detection of pressure ulcers. Swisher *et al*., have demonstrated the fabrication of a flexible device that can non-invasively map pressure induced damage [62]. Pressure ulcers develop when pressure is applied to a localised area in the body when an individual lies in the same position for a long period of time or if an individual has limited mobility. This flexible sensor array was composed of gold inkjet printed electrodes printed on a polyethylene naphthalate substrate and a conducting gel was used to reduce the influence of the highly resistive SC layer and improve adherence to skin. These flexible arrays were mounted on to skin and a frequency sweep of 100 Hz to 1 MHz was used to detect pressure induced tissue damage *in-vivo* on a rat model [62]. Using impedance spectroscopy across these flexible electrode arrays, the group observed that pressure damaged tissue had lower impedance compared to healthy or undamaged tissue. This decrease in impedance was attributed to the loss of cell membrane integrity. Their results demonstrates the feasibility of using impedance as a non-invasive method for the early detection of pressure ulcers.

Skin impedance is dominated by the high impedance of the SC layer, which comprises of compressed, keratinised flattened cells, and its influence decreases when the frequency range increases [63], [64]. Martinsen *et al.* found by means of finite element calculations, that viable skin represented about 10% of the measured impedance at 1 kHz and represented about 90% of impedance at 100 kHz, concluding that the SC dominates the lower frequency region [65]. Heikenfeld *et al*. also showed that for measurement frequencies between 1 Hz to 10 kHz, the SC dominates the overall impedance of the electrode skin contact [1]. However, what has not been thoroughly considered is that the measured impedance can vary depending on the activity and density of sweat glands which can form conductive ionic pathways as well as the thickness and anatomical position of the SC layer can change the electrical properties of skin [66], [67]. Yamamoto *et al*. were first to investigate and elucidate the electrical properties of the SC using impedance spectroscopy via tape stripping studies and demonstrated the difference in electrical contributions of the SC from the viable skin [68]. It was found that the SC had a high resistance, which reduced upon the removal of the barrier. This trend was also observed by Aberg (Fig.

1.5) where high resistances were observed before stripping and a gradual decrease in resistance leading to the formation of a semi-circle in the Nyquist plot was seen after 90 tape strips, implying that the status of the SC dominates until viable skin was exposed [63].

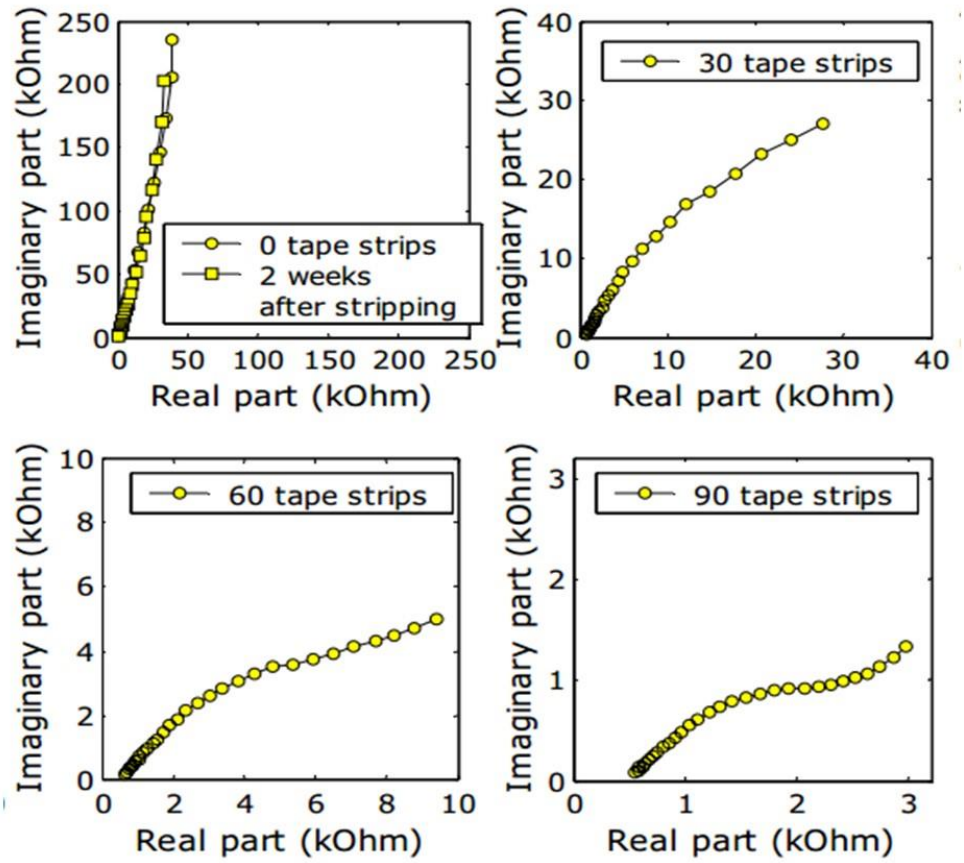

Figure 1.5 Nyquist plots depicting the influence of the barrier status of the SC before and after tape stripping, as the outermost layers of skin were removed a decrease in impedance was observed, reproduced from [63].

The hydration state of the SC has been well-researched, and stems from early work by Blank [69], [70]. According to Blank, the SC will be flexible as long as it contains 10-20% water but if it drops below 10% it could lead to skin barrier impairment [70]. An adequate amount of water present in the SC allows the skin barrier to remain intact giving the skin better elasticity and firmness. Electrical impedance has recently been used to monitor tissue water content of the skin barrier. Leveque *et al*. have explained that the keratin present in the SC is a medium of weak electrical conduction when it is dry [71]. Introducing water to the tightly bound keratin

chains allows the inter-chain spacing to expand as all water-binding sites of the keratin becomes occupied [72], [73]. From this, the water content and water-holding capacity of keratinized tissue in the SC governs the electrical impedance of the human tissue which can be used towards understanding skin barrier function. Therefore, skin tissue water content has been a parameter of interest for monitoring SC barrier function. In skin research, both transepidermal water loss (TEWL) and tissue water content have been used together to understand skin barrier function. Skin probes such as the Tewameter® and VapoMeter (Fig. 1.6a) have been used in clinical research studies to measure TEWL [74]. Skin tissue water content can be measured with commercial electrical skin probes such as the Corneometer® [75], [76], GPSkin Barrier® [76] and the Moisture MeterD (MMD) probes (Fig. 1.6b) [15]. These types of probes have been used in clinical research for quantitative evaluation of different parameters related to skin barrier function.

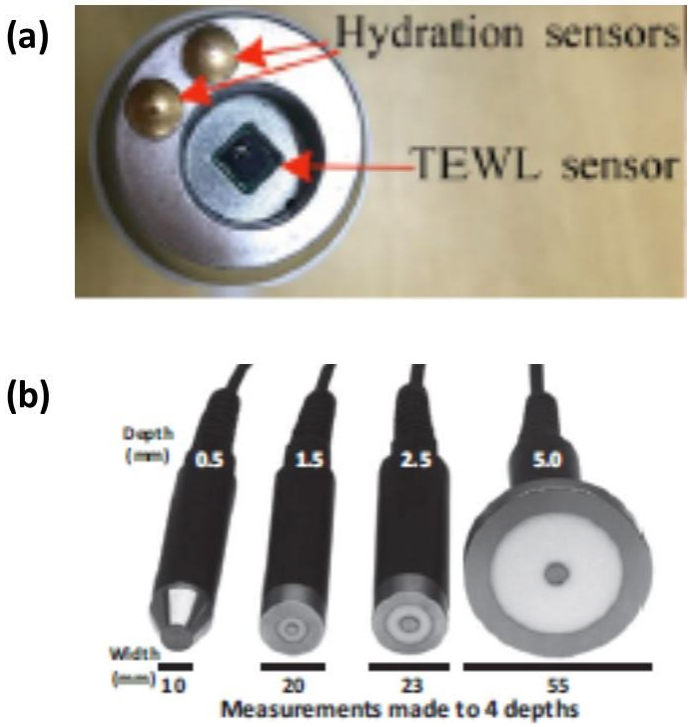

Figure 1.6 Images of (a) sensing tip of GPSkin Barrier® probe, reproduced from [76] *and (b) Delfin Moisture MeterD skin probes, reproduced from* [77].

TEWL is the rate at which water vapour is lost from the body across the skin and it has been used to determine the efficiency of the skin barrier function [78]. When the skin barrier has

been compromised by a skin condition or by physical or chemical irritants, the barrier function is altered and an increase in TEWL is observed. TEWL can be calculated by measuring the water vapour pressure gradient of the skin surface, the measured vapour pressure is based on the relative humidity and saturated vapour pressure which are dependent on temperature. In this case, relative humidity is measured using a capacitive sensor while temperature is measured by thermoresistors which are located within the chamber of the skin probe. Different chamber approaches have been used to measure TEWL, the open chamber method and closed chamber method. Open-chambers are open to the surrounding atmosphere and thus are easily influenced by external air convection therefore a draft shield is used to reduce air convection, while closed chamber methods are a more recent design in which the measuring chamber is enclosed from the surrounding atmosphere and measurements are thus not influenced by external air convection [79], [80]. De Paepe *et al*., have conducted a study to compare open-chamber (Tewameter®) and closed-chamber (VapoMeter) TEWL probes via *in-vivo* measurements of the human forearm [74]. It was noted that correct handling of the probes and standard ambient room conditions were important to achieve reproducible measurements because these have an effect on TEWL values measured [74]. Based on their tape-stripping study, it was observed that the VapoMeter gave significantly lower TEWL readings compared to the Tewameter® which could be a drawback for the closed chamber system. This lower reading was attributed to the fact that an open chamber system records stabilized TEWL values whereas the closed chamber system requires a few minutes to compute TEWL values based on the increasing rate of humidity within the chamber [74]. Despite this lower reading, both TEWL probes are still considered reliable for measuring TEWL as long as application pressure, humidity and temperature are kept consistent and a standardised protocol has been put in place.

Table 1.1 Measurement principles and measurement specifications for commercial skin probes that measure tissue water content.

Skin probe	Measurement Principle	Frequency	Stated Measurement Depth	Ref.
Corneometer® (Model 820 & Model 825)	Capacitance	40-75 kHz (Model 820) 0.9 to 1.2 MHz (Model 825)	30 - 45 µm (Model 820) < 15 µm (Model 825)	[76], [81], [82]
GPSkin Barrier®	Impedance	1 kHz	-	[76]
Skicon® (Model 100 & Model 200EX)	Conductance	3.5 MHz	< 15 µm	[81], [83]
Delfin MMD	Tissue Dielectric Constant	300 MHz	0.5 - 5.0 mm	[84]
Nova DPM (Model 900 & Model 9003)	Impedance	up to 1 MHz	40-60 µm	[81], [82]

Some skin probes have been designed to assess the tissue water content of skin. The use of these devices to evaluate tissue water content of skin has been documented in both normal and diseased skin [47], [76], [85], [86]. They are regularly used to monitor the skin water content of individuals that suffer from AD [87]. However, many factors may influence these skin measurements which can impact the final interpretation of results. These probes use electrical methods for assessing skin tissue water content which are based on measuring impedance or conductance, as a function of one or more different stimulating frequencies [82] as tabulated in Table 1.1. Both impedance and conductance are frequency-dependent and deriving physical parameters such as resistance, reactance and capacitance can be complicated. Measurement from the skin probes typically use two electrodes to apply an electric field, where in impedance it measures the opposition to the flow of electric current through the skin and depends upon resistance and reactance, while capacitance is the ability of a system to store charge which is calculated from reactance only. A range of frequencies and different electrode geometries are used to measure tissue water content. The electric field distribution depends on the complex permittivity of the tissue, which depends on the distribution of polar materials (i.e. water or ions) with depth through the various skin layers [82] which can potentially be influenced by electrode geometry and frequency range. The Corneometer® (Model CM 825) consists of an

interdigitated array of gold electrodes that are 75 µm wide with an interdigitated spacing of 75 µm [88], covered by a low dielectric vitrified material of 20 µm thickness that acts as the capacitive layer [75], [76]. Depending on the Corneometer® model, its stated measurement depth into skin varies between < 15 µm up to 45 µm, which is considered as a skin surface measurement. In contrast, the MMD probe uses concentric electrode configurations to measure deeper into the skin whereby the spacing between these concentric electrodes govern the effective measurement depth (0.5 to 5.0 mm depth) (Fig. 1.6b) [84]. Interdigitated electrodes compared to a concentric configuration reduce the contribution from the viable skin due to the close spacing between the electrodes [89]. This suggests that electrode geometry and electrode spacing of skin probes have an effect on the penetration depth measured.

The Corneometer® (Model CM 825) uses a frequency range of 0.9 - 1.2 MHz for its measurement [75], [76]. Literature surrounding the Corneometer® claims a measurement depth of < 15 µm [81] so it can measure tissue water content of the SC layer, which was previously mentioned to be 8 – 40 µm depending on various factors. In contrast, the MMD probe measures tissue dielectric constant (TDC), a measure of the localised skin tissue water content and its changes. This probe employs a frequency of 300 MHz and uses a concentric electrode configuration to measure deeper into the skin [84]. At this high frequency the electromagnetic wave reflected by the probe can measure both free and bound water in the tissue [84]. This is assuming that at this high frequency the charge between the electrodes causes an electric field, where the dipoles of free and bound water in tissue align themselves with the generated field in order to measure water content. This suggests that measurements from the various commercial skin probes are calculated based on the permittivity of the tissue, the penetration depth based on the frequency range and geometry used. These parameters should be taken into account when comparing studies that use these commercial skin probes. Other factors such as device application pressure, anatomical site and environmental conditions should also be considered when comparing studies conducted by different researcher groups since there is no standardised protocol for measuring skin tissue water content. Another factor that can affect skin probes would be interference on the skin surface. Substances present between the electrodes and the skin such as oil and dirt may affect the readings. Despite these factors, skin probes are useful tools for evaluating water content and water loss which have been related to skin barrier function. For example, Angelova-Fischer *et al*. investigated tissue water content and TEWL to assess the skin barrier function of AD sufferers [87]. They observed lower tissue water content for AD sufferers, which increased steadily as the flare-up subsided indicating

that the skin barrier was repairing itself [87]. An increase in TEWL was also observed for AD sufferers, indicating that the damaged barrier was allowing water to evaporate at a high rate from skin, while TEWL rates were lower in uninvolved (control) sites [87].

Another parameter that is important in skin barrier function is pH. The skin is known as the "acid mantle" due to its acidic pH which contributes to its optimal barrier function and has been broadly measured to be between pH 4.2 and 6.0 [90]. Research into pH and factors that affect it depend on both the external and internal influences [91]. Changes in pH has implications for the skin microbiome and enzymatic activity and elevations in pH can indicate dysregulation of the skin barrier function [92], [93]. Luebberding *et al*. showed skin pH ranges between 4.58 ± 0.29 and 5.12 ± 0.35 in healthy adult males and females, respectively [94]. However, disruption of the skin barrier function increases skin pH (pH > 6), and impairs healing by allowing bacteria or fungi to thrive [95], [96]. As such, dramatic alterations in skin pH can play a role in the pathogenesis of skin conditions.

pH is typically measured using a flat head potentiometric pH probe [93], [94], [97]. These pH probes consist of a flat-topped glass electrode for full skin contact. It is connected to a voltmeter that can measure the electrical potential due to the activity of hydrogen ions surrounding the glass membrane at the top of the probe [94]. The glass electrode response is governed by the Nernst equation, which is the relationship between the potential of the electrode and the concentration of the hydrogen species in a redox reaction. By using the Nernst equation, it can predict the cell potential of reactions that depend on pH and it predicts that for 1 unit change in pH, the potential will change by about 60 mV. Thus the voltage generated by the probe depends on the hydrogen ion concentration of skin. The measured skin pH is based on the extraction of water-soluble components of the SC as well as secretions from sebaceous and sweat glands [98], which reflects the skins barrier function. Another method to detect pH is through colorimetric optical detection using pH sensitive dyes [99], [100]. In this case, pH sensitive dye changes colour when it comes into contact with skin or sweat. The measured colour change can be compared to a reference colour range which can be used to determine the pH. Recently, Rogers and L'Oreal launched a prototype epidermal pH sensor based on pH sensitive dyes. The platform harvests sweat from the skin surface and uses colorimetric pH senstive dyes to optically measure pH. Their epidermal pH tracker uses a smart phone for imaging the colorimetric dyes and an algorithm processes the colour change before and after exposure to sweat is used to estimate pH [99]. This technique relies on a visual comparison of the colour measured against a colour reference scale which would be advantageous and user-

friendly when used in a wearable format for continuous monitoring. However, colour image processing can be a challenge because lighting and image capturing methods can influence the measured pH.

1.2.2 Skin matrices and their diagnostic opportunities for monitoring health

1.2.2.1 Sweat

Sweat is a matrix of analytical interest because of its accessibility as it can be easily generated through exercise or it can be induced using the drug, Pilocarpine. There are three glands present in skin: eccrine, apocrine and sebaceous glands. Gland distribution at the skin surface varies across the body. Eccrine glands are distributed across the skin and have their functions in excretion and thermoregulation by secreting water and electrolytes [101]. Apocrine glands secrete proteins and odour precursors and are distributed on the axillae, areola of nipple, and genital areas [102]. Sebaceous glands mainly secrete sebum which lubricates the skin and have also been associated in the development of acne [103]. In this case, sweat is produced mainly from the eccrine and apocrine glands [104], [105]. Sweat is composed mainly of water with electrolytes, such as sodium and potassium, analytes such as urea and lactate as well as amines, amino acids and metal ions [104]. Monitoring the change in analyte concentrations can potentially act as indicators for clinical conditions or hydration status in athletes [11]. For example, Cystic fibrosis (CF) is a disease that has been related to changes in the transport of sodium and chloride resulting in the formation of mucus in organs such as lungs and intestines [105]. It is clinically diagnosed through sweat chloride testing using pilocarpine iontophoresis to stimulate sweat, which is then quantitatively analysed for chloride using a chloridometer [106]. Other methods have been used to monitor this disease through sweat, such as the use of a calix[4]arene based sodium ionophore to selectively detect Na^+ in sweat in the form of a sweat sensor belt [107]. Participants wore this sensor during exercise to generate sweat and used a patch of polyimide/lycra® blend to wick fresh sweat into the sensor platform where the sodium ionophore selectively detected Na^+ from sweat. It was observed that participants suffering from CF had high levels of sodium [107]. This indicates that the sensor belt can potentially be used to monitor sodium levels of individuals who suffer from CF. The use of enzymes is another method to detect analytes from sweat. Analyte information such as lactate from sweat can be detected using an enzyme-based approach. For example, an epidermal sensor has been developed to selectively detect lactate in sweat using lactate oxidase (LOx) which monitored lactate levels to evaluate anaerobic/aerobic status and assess physical fitness of an

individual [23]. Wang's group fabricated a screen printed epidermal sensor that utilises a 3-electrode system, where the working electrode was functionalised with LOx and the resulting sensor was used to record sweat lactate profiles during prolonged exercise via amperometric methods [23]. Using this epidermal approach, dynamic changes in sweat lactate levels were observed. Sweat has also been used to monitor pH change by utilising universal indicator dyes such as bromothymol blue, methyl red and phenolphthalein as these dyes yield colorimetric responses over the relevant range (pH 5.0 to 7.0) [99]. Rogers' group have developed a wearable microfluidic patch that used optical detection by recording the colour change before and after exposure to sweat [108]. The research carried out developing this microfluidic pH patch has led towards the optimisation and production of the My Skin Track pH which will be discussed further in the section discussing epidermal sensors in this thesis. Overall, this demonstrates that sweat is a matrix that can be easily accessed because sweat glands are present all over the body and it can be used to detect analytes relevant to health. However, the main limitation of using sweat as a diagnostic matrix is sweat volume generation. Individuals have limited control in the amount and rate of sweat produced for sampling and analysis. Therefore techniques such as pilocarpine delivery or exercise are typically employed to generate large volumes of sweat.

1.2.2.2 Interstitial fluid (ISF)

The ISF is an attractive source of biomarkers. It is an extracellular fluid that surrounds tissue cells and has become a promising alternative source of biomarkers that can also be found in blood [109]. Analytes and small molecules found in blood and the surrounding vascularised tissue, such as glucose [110] and lactate [111] are readily exchanged by diffusion into the ISF [109]. As a result, the ISF is a good analytical skin matrix that can be used as a proxy for blood sampling, offering valuable information about an individuals' health. However, accessing this fluid still requires minimally invasive methods such as reverse iontophoresis and microneedles. One of the first commercially available electrochemical sensors was the GlucoWatch®. This sampled the ISF using reverse iontophoresis and an enzyme to selectively detect for glucose. It used reverse iontophoresis to extract glucose from skin, whereby current is passed over the skin to drive glucose from the ISF towards the skin surface. A hydrogel disc containing glucose oxidase (GOx) selectively catalyse glucose molecules [110]. However, the production of the GlucoWatch® was later discontinued due to errors in reading and skin damage due to multiple hours of reverse iontophoresis [1]. Another method of sampling ISF is through the use of

microneedles. Microneedles can be classified as solid, dissolvable or hollow and materials such as metals and polymers have been used to produce microneedles [112]. However, the choice in materials for microneedle fabrication is an important consideration because it should have sufficient mechanical strength to penetrate the skin but it cannot be too fragile that the needle might break in the skin. Microneedle lengths can vary between 250 to 2000 µm [113]–[115] which penetrate and create pathways through the SC layer of the epidermis. Hollow microneedles are a sub-class of microneedles. It contains a hollow bore in the centre of the needle whereby when inserted into the skin it produces a channel in the skin layers that can be used for drug delivery or extract fluids [114], [116], [117]. One example used a silicone-based hollow microneedle array that consists of 200–350 µm tall needle shafts which was supported by a glass substrate [117]. This hollow microneedle array was applied onto the earlobe used to extract ISF and detect glucose using a commercial glucose testing strip placed in contact with the reservoirs of the microneedle array. This type of microneedle was fabricated using a rigid silicone material which can elicit a foreign body response if the microneedle tip breaks in skin. Although, other alternative approaches for extracting ISF using microneedles have been reported using soft polymer materials such as a swellable hydrogel microneedle platform based on methacrylated hyaluronic acid [118]. In this type of microneedle, the biocompatible hydrogel swells to extract ISF that contains the target metabolites such as glucose and cholesterol. An efficient recovery method of these analytes from the hydrogel patch post the extraction was critical for subsequent glucose and cholesterol analysis [118]. Despite being a promising diagnostic fluid, reliable sampling of ISF is still a challenge and is a minimally invasive technique. As well as this, microneedles damage the skin and thus induce immunological responses that can cause localised skin irritation. However, a recent innovation in microneedle sampling is the Abbott Freestyle® Libre™, a commercial wearable device that extracts ISF for glucose monitoring and has been intended to replace blood glucose measurements. This wearable sensor is discussed in more detail in section 1.3.3.

1.2.2.3 Skin volatile emissions

The human body emits hundreds of volatile organic compounds (VOCs) via the skin derived from glandular excretions [22]. VOCs have currently attracted considerable scientific interest as this matrix offers a promising non-invasive route towards monitoring and understanding human physiology. These VOCs can reflect the metabolic conditions of an individual and can be used to target disease-specific VOCs [119]. VOCs are emitted from the three skin glands:

eccrine, apocrine and sebaceous glands which were previously mentioned in the section that discussed sweat. Emitted VOCs are comprised of a variety of compound classes such as alkanes, acids, alcohols, ketones and aldehydes that can be from both exogenous and endogenous sources [47], [120]. It has been reported that using these volatile profiles can potentially differentiate between healthy and diseased groups, such as melanoma [121]. To sample VOCs from skin the volatile emissions are typically absorbed into porous materials such as gauze [122] or polymer matrices [47] in a head space format. The collected VOC samples are analysed via gas chromatography-mass spectrometry (GC-MS). However, due to their low concentrations a suitable sampling method such as a pre-concentration step is typically employed to enrich the target VOCs [123]. Head space, solid phase microextraction (HS-SPME) pre-concentration is a sensitive, non-invasive, solvent free and easily performed method for VOC sampling [22]. Skin VOCs sampling has been used to investigate volatile emissions before and after SC barrier disruption [47] as well as unique volatile metabolic profiles of melanoma [121]. It has also been used to establish predictors for malaria infection [124] and has recently been studied for specific volatile emissions relating to Parkinsons disease [122].

1.3 Current state of the art in wearable and epidermal sensing

Wearable sensors are dominated by commercial wrist watch sensors such as the Fitbit®. This type of wearable physical activity monitor has become widely used to allow individuals to monitor their physical activity. Recent research are moving beyond this by developing innovative epidermal sensors that are leading to personalised health care. As previously mentioned, the skin surface and other matrices can serve as "windows" into the metabolic processes of the body. Translating this into wearable sensors can leverage this opportunity, however the fabrication and development of these sensors comes with challenges. For example, these type of sensors require soft flexible materials for mechanical stability when worn on the body to achieve the goal of continuous real-time monitoring. Reliable sampling methodologies are also important to consider in order to accurately detect and analyse the target biomarkers from skin as well as the use of biocompatible materials with skin.

As mentioned earlier, the GlucoWatch® was one of the first wearable biochemical sensors that was commercially deployed. This wearable device utilised hydrogel pads containing glucose enzymes to selectively detect glucose extracted from ISF via reverse iontophoresis [110]. The

glucose response was measured amperometrically by direct detection of H_2O_2 generated by the GOx catalysed reaction on the surface of a Pt-graphite working electrode. However, the GlucoWatch® ultimately failed as a product due to the repeated need for calibration and in some cases an unusual tingling sensation or skin damage after multiple hours of reverse iontophoresis [1], [110]. This demonstrates the challenges faced in the development of wearable chemical sensors compared to physical wearable sensors. The next sections will discuss the current innovations in wearable and epidermal sensing technology.

The emerging field of epidermal sensors presents an exciting opportunity to move away from invasive sampling as well as have wearable sensors that more integrated to the body compared to bulky wearable devices. Epidermal sensors are a sub-class of wearable sensors that are directly adhered to skin. The research field of epidermal sensors have been dominated by groups of Wang and Rogers among others. Interestingly, Wang and Rogers recently described the SC as an information barrier from the point of view of epidermal sensing [1]. The skin and other externally facing tissue surfaces are by design barriers to chemicals that can be used as diagnostic biomarkers and therefore access to chemical analytes is only possible by measuring fluids secreted from the body such sweat, tears and saliva [1]. Their groups have demonstrated that epidermal sensing can be achieved by using methods such as reverse iontophoresis or pilocarpine iontophoresis to extract these fluids from skin to detect target analytes [125]–[128]. However, other approaches for epidermal sensing has been achieved and other research groups have shown that tracking the electrical changes of the SC can determine its effectiveness and permeability as a protective barrier which is also important for health monitoring [14], [15], [129], [130]. Another sensing approach using epidermal sensors track electrical activity such as electromyography (EMG) or electrocardiography (ECG) [131]–[133].

Wang's research group have reported several tattoo-based epidermal sensors that employs screen-printing as a method of choice for fabrication. By directly screen-printing on to a temporary transfer tattoo paper substrate, they create epidermal sensors that directly adhere onto skin [134]. This group have developed screen-printable inks modified either for example by dispersing carbon fiber segments within the inks to enhance tensile strength [134] or by incorporating elastomeric materials such as polyurethane binders to induce stretchability [135]. These sensors rely methods such as defining electrode areas between the tattoo and skin to facilitate the flux of fresh perspiration over the sensor [23] or hydrogel coatings (i.e. agarose gel) on the electrode to contact the electrodes to skin to deliver the extracted fluid to the sensor [127]. They have shown that these screen-printed electrochemical sensors have the potential

for monitoring skin biomarkers such as ammonium in sweat [136] as well as glucose [127] and alcohol from skin ISF [137]

Rogers' research group has been another leading group in epidermal sensors. Their group has spent time understanding and exploiting the characteristics of soft materials to design skin conformal electronics and sensors. Their group uses lithography and etching techniques to design thin, low-modulus and stretchable epidermal sensors using materials such as polyimide and polymethyl methacrylate [14], [129], [138]. Innovative electrode geometries using serpentine and fractal designs have also been used to enhance stretchability of the epidermal sensors as well as encapsulation of these electrodes within soft polymer matrices to enhance robustness [14], [55], [138], [139]. Their developments in electronics integrated with soft materials for epidermal sensing have led to the deployment of two different epidermal sensors into market, the UV skin patch (Fig. 1.1a) [24] and more recently My Skin Track pH (Fig. 1.1b) [25] co-developed with L'Oreal (La Roche-Posay).

Both of these research groups have fabricated and optimised epidermal sensors to focus on changes in skin chemistry, such as using enzymes to target analytes from sweat as well as tracking its concentration change [127], monitoring changes in skin pH [100] as well as tracking alterations in the skins electrical properties due to hydration changes [15], [129]. These epidermal sensors and their sensing techniques among others will be discussed in detail in the next few sections.

1.3.1 Physiological monitoring via the SC

As previously discussed, the SC is a protective barrier against water loss. However, a damaged skin barrier typically seen in skin conditions such as AD allows for water loss and penetration of microbes and irritants. This causes excessive dryness and irritation of skin, therefore monitoring the water content of this barrier is a parameter of interest for these skin conditions. It can potentially predict and prevent flare-ups from manifesting or conditions worsening.

Several commercial skin probes are employed in clinical research to understand and quantitatively evaluate the tissue water content of skin. However, currently these commercial skin probes are expensive and not accessible to the individual. Therefore, researchers are currently developing various epidermal platforms that can non-invasively monitor the skin barrier function via its tissue water content to help personalise this type of measurement. Tissue water content is typically characterized using skin impedance [14], [15], [55], [56], [140],

thermal conductivity [140], [141] and raman spectroscopy [142], [143]. Impedance, represents one of the most established forms of assessing skin barrier function as well as giving reliable and direct measurements, due to the strong influence of water content on conductivity and permittivity of the skin [55]. Commercial probes have demonstrated the use of impedance for measuring tissue water content and now this approach is being used by epidermal sensors to monitor skin tissue water content.

Rogers' research group was the first to develop a truly conformable epidermal sensor that utilises impedance to track electrical changes in skin that correlate to tissue water content. The group uses lithography and reactive ion etching to fabricate an array of gold concentric serpentine electrodes (Fig. 1.7a, top left, inset) coated in a thin polymer matrix (approx. 5 μm), where both the serpentine design and polymer encapsulation was used to accommodate for the mechanical strain put on the platform when worn on the body (Fig. 1.7a, top left) [14]. This group have performed extensive studies using different patterns of stretchable periodic serpentine or fractal geometries for conducting tracks to determine its impact on mechanical strain. They have shown that different repeated line and loop patterns of conducting tracks can achieve mechanical strain limits suitable for epidermal sensor use [138]. In particular, the serpentine pattern commonly used as a conducting track in their epidermal platforms can achieve elastic stretchabilities between 6 - 61%, which depends on the arc angle of the serpentine patterns and application of the overall sensor platform [138]. Their group has used this platform to perform impedance to determine tissue water content in skin using a frequency range between 15 - 95 kHz, where they observed that their platform had the highest sensitivity at low frequencies [14]. The impedances measured for the inner forearm ranged between 25 and 50 kΩ, where an increase in impedance correlates to a decreased water content, which was related to a decrease in electrical conductivity of the keratinized tissue (Fig. 1.7a, bottom left). A MoistureMeterSC Compact (Delfin Technologies) was used to validate the epidermal sensor. Shanshan *et al*. also fabricated an epidermal hydration sensor (Fig. 1.7b, top right). This platform utilises an interdigitated electrode design based on soft conducting materials [15]. The finger lengths of the electrodes were 20 mm with 2 mm spacing fabricated using a polydimethylsiloxane (PDMS) mask. Silver nanowires dispersed in ethanol (average length, 10 μm and diameter, 90 nm) were drop-cast into the area defined by the mask and was heated to evaporate the ethanol [15]. This was then coated with another layer of PDMS to act as a support for the electrodes and a self-adhesive substrate was used to attach the sensor to skin. This platform utilises an interdigitated design, whereby the 90˚ bends would be considered

points of fracture. The overall thickness of the device was not reported. In Rogers' approach the concentric electrodes had smooth edges and curves with a substrate thickness of approx. 5 µm, both of which were considered key to reduce mechanical strain endured by the platform. Despite the geometry, when this interdigitated silver nanowires/PDMS was used as a strain sensor and it was able to record capacitive change as a function of tensile strain up to 100% which is far beyond that of a traditional thin film strain sensor [15]. This platform was also used to measure skin tissue water content. It was capable of measuring impedances approx. between 1 to 3 kΩ on the inner forearm at 100 kHz (Fig. 1.7b, bottom right) [15]. These impedance values were lower compared to measurements by Rogers' serpentine gold hydration platform, which was likely due to the differences in frequency range, electrode materials, and geometries. Despite these differences in impedance values recorded, the relative change observed for increasing and decreasing water content were the same.

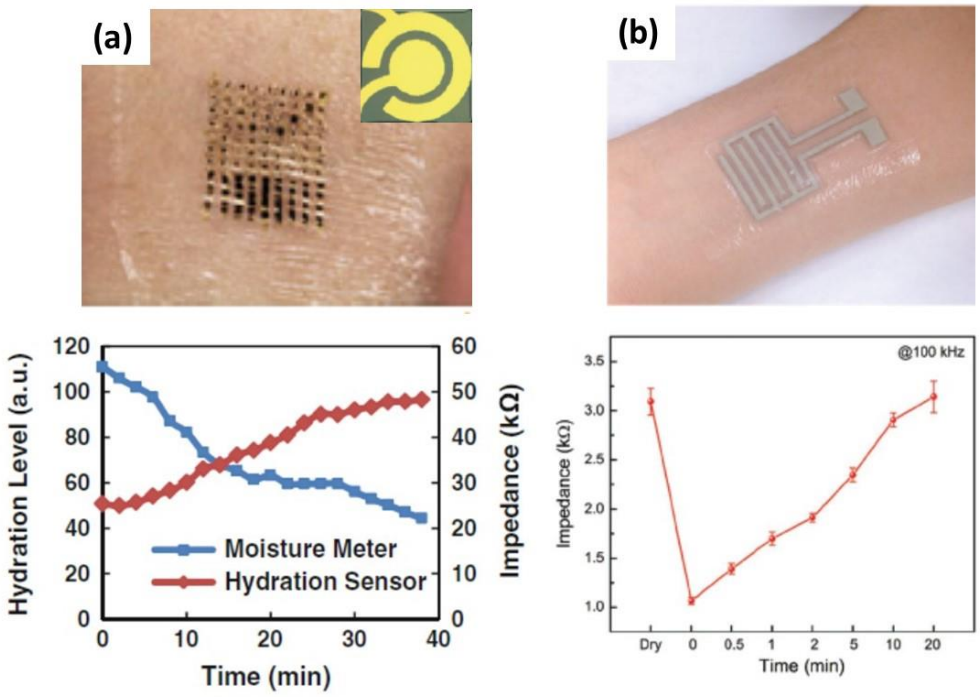

Figure 1.7 (a) Image of Rogers epidermal wearable based on concentric electrodes, reproduced from [14] *and Shanshan et al. epidermal wearable based on interdigitated electrodes, reproduced from* [15] *and its corresponding data tracking electrical changes due to changing tissue water content overtime.*

Another example of an innovative epidermal sensor is the UV skin patch co-developed by Rogers with La Roche-Posay. The patch is an ultra-thin (approx. 600 μm) breathable sensor that contains UV sensitive dyes that change colour upon exposure to UV radiation. UV radiation is comprised of UVA and UVB rays, where UVA rays penetrate deep into the dermis layers of skin and UVB rays superficially penetrate into the epidermis [144]. However, UVA rays are typically higher than UVB rays and literature data indicates that UVA rays potentially contribute to skin ageing and skin cancer [145], [146]. Rogers' group have proposed the use of colorimetric chemistries for UV detection in their epidermal UV patch. The chemistry for the UV detection involves a combination of a photoacid generator such as (4-phenoxyphenyl)diphenylsulfonium triflate (PPDPS-TF) and colour changeable dyes such as crystal violet lactone and Congo red for UVA and UVB detection [147]. The absorption of UV photons by the photosensitive activator generates an activated species that induces a change in the colour of the dye [147]. The photoacid generator is the PPDPS-TF, when it absorbs light it becomes more acidic which is detected by the pH sensitive dyes and induces the colour change in the UV patch, in this case the dyes change from colourless to bright colours with decreasing pH [147]. The UV patch was fabricated by roller printing the reference colours on a permeable polyurethane (PU) film (16 μm), the UV ink and blockers are screen-printed on top. Below the PU film a near field communications antenna was incorporated for wireless detection. This ultra-thin UV patch uses an adhesive patch to adhere to skin and its elastic properties allow for conformal contact with skin for continuous wear for up to 5 days. Optical imaging of the dyes were done before and after UV exposure and the change in colour is quantified with regards to the reference dyes. The application algorithm used was designed to determine the user's UV exposure by colour quantification as well as perform lighting correction [24]. It was validated against UV dosimeters and their analysis show strong correlation between the commercial dosimeters and UV epidermal patch picture analysis [24]. This UV skin patch was the first of its kind to be used in a large population to investigate skin UV exposure across a range of geographical locations.

Epidermal sensors have also been designed to intimately contact the skin to measure electrical activity such as electromyography (EMG), electroencephalography (EEG) and electrocardiography (ECG) [18], [131], [132], [148]. When monitoring electrical activity in the body via the skin, understanding the electrode-skin interface is crucial as this can determine the quality of the signal [149], [150]. Typically wet or semi-wet electrodes are used for these applications, however it would be more ideal to develop a wholly dry electrode system for this

application, given the deleterious drying effects over time for wet electrodes [15], [150]. For example, Greco *et al*. demonstrated the fabrication of conductive nanosheets by inkjet printing poly(3,4-ethylenedioxythiophene) polystyrene sulfonate (PEDOT:PSS) as temporary tattoo electrodes [131], [132]. The PEDOT:PSS tattoo electrodes had an overall thickness between 600-1200 nm and were capable of intimately contacting the rough skin surface, maximising the sensing area (Fig. 1.8a, top left) [132]. When the platform was subject to mechanical stress, the first stretch applied to the epidermal tattoo caused an irreversible change in resistance and an incomplete recovery to resistance was observed after 10% strain [131]. Although the sub-micrometre thickness of the tattoo nanosheets allowed for ultra-conformability to the complex surface of the skin, its functionality is limited by the amount of mechanical stress endured. These tattoo electrodes were used for surface electromyography (sEMG) and the recorded signals were compared with those recorded by state-of-the-art pre-gelled Ag/AgCl electrodes. Time domain and spectrograms of the EMG signals recorded during three series of grasping at different pressures (2, 3, 5 psi) (Fig. 1.8a, bottom left) and the measurements for both tattoo EMG electrodes and standard gel electrodes matched well at all contraction levels [131]. Another example of measuring electricity activity via the skin was demonstrated by Ren *et al*. where magneto-rheological lithography was used to fabricate microneedle array electrodes (MAE) [148]. These microneedle arrays were connected to conducting serpentine patterns directly printed on a 25 μm thick polyethylene terephthalate (PET) film to form the electrode platform (Fig. 1.8b, top right). Utilising the serpentine design with a thin substrate enhances the mechanical deformability and prevents fracture by decreasing the induced strain [148]. This epidermal wearable platform used 500 μm length needles to overcome the resistance of the SC barrier and reduced motion effects ensuring reliable monitoring of bio-signals. The electrode-skin interface impedance was monitored between 20 Hz and 10 kHz and its performance measuring different electrical signals were evaluated. The flexible MAE was able to record ECG, EMG and EEG signals. However, the dynamic ECG signal recorded by the flexible epidermal microneedle array was the most distinguishable and introduced the least signal noise (Fig. 1.8b, bottom right) [148]. This demonstrates the potential of a wearable microneedle arrays for ECG monitoring. However, as discussed earlier microneedles are a minimally invasive approach of contacting skin that have the potential to elicit an immune response which is not ideal.

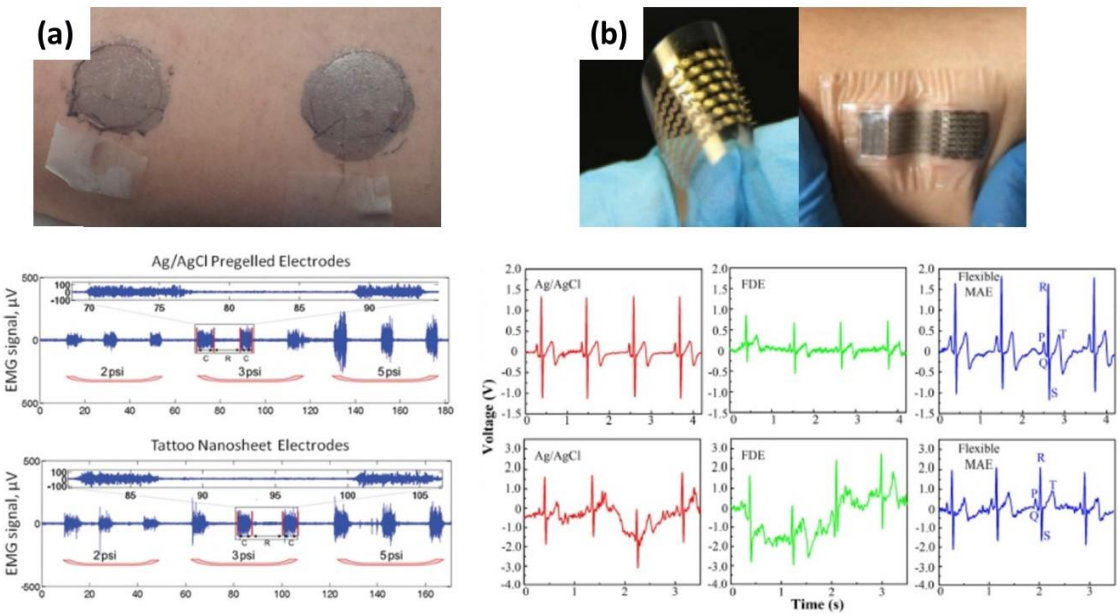

Figure 1.8 (a) Image of the PEDOT:PSS based epidermal sensor on forearm and comparison of the EMG signals recorded by the epidermal sensor versus standard gel electrodes during a series of different contraction levels, reproduced from [131] *and (b) image of the epidermal microneedle array during flexing and adhered on the forearm as well as the comparison of electrical signals recorded by the epidermal sensor against standard wet and dry electrodes, reproduced from* [148].

1.3.2 Biomarker analysis in sweat

As previously discussed, sweat is a sampling matrix that is easily accessible and can be conveniently sampled from different locations of the body. Epidermal sensors have exploited this which has led towards innovative sweat sampling approaches and in-situ analyte detection. Wang's research group has used iontophoresis to deliver a sweat inducing drug and subsequent enzyme-based detection for alcohol monitoring in sweat [126]. This tattoo platform consists of iontophoretic electrodes and a 3-electrode electrochemical cell, whereby the electrode system consisted Ag/ AgCl reference electrode while the counter and working electrode were printed with conductive carbon [126]. Alcohol oxidase (AOx) was then enzyme used to selectively detect ethanol from sweat. It was immobilized on the working electrode by drop-casting with bovine serum albumin (BSA) and chitosan, which was covered with agarose gel containing phosphate buffer saline (PBS) to provide consistent and stable electrolyte level. This enzyme-based detection relies on a Prussian-Blue mediator to detect changes in current due to the production of H_2O_2 generated from the AOx enzymatic reaction based on alcohol content of

the skin. Initially, calibration plots were obtained using 3 mM increments of the ethanol concentration, up to 36 mM in the buffer solution which corresponded to ethanol levels in sweat [126]. On-body alcohol monitoring with participants using this epidermal sensor was validated against a commercial breathalyser and has shown that it was capable of detecting changes in current related to alcohol consumption. However, it was noted that even though the participants consumed the same amount of alcohol, the blood alcohol content measured by the breathalyser varied which was attributed to their different alcohol metabolisms. Overall, this group has shown proof of concept of an epidermal sensor that monitors alcohol levels from sweat using enzyme-based detection which can potentially be used for continuous monitoring to warn individuals when they have consumed their alcohol limit.

A non-enzymatic approach for sweat analysis was demonstrated by Zaryanov *et al.* by modifying a commercial screen-printed sensor to selectively detect lactate [128]. The commercial screen-printed sensor has a carbon working electrode and carbon counter electrode. The working electrode was modified by electropolymerization of 3-aminophenylboronic acid (3-APBA) on to the electrode surface [128]. Phenylboronic acids (PBA) have been known to selectively bind to compounds with 1,2- and 1,3- diol functionalities, such as sugars and α-hydroxls such as lactate [151]. In order to reduce the influence of interference and further improve affinity to lactate, molecular imprinting (MIP) of lactate was also utilised. In MIP, 3-dimensional cavities are created within a polymer matrix complementary to size, shape, and functional group orientation of the target molecule [128], [152]. The size and shape of these cavities allow the target molecule to occupy the space for selective detection. By using PBA and MIP, the group has modified the sensor to selectively detect lactate in sweat. This modified sensor uses impedance to measure the response of the electrodes and an equivalent circuit was used to extract the resistance value attributed to lactate. It was observed that relative resistance decreased, as lactate concentration increased and lactate detection using the modified sensor is possible in the range from 3 to 100 mM, which corresponds to its concentration in human sweat [128]. However, this modified sensor was not subjected to *in-vivo* testing. The sweat was collected from participants using a Macroduct Sweat Collector, which uses pilocarpine to induce sweat production. This sensor was validated against a biosensor that uses enzyme-based detection and it was observed that the lactate concentration in sweat obtained by the modified sensor was in good correlation with the values obtained by the reference method. This demonstrates that a modified sensor that utilises PBA and MIP was valid for selective lactate detection in human sweat.

Another example of sweat analysis was through the use of ion-selective electrodes (ISE) integrated into a wearable platform. Glennon and co-workers have used a sodium ionophore to selectively detect Na^+ ions potentiometrically in sweat (Fig. 1.9a) [10]. Their prototype epidermal platform uses a microfluidic chip that contained an absorbent material to wick sweat from skin and across modified screen printed carbon electrodes. This microfluidic chip was housed in a pod-shaped platform so it can be worn on the body similar to wearing a watch. In their study, the ISE and reference polymer membranes were prepared by drop-casting these onto screen printed carbon electrodes before being placed in the housing unit [10]. During on-body trials, the platforms were pre-primed before use with 10^{-4} M NaCl to provide full contact with the electrodes and skin as well as establish a stable baseline to enable the arrival of sweat to be observed as a rapid increase in signal. The detection of sweat was observed as an increase in potential as Na^+ concentration increases. This wearable platform relies on an adjustable strap tightly wrapped around the limb to keep the device from losing contact with the skin and to ensure a steady flow of sweat was wicked towards the electrodes for detection. In order to generate high volumes of sweat, the participants were required to perform high intensity exercise with the wearable device strapped to their limb. This group has shown a novel wearable approach using a housed microfluidic chip that enables real-time potentiometric detection of Na^+ concentrations in sweat.

Figure 1.9 Images of the (a) components for SWEATCH, a sodium detection platform and how it is worn on the arm, reproduced from [10] *and (b) epidermal sensor that uses a detachable*

microfluidic system and a phone system for wireless communication and acquisition to detect various analytes in sweat, reproduced from [108].

Epidermal sensors have also been developed to detect sweat pH. The pH of sweat ranges from pH 5-6 and becomes more acidic with evaporation which is controlled by lactic acid and its volatile derivatives such as acetic and propionic acid, while sweat becomes alkaline due to ammonia build up linked to bacterial action [91]. Wang's group have developed an epidermal platform for real-time potentiometric monitoring of pH in sweat [153]. This epidermal sensor uses a polyaniline-based solid-contact ISE on screen printed electrodes printed on temporary tattoo paper to fabricate a pH sensitive wearable. For proper contact between the two electrodes and analyte solution, a rectangular-shaped region was defined around the reference and ISE electrodes. Polyaniline, a conducting polymer can be used to detect pH through its electrical response. The pH-sensitive conductivity of polyaniline is due to the reversible protonation process between the emeraldine salt and base forms [154]. The resulting platform showed rapid and near-instantaneous potentiometric responses to pH changes between pH 3-7 during *in-vitro* testing, which encompasses the pH range of human sweat [153]. Real-time pH sensing using this platform was carried out on a participant on a stationary bike and has shown that 10 min of cycling was required before a response was generated by the tattoo platform indicating that a high sweat flow was required to establish a stable pH reading [153]. However, once a high rate of sweat was generated, this platform was capable of detecting sweat pH that correlated with a glass pH electrode.

Sweat pH monitoring has also been integrated with Ca^{2+} detection. Ca^{2+} levels in sweat are dependent on pH [155], [156] and low levels of Ca^{2+} has been linked with hypocalcemia [157]. Nyein and co-workers have used an electrode array for their epidermal sensor which was patterned on PET using photolithography and then coated in an insulation layer. The electrode areas for Ca^{2+} detection and pH detection were defined using photolithography. This research group also used polyaniline for detecting pH changes, while a calcium ionophore-based sensor was used to selectively detect Ca^{2+} in the same platform [155]. Real-time on body trials using this epidermal platform required the subjects to cycle for 10 min to generate enough sweat for analysis. It was observed that the measured potential on the Ca^{+} electrode decreased as Ca^{2+} concentrations decreased and potential increased on the pH electrode as pH decreased. Real-time on-body analysis shows that concentrations of Ca^{2+} decreased with increasing pH which

was consistent with inductively coupled plasma - mass spectrometry (ICP-MS) and pH probe measurements [155], [157]. These on-body results affirm the potential of epidermal sensors in personal healthcare and in this instance real-time continuous analysis can alert the wearer regarding excessive loss or rise of electrolytes.

Rogers and co-workers have also recently developed a sophisticated epidermal wearable devices for sweat sampling and analysis. Their wearable chemical device was fabricated using lithography techniques as well as utilise thin, soft silicone materials such as PDMS to form the microfluidic system that samples and analyses sweat [99], [108]. This epidermal sensor was capable of sensing multiple parameters in sweat such as total sweat loss, pH, lactate, chloride, and glucose [99], [108]. Their first iteration of the microfluidic platform had the colorimetric sensor embedded in the device. Designated reservoirs contained the colorimetric assays to detect pH, chloride glucose, and lactate. A universal pH indicator that includes dyes such as bromothymol blue to produce a colorimetric response for pH detection, while colorimetric detection of chloride involved competitive binding between Hg^{2+} and Fe^{2+} with 2,4,6-tris(2-pyridyl)-s-triazine (TPTZ) [99]. In the presence of chloride ions, iron ions (Fe^{2+}) bind with TPTZ, whereas Hg^{2+} participates as HgCl2, thereby inducing a change in colour. Glucose and lactate concentrations were analysed by enzymatic reaction and the colour change induced by these reactions was used to correlate the concentration of the analytes to the relevant concentration in sweat. However, this platform was limited to single use and it did not afford real-time tracking of changes in analyte concentration because the reservoirs containing the colorimetric assays were embedded in the platform [99]. This issue was since resolved by developing a disposable microfluidic system that can attach/re-attach to and from the platform using small magnets (Fig. 1.9b) [108]. The microfluidic layer containing the colorimetric reagents and enzymes can be detached from the layer containing the electronic components via small magnets. In this new iteration, the platform detects glucose and lactate based on the generated electrical signals proportional to their concentration in a manner similar to the operation of a biofuel cell where the catalysis or enzymatic activity is used for energy production [108]. This eliminates the need for a potentiostat. The lactate sensor for example, uses an anode that consists of carbon nanotube (CNT) paper to provide a conductive, high–surface area substrate to immobilize LOx enzyme for selectively catalysing lactate oxidation and the redox mediator, tetrathiafulvalene for shuttling electrons between enzyme active sites and the underlying CNT paper [108]. Chitosan and polyvinyl chloride membrane coating was used to minimize leaching of the enzyme and the mediator from the electrode. A similar

approach was used for the glucose sensor, however GOx enzyme was directly dispersed in Nafion to ensure rapid interaction of glucose with the enzyme due to high ionic conductivity. The voltage generated across these biofuel cell–based sensors was proportional to the concentration of the glucose or lactate present. The colorimetric aspect of the epidermal device utilises silver chloranilate, which complexes with chloride ions to generate a species with a distinct purple colour when intensity is proportional to the chloride concentration and pH-sensitive dyes was used for determining pH. The change in colour was compared to colour reference markers, lightness values for the chloride assay and the R value from a red, green, blue (RGB) colour model for the pH assay. The resulting epidermal platform combines the use of an electronic and microfluidic functionality in one platform that simultaneously monitors multiple parameters which is highly advantageous and has culminated in the commercial development of the wearable pH sensor, My Skin Track pH (Fig. 1.1b).

1.3.3 Biomarker analysis in ISF

ISF is a matrix that is a rich source of biomarkers because it fills extracellular space in tissues, which means that ISF biomarkers can provide systemic information due to their origins in blood [158]. There are limited techniques for ISF sampling, including reverse iontophoresis [110], [159], suction blisters [160], [161], and microneedle patches [111], [114], [158], [162], [163]. As previously discussed, the GlucoWatch® was an example of a wearable sensor for extracting ISF using reverse iontophoresis. However, this sensor was discontinued because long periods of reverse iontophoresis caused skin damage. Suction blistering is another approach to extracting ISF, a vacuum is applied to a skin area. The suction separates the dermis and epidermis, and fluid from the surrounding tissues fills the gap, creating a blister and the blister fluid is extracted with a needle. This approach is time consuming because a vacuum has to be achieved in order to form the blister. It is also uncomfortable because it forms a pocket of fluid that could burst and become infected.

Recently, innovations in microfabrication and materials have progressed the development of microneedles into diagnostic sensors that can access ISF. For example, Bollella *et al*. have demonstrated the fabrication of a microneedle array for simultaneous monitoring of lactate and glucose in ISF [111]. This microneedle array was comprised of polycarbonate and consisted of 64 microneedles arranged as 4 x 4 arrays. Three of the arrays have been metallized in gold by electro-deposition of Au-multiwalled carbon nanotubes, while one array was metallized in

silver [111]. The gold electrodes were further modified by electropolymerization of methylene blue which functions as a mediator for the LOx and FAD-Glucose dehydrogenase enzymes. The LOx and FAD-Glucose dehydrogenase enzyme were drop-cast on separate microneedle arrays. To electrochemically characterise the microneedles, the modified microneedle arrays were tested on chitosan/agarose hydrogel embedded with artificial ISF. Amperometry was used to detect the enzymatic reactions from the surface of the microneedles. The lactate working electrode was capable of detecting linear ranges between 10 – 100 µM, while the glucose working electrode detected a linear range between 0.05 – 5 mM [111]. Their work has demonstrated the potential of However, these tests were carried out on artificial ISF in hydrogel skin mimics therefore further tests are required to evaluate the biocompatibility of these microneedle arrays *in vivo*.

As previously mentioned, hollow microneedles are a sub-class of microneedles that contains a hollow bore in the centre of the needle whereby when inserted into the skin it produces a channel in the skin layers. This class of microneedle has been used for drug/therapeutic delivery [164], [165] and extraction of fluids [114], [117], [166]. Recently, hollow microneedles have been modified by integrating responsive materials or miniaturised sensing systems within the hollow bore of the microneedle. For example, Miller *et al*. developed a hollow microneedle sensor where each bore had been filled with a modified carbon paste material that was tailored to detect pH, glucose, or lactate [167]. Flat flexible cable assemblies were used to prepare the sensor devices and laser ablation was used to create openings in the polyester insulating layer to the tin-plated copper conductors. These openings were filled with the modified carbon pastes. One of the modified pastes was a glucose oxidase paste that consisted of GOx mixed with polyethyleneimine, rhodium on carbon and mineral oil, similar materials were also used to fabricate the lactate oxidase paste but LOx was used for selective detection of glucose [167]. The pH paste consisted of graphite, mineral oil and a Fast Blue RR salt. The hollow microneedles were comprised of an acrylate-based polymer and the hollow microneedle pattern was fabricated using a lithography approach. These hollow microneedles were aligned and adhered on top of these openings with double-sided tape. This was tested in a 3-electrode chemical cell against Ag/AgCl reference and Pt counter electrodes. Glucose and lactate were detected based on enzymatic reactions and this sensor was capable of detecting concentrations between 2 to 12 mM for both analytes. For detecting alterations in pH, a pH range of 5 to 8 and the response was measured by evaluating the shift of the anodic peak potential position of the quinone moiety on the immobilized Fast Blue RR salt [167]. Many implantable continuous

monitoring systems succumb to biofouling when adhered to skin, therefore a coating material was investigated. Lipidure®, a copolymer of butyl methacrylate and 2-methacryloyloxyethyl phosphorylcholine, was chosen as the coating material. Uncoated and Lipidure® microneedles were tested and it was observed that there was uniform macrophage coverage on the uncoated materials; on the other hand, the coated materials displayed little to no biofouling [167]. This group demonstrated the fabrication of a hollow microneedle-based sensor that was capable of detecting multiple analytes in physiologically relevant tissue environments as well as reduce biofouling by using a biocompatible polymer coating. This microneedle array can potentially be used as an epidermal sensor for multiple analyte detection in ISF but further studies would be required to determine its sensing capabilities *in-vivo.*

Ribet *et al.* developed another interesting example of a hollow microneedle integrated with an electrochemical sensor for glucose monitoring [162]. This hollow microneedle patch consists of a miniaturized electrochemical sensing probe and a single silicon-based needle (700 µm, length). The developed sensor is a 3-electrode electrochemical enzymatic- based glucose sensor, where platinum electrode deposition was employed to fabricate the 3 electrodes, while GOx and BSA was used to functionalise the working electrode. To crosslink the enzymatic membrane, glutaraldehyde was used. This modified electrode was slotted into the hollow needle and by facing the sensing electrodes on the tip of the hollow needle towards the dermal space of skin, real-time measurements can potentially be performed. As a proof of concept, amperometric *in-vivo* performance of the electrode was tested on a human forearm. It was observed that this microneedle sensor had a similar trend with the blood glucose data collected via finger prick method, with only approximately 10 min of lag time between their microneedle sensor and commercial glucometer [162]. These research groups have shown the potential of microneedle platforms for the extraction and analysis of ISF using innovative designs and materials. However, their studies did not fully address the issue of safety and the possibility of pain or discomfort caused by insertions into skin.

A less invasive approach of extracting ISF was through the use of reverse iontophoresis to extract ISF by passing a current over the surface of the skin. Wang's research group have presented an enzyme-based epidermal tattoo platform that combines reverse iontophoretic extraction of glucose from ISF and amperometry to detect changes in current due to glucose levels [127]. Similar to their epidermal alcohol sweat sensor, this epidermal glucose sensor also uses an enzyme, GOx and Prussian-Blue mediator. It was important to ensure proper contact between the skin and the platform during reverse iontophoresis for efficient glucose extraction

and to avoid skin irritation. Therefore additional Ag/AgCl reverse iontophoresis electrodes and hydrogel coatings were incorporated for efficient extraction and delivery of ISF to the electrodes [127]. This epidermal sensor was able to linearly respond to glucose between 10 - 100 μM, which is broadly within range of blood glucose levels (3-8 mM healthy people and 2-40 mM in diabetics [168]). As proof of concept, the epidermal glucose sensor was used for on-body trials where glucose levels were monitored before and after food consumption and was found to be capable of detecting spikes in glucose levels due to food consumption. However, a delayed sensor response was observed due to the low current density (0.2 mA/cm^2) used to extract the ISF which slowed down extraction causing a lag in the observed glucose response [127]. Glucose levels in the ISF closely follow blood glucose, albeit with a slight time delay which has been estimated to be between 5-10 minutes [169]. Wang's research group had to compensate for this sensor lag by asking the participants during on-body trials to fast, followed by food consumption to detect the spike in glucose levels.

Wang's research group has further modified an epidermal platform for simultaneous detection of analytes in sweat and ISF using a single epidermal platform. This epidermal platform demonstrates induction of sweat via transdermal pilocarpine delivery, alongside extraction of the ISF [125]. The dual iontophoretic system combining two iontophoretic operations was demonstrated, for the first time, with iontophoretic ISF extraction at the cathode compartment and iontophoretic delivery of the sweat-inducing pilocarpine agent at the anode compartment (Fig. 1.10). This iontophoretic-based sensor was based on two mechanisms, electrorepulsion and electro-osmosis. The epidermal sensor delivers the positively charged pilocarpine drug at the anode by electrorepulsion (iontophoretic delivery), allowing the delivered drug to generate sweat, which was localized at the pilocarpine loaded gel in the anode compartment [125]. Simultaneously, cationic electro-osmotic flux toward the cathode was due to the overall negative charge of human skin, leading to the migration of positive ions and of neutral molecules, such as glucose [125].

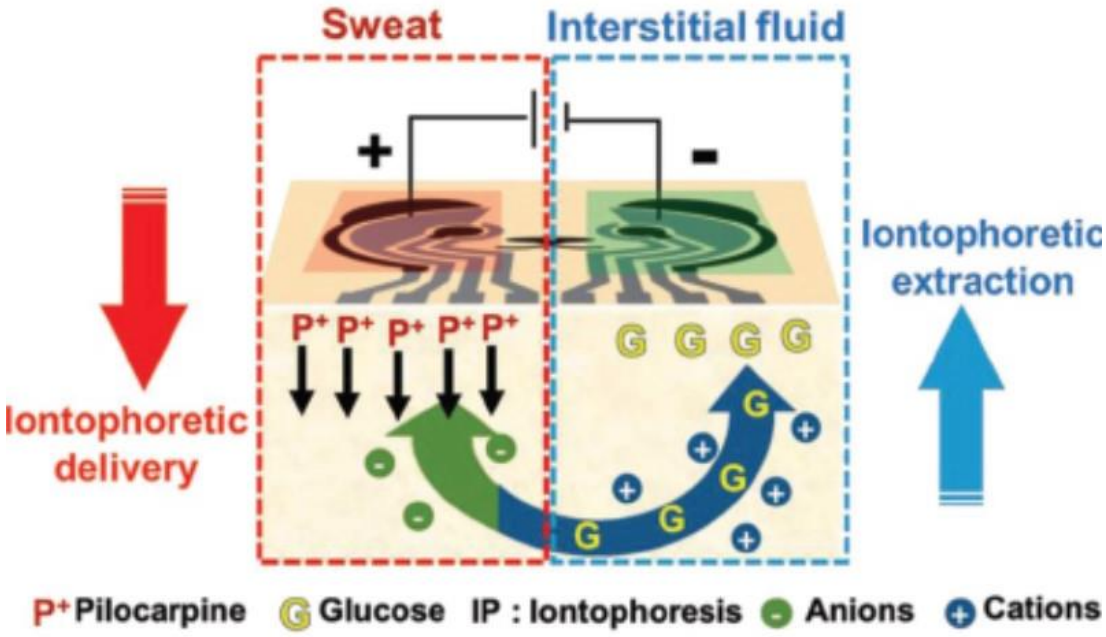

Figure 1.10 Schematic representation of the iontophoretic set-up of the epidermal platform for simultaneous monitoring of alcohol in sweat and glucose in ISF from skin, reproduced from [125].

This dual measurement epidermal sensor incorporated an amperometric biosensor at the anode to measure alcohol in generated sweat, while the another biosensor at the cathode detected the extracted ISF glucose [125]. Both electrodes were composed of a screen-printed electrochemical cell using Prussian blue mediator, the corresponding enzyme bioreceptors (GOx for glucose and AOx for alcohol), and chitosan for enzyme immobilization. On-body tests involved the consumption of food and alcoholic beverages to induce spikes in blood glucose and alcohol levels. The subjects showed an increased response in blood glucose and alcohol levels. Although, this prototype was demonstrated on healthy subjects, future efforts using this glucose-alcohol sensor will focus on larger population studies for monitoring glucose and related alcohol effects in diabetes and pre-diabetes subjects. This new hybrid platform shows the potential of a dual fluid sampling and analysis platform.

Abbott have recently launched a wearable glucose monitoring system called the Freestyle® Libre™ [170]. This device (35 mm x 5 mm) houses a thin microneedle which can be inserted into skin to access the ISF and can wirelessly monitor glucose levels over 14 days [170], [171]. This wearable glucose monitoring system uses enzyme-based electrochemical detection using a screen printed platform. This wearable system is worn on the upper arm and a hand-held

reader is used to scan the sensor to receive a glucose result along with historic results with a 15-min frequency for up to 8 h [170]. The device has been evaluated against blood glucose measurements and has shown that the Freestyle® Libre™ has an overall accuracy similar to continuous blood glucose monitoring [170], [172], with a mean lag time of 4.5 - 4.8 min between the Freestyle® Libre™ and reference blood glucose meter [170].This was a considerably shorter lag time compared to the previously discussed epidermal platforms that extracted and compared ISF to a glucometer. The accuracy of the results was demonstrated against capillary blood glucose reference values and the overall mean absolute relative difference was 11.4% [170]. This device used a single needle inserted into the skin which can cause irritation overtime and an adhesive layer to adhere the device on to the skin surface to keep it in place. This commercial wearable sensor is an example of a realised epidermal platform for continuous glucose monitoring which reduces the need to sample blood using the "finger-prick" approach.

1.3.4 Sampling and analysis of skin volatile emissions

As discussed previously, a promising approach for monitoring the physiological state can be through the detection and analysis of volatile organic compounds (VOCs). However, due to their low rates of emission, careful consideration is required to develop VOCs sampling approaches. Jiang *et al*. devloped a non-invasive wearable VOC sampler that uses a PDMS membrane sandwiched between stainless steel mesh [173]. The PDMS membrane used the mesh as a spacer which was placed on skin covered by aluminium foil and was kept in place by tape (Fig. 1.11a). The membrane varied in sizes: 6, 11, and 17 mm diameter and these were left on skin for 60 min to absorb VOCs before being placed into the desorption unit of the GC-MS. Analytes were desorbed from the membrane and a custom library was used to analyse the spectra and identify the emitted compounds. The group observed that for most compounds, the extraction amount was linearly proportional to the size of the membrane and the larger membrane size provided better sensitivity [173]. This wearable PDMS membrane was used to monitor ethanol, before and after drinking one shot of whiskey. The maximum peak for ethanol release was around 50 min after drinking whiskey and was shown to have good agreement with blood alcohol concentration [173]. However, this sampling method has difficulty detecting semi- and low-volatility compounds such as 1-tetradecanol and 1-octadecanol indicating that the sampling time was not sufficient to reach extraction equilibrium for these low volatile compounds [173]. Duffy *et al*. have also devised a sampling method that uses a solid phase

micro extraction (SPME) fibre to directly adsorb volatiles from the skin without contacting the skin [47]. A wearable format for enclosed headspace sampling of skin was used, where the SPME fibre was comprised of 50/30 μm divinylbenzene/ carboxen/polydimethylsiloxane Stableflex (2 cm length) and was placed in a glass funnel (Fig. 1.11b) [47]. The individual wears the glass funnel with the SPME fibre for 15 min to allow volatiles from skin to absorb into the fibre and reach equilibrium with the headspace. GC-MS was used to separate and identify the volatile metabolites after desorbtion from the fibre. A total of 37 compounds were identified such as hexanal, nonanoic acid, squalane and squalene [47]. Our group also investigated alterations in skin VOC emissions before and after SC barrier disruption which was simulated via a tape-stripping method. Principle component analysis (PCA) was performed on the total ion chromatogram data collected, to categorise the skin volatile profiles before and after barrier disruption. From our analysis, downregulation of squalane was observed which may be attributed to the removal of sebaceous components and oxidation products from the skin surface after tape stripping. The upregulation of glycine was also observed, which may indicate a perturbation to the skin's natural moisturising factor production [47]. This wearable VOC sampler uses a rigid glass housing for head space sampling, which contradicts the epidermal platform approaches discussed earlier whereby soft, stretchable materials have been central to their development. Despite this limitation in housing, this wearable sampler approach provides valuable information towards understanding the variation in the skin volatile profiles of individuals with a compromised skin barrier.

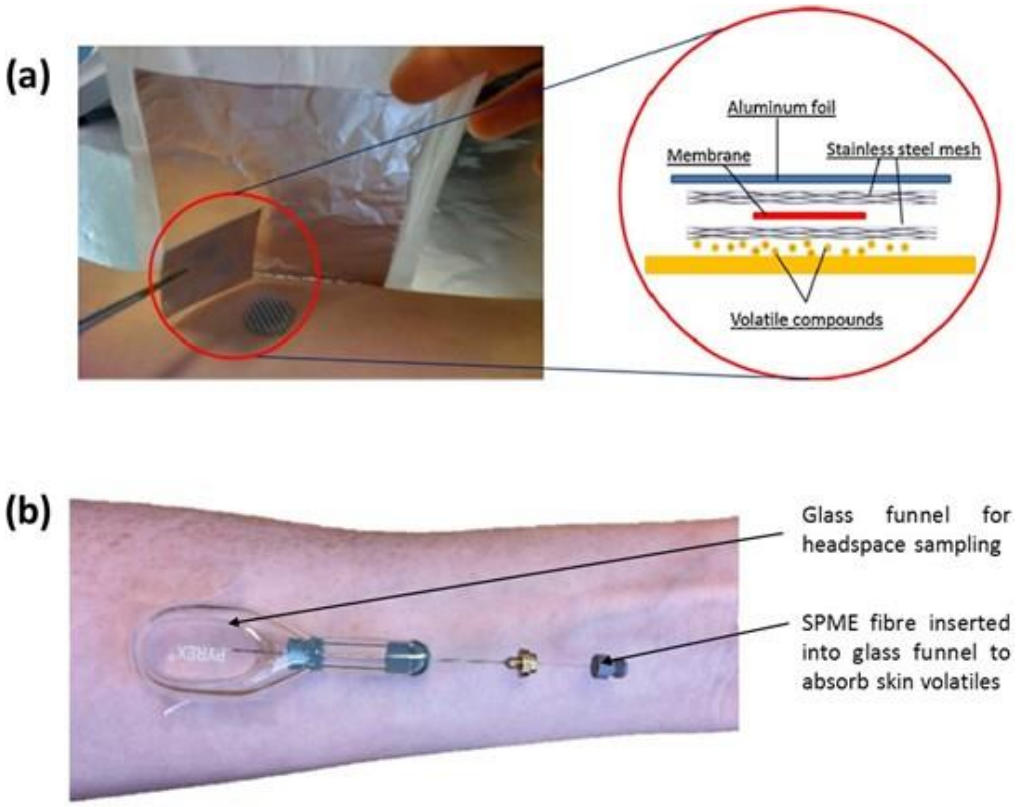

Figure 1.11 Images of the (a) PDMS membrane sandwich for skin VOC sampling, reproduced from [173] *and (b) wearable head space sampler integrating SPME fibre for skin VOC sampling, reproduced from* [47].

Recently researchers have devised other approaches to sample VOCs, reducing the use of rigid materials used for wearable sampling and are currently developing new soft conformable materials for wearable sensing. Jin *et al.* have reported as proof of concept, a sophisticated self-healing wearable material for VOCs detection [174]. This wearable sensor is based on three parts: a self-healable polymer substrate made from self-healing disulfide-crosslinked PU, a self-healing silver polymer composite made of silver and PU diol and functionalised gold nanoparticle (GNP) solutions [174]. GNPs were functionalized with 3-ethoxythio-phenol, benzylmercaptan, tert-dodec- anethiol, hexanethiol or decanethiol were dispersed in toluene and sodium borohydride was used as a reducing agent to produce the thiol capped GNPs [174]. The molecularly functionalised GNP were drop-casted on to the silver polymer. This wearable sensor uses chemiresistive transduction where the signal response from the sensing material functionalised with GNP interacts with the target volatile emission and its electrical resistance changes in response to the volatile emission. This group used 11 standard VOCs found in

healthy human skin, to characterise this sensor array [174]. The array measured electrical changes in resistance before and after exposure to the standard VOCs. The group monitored VOCs between 0.5 – 20 ppm to investigate the differences in response signals which were analysed using PCA. The spatial distance between each VOC represents the discrimination capability of the sensor array (i.e. large space suggests desirable discrimination) [174]. The self-healing capability of this sensor array was a desirable feature for wearable sensors due to its ability to heal in damaged areas which would prove useful during strenuous movements. The self-healing mechanism was based on reformation of hydrogen and disulfide bonds between the polymer chains. This mechanical reinforcement allows this wearable sensor to be more durable against damage. However, it was shown that overtime mechanical damage affects the functionality of the sensor array making the sensor less sensitive to VOCs [174]. This self-healing sensor requires healing time, the rearrangement of the GNP films govern the healing efficiency and to achieve a fully healed sensing platform with low signal-to-noise ratio, 24 h was required [174]. It should be noted that this sensor was a proof of concept and has not been in used in a participant studies, therefore the materials biocompatibillty to skin and the effect of skin humidity should be carefully considered. Despite this, the reported self-healable VOCs sensor would be expected to play a significant role in smart wearable technology once issues with sensor sensitivity are further optimised.

Another interesting approach for detecting and differentiating volatiles was through the use of chemo-responsive dyes. Rakow *et al.* reported the development of an optical-chemical sensing method that utilises colour change induced by an array of metalloporphyrin dyes[175], [176]. Metalloporphyrin dyes were chosen for detecting volatile compounds because of their open coordination sites for axial ligation, their large spectral shifts upon binding and their intense colour [175]. The array of dyes were stamped onto a flexible thin PET film and dried under nitrogen before exposure to the volatile compounds. This colorimetric array was imaged before and after exposure to different commercial coffees A difference map (i.e. red minus red, green minus green, blue minus blue) was generated for each analysis, and the resulting colour difference profiles can be used to obtain a fingerprint specific to the volatile compound for each coffee aroma [176]. This colorimetric approach was recently adapted by our research group to investigate VOCs from skin. The wearable sensor array is a prototype that uses chemically responsive dyes such as pH sensitive, solvatochromic and porphyrins which are immobilised in a porous sol-gel matrix and drop-casted onto flexible thin layer chromatography (TLC) plates. The dyes use a range of intermolecular interactions such as Lewis/Brønsted acid-

base, hydrogen bonding and metal-ion coordination for detecting different volatiles. This wearable sensor array can potentially be used for detecting specific volatile compounds such as ammonia which is a known biomarker found in breath for individuals that suffer from kidney disease or failure [177], [178]. This demonstrates a simple colorimetric approach has the potential for non-invasively detecting and analysing volatile compounds that may be helpful for skin diagnosis and health management in the future.

This discussion has demonstrated innovative ways to sample and sense skin VOCs. The importance of an effective representative sampling approach in collecting VOCs is important for the understanding of this matrix. Their work has shown that monitoring skin VOC profiles have the potential to differentiate between healthy and diseased states, however a library of the volatile compounds emitted from the skin need to be constantly updated for comprehensive skin volatile analysis.

1.4 Conclusion

The expanding field of epidermal sensors haves opened up new prospects for real-time health monitoring and personalised healthcare. On-going research in the development of these epidermal sensors shows constant improvements in electronics and strategies for electrical and biochemical sensing as well as innovative smart responsive materials. The use of expensive commercial probes and invasive sampling methods such as the "finger-prick" method will be reduced in future due to the rise in epidermal sensors. The use of these epidermal sensors employ less intrusive sensing and analysis methods by sampling from more accessible matrices compared to sampling blood. Skin ISF and sweat are the most commonly used skin matrices for sensing and analysis using these epidermal wearables due to their rich chemistry and accessibility. These matrices have shown the most promising results for tracking a wide array of analytes that correlated well with the validation approaches used, such as measuring glucose in ISF and comparing it against a standard glucometer. Thorough understanding of these skin matrices and innovations in materials and sensor fabrications have led to the development of the Abbott Freestyle® Libre™ and My Skin Track pH, epidermal sensors that have been recently launched into market. These epidermal sensors have shown that real-time monitoring can be achieved and a more comprehensive understanding of an individuals' health can be provided to them and their clinicians.

Particular challenges still need to be addressed by researchers, ideally these epidermal sensors should be capable of withstanding rigorous bodily movements without affecting significantly affecting sensor performance as well as reliably monitor target analytes or electrical signals. . It would be ideal for the epidermal sensor to be worn for long periods of time to enable continuous long-term monitoring of an individual. However this would require thin, low-modulus materials that are stretchable and flexible in order to mechanically match the properties skin. Epidermal sensors that rely on chemical or biological sensing must be able to detect target chemicals rapidly as well as be able to discriminate between the target analyte and co-existing interfering components. This requires a good extraction or collection method of the biofluids that contain the target analyte because it is possible for these fluids to be dilute or secreted in miniscule volumes, while a selective membrane can ensure that only target analytes are detected. Electrode stability overtime should also be considered because the electrode response should remain constant overtime. However, continuous exposure to biofluids may lead to biofouling or irreversible non-specific adsorption on the transducer surface which can interfere with the measurements. Despite these challenges, epidermal sensors have shown their

potential for personal health monitoring. Continued optimisation in fabrication methods, materials and sensing modes will further progress epidermal sensors so they can be applied to a broader range of biomedical and fitness applications and provide a low-cost solution to personalised healthcare.

In this thesis, the development of an epidermal sensor using a tattoo platform will be shown. The main challenges addressed in this body of work is fabricating a robust wearable tattoo platform that is also capable of reliably measuring the electrical properties of skin related to changes in water content. It also investigates the impact of adherence methods using conducting and non-conducting adhesives to enhance adherence of the tattoo platform on skin. A reliable adherence method is required for epidermal sensors to allow the electrodes to be continuously adhered to skin in order to reliably measure its electrical properties but also allow the platform to withstand mechanical deformation over time.

1.5 Thesis outline

The purpose of this work is to develop a new epidermal platform approach for monitoring physiological activity related to skin barrier function as well as biomarker analysis in skin. The thesis proposes a planar concentric electrode design based on soft and flexible materials that can be adhered directly to skin as a wearable tattoo-type platform. The transduction method of choice for this research is non-faradaic impedance spectroscopy.

Chapter 2 reports on the first prototype of the screen-printed silver-based electrodes. This screen-printed platform is utilised to track changes in water content in a hydrogel skin mimic, porcine skin and human skin using impedance spectroscopy. Equivalent circuit models for each system are proposed. The initial results of this prototype demonstrates its potential as an epidermal sensor for the non-invasive assessment of the skin barrier. Though this prototype comprised of flexible materials, it did not fully conform to skin and is more suited for single use measurements.

Chapter 3 focuses on improving the durability and adherence of the epidermal sensor to skin. This research investigates two approaches for enhancing adherence by way of electrode ink formulation as well as the use of conducting adhesive (CA) films. It is shown that the presence of an elastomer in the ink formulation has a positive impact on the mechanical properties of the epidermal sensor. The CA film is incorporated into the platform as a means of improving its adherence to skin. Although the CA improves the mechanical robustness of the epidermal platform, it is shown that the CA had deleterious effects on its electrical properties due to the CAs high resistance.

Chapter 4 attempts to overcome the issues in Chapter 3 by proposing an alternative adherence strategy to skin. This research investigates the use of a thinner non-conducting adhesive layer whereby pores are machined into the adhesive film to allow for electrical contact as well as incorporate good mechanical properties into the epidermal sensor. The viable tissue resistance values measured by this platform are shown to correlate with tissue dielectric constant measurements from a commercial probe in a participant study. Chapters 2-4 demonstrates that selection of ink formulation and adherence methodologies are important considerations in the fabrication and performance of epidermal sensors.

Chapter 5 seeks to adapt the tattoo platform to facilitate biomarker analysis through the use of responsive materials. This research investigates the use of phenyl boronic acid (PBA) functionalized hydrogels for chemical sensing ultimately for application in epidermal sensing.

PBA functionalized hydrogels are a promising smart material for the detection of monosaccharides such as glucose and α-hydroxyls such as lactate. The PBA hydrogels in this study use a quaternised nitrogen atom along the monomer chain attached to the phenyl group. The electrical responses of these PBA hydrogel systems are investigated under different pH conditions and its applicability for detecting different analytes such as glucose, lactate and ascorbic acid are also examined to understand its potential as an epidermal chemical sensing interface.

Chapter 6 discusses conclusions and recommendations for future work arising from this thesis.

1.6 References

[1] J. Heikenfeld, A. Jajack, J. Rogers, P. Gutruf, L. Tian, T. Pan, R. Li, M. Khine, J. Kim, J. Wang, and J. Kim, "Wearable sensors: Modalities, challenges, and prospects," *Lab Chip*, vol. 18, no. 2, pp. 217–248, 2018.

[2] J. Takacs, C. L. Pollock, J. R. Guenther, M. Bahar, C. Napier, and M. A. Hunt, "Validation of the Fitbit One activity monitor device during treadmill walking," *J. Sci. Med. Sport*, vol. 17, no. 5, pp. 496–500, 2014.

[3] J. E. Sasaki, A. Hickey, M. Mavilia, J. Tedesco, D. John, S. K. Keadle, and P. S. Freedson, "Validation of the Fitbit Wireless Activity Tracker for Prediction of Energy Expenditure," *J. Phys. Act. Heal.*, vol. 12, no. 2, pp. 149–154, 2014.

[4] G. Farnell and J. Barkley, "The effect of a wearable physical activity monitor (Fitbit One) on physical activity behaviour in women: A pilot study," *J. Hum. Sport Exerc.*, vol. 12, no. 4, pp. 1230–1237, 2017.

[5] K. M. Diaz, D. J. Krupka, M. J. Chang, J. Peacock, Y. Ma, J. Goldsmith, J. E. Schwartz, and K. W. Davidson, "Fitbit ®: An Accurate and Reliable Device for Wireless Physical Activity Tracking," *Int. J. Cardiol.*, vol. 185, pp. 138–140, 2015.

[6] R. Sashikumar and R. Kannan, "Salivary glucose levels and oral candidal carriage in type II diabetics," *Oral Surgery, Oral Med. Oral Pathol. Oral Radiol. Endodontology*, vol. 109, no. 5, pp. 706–711, 2010.

[7] R. S. P. Malon, S. Sadir, M. Balakrishnan, E. P. Córcoles, and E. P. Rcoles, "Saliva-Based Biosensors: Noninvasive Monitoring Tool for Clinical Diagnostics," *Biomed Res. Int.*, vol. 2014, pp. 1–20, 2014.

[8] H. Yao, C. Marcheselli, A. Afanasiev, I. Lähdesmäki, and B. A. Parviz, "A soft hydrogel contact lens with an encapsulated sensor for tear glucose monitoring," *Proc. IEEE Int. Conf. Micro Electro Mech. Syst.*, pp. 769–772, 2012.

[9] M. X. Chu, K. Miyajima, D. Takahashi, T. Arakawa, K. Sano, S. I. Sawada, H. Kudo, Y. Iwasaki, K. Akiyoshi, M. Mochizuki, and K. Mitsubayashi, "Soft contact lens biosensor for in situ monitoring of tear glucose as non-invasive blood sugar assessment," *Talanta*, vol. 83, no. 3, pp. 960–965, 2011.

[10] T. Glennon, C. O'Quigley, M. McCaul, G. Matzeu, S. Beirne, G. G. Wallace, F.

Stroiescu, N. O'Mahoney, P. White, and D. Diamond, "SWEATCH : A Wearable Platform for Harvesting and Analysing Sweat Sodium Content," *Electroanalysis*, vol. 28, no. 6, pp. 1283–1289, 2016.

[11] A. J. Bandodkar and J. Wang, "Non-invasive wearable electrochemical sensors: A review," *Trends in Biotechnology*, vol. 32. pp. 363–371, 2014.

[12] A. J. Bandodkar, W. Jia, and J. Wang, "Tattoo-Based Wearable Electrochemical Devices: A Review," *Electroanalysis*, vol. 27, no. 3, pp. 562–572, 2015.

[13] H. Jin, Y. S. Abu-Raya, and H. Haick, "Advanced Materials for Health Monitoring with Skin-Based Wearable Devices," *Adv. Healthc. Mater.*, 2017.

[14] X. Huang, W.-H. Yeo, Y. Liu, and J. A. Rogers, "Epidermal differential impedance sensor for conformal skin hydration monitoring.," *Biointerphases*, vol. 7, no. 1–4, p. 52, Dec. 2012.

[15] S. Yao, A. Myers, A. Malhotra, F. Lin, A. Bozkurt, J. F. Muth, and Y. Zhu, "A Wearable Hydration Sensor with Conformal Nanowire Electrodes," *Adv. Healthc. Mater.*, vol. 6, no. 6, pp. 1–8, 2017.

[16] J. Malvehy, A. Hauschild, C. Curiel-Lewandrowski, P. Mohr, R. Hofmann-Wellenhof, R. Motley, C. Berking, D. Grossman, J. Paoli, C. Loquai, J. Olah, U. Reinhold, H. Wenger, T. Dirschka, S. Davis, C. Henderson, H. Rabinovitz, J. Welzel, D. Schadendoff, and U. Birgersson, "Clinical performance of the Nevisense system in cutaneous melanoma detection: an international, multicentre, prospective and blinded clinical trial on efficacy and safety," *Br. J. Dermatol.*, vol. 171, no. 5, pp. 1099–1107, 2014.

[17] Y. Chen, B. Lu, Y. Chen, and X. Feng, "Breathable and Stretchable Temperature Sensors Inspired by Skin," *Sci. Rep.*, vol. 5, no. 1, p. 11505, 2015.

[18] L. Bareket, L. Inzelberg, D. Rand, M. David-Pur, D. Rabinovich, B. Brandes, and Y. Hanein, "Temporary-tattoo for long-term high fidelity biopotential recordings," *Sci. Rep.*, vol. 6, p. 25727, 2016.

[19] A. Ní Annaidh, K. Bruyère, M. Destrade, M. D. Gilchrist, and M. Otténio, "Characterization of the anisotropic mechanical properties of excised human skin," *J. Mech. Behav. Biomed. Mater.*, vol. 5, no. 1, pp. 139–148, 2012.

[20] F. H. Silver, J. W. Freeman, and D. DeVore, “Viscoelastic properties of human skin and processed dermis.,” *Skin Research and Technology*, vol. 7, no. 1. pp. 18–23, 2001.

[21] X. Liang and S. A. Boppart, “Biomechanical Properties of In Vivo Human Skin From Dynamic Optical Coherence Elastography,” *IEEE Trans Biomed Eng.*, vol. 57, no. 4, pp. 953–959, 2010.

[22] E. Duffy and A. Morrin, “Endogenous and microbial volatile organic compounds in cutaneous health and disease,” *TrAC - Trends Anal. Chem.*, vol. 111, pp. 163–172, 2019.

[23] W. Jia, A. J. Bandodkar, G. Valdés-Ramírez, J. R. Windmiller, Z. Yang, J. Ramírez, G. Chan, and J. Wang, “Electrochemical tattoo biosensors for real-time noninvasive lactate monitoring in human perspiration,” *Anal. Chem.*, vol. 85, no. 14, pp. 6553–6560, 2013.

[24] Y. Shi, M. Manco, D. Moyal, G. Huppert, H. Araki, A. Banks, H. Joshi, R. McKenzie, A. Seewald, G. Griffin, E. Sen-Gupta, D. Wright, P. Bastien, F. Valceschini, S. Seité, J. A. Wright, R. Ghaffari, J. Rogers, G. Balooch, and R. M. Pielak, “Soft, stretchable, epidermal sensor with integrated electronics and photochemistry for measuring personal UV exposures,” *PLoS One*, vol. 13, no. 1, pp. 1–15, 2018.

[25] “L’Oréal Unveils Prototype Of First-Ever Wearable Microfluidic Sensor To Measure Skin pH Levels,” *Website*, 2019. [Online]. Available: https://www.prnewswire.com/news-releases/loreal-unveils-prototype-of-first-ever-wearable-microfluidic-sensor-to-measure-skin-ph-levels-300773342.html. [Accessed: 04-Feb-2019].

[26] J. E. Lai-Cheong and J. A. McGrath, “Structure and function of skin, hair and nails,” *Med. (United Kingdom)*, vol. 37, no. 5, pp. 223–226, 2009.

[27] G. K. Menon, G. W. Cleary, and M. E. Lane, “The structure and function of the stratum corneum,” *Int. J. Pharm.*, vol. 435, pp. 3–9, 2012.

[28] A. Baroni, E. Buommino, V. De Gregorio, E. Ruocco, V. Ruocco, and R. Wolf, “Structure and function of the epidermis related to barrier properties,” *Clin. Dermatol.*, vol. 30, no. 3, pp. 257–262, 2012.

[29] A. K. Dąbrowska, F. Spano, S. Derler, C. Adlhart, N. D. Spencer, and R. M. Rossi,

"The relationship between skin function, barrier properties, and body-dependent factors," *Ski. Res. Technol.*, vol. 24, no. 2, pp. 165–174, 2018.

[30] S. Paliwal, B. Hee, K. Y. Tsai, and S. Mitragotri, "Diagnostic opportunities based on skin biomarkers," vol. 50, pp. 546–556, 2013.

[31] J. A. McGrath, R. A. J. Eady, and F. M. Pope, "Anatomy and Organization of Human Skin," in *The Rook's Textbook of Dermatology*, 2004, pp. 45–128.

[32] K. A. Holbrook and G. F. Odland, "Regional differences in the thickness (cell layers) of the human stratum corneum: an ultrastructural analysis.," *J. Invest. Dermatol.*, vol. 62, no. 4, pp. 415–422, 1974.

[33] R. R. Wickett and M. O. Visscher, "Structure and function of the epidermal barrier," *Am. J. Infect. Control*, vol. 34, no. 10, pp. S98–S110, 2006.

[34] S. Cazzaniga, P. Elsner, M. Bruze, M.-L. A. Schuttelaar, T. . Diepgen, L. Naldi, R. F. Ofenloch, M. Goncalo, and A. Svensson, "Prevalence of skin disease in a population-based sample of adults from five European countries," *Br. J. Dermatol.*, vol. 178, pp. 1111–1118, 2017.

[35] S. Barbarot, S. Auziere, A. Gadkari, G. Girolomoni, L. Puig, E. L. Simpson, D. J. Margolis, M. de Bruin-Weller, and L. Eckert, "Epidemiology of atopic dermatitis in adults: Results from an international survey," *Allergy*, vol. 73, no. 6, pp. 1284–1293, 2018.

[36] A. B. Simonsen, J. D. Johansen, M. Deleuran, C. G. Mortz, L. Skov, and M. Sommerlund, "Children with atopic dermatitis may have unacknowledged contact allergies contributing to their skin symptoms," *J. Eur. Acad. Dermatology Venereol.*, vol. 32, no. 3, pp. 428–436, 2018.

[37] E. Guttman-Yassky, K. E. Nograles, and J. G. Krueger, "Contrasting pathogenesis of atopic dermatitis and psoriasis - Part I: Clinical and pathologic concepts," *J. Allergy Clin. Immunol.*, vol. 127, no. 5, pp. 1110–1118, 2011.

[38] N. Morar, S. A. G. Willis-Owen, M. F. Moffatt, and W. O. C. M. Cookson, "The genetics of atopic dermatitis," *J. Allergy Clin. Immunol.*, vol. 118, no. 1, pp. 24–34, 2006.

[39] M. J. Cork, S. G. Danby, Y. Vasilopoulos, J. Hadgraft, M. E. Lane, M. Moustafa, R.

H. Guy, A. L. MacGowan, R. Tazi-Ahnini, and S. J. Ward, “Epidermal barrier dysfunction in atopic dermatitis,” *J. Invest. Dermatol.*, vol. 129, no. 8, pp. 1892–1908, 2009.

[40] C. N. A. Palmer, A. D. Irvine, A. Terron-Kwiatkowski, Y. Zhao, H. Liao, S. P. Lee, D. R. Goudie, A. Sandilands, L. E. Campbell, F. J. D. Smith, G. M. O’Regan, R. M. Watson, J. E. Cecil, S. J. Bale, J. G. Compton, J. J. DiGiovanna, P. Fleckman, S. Lewis-Jones, G. Arseculeratne, A. Sergeant, C. S. Munro, B. El Houate, K. McElreavey, L. B. Halkjaer, H. Bisgaard, S. Mukhopadhyay, and W. H. I. McLean, “Common loss-of-function variants of the epidermal barrier protein filaggrin are a major predisposing factor for atopic dermatitis.,” *Nat. Genet.*, vol. 38, no. 4, pp. 441–446, 2006.

[41] M. Lodén, “Effect of moisturizers on epidermal barrier function,” *Clin. Dermatol.*, vol. 30, no. 3, pp. 286–296, 2012.

[42] S. Weidinger and N. Novak, “Atopic dermatitis,” *Lancet*, vol. 387, pp. 1109–1122, 2016.

[43] C. Lee Eberting, “Repairing a Compromised Skin Barrier in Dermatitis: Leveraging the Skin’s Ability to Heal Itself,” *J. Allergy Ther.*, vol. 5, no. 5, p. 1000187, 2014.

[44] H. Pickett, “Shave and Punch Biopsy for Skin Lesions,” *Am. Fam. Physician*, vol. 84, no. 9, pp. 995–1002, 2011.

[45] P. Clarke, “Nonmelanoma Skin Cancers - treatment options,” *Aust. Fam. Physician*, vol. 41, no. 7, pp. 476–480, 2012.

[46] X. Jing, C. W. Michael, and C. G. A. Theoharis, “The use of Immunocytochemical Study in the Cytologic Diagnosis of Melanoma: Evaluation of three Antibodies,” *Diagn. Cytopathol.*, vol. 41, no. 2, pp. 126–130, 2011.

[47] E. Duffy, M. R. Jacobs, B. Kirby, and A. Morrin, “Probing skin physiology through the volatile footprint: Discriminating volatile emissions before and after acute barrier disruption,” *Exp. Dermatol.*, vol. 26, no. 10, pp. 919–925, 2017.

[48] S. J. Bashir, A. L. Chew, A. Anigbogu, F. Dreher, and H. I. Maibach, “Physical and physiological effects of stratum corneum tape stripping,” *Skin Res. Technol.*, vol. 7, no. 1, pp. 40–48, 2001.

[49] M.-L. Clausen, H.-C. Slotved, K. A. Krogfelt, and T. Agner, “Tape Stripping Technique for Stratum Corneum Protein Analysis,” *Sci. Rep.*, vol. 6, p. 19918, 2016.

[50] S. Grimnes and Ø. G. Martinsen, *Bioimpedance and Bioelectricity Basics*. Elsevier, 2008.

[51] H. P. Schwan, “Electrical properties of tissues and cell suspensions: mechanisms and models,” *Adv. Med. Phys.*, pp. 70–71, 1994.

[52] D. A. Dean, T. Ramanathan, D. Machado, and R. Sundararajan, “Electrical impedance spectroscopy study of biological tissues,” *J. Electrostat.*, vol. 66, pp. 165–177, 2008.

[53] S. Grimnes and Ø. G. Martinsen, “Alpha-dispersion in human tissue,” *J. Phys. Conf. Ser.*, vol. 224, p. 12073, 2010.

[54] U. Birgersson, “Electrical Impedance of Human Skin and Tissue Alterations: Mathematical Modeling and Measurements,” Karolinska Institutet, Stockholm, Sweden, 2012.

[55] X. Huang, H. Cheng, K. Chen, Y. Zhang, Y. Zhang, Y. Liu, C. Zhu, S.-C. Ouyang, G.-W. Kong, C. Yu, Y. Huang, and J. a Rogers, “Epidermal impedance sensing sheets for precision hydration assessment and spatial mapping.,” *IEEE Trans. Biomed. Eng.*, vol. 60, no. 10, pp. 2848–57, Oct. 2013.

[56] K. De Guzman and A. Morrin, “Screen-printed Tattoo Sensor towards the Non-invasive Assessment of the Skin Barrier,” *Electroanalysis*, vol. 29, no. 1, pp. 188–196, 2017.

[57] E. A. White, M. E. Orazem, and A. L. Bunge, “Characterization of damaged skin by impedance spectroscopy: Chemical damage by dimethyl sulfoxide,” *Pharm. Res.*, vol. 30, pp. 2607–2624, 2013.

[58] E. A. White, M. E. Orazem, and A. L. Bunge, “Characterization of damaged skin by impedance spectroscopy: Mechanical damage,” *Pharm. Res.*, vol. 30, no. 8, pp. 2036–2049, 2013.

[59] P. Mohr, U. Birgersson, C. Berking, C. Henderson, U. Trefzer, L. Kemeny, C. Sunderkötter, T. Dirschka, R. Motley, M. Frohm-Nilsson, U. Reinhold, C. Loquai, R. Braun, F. Nyberg, and J. Paoli, “Electrical impedance spectroscopy as a potential adjunct diagnostic tool for cutaneous melanoma,” *Ski. Res. Technol.*, vol. 19, no. 2, pp.

75–83, 2013.

[60] S. Laufer, A. Ivorra, V. E. Reuter, B. Rubinsky, and S. B. Solomon, “Electrical impedance characterization of normal and cancerous human hepatic tissue,” *Physiol. Meas.*, vol. 31, no. 7, pp. 995–1009, 2010.

[61] L. Helen, B. D. O’Donnell, W. Messina, C. O’Mahony, O. M. A. Ahmed, and E. J. Moore, “Impedance Sensor to Detect Substance Change at the Needle Tip,” *Electroanalysis*, vol. 29, no. 11, pp. 2533–2540, 2017.

[62] S. L. Swisher, M. C. Lin, A. Liao, E. J. Leeflang, Y. Khan, F. J. Pavinatto, K. Mann, A. Naujokas, D. Young, S. Roy, M. R. Harrison, A. C. Arias, V. Subramanian, and M. M. Maharbiz, “Impedance sensing device enables early detection of pressure ulcers in vivo.,” *Nat. Commun.*, vol. 6, p. 6575, 2015.

[63] P. Åberg, *Skin cancer as seen by electrical impedance*. 2004.

[64] U. Birgersson, E. Birgersson, P. Aberg, I. Nicander, and S. Ollmar, “Non-invasive bioimpedance of intact skin: mathematical modeling and experiments.,” *Physiol. Meas.*, vol. 32, no. 1, pp. 1–18, 2011.

[65] Ø. G. Martinsen, S. Grimnes, and E. Haug, “Measuring depth depends on frequency in electrical skin impedance measurements,” *Ski. Res. Technol.*, vol. 5, no. 3, pp. 179–181, 1999.

[66] C. Tronstad, G. K. Johnsen, S. Grimnes, and Ø. G. Martinsen, “A study on electrode gels for skin conductance measurements,” *Physiol. Meas.*, vol. 31, no. 10, pp. 1395–1410, 2010.

[67] Z. Sonner, E. Wilder, J. Heikenfeld, G. Kasting, F. Beyette, D. Swaile, F. Sherman, J. Joyce, J. Hagen, N. Kelley-Loughnane, and R. Naik, “The microfluidics of the eccrine sweat gland, including biomarker partitioning, transport, and biosensing implications,” *Biomicrofluidics*, vol. 9, p. 31301, 2015.

[68] T. Yamamoto and Y. Yamamoto, “Electrical properties of the epidermal stratum corneum,” *Med. Biol. Eng. Comput.*, vol. 14, no. 2, pp. 151–158, 1976.

[69] I. H. Blank, “Factors which influence the water content of the stratum corneum*,” *J. Biophys. Biochem. Cytol.*, pp. 433–441, 1951.

[70] I. H. Blank, “Further Observations on Factors Which Influence the Water Content of the Stratum Corneum,” *J. Invest. Dermatol.*, vol. 21, no. 1, pp. 259–271, 1953.

[71] J. L. Leveque and J. De Rigal, “Impedance Methods for Studying Skin Moisturization,” *J. Soc. Cosmet. Chem.*, vol. 34, pp. 419–428, 1983.

[72] S. Björklund, T. Ruzgas, A. Nowacka, I. Dahi, D. Topgaard, E. Sparr, and J. Engblom, “Skin membrane electrical impedance properties under the influence of a varying water gradient,” *Biophys. J.*, vol. 104, no. 12, pp. 2639–2650, 2013.

[73] G. K. Johnsen, Ø. G. Martinsen, and S. Grimnes, “Sorption studies of human keratinized tissues,” *J. Phys. Conf. Ser.*, vol. 224, p. 12094, 2010.

[74] K. De Paepe, E. Houben, R. Adam, F. Wiessemann, and V. Rogiers, “Validation of the VapoMeter, a closed unventilated chamber system to assess transepidermal water loss vs. the open chamber Tewameter®,” *Ski. Res. Technol.*, vol. 11, no. 1, pp. 61–69, 2005.

[75] P. Clarys, R. Clijsen, J. Taeymans, and A. O. Barel, “Hydration measurements of the stratum corneum: comparison between the capacitance method (digital version of the Corneometer CM 825®) and the impedance method (Skicon-200EX®),” *Ski. Res. Technol.*, vol. 18, no. 3, pp. 316–323, 2012.

[76] L. Ye, Z. Wang, Z. Li, C. Lv, and M. Q. Man, “Validation of GPSkin Barrier ® for assessing epidermal permeability barrier function and stratum corneum hydration in humans,” *Ski. Res. Technol.*, vol. 25, no. 1, pp. 25–29, 2019.

[77] H. N. Mayrovitz, A. Grammenos, K. Corbitt, and S. Bartos, “Young adult gender differences in forearm skin-to-fat tissue dielectric constant values measured at 300 MHz,” *Ski. Res. Technol.*, vol. 22, no. 1, pp. 81–88, 2016.

[78] F. Gioia and L. Celleno, “The dynamics of transepidermal water loss (TEWL) from hydrated skin,” *Ski. Res. Technol.*, vol. 8, pp. 178–186, 2002.

[79] J. Du Plessis, A. Stefaniak, F. Eloff, S. John, T. Agner, T. C. Chou, R. Nixon, M. Steiner, A. Franken, I. Kudla, and L. Holness, “International guidelines for the in vivo assessment of skin properties in non-clinical settings: Part 2. transepidermal water loss and skin hydration,” *Ski. Res. Technol.*, vol. 19, no. 3, pp. 265–278, 2013.

[80] D. Martini, D. Angelino, C. Cortelazzi, I. Zavaroni, G. Bedogni, M. Musci, C. Pruneti,

G. Passeri, M. Ventura, D. Galli, P. Mirandola, M. Vitale, A. Dei Cas, R. C. Bonadonna, S. Di Nuzzo, M. B. De Felici, and D. Del Rio, "Claimed effects, outcome variables and methods of measurement for health claims proposed under European community regulation 1924/2006 in the framework of maintenance of skin function," *Nutrients*, vol. 10, no. 1, 2018.

[81] J. W. Fluhr, M. Gloor, S. Lazzerini, P. Kleesz, R. Grieshaber, and E. Berardesca, "Comparative study of five instruments measuring stratum corneum hydration (Corneometer CM 820 and CM 825, Skicon 200, Nova DPM 9003, DermaLab). Part I. In vitro," *Ski. Res. Technol.*, vol. 5, no. 3, pp. 161–170, 1999.

[82] E. Berardesca, "EEMCO guidance for the assessment of stratum corneum hydration: Electrical methods," *Ski. Res. Technol.*, vol. 3, pp. 126–132, 1997.

[83] K. I. O'Goshi and J. Serup, "Skin conductance; validation of Skicon-200EX® compared to the original model, Skicon-100®," *Ski. Res. Technol.*, vol. 13, pp. 13–18, 2007.

[84] H. N. Mayrovitz, D. N. Weingrad, and S. Davey, "Tissue dielectric constant (TDC) measurements as a means of characterizing localized tissue water in arms of women with and without breast cancer treatment related lymphedema," *Lymphology*, vol. 47, no. 3, pp. 142–150, 2014.

[85] A. Bornkessel, M. Flach, M. Arens-Corell, P. Elsner, and J. W. Fluhr, "Functional assessment of a washing emulsion for sensitive skin: Mild impairment of stratum corneum hydration, pH, barrier function, lipid content, integrity and cohesion in a controlled washing test," *Ski. Res. Technol.*, vol. 11, no. 1, pp. 53–60, 2005.

[86] P. G. Sator, J. B. Schmidt, and H. Hönigsmann, "Comparison of epidermal hydration and skin surface lipids in healthy individuals and in patients with atopic dermatitis," *J. Am. Acad. Dermatol.*, vol. 48, no. 3, pp. 352–358, 2003.

[87] I. Angelova-Fischer, A. Bauer, U. C. Hipler, I. Petrov, J. Kazandjieva, T. Bruckner, T. Diepgen, N. Tsankov, M. Williams, T. W. Fischer, P. Elsner, and J. W. Fluhr, "The Objective Severity Assessment of Atopic Dermatitis (OSAAD) score: Validity, reliability and sensitivity in adult patients with atopic dermatitis," *Br. J. Dermatol.*, vol. 153, pp. 767–773, 2005.

[88] A. O. Barel and P. Clarys, “In vitro calibration of the capacitance method (Corneometer CM 825) and conductance method (Skicon-200) for the evaluation of the hydration state of the skin,” *Ski. Res. Technol.*, vol. 3, no. 2, pp. 107–113, 1997.

[89] S. Grimnes and Ø. G. Martinsen, *Bioimpedance and Bioelectricity Basics*. Elsevier, 2008.

[90] I. H. Blank, “Measurement of pH of the Skin Surface III. Measurements on the arms of children withh no apparent skin lesions,” *J. Invest. Dermatol.*, vol. 2, no. 5, pp. 231–234, 1939.

[91] J. L. Parra and M. Paye, “EEMCO guidance for the in vivo assessment of skin surface pH,” *Skin Pharmacol. Appl. Skin Physiol.*, vol. 16, pp. 188–202, 2003.

[92] H. Öhman and A. Vahlquist, “The pH gradient over the stratum corneum differs in X-linked recessive and autosomal dominant ichthyosis: A clue to the molecular origin of the ‘acid skin mantle’?,” *J. Invest. Dermatol.*, vol. 111, no. 4, pp. 674–677, 1998.

[93] B. Eberlein-Konig, T. Schafer, J. Huss-Marp, U. Darsow, M. Mohrenschlager, O. Herbert, D. Abeck, U. Kramer, H. Behrendt, and J. Ring, “Skin surface pH, stratum corneum hydration, trans-epidermal water loss and skin roughness related to atopic eczema and skin dryness in a population of primary school children,” *Acta Derm. Venereol.*, vol. 80, no. 3, pp. 188–191, 2000.

[94] S. Luebberding, N. Krueger, and M. Kerscher, “Skin physiology in men and women: In vivo evaluation of 300 people including TEWL, SC hydration, sebum content and skin surface pH,” *Int. J. Cosmet. Sci.*, vol. 35, pp. 477–483, 2013.

[95] C. R. Kruse, K. Nuutila, C. C. Y. Lee, E. Kiwanuka, M. Singh, E. J. Caterson, E. Eriksson, and J. A. Sørensen, “The external microenvironment of healing skin wounds,” *Wound Repair Regen.*, vol. 23, no. 4, pp. 456–464, 2015.

[96] L. A. Schneider, A. Korber, S. Grabbe, and J. Dissemond, “Influence of pH on wound-healing: A new perspective for wound-therapy?,” *Arch. Dermatol. Res.*, vol. 298, no. 9, pp. 413–420, 2007.

[97] J. M. Jungersted, H. Scheer, M. Mempel, H. Baurecht, L. Cifuentes, J. K. Høgh, L. I. Hellgren, G. B. E. Jemec, T. Agner, and S. Weidinger, “Stratum corneum lipids, skin barrier function and filaggrin mutations in patients with atopic eczema,” *Allergy*, vol.

65, no. 7, pp. 911–918, 2010.

[98] M. H. Schmid-Wendtner and H. C. Korting, “The pH of the skin surface and its impact on the barrier function,” *Skin Pharmacol. Physiol.*, vol. 19, pp. 296–302, 2006.

[99] A. Koh, D. Kang, Y. Xue, S. Lee, R. M. Pielak, J. Kim, T. Hwang, S. Min, A. Banks, P. Bastien, M. C. Manco, L. Wang, K. R. Ammann, K. I. Jang, P. Won, S. Han, R. Ghaffari, U. Paik, M. J. Slepian, G. Balooch, Y. Huang, and J. A. Rogers, “A soft, wearable microfluidic device for the capture, storage, and colorimetric sensing of sweat,” *Sci. Transl. Med.*, vol. 8, no. 366, 2016.

[100] A. Tamayol, M. Akbari, Y. Zilberman, M. Comotto, E. Lesha, L. Serex, S. Bagherifard, Y. Chen, G. Fu, S. K. Ameri, W. Ruan, E. L. Miller, M. R. Dokmeci, S. Sonkusale, and A. Khademhosseini, “Flexible pH-Sensing Hydrogel Fibers for Epidermal Applications,” *Adv. Healthc. Mater.*, vol. 5, no. 6, pp. 711–719, 2016.

[101] C.-Y. Cui and D. Schlessinger, “Eccrine sweat gland development and sweat secretion,” *Exp Dermatol*, vol. 24, no. 9, pp. 644–650, 2015.

[102] K. Saga, “Structure and function of human sweat glands studied with histochemistry and cytochemistry,” *Prog. Histochem. Cytochem.*, vol. 37, no. 4, pp. 323–386, 2002.

[103] C. C. Zouboulis, “Acne and sebaceous gland function,” *Clin. Dermatol.*, vol. 22, pp. 360–366, 2004.

[104] A. Mena-Bravo and M. D. Luque de Castro, “Sweat: A sample with limited present applications and promising future in metabolomics,” *J. Pharm. Biomed. Anal.*, vol. 90, pp. 139–147, 2014.

[105] S. Jadoon, S. Karim, M. R. Akram, A. Kalsoom Khan, M. A. Zia, A. R. Siddiqi, and G. Murtaza, “Recent developments in sweat analysis and its applications,” *Int. J. Anal. Chem.*, vol. 2015, 2015.

[106] V. A. LeGrys, J. R. Yankaskas, L. M. Quittell, B. C. Marshall, and P. J. Mogayzel, “Diagnostic Sweat Testing: The Cystic Fibrosis Foundation Guidelines,” *J. Pediatr.*, vol. 151, no. 1, pp. 85–89, 2007.

[107] B. Schazmann, D. Morris, C. Slater, S. Beirne, C. Fay, R. Reuveny, N. Moyna, and D. Diamond, “A wearable electrochemical sensor for the real-time measurement of sweat sodium concentration,” *Anal. Methods*, vol. 2, no. 4, p. 342, 2010.

[108] A. J. Bandodkar, P. Gutruf, J. Choi, K. Lee, Y. Sekine, J. T. Reeder, W. J. Jeang, A. J. Aranyosi, S. P. Lee, J. B. Model, R. Ghaffari, C.-J. Su, J. P. Leshock, T. Ray, A. Verrillo, K. Thomas, V. Krishnamurthi, S. Han, J. Kim, S. Krishnan, T. Hang, and J. A. Rogers, "Battery-free, skin-interfaced microfluidic/electronic systems for simultaneous electrochemical, colorimetric, and volumetric analysis of sweat," *Sci. Adv.*, vol. 5, no. 1, p. eaav3294, 2019.

[109] S. R. Corrie, J. W. Coffey, J. Islam, K. A. Markey, and M. A. F. Kendall, "Blood, sweat, and tears: Developing clinically relevant protein biosensors for integrated body fluid analysis," *Analyst*, vol. 140, pp. 4350–4364, 2015.

[110] M. J. Tierney, J. A. Tamada, R. O. Potts, L. Jovanovic, and S. Garg, "Clinical evaluation of the GlucoWatch® biographer: A continual, non-invasive glucose monitor for patients with diabetes," *Biosens. Bioelectron.*, vol. 16, pp. 621–629, 2001.

[111] P. Bollella, S. Sharma, A. E. G. Cass, and R. Antiochia, "Minimally-invasive Microneedle-based Biosensor Array for Simultaneous Lactate and Glucose Monitoring in Artificial Interstitial Fluid," *Electroanalysis*, vol. 31, pp. 374–382, 2019.

[112] S. H. Bariya, M. C. Gohel, T. A. Mehta, and O. P. Sharma, "Microneedles: An emerging transdermal drug delivery system," *J. Pharm. Pharmacol.*, vol. 64, no. 1, pp. 11–29, 2012.

[113] M. W. Zhu, H. W. Li, X. L. Chen, Y. F. Tang, M. H. Lu, and Y. F. Chen, "Silica needle template fabrication of metal hollow microneedle arrays," *J. Micromechanics Microengineering*, vol. 19, p. 115010, 2009.

[114] P. R. Miller, R. M. Taylor, B. Q. Tran, G. Boyd, T. Glaros, V. H. Chavez, R. Krishnakumar, A. Sinha, K. Poorey, K. P. Williams, S. S. Branda, J. T. Baca, and R. Polsky, "Extraction and biomolecular analysis of dermal interstitial fluid collected with hollow microneedles," *Commun. Biol.*, vol. 1, no. 173, pp. 1–11, 2018.

[115] K. Y. Seong, M. S. Seo, D. Y. Hwang, E. D. O'Cearbhaill, S. Sreenan, J. M. Karp, and S. Y. Yang, "A self-adherent, bullet-shaped microneedle patch for controlled transdermal delivery of insulin," *J. Control. Release*, vol. 265, pp. 48–56, 2017.

[116] Y.-C. Kim, J.-H. Park, and M. R. Prausnitz, "Microneedles for drug and vaccine delivery," *Adv. Drug Deliv. Rev.*, vol. 64, no. 14, pp. 1547–1568, 2012.

[117] E. V. Mukerjee, S. D. Collins, R. R. Isseroff, and R. L. Smith, “Microneedle array for transdermal biological fluid extraction and in situ analysis,” *Sensors Actuators, A Phys.*, vol. 114, no. 2–3, pp. 267–275, 2004.

[118] H. Chang, M. Zheng, X. Yu, A. Than, R. Z. Seeni, R. Kang, J. Tian, D. P. Khanh, L. Liu, P. Chen, and C. Xu, “A Swellable Microneedle Patch to Rapidly Extract Skin Interstitial Fluid for Timely Metabolic Analysis,” *Adv. Mater.*, vol. 29, p. 1702243, 2017.

[119] M. Shirasu and K. Touhara, “The scent of disease: Volatile organic compounds of the human body related to disease and disorder,” *J. Biochem.*, vol. 150, no. 3, pp. 257–266, 2011.

[120] M. Gallagher, C. J. Wysocki, J. J. Leyden, A. I. Spielman, X. Sun, and G. Preti, “Analyses of volatile organic compounds from human skin,” *Br. J. Dermatol.*, vol. 159, no. 4, pp. 780–791, 2008.

[121] T. Abaffy, M. G. Möller, D. D. Riemer, C. Milikowski, and R. A. DeFazio, “Comparative analysis of volatile metabolomics signals from melanoma and benign skin: A pilot study,” *Metabolomics*, vol. 9, no. 5, pp. 998–1008, 2013.

[122] D. K. Trivedi, E. Sinclair, Y. Xu, D. Sarkar, C. Walton-Doyle, C. Liscio, P. Banks, J. Milne, M. Silverdale, T. Kunath, R. Goodacre, and P. Barran, “Discovery of Volatile Biomarkers of Parkinson’s Disease from Sebum,” *ACS Cent. Sci.*, vol. 5, pp. 599–606, 2019.

[123] S. K. Pandey and K. H. Kim, “Human body-odor components and their determination,” *TrAC - Trends Anal. Chem.*, vol. 30, no. 5, pp. 784–796, 2011.

[124] C. M. De Moraes, C. Wanjiku, N. M. Stanczyk, H. Pulido, J. W. Sims, H. S. Betz, A. F. Read, B. Torto, and M. C. Mescher, “Volatile biomarkers of symptomatic and asymptomatic malaria infection in humans,” *Proc. Natl. Acad. Sci.*, vol. 115, no. 22, pp. 5780–5785, 2018.

[125] J. Kim, J. R. Sempionatto, S. Imani, M. C. Hartel, A. Barfidokht, G. Tang, A. S. Campbell, P. P. Mercier, and J. Wang, “Simultaneous Monitoring of Sweat and Interstitial Fluid Using a Single Wearable Biosensor Platform,” *Adv. Sci.*, vol. 5, no. 10, p. 1800880, 2018.

[126] J. Kim, I. Jeerapan, S. Imani, T. N. Cho, A. Bandodkar, S. Cinti, P. P. Mercier, and J. Wang, "Noninvasive Alcohol Monitoring Using a Wearable Tattoo-Based Iontophoretic-Biosensing System," *ACS Sensors*, vol. 1, no. 8, pp. 1011–1019, 2016.

[127] A. J. Bandodkar, W. Jia, C. Yardımcı, X. Wang, J. Ramirez, and J. Wang, "Tattoo-Based Noninvasive Glucose Monitoring: A Proof-of-Concept Study," 2014.

[128] N. V. Zaryanov, V. N. Nikitina, E. V. Karpova, E. E. Karyakina, and A. A. Karyakin, "Nonenzymatic sensor for lactate detection in human sweat," *Anal. Chem.*, vol. 89, pp. 11198–11202, 2017.

[129] X. Huang, H. Cheng, K. Chen, Y. Zhang, Y. Zhang, Y. Liu, C. Zhu, S.-C. Ouyang, G.-W. Kong, C. Yu, Y. Huang, and J. A. Rogers, "Epidermal impedance sensing sheets for precision hydration assessment and spatial mapping.," *IEEE Trans. Biomed. Eng.*, vol. 60, no. 10, pp. 2848–57, Oct. 2013.

[130] K. De Guzman, G. Al-Kharusi, T. Levingstone, and A. Morrin, "Robust epidermal tattoo electrode platform for skin physiology monitoring," *Anal. Methods*, vol. 11, no. 11, pp. 1460–1468, 2019.

[131] A. Zucca, C. Cipriani, Sudha, S. Tarantino, D. Ricci, V. Mattoli, and F. Greco, "Tattoo Conductive Polymer Nanosheets for Skin-Contact Applications," *Adv. Healthc. Mater.*, vol. 4, no. 7, pp. 983–990, 2015.

[132] L. M. Ferrari, S. Sudha, S. Tarantino, R. Esposti, F. Bolzoni, P. Cavallari, C. Cipriani, V. Mattoli, and F. Greco, "Ultraconformable Temporary Tattoo Electrodes for Electrophysiology," *Adv. Sci.*, vol. 5, no. 3, p. 1700771, 2018.

[133] Y. Liu, J. J. S. Norton, R. Qazi, Z. Zou, K. R. Ammann, H. Liu, L. Yan, P. L. Tran, K.-I. Jang, J. W. Lee, D. Zhang, K. A. Kilian, S. H. Jung, T. Bretl, J. Xiao, M. J. Slepian, Y. Huang, J.-W. Jeong, and J. A. Rogers, "Epidermal mechano-acoustic sensing electronics for cardiovascular diagnostics and human-machine interfaces," *Sci. Adv.*, vol. 2, no. 11, Nov. 2016.

[134] J. R. Windmiller, A. J. Bandodkar, G. Valdés-Ramírez, S. Parkhomovsky, A. G. Martinez, and J. Wang, "Electrochemical sensing based on printable temporary transfer tattoos," *Chem. Commun.*, vol. 48, no. 54, p. 6794, 2012.

[135] A. J. Bandodkar, I. Jeerapan, J. M. You, R. Nuñez-Flores, and J. Wang, "Highly

Stretchable Fully-Printed CNT-Based Electrochemical Sensors and Biofuel Cells: Combining Intrinsic and Design-Induced Stretchability," *Nano Lett.*, vol. 16, no. 1, pp. 721–727, 2016.

[136] T. Guinovart, A. J. Bandodkar, J. R. Windmiller, F. J. Andrade, and J. Wang, "A potentiometric tattoo sensor for monitoring ammonium in sweat.," *Analyst*, vol. 138, no. 22, pp. 7031–8, 2013.

[137] A. S. Campbell, J. Kim, and J. Wang, "Wearable electrochemical alcohol biosensors," *Curr. Opin. Electrochem.*, vol. 10, pp. 126–135, 2018.

[138] J. A. Fan, W.-H. Yeo, Y. Su, Y. Hattori, W. Lee, S.-Y. Jung, Y. Zhang, Z. Liu, H. Cheng, L. Falgout, M. Bajema, T. Coleman, D. Gregoire, R. J. Larsen, Y. Huang, and J. A. Rogers, "Fractal design concepts for stretchable electronics," *Nat. Commun.*, vol. 5, p. 3266, 2014.

[139] W. H. Yeo, Y. S. Kim, J. Lee, A. Ameen, L. Shi, M. Li, S. Wang, R. Ma, S. H. Jin, Z. Kang, Y. Huang, and J. A. Rogers, "Multifunctional epidermal electronics printed directly onto the skin," *Adv. Mater.*, vol. 25, no. 20, pp. 2773–2778, 2013.

[140] S. Krishnan, Y. Shi, R. C. Webb, Y. Ma, P. Bastien, K. E. Crawford, A. Wang, X. Feng, M. Manco, J. Kurniawan, E. Tir, Y. Huang, G. Balooch, R. M. Pielak, and J. A. Rogers, "Multimodal epidermal devices for hydration monitoring," *Microsystems Nanoeng.*, vol. 3, p. 17014, 2017.

[141] S. R. Madhvapathy, Y. Ma, M. Patel, S. Krishnan, C. Wei, Y. Li, S. Xu, X. Feng, Y. Huang, and J. A. Rogers, "Epidermal Electronic Systems for Measuring the Thermal Properties of Human Skin at Depths of up to Several Millimeters," *Adv. Funct. Mater.*, vol. 28, p. 1802083, 2018.

[142] P. J. Caspers, G. W. Lucassen, H. A. Bruining, and G. J. Puppels, "Automated depth-scanning confocal Raman microspectrometer for rapid in vivo determination of water concentration profiles in human skin," *J. Raman Spectrosc.*, vol. 31, pp. 813–818, 2000.

[143] M. Egawa and H. Tagami, "Comparison of the depth profiles of water and water-binding substances in the stratum corneum determined in vivo by Raman spectroscopy between the cheek and volar forearm skin: Effects of age, seasonal changes and

artificial forced hydration," *Br. J. Dermatol.*, vol. 158, pp. 251–260, 2008.

[144] B. D. Wilson, S. Moon, and F. Armstrong, "Comprehensive Review of Ultraviolet Radiation and the Current Status on Sunscreens," *Clin. Aesthetic Dermatology*, vol. 5, pp. 18–23, 2012.

[145] L. Baumann, "Skin ageing and its treatment," *J. Pathol.*, vol. 211, pp. 241–251, 2007.

[146] J. D'Orazio, S. Jarrett, A. Amaro-Ortiz, and T. Scott, "UV radiation and the skin," *Int. J. Mol. Sci.*, vol. 14, pp. 12222–12248, 2013.

[147] H. Araki, J. Kim, S. Zhang, A. Banks, K. E. Crawford, X. Sheng, P. Gutruf, Y. Shi, R. M. Pielak, and J. A. Rogers, "Materials and Device Designs for an Epidermal UV Colorimetric Dosimeter with Near Field Communication Capabilities," *Adv. Funct. Mater.*, vol. 27, p. 1604465, 2017.

[148] L. Ren, S. Xu, J. Gao, Z. Lin, Z. Chen, B. Liu, L. Liang, and L. Jiang, "Fabrication of flexible microneedle array electrodes for wearable bio-signal recording," *Sensors (Switzerland)*, vol. 18, no. 4, pp. 1–11, 2018.

[149] G. Li, S. Wang, and Y. Y. Duan, "Towards gel-free electrodes: A systematic study of electrode-skin impedance," *Sensors Actuators, B Chem.*, vol. 241, no. October 2016, pp. 1244–1255, 2017.

[150] G. Li, S. Wang, and Y. Y. Duan, "Sensors and Actuators B : Chemical Towards conductive-gel-free electrodes : Understanding the wet electrode , semi-dry electrode and dry electrode-skin interface impedance using electrochemical impedance spectroscopy fitting," *Sensors Actuators B. Chem.*, vol. 277, no. April, pp. 250–260, 2018.

[151] B. Pappin, M. J., and T. A., "Boron-Carbohydrate Interactions," in *Carbohydrates - Comprehensive Studies on Glycobiology and Glycotechnology*, 2012.

[152] M. P. Divya, Y. S. Rajput, R. Sharma, and G. Singh, "Molecularly imprinted polymer for separation of lactate," *J. Anal. Chem.*, vol. 70, no. 10, pp. 1213–1217, 2015.

[153] A. J. Bandodkar, V. W. S. Hung, W. Jia, G. Valdés-Ramírez, J. R. Windmiller, A. G. Martinez, J. Ramírez, G. Chan, K. Kerman, and J. Wang, "Tattoo-based potentiometric ion-selective sensors for epidermal pH monitoring.," *Analyst*, vol. 138, pp. 123–128, Jan. 2013.

[154] T. Lindfors and A. Ivaska, “pH sensitivity of polyaniline and its substituted derivatives,” *J. Electroanal. Chem.*, vol. 531, no. 1, pp. 43–52, 2002.

[155] H. Y. Y. Nyein, W. Gao, Z. Shahpar, S. Emaminejad, S. Challa, K. Chen, H. M. Fahad, L. C. Tai, H. Ota, R. W. Davis, and A. Javey, “A Wearable Electrochemical Platform for Noninvasive Simultaneous Monitoring of Ca2+ and pH,” *ACS Nano*, vol. 10, no. 7, pp. 7216–7224, 2016.

[156] W. G. Robertson, “Measurement of Ionised Calcium in Body Fluids—A Review,” *Ann. Clin. Biochem.*, vol. 13, no. 1–6, pp. 540–548, 1976.

[157] M. S. Cooper and N. J. L. Gittoes, “Diagnosis and management of hypocalcaemia,” *BMJ*, vol. 336, pp. 1298–1302, 2008.

[158] C. Kolluru, M. Williams, J. Chae, and M. R. Prausnitz, “Recruitment and Collection of Dermal Interstitial Fluid Using a Microneedle Patch,” *Adv. Healthc. Mater.*, vol. 8, no. 3, 2019.

[159] A. Sieg, R. H. Guy, and M. B. Delgado-Charro, “Noninvasive glucose monitoring by reverse iontophoresis in vivo: Application of the internal standard concept,” *Clin. Chem.*, vol. 50, no. 8, pp. 1383–1390, 2004.

[160] M. M. Niedzwiecki, P. Samant, D. I. Walker, V. Tran, D. P. Jones, M. R. Prausnitz, and G. W. Miller, “Human Suction Blister Fluid Composition Determined Using High-Resolution Metabolomics,” *Anal. Chem.*, vol. 90, no. 6, pp. 3786–3792, 2018.

[161] S. N. Thennadil, J. L. Rennert, B. J. Wenzel, K. H. Hazen, T. L. Ruchti, and M. B. Block, “Comparison of Glucose Concentration in Interstitial Fluid, and Capillary and Venous Blood During Rapid Changes in Blood Glucose Levels,” *Diabetes Technol. Ther.*, vol. 3, pp. 357–365, 2001.

[162] F. Ribet, G. Stemme, and N. Roxhed, “Real-time intradermal continuous glucose monitoring using a minimally invasive microneedle-based system,” *Biomed. Microdevices*, vol. 20, no. 4, 2018.

[163] P. Bollella, S. Sharma, A. E. G. Cass, and R. Antiochia, “Microneedle-based biosensor for minimally-invasive lactate detection,” *Biosens. Bioelectron.*, vol. 123, no. August 2018, pp. 152–159, 2019.

[164] L. Daugimont, N. Baron, G. Vandermeulen, N. Pavselj, D. Miklavcic, M. C. Jullien,

G. Cabodevila, L. M. Mir, and V. Préat, “Hollow microneedle arrays for intradermal drug delivery and DNA electroporation,” *J. Membr. Biol.*, vol. 236, pp. 117–125, 2010.

[165] B. Gualeni, S. A. Coulman, D. Shah, P. F. Eng, H. Ashraf, P. Vescovo, G. J. Blayney, L. D. Piveteau, O. J. Guy, and J. C. Birchall, “Minimally invasive and targeted therapeutic cell delivery to the skin using microneedle devices,” *Br. J. Dermatol.*, vol. 178, no. 3, pp. 731–739, 2018.

[166] C. G. Li, C. Y. Lee, K. Lee, and H. Jung, “An optimized hollow microneedle for minimally invasive blood extraction,” *Biomed. Microdevices*, vol. 15, no. 1, pp. 17–25, 2013.

[167] P. R. Miller, S. A. Skoog, T. L. Edwards, D. M. Lopez, D. R. Wheeler, D. C. Arango, X. Xiao, S. M. Brozik, J. Wang, R. Polsky, and R. J. Narayan, “Multiplexed microneedle-based biosensor array for characterization of metabolic acidosis,” *Talanta*, vol. 88, pp. 739–742, 2012.

[168] R. Badugu, J. R. Lakowicz, and C. D. Geddes, “Noninvasive Continuous Monitoring of Physiological Glucose Using a Monosaccharide-Sensing Contact Lens,” *Anal. Chem.*, vol. 76, pp. 610–618, 2004.

[169] K. Rebrin, N. F. Sheppard, and G. M. Steil, “Use of Subcutaneous Interstitial Fluid Glucose to Estimate,” *J. Diabetes Sci. Technol.*, vol. 4, no. 5, pp. 1087–1098, 2010.

[170] T. Bailey, B. W. Bode, M. P. Christiansen, L. J. Klaff, and S. Alva, “The Performance and Usability of a Factory-Calibrated Flash Glucose Monitoring System,” *Diabetes Technol. Ther.*, vol. 17, no. 11, pp. 787–794, 2015.

[171] F. Ribet, G. Stemme, and N. Roxhed, “Microneedle-based system for minimally invasive continuous monitoring of glucose in the dermal interstitial fluid,” *Proc. IEEE Int. Conf. Micro Electro Mech. Syst.*, pp. 408–411, 2018.

[172] A. F. Ólafsdóttir, S. Attvall, U. Sandgren, S. Dahlqvist, A. Pivodic, S. Skrtic, E. Theodorsson, and M. Lind, “A Clinical Trial of the Accuracy and Treatment Experience of the Flash Glucose Monitor FreeStyle Libre in Adults with Type 1 Diabetes,” *Diabetes Technol. Ther.*, vol. 19, no. 3, pp. 164–172, 2017.

[173] R. Jiang, E. Cudjoe, B. Bojko, T. Abaffy, and J. Pawliszyn, “A non-invasive method

for in vivo skin volatile compounds sampling," *Anal. Chim. Acta*, vol. 804, no. August, pp. 111–119, 2013.

[174] H. Jin, T. P. Huynh, and H. Haick, "Self-Healable Sensors Based Nanoparticles for Detecting Physiological Markers via Skin and Breath: Toward Disease Prevention via Wearable Devices," *Nano Lett.*, vol. 16, no. 7, pp. 4194–4202, 2016.

[175] K. S. Suslick and N. A. Rakow, "A colorimetric sensor array for odour visualization," *Nature*, vol. 406, no. 6797, pp. 710–713, 2000.

[176] B. A. Suslick, L. Feng, and K. S. Suslick, "Discrimination of complex mixtures by a colorimetric sensor array: Coffee aromas," *Anal. Chem.*, vol. 82, no. 5, pp. 2067–2073, 2010.

[177] S. Davies, P. Spanel, and D. Smith, "Quantitative analysis of ammonia on the breath of patients in end-stage renal failure," *Kidney Int.*, vol. 52, no. 1, pp. 223–228, 1997.

[178] P. Le Maout, J. L. Wojkiewicz, N. Redon, C. Lahuec, F. Seguin, L. Dupont, S. Mikhaylov, Y. Noskov, N. Ogurtsov, and A. Pud, "Polyaniline nanocomposites based sensor array for breath ammonia analysis. Portable e-nose approach to non-invasive diagnosis of chronic kidney disease," *Sensors Actuators, B Chem.*, vol. 274, no. April, pp. 616–626, 2018.

Chapter 2

Fabrication and Characterisation of Tattoo Sensor for the Non-Invasive Assessment of the Skin Barrier

2.1 Introduction

The human skin barrier is the interface between the complex physiology of the body and the influences of external environment, and this main barrier of protection is provided by the SC layer found in the epidermis [1], [2]. The primary role of the SC is to maintain the hydration gradient of the skin by keeping the skin hydrated and preventing transepidermal water loss. An alteration in the skin barrier is often described as a reduced barrier function due to altered lipid composition and organisation within the SC [3], [4] . This alteration in skin barrier function manifests as skin dryness and/or inflammation commonly seen in patients with skin disorders/diseases such as atopic dermatitis [5], [6]. Development of devices that can be used for early diagnosis or continuous monitoring of the skin barrier can help manage or prevent the progression of an individuals' skin disorder/disease.

Wearable sensors such as, epidermal sensors have received considerable notice recently for their potential in continuous on-body monitoring. As mentioned in Chapter 1, Epidermal sensors are a type of skin-based Fwearable platform that are 'worn' directly on the skin and are a promising means of non-invasively assessing the health status of an individual. Fabrication of these sensors and devices require materials and fabrication methodologies that allow electrically conducting materials conform and flow with the mechanics of skin as well as deliver good electrical performance.

In this chapter the development and characterisation of a screen-printed tattoo sensor for the non-invasive assessment of the skin barrier is presented. Impedance spectroscopy was the transduction method used to non-invasively interrogate the skin with the screen printed electrode. The screen-printed silver tattoo sensor comprising two concentric circle electrodes was applied and characterised initially on a hydrogel. It was shown that the tattoo was capable of tracking changes in water content in the hydrogel using impedance spectroscopy. The tattoo sensors were then applied to porcine and human skin and impedance spectroscopy was again used to interrogate the skin at the outer stratum corneum (SC). As mentioned earlier, the SC is a layer of great interest from a dermatological point of view since it plays a critical role in the barrier function of the skin by protecting underlying tissue from infection, dehydration, chemical irritants and mechanical stress. Hydration changes were tracked in the skin using the impedance approach and validated against a tissue dielectric constant (TDC) measurement taken with the MoistureMeterD (MMD, Delfin Technologies). Using the tattoo sensors the impedimetric results obtained were modelled into a proposed circuit model representative of the

systems measured. From this study, the potential of using wearable tattoo electrodes combined with impedance spectroscopy as a transduction technique to investigate skin barrier hydration status offers considerable promise towards the monitoring of and self-management of skin health.

2.2 Materials and methods

2.2.1 Materials

Acheson Electrodag PF-410 silver conductive ink was purchased from Nor-Cote International Ltd. Temporary transfer tattoo paper substrate was from Sports Ink™ (Dublin, Ireland). Strip boards were purchased from Maplin Electronics. Mill Max spring loaded contacts (Gold plated copper alloy, 0906-4-15-20-75-14-11-0) were purchased from Farnell Components (Ireland). Poly (ethylene glycol) diglycidyl ether (PEDGE, average Mn 500, 475696) was purchased from Sigma-Aldrich. Jeffamine® EDR-148 polyetheramine was donated from Huntsman Chemical Company (US). The human skin equivalent (Labskin) (Batch 170105) was obtained from Innoven UK Ltd. (www.innovenn.co.uk/labskin, York, England, UK).

2.2.2 Tattoo sensor design, fabrication and application

A two-concentric circle design was utilised for the tattoo sensor (Fig. 2.1a) and are screen-printed from silver ink. The tattoo has an overall diameter of 20 mm with the inner and outer electrodes separated by a distance of 3 mm. The electrical signal propagation of the tattoo electrodes into skin displayed in Fig. 2.1c.

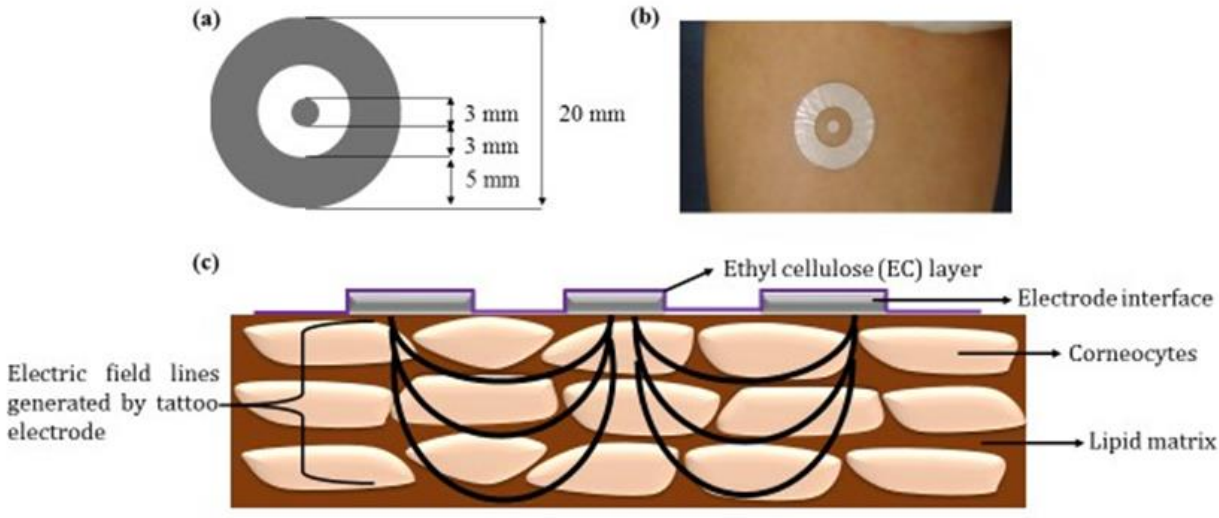

Figure 2. 1 (a) Tattoo sensor schematic and dimensions, (b) Tattoo electrodes as applied on the inner forearm imaged using a Nikon D3300 and (c) side-profile schematic of the electrical signal from the tattoo electrodes on the skin.

Screen printing was the fabrication technique used to print the tattoo electrodes because it is a simple low-cost fabrication method that is capable of mass printing electrodes. This fabrication technique produces thick films compared to thin films produced by inkjet printing. Initial thin film electrodes printed via inkjet printing produced fragile films that could not be properly contacted to the potentiostat using thin wires and pins as they became damaged easily. Therefore, screen printing was chosen to fabricate the tattoo electrodes. Screen printing of the tattoo electrodes were performed using a DEK screen printer. A screen containing the desired configuration pattern, in this case a repeating two concentric circle pattern (Fig. 2.2d) was mounted on a frame in the printer. A metal flood blade and rubber squeegee was utilised to pass ink at 40 mm/s over the screen and transfer the image onto the temporary tattoo substrate placed underneath. The PF410 silver ink patterns were then cured at 120 ^{o}C for 5 min.

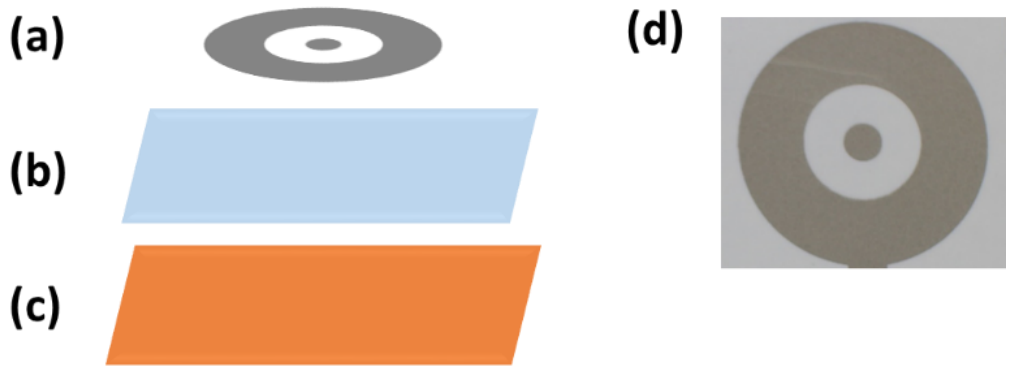

Figure 2.2 Schematic of screen printed tattoo electrodes: (a) two concentric design for tattoo electrodes, (b) clear thin ethyl cellulose (EC) transfer layer, (c) tattoo paper with starch-dextrin water release layer and (d) image of the screen printed tattoo electrodes.

The process to transfer the tattoo onto skin has been previously reported by Windmiller *et al.* [7]. The tattoo electrodes were applied onto the desired substrate by directly placing it onto the hydrogel or skin (Fig. 2.3a), dabbing the backing paper with water for 1 min (Fig. 2.3b) to release the backing paper (Fig. 2.3c) from the tattoo design. The tattoo electrode is then held down by the EC layer on the hydrogel or skin. Filter paper was used to wick away excess water.

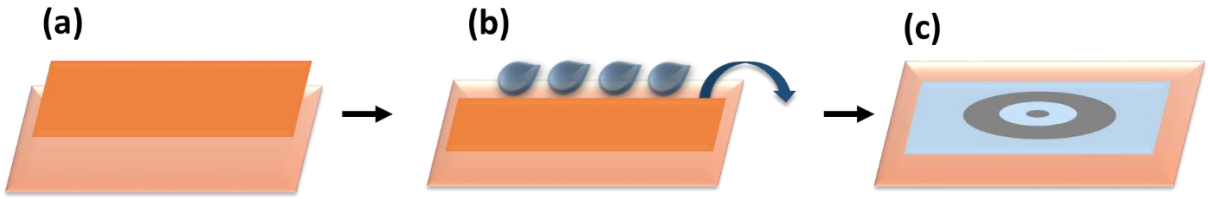

Figure 2.3 Schematic of tattoo electrodes application: (a) Tattoo is flipped and then positioned onto desired area, (b) backing paper is wetted for approximately one minute while holding the tattoo steady on the area and (c) tattoo electrode pattern is released on the target substrate.

2.2.3 Impedance analysis

Two gold pins (7 mm apart) were soldered on to a strip board and used to contact with the inner and outer tattoo electrodes and connect to the potentiostat. Impedance spectroscopy was performed using an Autolab PGSTAT128N workstation. The frequency range scanned was from 0.1 Hz to 1 MHz with an amplitude of 0.01 V, unless stated otherwise. All spectra collected on hydrogel were recorded at 0 V set potential. The same frequency range was used for the porcine and human skin experiments with an amplitude of 0.03 V and set potential of 0.1 V.

2.2.4 Delfin MoistureMeterD (MMD) analysis

Tissue dielectric constant (TDC) measurements were made with the MoistureMeterD (MMD,Delfin Technologies, Finland) probes. This device measures skin and the skin-to-fat TDC at a frequency of 300 MHz by placing the small hand held probe to the skin for 10 s. Different MMD probes can be used with outer diameters from 10 to 55 mm, for an effective measurement depth of 0.5 to 5 mm respectively. Effective measurement depth is defined as the depth at which the 300 MHz electric field decreases to 1/*e* of its surface field [8], [9]. Measurements were done on hydrogel, porcine skin and human skin in a similar manner where the 1.5 mm effective measurement depth probe was used for the hydrogel and the 0.5 mm effective depth probe was used for porcine and human skin.

2.2.5 Hydrogel preparation

Poly(ethylene glycol)diglycidyl ether (PEDGE) –Jeffamine® hydrogels of approx. 10 mm depth were used in all experiments. These were prepared using a protocol previously reported [10].

This was prepared by weighing out and mixing 9.426 g PEDGE, 14.923 g DIW and 2.651g Jeffamine® EDR-148 and stirred for 5 min to get a homogenous mixture. This mixture was poured into a small crystallizing dish and placed in the refrigerator (4 ˚C) overnight to cure.

Hydrogels were synthesized with varying amine-epoxy networks (1:1, 1:1.2 and 1:2 amine:epoxy) to determine if the tattoo electrodes can determine the effect different crosslinking parameters. To synthesise the hydrogels with different crosslinking parameters a method previously reported by Mac Kenna *et al.* was used [10]. Similar tattoo application from Section 2.2.2 and dehydration and hydration procedures from Section 2.2.6 were followed.

2.2.6 Hydrogel dehydration and hydration

Before analysis, hydrogels were removed from the fridge and left to acclimatize to room temperature for at least 1 h.

To monitor water loss, tattoo electrodes were applied to the surface of the hydrogels, (according to Section 2.2.2) and an impedance spectrum taken at hourly intervals using the tattoo electrodes by way of contacting the two gold pins to the inner and outer electrodes.

To monitor water uptake, an impedance measurement of the hydrogel in its initial state was first taken using a tattoo. Following this, the tattoo was removed and the hydrogel was submerged in DIW for different time intervals (1, 3, 5, 10 and 15 min). Each time the hydrogel was removed from water, a fresh tattoo sensor was applied, and an impedance spectrum taken again. This analysis was validated against TDC measurements taken with the MMD probe (1.5 mm effective measurement depth).

2.2.7 Skin dehydration and hydration

Porcine skin was purchased from the local butcher and was cut into 6 cm x 6 cm pieces and allowed to soak in DIW for 24 hr. To monitor porcine skin dehydration, the porcine skin was removed from the water and patted dry gently and kept at room temperature. A tattoo sensor was applied to the porcine skin as described in Section 2.2.2 and impedance measurements taken every h for 4 h using the same tattoo throughout.

To monitor porcine skin hydration, a tattoo sensor was placed on dry porcine skin and an impedance spectrum was collected using the tattoo electrodes. The tattoo was removed and a

piece of cotton wool was soaked with DIW and applied to the porcine skin for 1 min. An impedance measurement was then taken using a fresh tattoo. The tattoo was removed and the process of topically applying water to the skin was repeated. A fresh tattoo was used for the impedance measurement after each application of water. A TDC measurement with the MMD probe (0.5 mm effective depth) was also taken after each topical water application.

To monitor human skin dehydration, an area of the inner forearm was first pre-treated with a piece of cotton wool saturated with 1 mL DIW. A tattoo sensor was then applied on this area of the inner forearm and impedance spectra were taken at defined intervals. The measurements were validated by taking a TDC measurement with the MMD probe (0.5 mm effective depth). One volunteer was used and informed consent was obtained. To characterise the human skin equivalent (Labskin), the tattoo was applied on to the surface of the skin and an impedance spectra was taken. The human skin equivalent has a robust structure owing to the use of fibrin in constructing a synthetic dermal matrix, which contains primary human fibroblasts. All living skin equivalents were incubated in a regulated environment at 37 ◦C in 5% (v/v) carbon dioxide and air. The impedimetric results were compared to human skin measurements of participants using the tattoo and MMD probe [11]. Informed consent was received from all participants (aged 22-28).

2.2.8 Optical microscopy

A Nikon D3300 AF-P 18-55 VR camera was used to image the tattoo electrodes applied on the hydrogel and porcine skin. A Keyence Digital Inspection Microscope (3D VHX-2000) was used to take high resolution images of surface adherence of the tattoo electrodes on different target substrates. A VH-ZOOR lens was used and images were taken at x30.

2.2.9 Varying electrode configuration

Schematic designs of the tattoo with varying areas and distances are displayed in Fig. 2.4. All tattoo electrodes were applied on the hydrogel according to Section 2.2.2 and measured with gold pin contacts (5 mm apart). Using the method in Section 2.2.6, the hydrogels were measured using impedance spectroscopy.

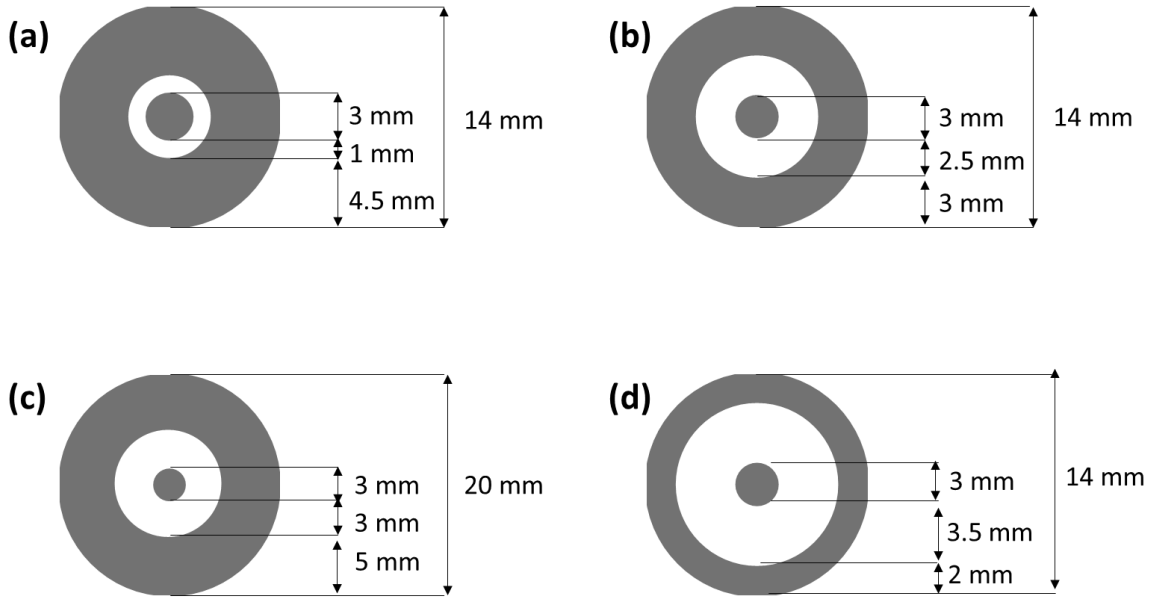

Figure 2.4 Dimensions of tattoo electrodes with varying distances between the inner and outer electrode: (a) 1mm, (b) 2.5 mm, (c) 3 mm and 3.5 mm distance.

2.3 Results and discussion

2.3.1 Physical characterisation of the tattoo electrodes

The tattoo sensor design consists of two concentric circle electrodes similar to the MMD. This design was based on coaxial transmission lines, where two concentric circle electrodes were made of a conducting material, in this case silver ink screen printed onto tattoo paper. The 3 mm distance between the electrodes represents the signal propagation distance into the medium that is being investigated. According to Hamed *et al.*, the advantage of having concentric electrodes is that the signal radiates from all directions as it passes through the medium investigated and that the propagating signal doesn't suffer any leakage compared to a different geometry [12].

The tattoo electrodes were applied on different surfaces to assess their conformability and adherence. In the first instance, they were applied onto hydrogels which was used as a physical mimic of soft tissue (Fig. 2.5a). It was observed that the silver electrodes adhere well to its flat, smooth surface. The EC layer can be observed in the image (Fig. 2.5b) as a transparent overlay which serves to hold the electrodes in position. This thin EC layer is released during the transfer process on the target substrate and is laminated to the surface based on van der Waal interactions [13], [14].

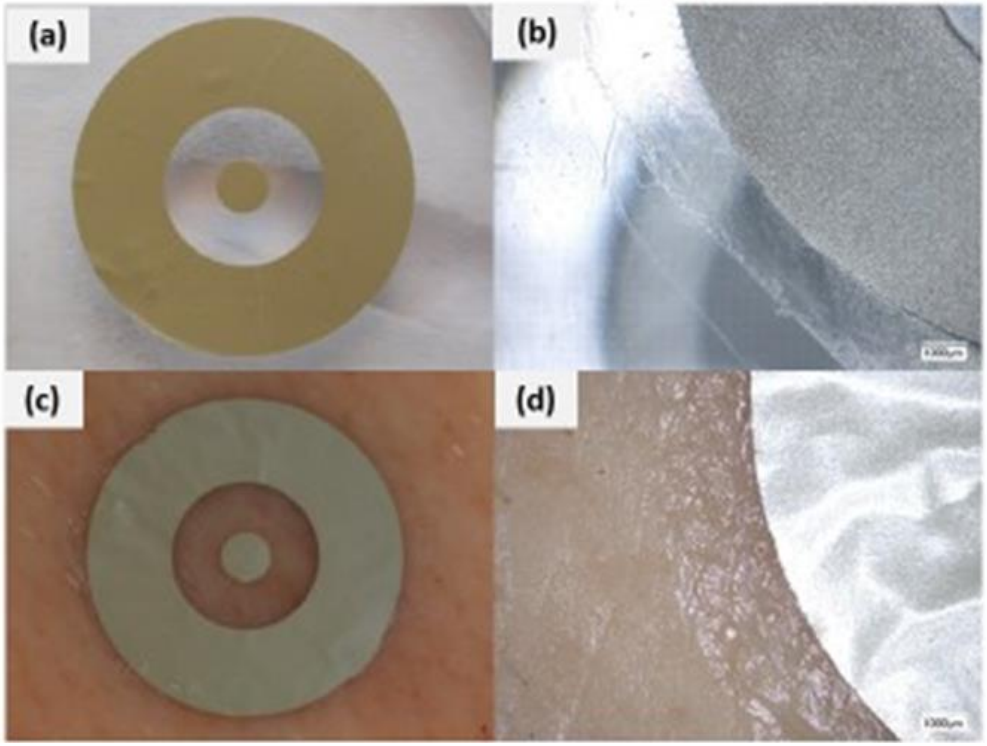

Figure 2.5 Silver tattoo electrodes applied on (a)–(b) hydrogel and (c)–(d) porcine skin. Magnified images of the electrodes on (b) hydrogel and (d) porcine skin.

The tattoo electrodes were also applied to and imaged on porcine skin (Fig. 2.5c). Porcine skin is well-known to have similarities to the human skin in many ways including in structure, thickness and hair follicle content [15]. From the magnified image in Fig. 2.2d, it can be seen that the tattoo adheres to the porcine skin, whereby the electrodes lie over the surface and rely on the more intimate contact of the transparent EC layer with the skin to hold it in place. Using a hand-held micrometre, the thickness of the printed electrodes was measured to be 10 ± 0.002 µm. Given that the skin roughness is reported as approx. 30 µm, it has been calculated that layers thicker than about 4 µm will not achieve conformal contact with skin [16]. Thus, due to their thickness, these screen-printed tattoo electrodes cannot have conformal contact with skin. The overlaying EC layer has a critical role in holding the electrodes in place given its ability to conformally contact with the skin surface because of its thinner (4 ± 0.002 µm) and more flexible form.

2.3.2 Characterisation of silver tattoo platform on hydrogel

Impedance measurements on hydrogels were first taken using tattoo electrodes which were applied according to Section 2.2.2. The Nyquist plot show the relationship between the real and imaginary components of complex impedance of the hydrogel when measured by the tattoo (Fig. 2.6). The spectrum suggests that two well-defined regions were observed by the tattoo electrodes whereby 2 distinct regions are observed: a time constant formed at the higher frequency range (semi-circular arc) while a second feature potentially including a second time constant was observed at the lower frequency range. The higher frequency range time constant was attributed to the bulk hydrogel. The lower frequency range includes a second possible time constant forming, which would be attributed to the tattoo electrode-hydrogel interface. It is possible that other contributions, such as, polarization of the electrode-hydrogel interface or diffusional properties were present in the lower frequency region [17], [18]. Another potential contribution at the lower frequency range would be changes in adherence over time. The tattoo electrodes are flexible, however the change at hydrogel surface could cause the tattoo electrodes to buckle or over stretch over time which could affect the electrical signal measured. These different contributions at the lower frequency make it challenging to model the electrode-hydrogel interface.

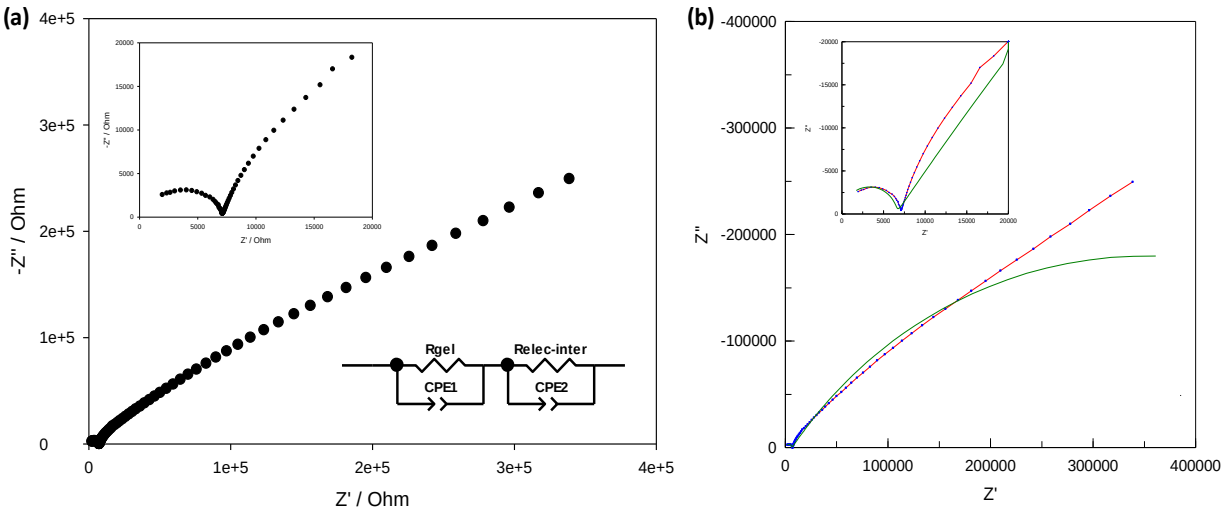

Figure 2.6. (a) Nyquist plot of PEDGE-Jeffamine hydrogel measured by the screen printed electrodes. Inset (top left) shows magnification of the plot at the higher frequency range and the inset (bottom right) shows the proposed circuit and (b) fitted impedance spectra, data points are in blue, interconnected with a red line, and the fits are shown in green).

Impedance spectroscopy can distinguish the individual contributions by modelling the data with a proposed circuit model. The circuit contains components that are representative of the system that is being studied. In this study the proposed circuit comprises of a constant phase element (CPE1) in parallel with a resistor (R_{gel}) representing the bulk hydrogel matrix, connected in series to a CPE (CPE2) and resistor ($R_{elec\text{-}inter}$) representing the tattoo electrode-hydrogel interface for the formation of the second time constant. The CPE component is typically used in circuits reflecting real cells that do not behave as ideal capacitors, which has been associated with surface roughness or non-uniform current distribution [20]. The corresponding Bode plot fitting can be seen in, Appendix, Fig. A2.A. The water content of the hydrogels was then varied over time via drying and immersion in water according to Section 2.2.6. The resulting Nyquist plots are shown in Fig. 2.7a & 2.7b. On varying the water content of the hydrogels, it was observed that the diameter of the high frequency semi-circular arc varied. In Fig. 2.7a, it can be seen that over time under drying conditions, the diameter of the arc increases across the real axis (Z'). It was also observed that there a trend of decreased overall impedance at the low frequency range and it was also observed that there was variation at these frequencies over time as the gel dehydrated. This suggests that there could potentially be changes in electrode adherence over time between the tattoo electrodes and the hydrogel surface. This change in adherence over time

due to dehydration of the hydrogel surface could affect the electrical signal generated by the tattoo electrodes. This indicates that consistent electrode contact and adherence over time on the target substrate are important considerations if the tattoo electrodes were to be used over a long period of time. However in this study, the bulk hydrogel matrix comprising of the polymer network interacting with both free and bound water [19] in the higher frequency range was the region of interest.

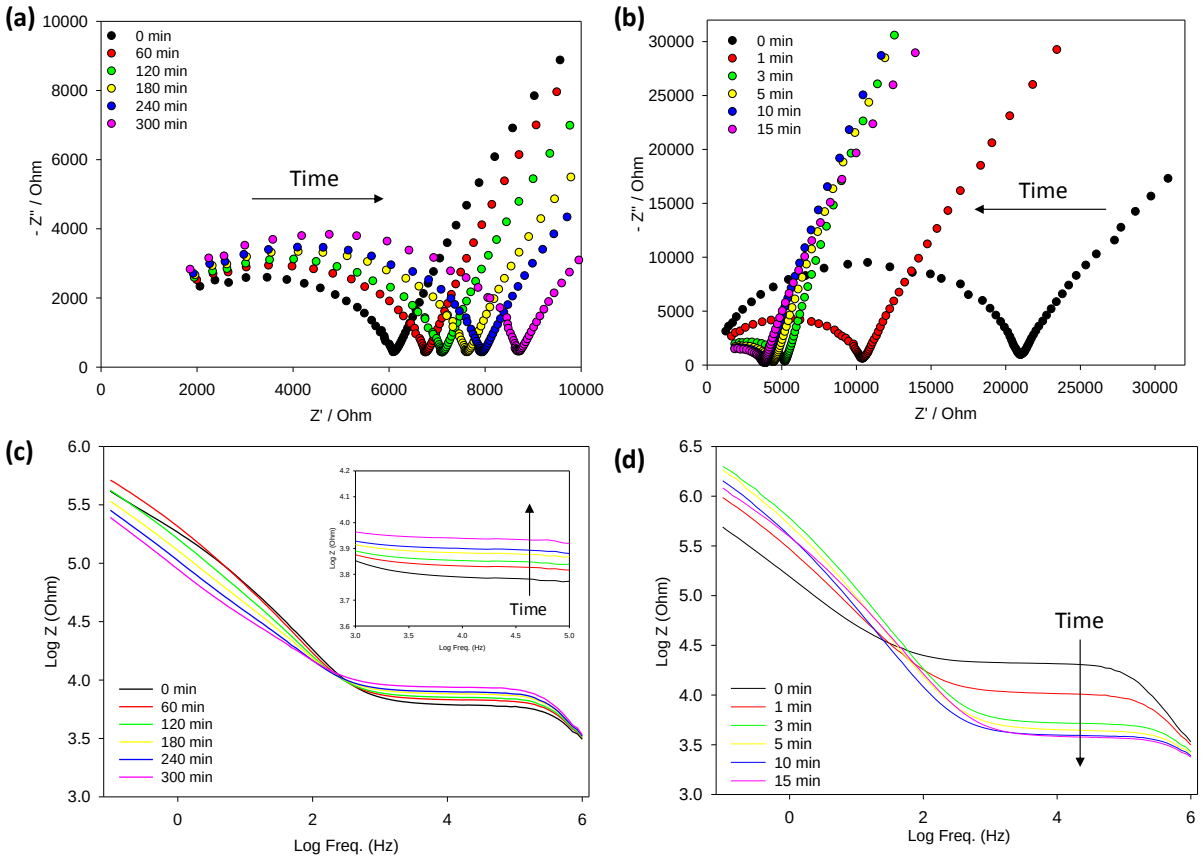

Figure 2.7 Representative Nyquist plots to show the magnification at the high frequency range PEDGE-Jeffamine hydrogels measured by the screen printed electrodes (a) dehydration and (b) hydration over time and corresponding representative (c) Impedance and (d) phase plots (n=3).

This result is attributed to the reduction of free water inside the polymer network [21] which leads to a collapse of the network due to a compressive stress induced as water evaporates. Fig. 2.77b shows the Nyquist plots during a hydration experiment. It can be seen that the opposite

effect occurs here whereby the diameter of the high frequency semi-circular arc decreases over time on the real axis (Z'). This decrease in diameter can be attributed to a diffusionally-controlled water uptake in the polymer. This uptake causes the hydration of the polymer chains which causes expansion. Over time, the polymer network relaxes and reaches equilibrium with the water. Using the proposed circuit in Fig. 2.6, values for R_{gel} were plotted against time. It can be seen that the value for R_{gel} increases linearly with time (Fig. 2.8a), reflecting the increase in hydrogel resistance as free water is lost from the network. This was validated by the MMD probe where a decrease in TDC was observed which indicates a decrease in water content (Fig. 2.8b).

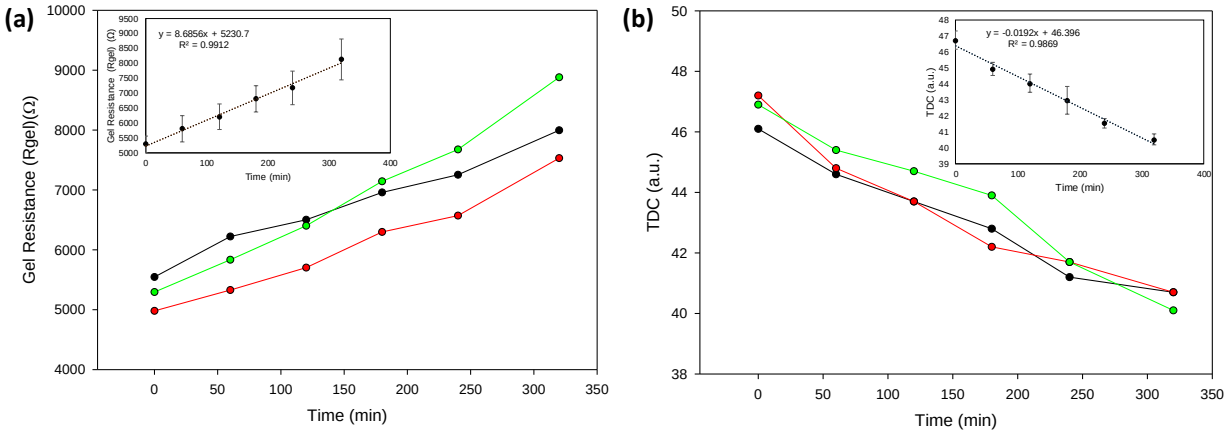

Figure 2.8 (a) Extracted R_{gel} values for hydrogel dehydration measured by the tattoo electrodes. Inset top left shows error bars and equation of the line. (b) TDC data taken by MMD probe on hydrogels plotted against time and inset top right shows error bars and equation of the line (n=3).

For the hydration experiment, the value for Rgel decreases exponentially as water is absorbed into the gel over time (Fig. 2.9a). This was further validated by the MMD probe where an increase in TDC was observed which indicates an increase in water content (Fig. 2.9b). As expected, different kinetics are observed for the dehydration and hydration experiments (Fig. 2.8 and 2.9). In the case of dehydration, the rate of change is observed as constant over the timescale of this experiment (300 min). The dominant kinetics in this experiment are likely to be evaporation-related. This surface-confined evaporation process is competing with a diffusional process from the bulk to the surface of the hydrogel, driven by the water concentration gradient generated via surface evaporation. In contrast, in the hydration experiment, the rate of change is much more rapid and is not constant. Equilibrium swelling is

reached within 6 min (Fig. 2.9a). It is important to note that the tattoo and MMD probe measurements have relatively shallow penetration depths relative to the depth of the hydrogel (10 mm).

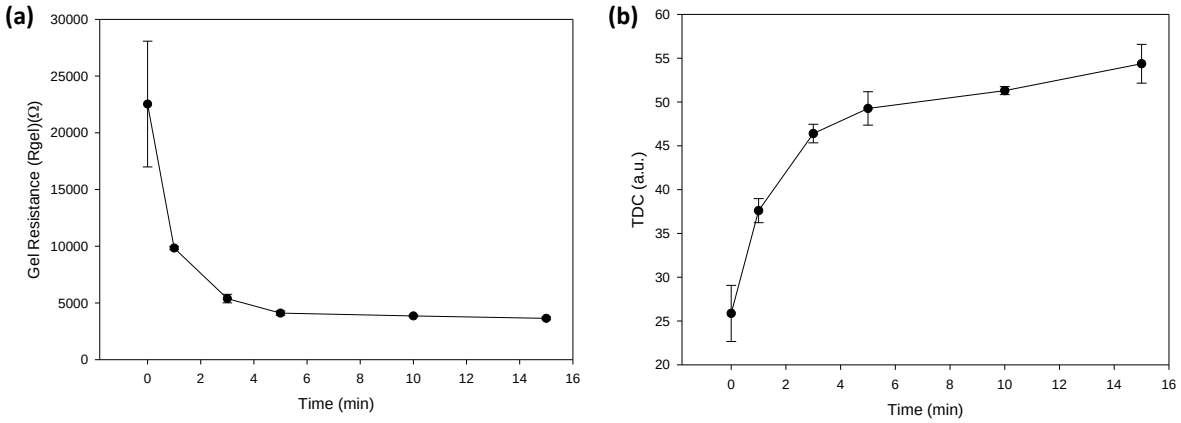

Figure 2.9 (a) Extracted R_{gel} values for hydrogel hydration measured by the tattoo electrodes and (b) TDC data taken by MMD probe on hydrogels plotted against time (n=3).

Thus, it is likely that this equilibrium state reached within this time is surface-localised. The graph displayed in Fig. 2.10 supports this conclusion as it shows the kinetics using gravimetric data taken during the hydration experiment. It was observed that the dehydration of the hydrogel is linear indicating that dehydration is a slow process, while the hydration of the hydrogel is not linear because the hydrogel absorbs water rapidly. The kinetics represented by the gravimetric data are different to the kinetics observed in the electrical data. This is because the gravimetric data represents the combined kinetics processes related to the bulk and surface of the gel, whereas the impedance and TDC data are surface confined measurements and hence only track changes within the surface layers.

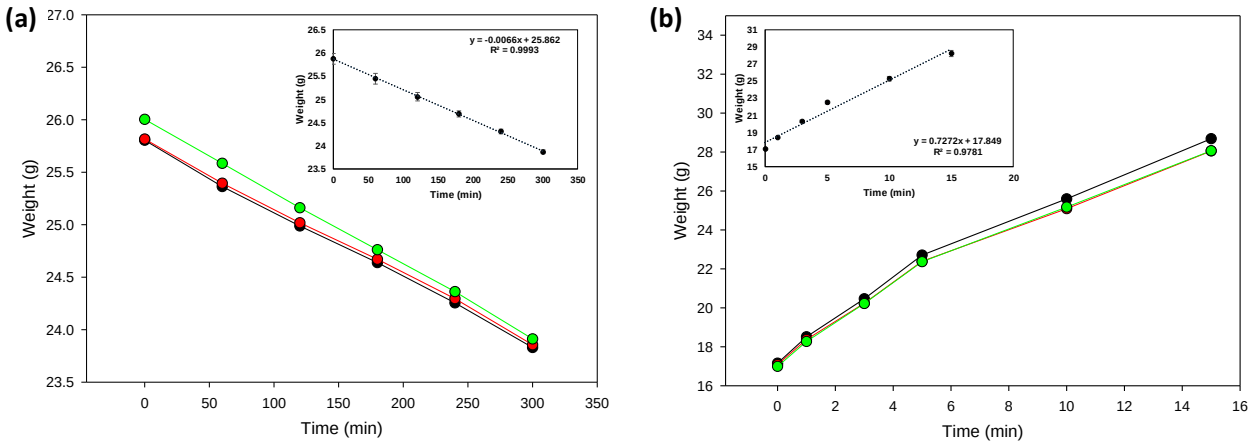

Figure 2.10 Gravimetric measurements of bulk hydrogel during (a) dehydration and (b) hydration of the hydrogel (n=3).

2.3.3 Effect of varying electrode configuration

Silver tattoos with varying configurations were investigated using impedance on hydrogels to determine how electrode configuration might influence the penetration depth of the tattoo. The distances were varied between 1mm, 2.5 mm, 3.0 mm and 3.5 mm distances between the inner and outer electrodes. The 3.0 mm tattoo electrode has an overall diameter of 20 mm while 1 mm, 2.5 mm and 3.5 mm have an overall diameter of 14 mm, therefore there is also a change in electrode area of the outer electrode that will be in contact with the hydrogel. The results were labelled based on the distance between the inner and outer electrode, while the area for each electrode configuration has been tabulated in Table 2.1. The Nyquist plots representing the different configurations can be seen in Figure 2.11. The resulting Nyquist plots observed show the formation of a semi-circular arc in the higher frequency range which was associated to the bulk hydrogel matrix and the formation of a second semi-circular arc associated with the tattoo electrode interface as mentioned early in Section 2.3.2.

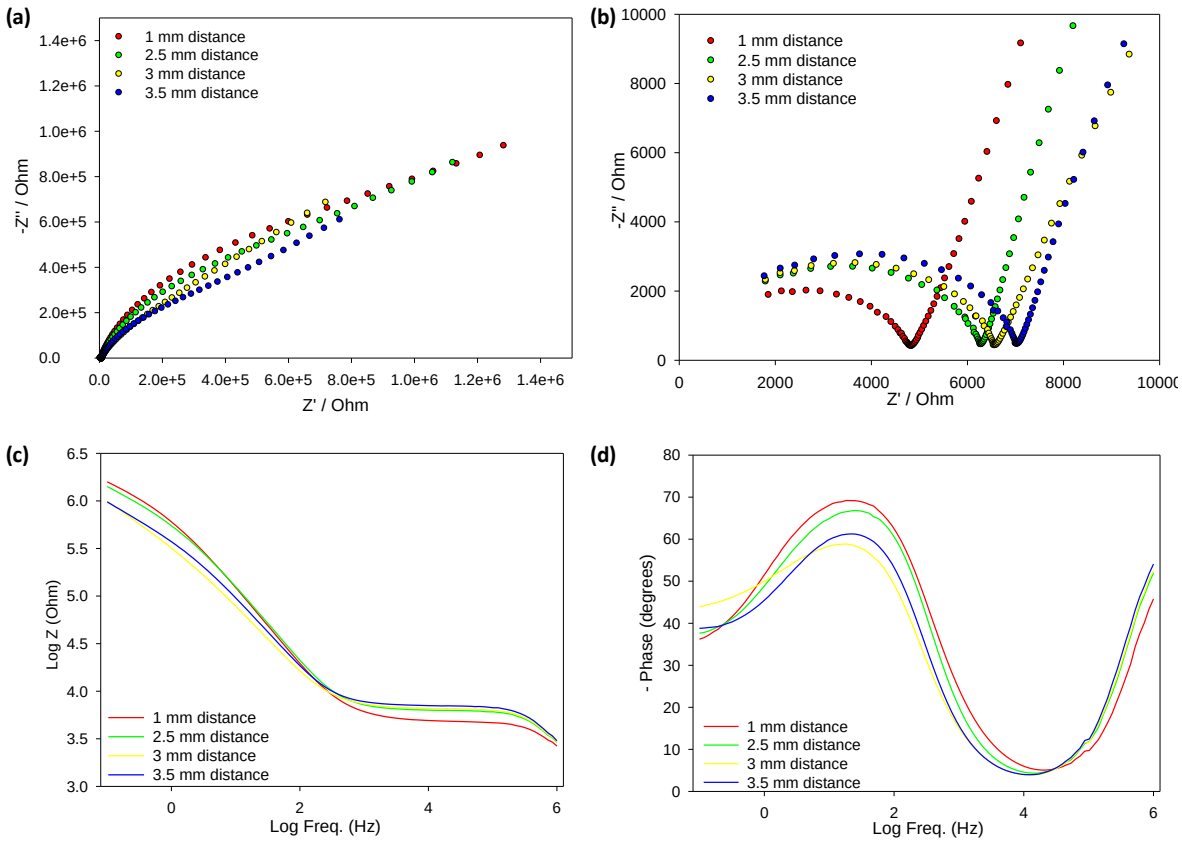

Figure 2.11 (a) Representative Nyquist plots of the PEDGE:Jeffamine hydrogels measured with screen printed electrodes varying in electrode configuration. (b) Magnification of the high frequency region and corresponding representative (c) Impedance and (d) phase plots (n=3).

The resulting Nyquist plots were fitted into the proposed equivalent circuit to compare the R_{gel} and $R_{elec\text{-}inter}$ values. The extracted R_{gel} values displayed in Fig. 2.12 show an increase in impedance as the distance between the inner and outer electrodes increases. It was expected that a change in electrode distance and electrode configuration would affect the measured impedance. The increasing trend seen for R_{gel} values is a result of the change in electrode distance but not area in contact with the hydrogel (n=3) (Table 2.1). It was expected that the electrode with a largest outer electrode area would have the lowest impedance as it is the largest contact with the hydrogel but the inner electrode area was kept constant which possibly made the electrode distance a dominant factor compared to outer electrode area. R. Ahmed *et al.*, has provided studies demonstrating that impedance of an electrochemical cell is affected by a change in electrode geometry [22]. Further understanding is required in order to understand the

influence and implications of changing these dimensions on the impedance measured for a wearable sensor which can become more complicated. This suggests that electrode design and configuration are parameters that can be used in future development of the electrodes but for the purpose of this study, the electrode with a 3.0 mm distance between the inner and outer electrode was chosen to be used for the study.

Table 2.1. Dimensions of the varying electrode configurations.

Distance between inner and outer electrodes	Area of inner electrode	Area of outer electrode
1.0 mm	7.07 mm^2	134.31 mm^2
2.5 mm	7.07 mm^2	109.76 mm^2
3.0 mm	7.07 mm^2	250.54 mm^2
3.5 mm	7.07 mm^2	67.35 mm^2

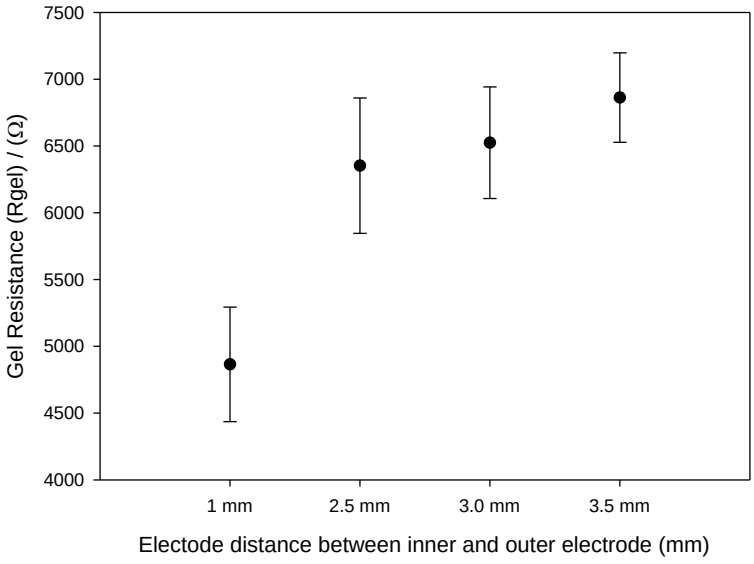

Figure 2.12 Extracted R_{gel} values for PEDGE: Jeffamine hydrogels measured with screen printed electrodes with varying electrode configurations (n=3).

2.3.4 Effect of hydrogel crosslinking ratios on hydration measurements

A series of hydrogels were prepared in which the molar ratio of the Jeffamine®:PEDGE (amine:epoxide) was adjusted according to the hydrogels synthesised by Mac Kenna *et al*. [10].

The relationship between the amine:epoxide molar ratios (1:1, 1:1.2 and 1:2 amine:epoxy and dehydration behaviour of the hydrogel were investigated impedimetrically. Different amine:epoxide ratios were used to mimic different skin types as an initial study before proceeding to porcine skin for that reason the tattoo electrodes were used to take once off measurements of the hydrogels over time. The tattoo electrodes were used to measure the changes in water content and corresponding gravimetric and hydration measurements using the MMD probe were also taken (n=1). The resulting Nyquist plots observed show the formation of a semi-circular arc in the higher frequency range which was associated to the bulk hydrogel matrix and the formation of a second semi-circular arc associated with the tattoo electrode interface as mentioned early in Section 2.3.2. The water content of the hydrogels were varied over time via drying and immersion in water according to Section 2.2.6. It was evident in the Nyquist plots (not shown) that varying the water affected the semi-circular arc attributed to the bulk hydrogel matrix, as discussed previously. Using the proposed circuit for the hydrogel system, values for R_{gel} were plotted against time and compared to TDC values from the MMD probe as seen in Fig. 2.13. Hydrogel ratios of 1.0:1.0 and 1.2:1.0 PEDGE:Jeffamine network showed similar slow dehydration profiles during the 300 min . As mentioned before this increasing trend in resistance is due to the compression of the hydrogel network over time as the water is lost. The polymer network containing the 2.0:1.0 PEDGE:Jeffamine network showed the largest change in R_{gel} after 180 min (Fig. 2.13a), suggesting that the higher epoxide content causes the polymer network to become denser at a faster rate as water evaporates from the surface compared to the hydrogels with lower epoxide ratios.

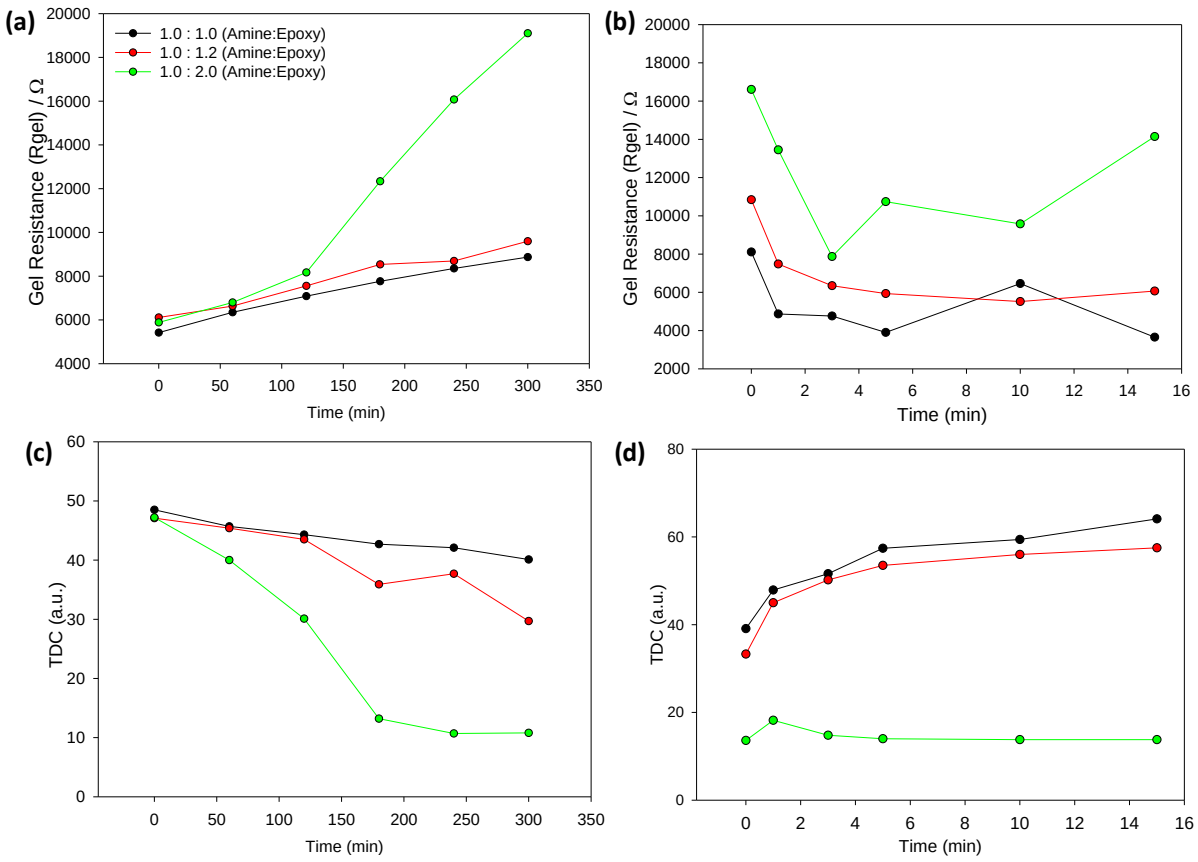

Figure 2.13 Different hydrogel crosslinking ratios measured using the tattoo electrodes during (a) dehydration and (b) hydration. Corresponding TDC measurements during (c) dehydration and (d) hydration (n=1).

This indicates that the properties of the crosslinked hydrogels depend on their crosslinking density, namely the ratio of moles of crosslinker to the moles of polymer units [23] which will affect the swelling property of the hydrogels. It is evident in the hydration experiments in Fig. 2.12 b that the 1.0:1.0 and 1.2:1.0 PEDGE :Jeffamine network produced the lower hydration response as it shows the lowest R_{gel} values while 2.0:1.0 PEDGE:Jeffamine network yielded the poorest response to water which is also supported by the TDC measurements (Fig. 2.13 (c) and (d).) and gravimetric data (Fig. 2.14)). This could be attributed to the probability of defects in the hydrogen bond network as increased cross-linking restricts the water uptake into the polymer network [24]. Mac Kenna *et al*. has attributed the poor swelling response to high crosslinking and poor ionisation whereby the network structure of the hydrogel becomes tighter, impairing the ionisation by electrostatic effects exerted by adjacent ionised amines [10]. This study was

able to verify that the tattoo electrodes were capable of tracking the surface changes in water content but also distinguish the different swelling responses of the different hydrogel networks.

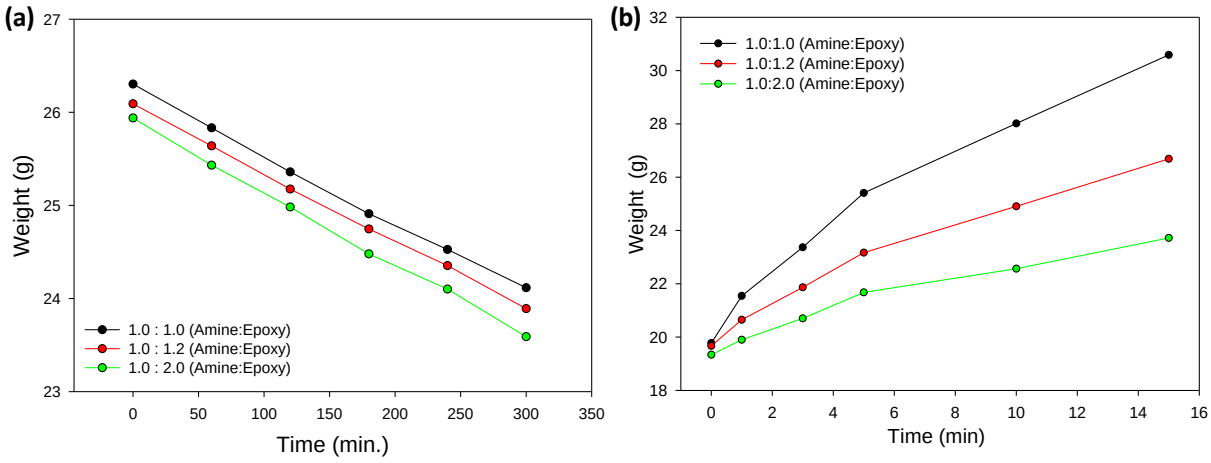

Figure 2.14 Gravimetric measurements of bulk hydrogels with varying PEDGE:Jeffamine crosslinking ratios (a) dehydration and (b) hydration (n=1).

2.3.5 Impedance analysis of porcine skin

Tattoo electrodes were applied to porcine skin and impedance measurements were taken in order to assess its performance. Porcine skin has been increasingly used as a mimic for human skin as it has anatomical and physiological similarities. Porcine skin has an SC thickness of approximately. 20-30 µm, which is comparable to that in humans [25], [26]. The human and porcine SC contains keratin protein in corneocytes and it is the hydration state of the keratinized tissue that can be important for its barrier function.

Initially, the tattoo electrodes were applied to porcine skin (according to Section 2.2.2.) that had been immersed in water for 24 hr. The resulting Nyquist plot can be seen in Fig. 2.15. The plot presents two well-defined regions: a semi-circle at high frequencies and the opening of a second semi-circle at lower frequencies. The semi-circle at high frequency range represents the time constant for the skin, whereas the opening of the semi-circle at lower frequency range can be attributed to the electrode-skin interface. Several equivalent circuits for skin have been proposed in literature [27]–[29] and a circuit commonly cited has been modified and used here [30]–[32].The circuit consists of ohmic resistance of the deeper viable tissue of the epidermis (R_{vt}) in

series with two parallel combinations of resistors and CPEs. The first parallel combination represents the resistance associated with the SC (R_{sc}) in combination with a related CPE (CPE1). Overall, this time constant represents the impedance associated with the ion conductive pathways of the intra- and extra-cellular compartments of the SC [30]–[32]. The second combination of resistor ($R_{elec/inter}$) and CPE (CPE2) represents the electrode-skin interface. The corresponding Bode plot fitting can be seen in, Appendix, Fig. A2.B.

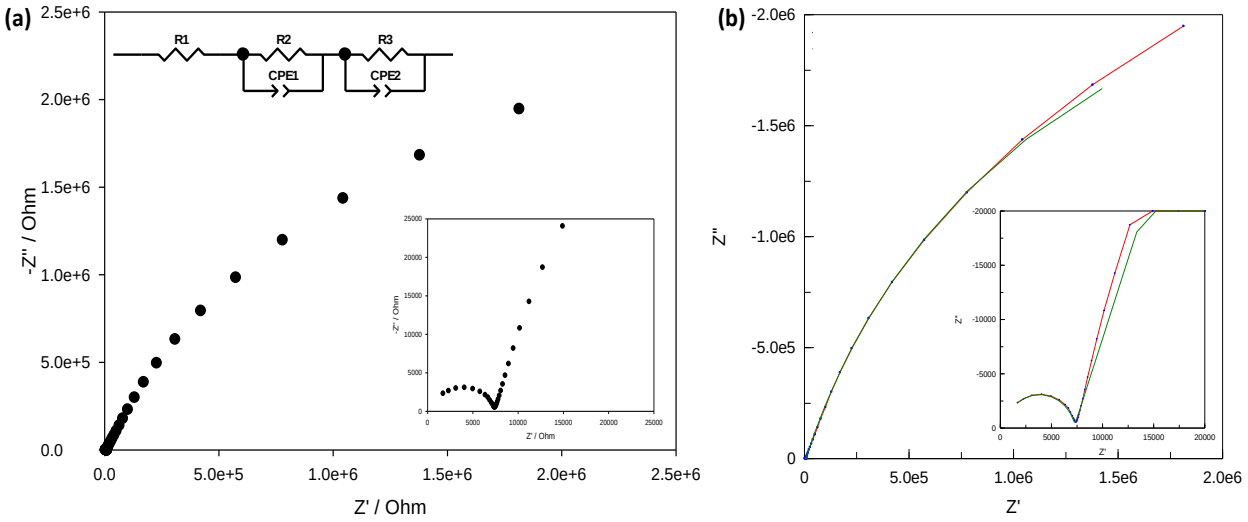

Figure 2.15 (a) Nyquist plot of porcine skin after 24 hr in DIW measured by the screen printed electrodes. Inset (bottom right) shows magnification of the plot at the higher frequency range and the inset (top left) shows the proposed circuit and (b) fitted impedance spectra, data points are in blue, interconnected with a red line, and the fits are shown in green).

Using a similar approach to the hydrogel study, the water content of the SC of porcine skin (according to Section 2.2.7) was varied via dehydration (via drying) and hydration (via topical water application). The resulting Nyquist plots are shown in Fig. 2.16a & b. It can be seen that both upon drying and exposure to water, the diameter of the high frequency semi-circular arc, representing the time constant for the SC varied. In Fig. 2.16a, it can be seen that over time under drying conditions the diameter of the semi-circular arc at high frequencies increased. This result is attributed to changes in the electrical conductivity of the keratinized tissue of the SC [32]. The water loss in the SC causes the inter-chain packing of the keratin to become dense

which results in an increased SC resistance [33]. Fig. 2.16b, shows the Nyquist plots after a number of topical applications of water. The semi-circular arc diameter at high frequency decreases as the number of topical applications of water increases. This decrease in diameter is attributed to the uptake of water by the SC whereby the packing of the keratin expands with larger inter-chain spacing, as a result reducing the impedance of the SC. As such, the water content of the SC can be understood as a hydration state of the keratin protein.

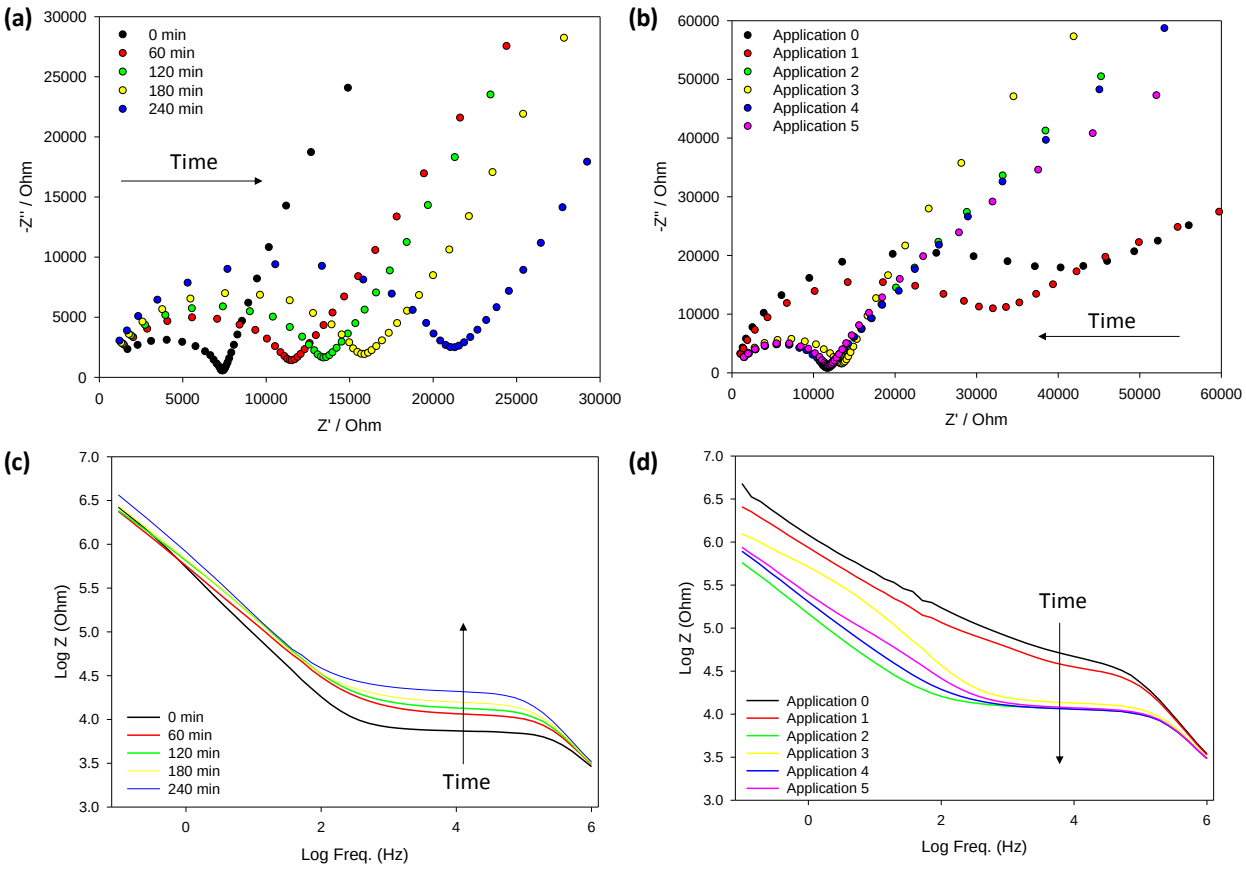

Figure 2.16 Representative Nyquist plots of porcine skin magnified at the high frequency range (a) dehydration and (b) hydration and corresponding representative (c) Impedance and (d) phase plots (n=3).

At low hydration levels, the keratin structures are densely packed. While fully hydrated structures have expanded corneocytes and wide inter-chain spacing whereby all water binding sites within the keratin are occupied. This hydrophilic property of the keratin can impart the

observed varying electrical behaviours to the SC upon hydration and dehydration. Using the proposed circuit, extracted values for the R_{sc} were plotted for the dehydration and hydration experiments. It can be seen that for the dehydration of porcine skin, the value of R_{sc} increases linearly with time (Fig. 2.17a). It is interesting to note that the corresponding plot for the TDC values shows a different kinetic profile whereby a minimum TDC value is reached after 120 min, indicating that an equilibrium state was being reached. The differences could be due to the different electric field penetration depths for the tattoo and the MMD probe.

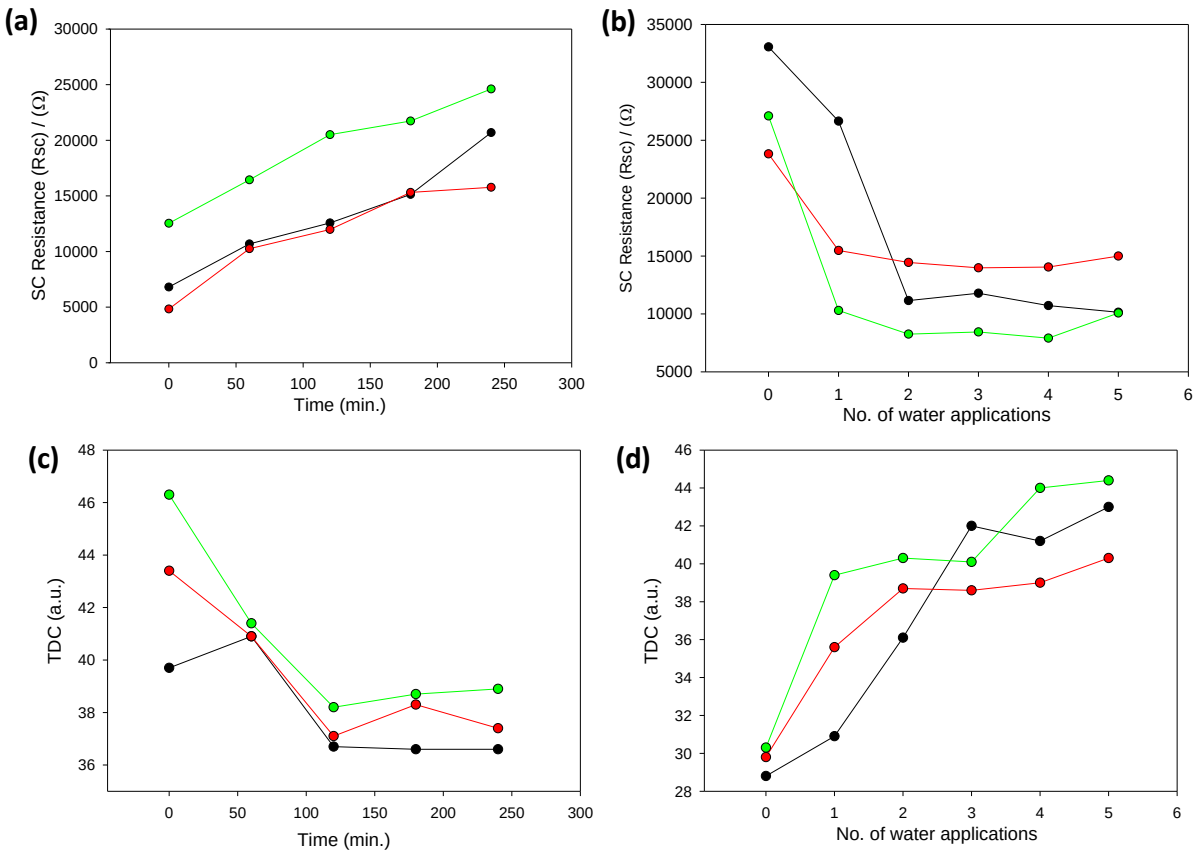

Figure 2.17 Dehydration and hydration results observed for the porcine skin using (a)-(b) extracted resistance measurements (Rsc) from the tattoo electrodes and (c)-(d) TDC measurements taken by the MMD probe (n=3).

The effective depth of the MMD probe was 0.5 mm which is significantly deeper than the depth of the SC (20-30 µm). Thus, the measurements taken by the MMD probe are likely to be measuring the water content from the outer surface down to a depth of approximately 0.5 mm.

The tattoo on the other hand, will likely have a much shallower depth of penetration, which is not likely to exceed the depth of SC given the frequency range used (up to 1 MHz). In the same manner as observed for the hydration of the hydrogel, the value of Rsc decreases rapidly as the water is imbibed by diffusion into the SC (Fig. 2.17b), before reaching equilibrium. This suggests the keratin sites of the SC became fully swollen after just 2 topical water applications. The kinetics observed for the tattoo-based measurements are in broad agreement with those observed the MMD probe (Fig. 2.17c and d).

2.3.6 Impedance analysis of human skin and its challenges

As a proof of concept, a human skin equivalent (HSE) was characterised and compared against human skin. These skin equivalents are available as full thickness living skin equivalent models, consisting of a dermal equivalent of polymerized fibrin containing primary adult human fibroblasts and a well differentiated, air-exposed epidermis [34]. The tattoo electrodes were applied on the HSE and an impedance measurement was taken. It was observed that there were two distinct regions, a semi-circle at the low frequency range potentially attributed to the HSE and a semi-circle at the high frequency range attributed to the skin-electrode interface (Fig. 2.18a). The tattoo electrodes were also applied on to human skin and an impedance measurement was taken, a single semi-circle was observed (Fig. 2.18b). It can been seen that HSE has a lower resistance compared to human skin, indicating that the HSE is less resistive than human skin. This trend was also observed in the Bode plots seen in the Appendix, Fig. A2.C where the HSE had a lower overall impedance compared to human skin. This result was validated by TDC measurements conducted by E. Duffy et *al*. which showed the HSE to have a higher TDC (56.3 ± 5.7) than human skin (Male TDC: 36.0 ± 4.0 female TDC: 29.9 ± 2.1) [11]. This could be due to the HSE being kept in a regulated environment compared to human skin where it is exposed to a constantly changing environment. It was also observed that the tattoo measurements indicate that the impedance measured for male skin had a smaller semi-circle while the measured impedance for women had a larger semi-circle. This suggest that there is potential for epidermal sensors to differentiate between parameters such as gender, age or skin type based on the electrical signal measured. Dabrowska *et al*., has discussed that skin properties can vary among individuals of different age, gender, ethnicity and skin types [35]. The hydration levels and permeability of skin can change due to age, environment, nutrition and disease which in turn can have an effect on elasticity, skin roughness and susceptibility of microbes penetrating the

skin barrier [35]. However, further investigation of a larger population using the tattoo electrodes would be required in order to fully understand these electrical signals from skin and its relationship between gender, age, anatomical site and skin type.

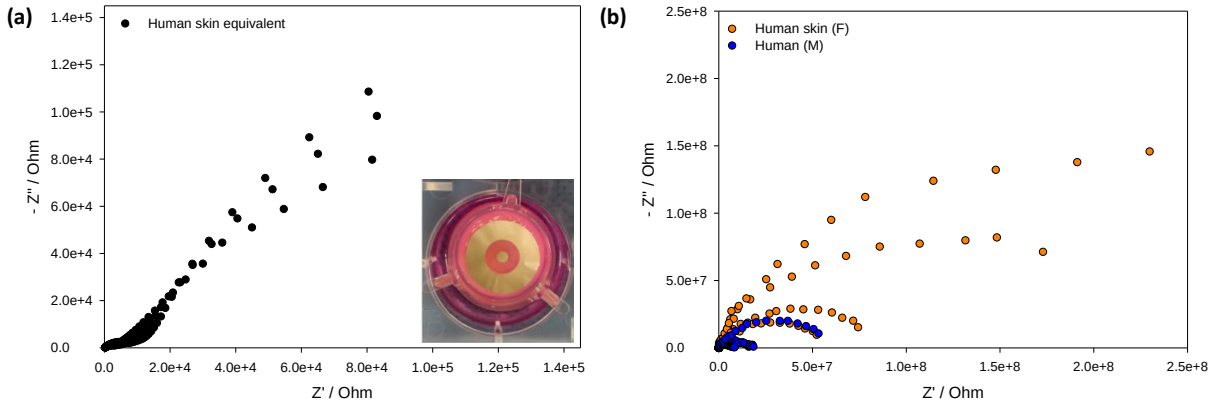

Figure 2.18 Nyquist plots of (a) human skin equivalent (n=3), bottom right inset image of labskin with tattoo electrodes and (b) human skin (n=8) measured using the tattoo sensor.

Nguyen *et al*. demonstrated that the contact impedance in the more invasive case such as having electrodes under the skin were significantly lower than the non-invasive case [36]. The issue with using an invasive or implantable sensor would be irritation, discomfort and possibly infection. This opens up an opportunity for non-invasive wearable sensors. As another proof of concept, the tattoo electrodes were applied to human skin in order to determine if impedance spectra could be taken on live tissue using this tattoo. In this case, a wearable tattoo-based sensor was applied to the inner forearm of the skin after pre-treatment and an impedance measurement was taken. A tattoo was then applied and 4 impedance spectra were taken sequentially using the same tattoo. Unlike the porcine skin pieces which were fully immersed in water before the dehydration experiment, the human skin was topically treated with water. The resulting Nyquist plots can be seen in Fig. 2.19, whereby the Nyquist plot at t=0 shows a single semi-circular arc that doesn't fully close. It can be seen by the scale of the real axis, that the resistances associated with human skin are significantly greater than those of porcine skin. Overtime, as water within the SC is lost, the diameter of the semi-circular arc increases. A similar trend was observed in the Bode plots where an increase in impedance was observed when there was a decrease in water content. The corresponding Bode plots are shown in the Appendix, Fig. A2.D.

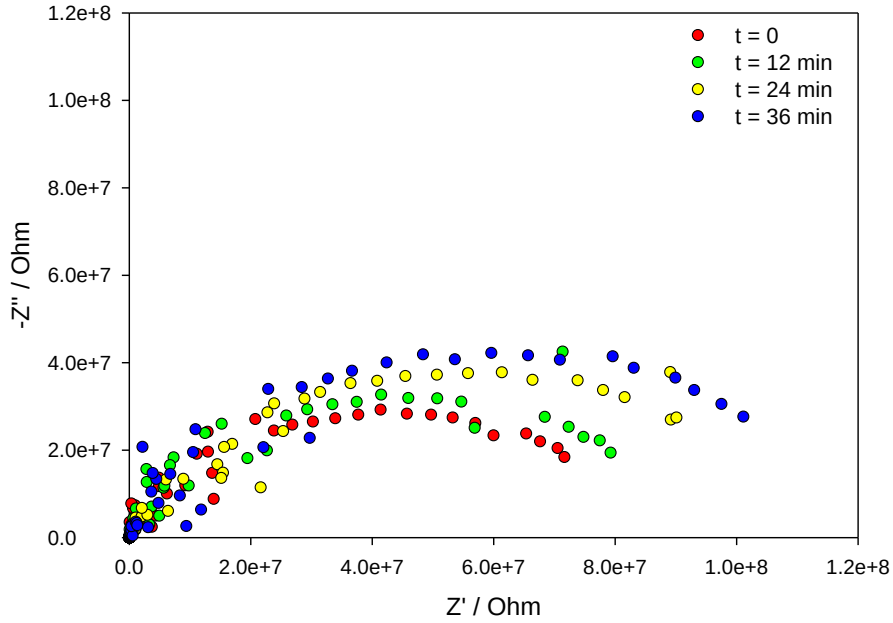

Figure 2.19 Nyquist plots showing impedance measurements of skin drying over time using the screen printed silver platform. Corresponding Bode plots can be found in Appendix, Fig. A2.D.

It is important to note that these Nyquist plots likely contain convoluted data relating to both the SC as well as the electrode-skin interface. Non-invasive impedance measurements of skin are dependent on the measuring frequency where higher frequency measurements reflect the deeper, viable layer while low frequency measurements are dominated by the SC [37], [38]. It was also observed that there was noise at the lower frequency (approx. 100 Hz) indicating that there could be potentially issues with skin adherence of the tattoo electrodes over time. For a two concentric electrode system, Martinsen *et al.* found by means of finite element calculations, that viable skin represented about 10% of the measured impedance at 1 kHz and represented about 90% of impedance at 100 kHz. Therefore the SC dominates in the lower frequencies below approx. 1 kHz [37] in human skin. It is possible that effects from the SC and viable skin can be observed between 1 kHz and 1 MHz, while lower frequencies represent possibly be a combination of effects from the SC-electrode interface. Total impedance values taken at 1 kHz were plotted against time (Fig. 2.20). A trend of increasing impedance was observed, which could be attributed to the change in the hydration levels of the skin over time. These measurements correlate with decreasing TDC values as measured by the MMD probe (Fig. 2.20). This trend is

consistent with decreasing electrical conductivity with decreasing hydration. A similar trend of increased impedance and decreased hydration levels from another epidermal sensor platform and hydration probe were observed when Huang *et al.* monitored hydration states of skin impedimetrically [39]. In this instance, the epidermal sensors were coupled with epidermal electronics and the devices were fabrications using lithographic procedures. This was repeated for a longer period of time (data shown in Appendix, Fig. A2.E), a similar trend was observed were impedance was low when there is high water content and impedance was high when there is low water content. However, it was observed that the tattoo electrodes were slowly buckling over time which indicates that this platform might not be suitable for long term measurement.

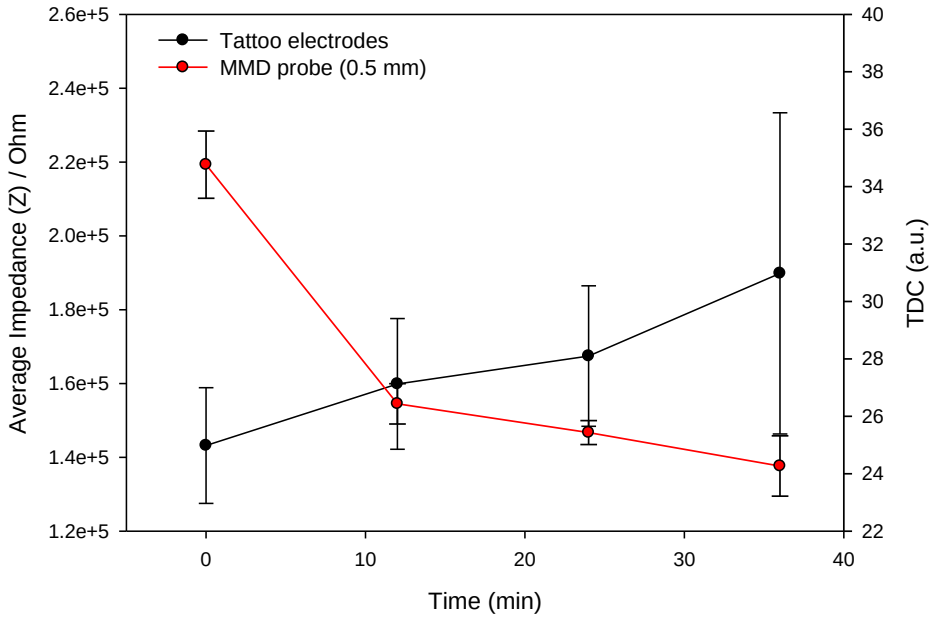

Figure 2.20 Isolated Z values taken from impedance spectra using the tattoo electrodes on human skin during dehydration and corresponding TDC measurements (n=3).

Overall, the screen-printed tattoo electrodes reported here were capable of detecting electrical changes in the SC which were related to hydration levels and were validated by the MMD probe. Impedance as a technique is highly sensitive and non-invasive and here, when combined with an epidermal tattoo platform has the potential to be used to interrogate and track human skin barrier hydration status.

2.4 Conclusion

The purpose of this study was to fabricate and characterise a low-cost, non-invasive screen-printed tattoo sensor to monitor skin barrier quality for the future application in health monitoring. The work demonstrated that a tattoo sensor comprising two concentric electrodes can be easily fabricated at large-scale using a screen-printing method. The tattoo sensor was shown to be able to impedimetrically track changes in hydration state of a soft tissue mimic and porcine skin which were then validated by TDC measurement. It was observed that there was an increase in impedance when water content was low, while a decrease in impedance indicated an increased water content. Preliminary results on a human skin equivalent indicate that it had a lower skin resistance compared to human skin. This could be due to the regulated environment where the HSE was kept compared to human skin which is constantly exposed to a changing environment. However, the HSE can potentially be employed as an early testing system for *in vivo* experiments using the tattoo sensors. It can potentially be used to test materials that haven't been used before on human skin as well investigations that would not be suitable on humans such microbial studies or new skin moisturising formulations. However, these HSEs can be expensive and require a constantly regulated environment because it can become contaminated when exposed to a non-regulated environment. Initial results on human skin were also presented and show promise for the non-invasive assessment of skin barrier status through impedance measurements. It was observed that the changes in water content can be tracked using the tattoo sensor. However, there are issues with skin adherence over time indicating that this platform is more suited for single measurements. Developing epidermal sensors that can move and flow with the skin is an on-going challenge in this research area. Thus, part of our future effort will be aimed at developing materials whereby thinner and more conformal conducting materials can be fabricated in to tattoos to enhance electrode-skin contact, adherence and mechanical stability under stress. This will open up new opportunities for the innovative approaches in material science that can address issues such as durability and long-term use of the tattoo-based sensor. Future efforts can also be focussed on tracking changes in skin barrier function using epidermal sensors. Tracking acute changes to the skin barrier using a wearable such as this could aid in diagnosis and management of diseases such as atopic dermatitis and psoriasis. Other skin properties, such as skin pH and TEWL will be considered as sensing targets. The tattoo-based sensor approach reported here has promise in health diagnostics as well as potential in human performance applications. In summary, this tattoo sensor is a step towards a simple and low-

cost, non-invasive wearable capable of measuring the impedance of skin and changes related to skin barrier function.

2.5 References

[1] J. A. Bouwstra and M. Ponec, "The skin barrier in healthy and diseased state," *Biochim. Biophys. Acta*, vol. 1758, no. 12, pp. 2080–2095, 2006.

[2] J. A. Segre, "Epidermal barrier formation and recovery in skin disorders," *J. Clin. Invest.*, vol. 116, no. 5, pp. 1150–1158, 2006.

[3] A. P. M. Lavrijsen, J. A. Bouwstra, G. S. Gooris, A. Weerheim, H. E. Bodde, and M. Ponec, "Reduced skin barrier function parallels abnormal stratum corneum lipid organization in patients with lamellar ichthyosis," *J. Invest. Dermatol.*, vol. 105, no. 4, pp. 619–624, 1995.

[4] D. Bommannan, R. O. Potts, and R. H. Guy, "Examination of the effect of ethanol on human stratum corneum in vivo using infrared spectroscopy," *J. Control. Release*, vol. 16, no. 3, pp. 299–304, 1991.

[5] Y. Werner and M. Lindberg, "Transepidermal Water Loss in Dry and Clincally Normal Skin in Patients with Atopic Dermatitis," *Acta Derm Venereol*, 1985.

[6] A. Di Nardo, P. Wertz, A. Giannetti, and S. Seidenari, "Ceramide and cholesterol composition of the skin of patients with atopic dermatitis," *Acta Derm. Venereol.*, vol. 78, no. 1, pp. 27–30, 1998.

[7] J. R. Windmiller, A. J. Bandodkar, G. Valdés-Ramírez, S. Parkhomovsky, A. G. Martinez, and J. Wang, "Electrochemical sensing based on printable temporary transfer tattoos," *Chem. Commun.*, vol. 48, no. 54, pp. 6794–6796, 2012.

[8] H. N. Mayrovitz, A. Grammenos, K. Corbitt, and S. Bartos, "Age-related changes in male forearm skin-to-fat tissue dielectric constant at 300 MHz," *Clin. Physiol. Funct. Imaging*, pp. 1–7, 2015.

[9] H. N. Mayrovitz, A. Grammenos, K. Corbitt, and S. Bartos, "Young adult gender differences in forearm skin-to-fat tissue dielectric constant values measured at 300 MHz," *Ski. Res. Technol.*, vol. 22, no. 1, pp. 81–88, 2016.

[10] N. Mac Kenna, P. Calvert, and A. Morrin, "Impedimetric transduction of swelling in pH-responsive hydrogels," *Analyst*, vol. 140, no. 9, pp. 3003–3011, 2015.

[11] E. Duffy, K. De Guzman, R. Wallace, R. Murphy, and A. Morrin, “Non-Invasive Assessment of Skin Barrier Properties: Investigating Emerging Tools for In Vitro and In Vivo Applications,” *Cosmetics*, vol. 4, p. 44, 2017.

[12] S. H. Hamed, B. Altrabsheh, T. Assa’d, S. Jaradat, M. Alshra’ah, A. Aljamal, H. S. Alkhatib, and A. M. Almalty, “Construction, in vitro and in vivo evaluation of an in-house conductance meter for measurement of skin hydration,” *Med. Eng. Phys.*, vol. 34, no. 10, pp. 1471–1476, 2012.

[13] D.-H. Kim, N. Lu, R. Ma, Y.-S. Kim, R.-H. Kim, S. Wang, J. Wu, S. M. Won, H. Tao, A. Islam, K. J. Yu, T. Kim, R. Chowdhury, M. Ying, L. Xu, M. Li, H.-J. Chung, H. Keum, M. McCormick, P. Liu, Y.-W. Zhang, F. Omenetto, Y. Huang, T. Coleman, and J. A. Rogers, “Epidermal Electronics,” vol. 333, pp. 838–843, 2011.

[14] A. Zucca, C. Cipriani, Sudha, S. Tarantino, D. Ricci, V. Mattoli, and F. Greco, “Tattoo Conductive Polymer Nanosheets for Skin-Contact Applications,” *Adv. Healthc. Mater.*, vol. 4, no. 7, pp. 983–990, 2015.

[15] A. Summerfield, F. Meurens, and M. E. Ricklin, “The immunology of the porcine skin and its value as a model for human skin,” *Mol. Immunol.*, vol. 66, no. 1, pp. 14–21, 2015.

[16] S. Wang, M. Li, J. Wu, D.-H. Kim, N. Lu, Y. Su, Z. Kang, Y. Huang, and J. A. Rogers, “Mechanics of Epidermal Electronics,” *J. Appl. Mech.*, vol. 79, no. 3, p. 31022, 2012.

[17] R. R. Silva, S. V. De Lima, G. H. R. C. Silva, H. P. De Oliveira, M. D. L. Oliveira, and C. a S. Andrade, “Dielectric behavior of alginate-based hydrogel containing neomycin-loaded lipid nanovesicles under influence of electrical potentials,” *J. Braz. Chem. Soc.*, vol. 27, no. 1, pp. 77–83, 2016.

[18] H. Warren, R. D. Gately, P. O’Brien, R. Gorkin, and M. In Het Panhuis, “Electrical conductivity, impedance, and percolation behavior of carbon nanofiber and carbon nanotube containing gellan gum hydrogels,” *J. Polym. Sci. Part B Polym. Phys.*, vol. 52, no. 13, pp. 864–871, 2014.

[19] D. Pasqui, M. De Cagna, and R. Barbucci, “Polysaccharide-based hydrogels: The key role of water in affecting mechanical properties,” *Polymers (Basel).*, vol. 4, no. 3, pp.

1517–1534, 2012.

[20] J.-B. Jorcin, M. E. Orazem, N. Pébère, and B. Tribollet, “CPE analysis by local electrochemical impedance spectroscopy,” *Electrochim. Acta*, vol. 51, no. 8–9, pp. 1473–1479, 2006.

[21] Y. Sekine and T. Ikeda-Fukazawa, “Structural changes of water in a hydrogel during dehydration,” *J. Chem. Phys.*, vol. 130, no. 3, pp. 1–8, 2009.

[22] R. Ahmed and K. Reifsnider, “Study of Influence of Electrode Geometry on Impedance Spectroscopy,” *Int. J. Electrochem. Sci*, vol. 6, pp. 1159–1174, 2011.

[23] F. Ganji, S. Vasheghani-Farahani, and E. Vasheghani-Farahani, “Theoretical Description of Hydrogel Swelling: A Review,” *Iran. Polym. J.*, vol. 19, no. 5, pp. 375–398, 2010.

[24] T. Terada, Y. Maeda, and H. Kitano, “Raman Spectroscopic Study on Water in Polymer Gels,” *J. Phys. Chem.*, vol. 97, no. 14, pp. 3619–3622, 1993.

[25] D. Bissett and J. McBride, “The use of the domestic pig as an animal model of human dry skin and for comparison of dry and normal skin properties,” *J Soc Cosmet Chem*, vol. 326, pp. 317–326, 1983.

[26] S. a. Hammond, C. Tsonis, K. Sellins, K. Rushlow, T. Scharton-Kersten, I. Colditz, and G. M. Glenn, “Transcutaneous immunization of domestic animals: Opportunities and challenges,” *Adv. Drug Deliv. Rev.*, vol. 43, no. 1, pp. 45–55, 2000.

[27] S. J. Dorgan and R. B. Reilly, “A model for human skin impedance during surface functional neuromuscular stimulation.,” *IEEE Trans. Rehabil. Eng.*, vol. 7, no. 3, pp. 341–348, 1999.

[28] F. Clemente, P. Arpaia, and C. Manna, “Characterization of human skin impedance after electrical treatment for transdermal drug delivery,” *Meas. J. Int. Meas. Confed.*, vol. 46, no. 9, pp. 3494–3501, 2013.

[29] R. Ivanic, I. Novotny, V. Rehacek, V. Tvarozek, and M. Weis, “Thin film non-symmetric microelectrode array for impedance monitoring of human skin,” *Thin Solid Films*, vol. 433, pp. 332–336, 2003.

[30] T. Yamamoto and Y. Yamamoto, “Non-linear electrical properties of skin in the low frequency range.,” *Med. Biol. Eng. Comput.*, vol. 19, no. 3, pp. 302–310, 1981.

[31] E. A. White, M. E. Orazem, and A. L. Bunge, “Characterization of damaged skin by impedance spectroscopy: Chemical damage by dimethyl sulfoxide,” *Pharm. Res.*, vol. 30, pp. 2607–2624, 2013.

[32] J. L. Leveque and J. De Rigal, “Impedance Methods for Studying Skin Moisturization,” *J. Soc. Cosmet. Chem.*, vol. 34, pp. 419–428, 1983.

[33] S. Björklund, T. Ruzgas, A. Nowacka, I. Dahi, D. Topgaard, E. Sparr, and J. Engblom, “Skin membrane electrical impedance properties under the influence of a varying water gradient,” *Biophys. J.*, vol. 104, no. 12, pp. 2639–2650, 2013.

[34] R. Bojar, “Studying the Human Skin Microbiome Using 3D In Vitro Skin Models,” *Appl. Vitr. Toxicol.*, vol. 1, no. 2, pp. 165–171, 2015.

[35] A. K. Dąbrowska, F. Spano, S. Derler, C. Adlhart, N. D. Spencer, and R. M. Rossi, “The relationship between skin function, barrier properties, and body-dependent factors,” *Ski. Res. Technol.*, vol. 24, pp. 165–174, 2018.

[36] D. T. Nguyen, R. Kosobrodov, M. A. Barry, W. Chik, C. Jin, T. I. Oh, A. Thiagalingam, and A. McEwan, “Electrode-Skin contact impedance: In vivo measurements on an ovine model,” *J. Phys. Conf. Ser.*, vol. 434, p. 12023, Apr. 2013.

[37] Ø. G. Martinsen, S. Grimnes, and E. Haug, “Measuring depth depends on frequency in electrical skin impedance measurements,” *Ski. Res. Technol.*, vol. 5, no. 3, pp. 179–181, 1999.

[38] U. Birgersson, E. Birgersson, and S. Ollmar, “Estimating electrical properties and the thickness of skin with electrical impedance spectroscopy: Mathematical analysis and measurements,” *J Electr Bioimp*, vol. 3, pp. 51–60, 2012.

[39] X. Huang, W.-H. Yeo, Y. Liu, and J. A. Rogers, “Epidermal differential impedance sensor for conformal skin hydration monitoring.,” *Biointerphases*, vol. 7, no. 1–4, p. 52, Dec. 2012.

Chapter 3

Approaches to Enhance Skin Adherence of Tattoo Sensor

3.1 Introduction

In Chapter 2, a tattoo sensor platform using a flexible commercial ink was fabricated and characterised as a wearable sensor to impedimetrically measure the electrical characteristics of skin. This initial platform showed promise for the non-invasive assessment of the skin barrier and it allowed for good electrical contact with skin for single measurements. However, it did not possess the appropriate mechanical properties for longer-term wear. Therefore strategies to allow for improved mechanical stability and electrical contact are required to improve the wearability in terms of robustness and to develop this wearable sensor for long-term monitoring.

Across the development of skin-based wearable sensors, it is clear that these sensors need to adhere well to the complex three dimensional curvature of the human body [1]. In order for these sensors to remain consistently adhered to skin overtime and during motion, different strategies have been employed. For example the use of adhesives to adhere onto skin as well as the development of stretchable materials to allow for the wearable device to stretch and move when worn on the body are being developed. Medical grade adhesives can be used to mount a planar sensor directly on to the skin and ensure consistent adherence to skin [2], [3]. The main purpose of the adhesive is to reduce delamination of the wearable device keeping it in place. Importantly, adhesives are typically resistive in nature, resulting in the physical and electrical isolation of the sensor from the skin [2], [4], which in many cases is ideal. Some wearable devices that use microfluidic channels to transport sweat from the skin to the sensor rely on adhesives to mount the sensor as well as defining the channel or sampling area dimensions. For example Wang's research group uses adhesives in their wearable sensors. They have reported the fabrication of a screen printed potentiometric tattoo sensor for monitoring ammonium in sweat and used adhesives to help mount the sensor onto skin [4]. Two strips made of Kapton® adhesive were placed on both sides of the tattoo to create a pathway where sweat is able to flow through, keeping electrical contact between the electrodes and skin [4] Their platform was capable of working in a range between 10^{-4} - 0.1 M ammonium in sweat however, during on-body testing had issues regarding delamination and therefore additional strips of Kapton® adhesive was used to hold the wearable sensor in place [4]. The group used a similar approach where the adhesive provided attachment of the epidermal microfluidic device onto skin as well as using it to define a sampling area for sweat collection [2]. This adhesive layer included 4 x 2 mm diameter pores matching with four sweat collection inlets of the microfluidic device that captured sweat generated by a participant [2]. However, they

observed that the use of adhesives can occlude pores of skin which can possibly influence the sweat rate of the individual [2]. Overall adhesives are a simple and effective approach to mount sensors to skin.

Another approach for skin adherence is through intermolecular forces such as, Van der Waals interactions where these forces alone have been used to adhere wearable epidermal devices without the need for adhesive fixtures [5]. These sensors require physical and mechanical properties that are well matched to the skin in order to adhere to the skin properly. The fabrication of these wearable devices involve thin-film substrates with good stretchability as well as a low effective moduli in order to minimise the deformation induced by delamination and buckling of a sensor [5]. Huang *et al*. reported the fabrication of an epidermal hydration sensor that has mechanical properties that enable its integration with skin by Van der Waals interactions [6]. The fabrication method uses lithography techniques, ultra-thin silicone substrates and serpentine electrode configurations to integrate with the skin which can allow for good adherence and compliant movement with the skin [6]. Ameri *et al*. reported the fabrication of an ultra-thin graphene electronic tattoo with a thickness of 463 ± 30 nm fabricated via a "wet-transfer, dry patterning method" [7]. Due to its ultra-thin composition it can be directly laminated onto skin via Van der Waals forces for several hours. However issues of consistent adherence remains an issue with this platform. In order for their electronic tattoo to remain functional on skin a liquid bandage (silicone acrylate polymer) was required to keep the electrodes adhered to skin. The use of Van der Waals interactions to adhere to skin has the potential for adhering sensors to skin if the sensors are thin and light-weight, however these forces are weak and prove to be a potential issue if the sensors delaminate over time or during strenuous movement of the body.

Another interesting new approach for skin adherence of sensors is through stronger interfacial bonds between a sensing system and skin. Hydrogel materials, having a versatile chemistry have been used to demonstrate this concept. Hydrogels are three-dimensional polymer networks capable of holding large amounts of water, which can also be tailored to have a similar structure to biological soft tissue and mimic natural tissues properties [8]. Hydrogels (as will be demonstrated in Chapter 5) can also be designed as sensor transducers that can be tailored to respond to their environment or target stimuli. Research groups are currently exploiting hydrogels by developing bio-inspired skin adhesive materials. For example, Han *et al*. have designed a polydopamine–

polyacrylamide (PDA–PAM) based hydrogel that possesses stretchability, self-healing capabilities and tissue adhesiveness [9]. Polydopamine (PDA) was utilised due to its structural similarities to the adhesive protein of mussels [10] and has also been used to prepare self-healable hydrogels because of its catechol groups [11]. The innovation in their hydrogel design is the prevention of over oxidation of PDA during hydrogel synthesis in order to maintain enough free catechol groups in the hydrogel [9]. The free catechol groups in PDA could interact with amine or thiol groups to form cation–π or π–π interactions with various surfaces, in this case skin [9]. The group were able to demonstrate that this hydrogel could endure mechanical strain of over 3000 % and the adhesiveness of the hydrogel has allowed it to conform readily to the dynamic skin surface [9]. However, it is critical that there was enough free catechol groups present within the PDA-PAM hydrogel because its adhesion relies on the interaction between the free catechols to interact with thiols or amines for robust skin adhesion [9]. Another research group has studied the use of ionic hydrogels as a promising material for robust adhesion in wearable devices. This group explores the use of a zwitterionic hydrogel crosslinked with polyvinyl alcohol [12]. In this case, zwitterionic (poly[2- (methacryloyloxy)ethyl]dimethyl-(3-sulfopropyl), PSBMA) chains were used to provide ionic conductivity to enhance sensitivity to strains, whereas the PVA matrix provides support [12]. Adhesion of this hydrogel system relies on the zwitterionic chains on the surface of hydrogels to provide electrostatic or dipole–dipole interactions with the skin [12]. Their robust adhesion on skin has allowed for strains between 0-300 % and allows for reliable detection of joints bending as well as monitoring wrist pulse before and after exercise [12]. However, this hydrogel system becomes rigid and loses its adhesion property overtime therefore had a short wearable life where adhesion strength to porcine skin remained almost constant after four cycles via shear testing [12]. The use of interfacial bonds to create tissue adhesion between a hydrogel system and skin is a promising novel material of directly attaching wearable sensors to skin.

Wearable sensors require mechanical properties that are well matched to the skin in order to maintain consistent and reliable contact as well as adherence during measurements on skin. Research groups have explored the use of polymer materials to induce flexibility and stretchability into wearable sensors in order to move and stretch with the body. For example several research groups have encapsulated their non-printed skin-based sensors using soft materials such as, poly (dimethyl siloxane) (PDMS) [13], [14] or polyimide combined with ecoflex [15], [16] to best match the Young's modulus of the epidermis which is approximately 0.14 - 0.6 MPa [5]. For

example, Roger's group uses lithography techniques to fabricate their wearable sensors. Their group has employed fractal or serpentine electrode designs and used soft, polymer encapsulation methods to induce stretchability into the wearable sensor. Although this approach allows for improved stretchability, it does require complex and expensive techniques in order to fabricate the wearable device.

Another strategy for fabricating flexible and stretchable materials for wearable sensors is by use of new printable metal ink formulations. These inks can be tailored to have desirable properties for wearable sensors [17], [18]. They can be printed using conventional printing methods such as screen- or ink-jet printing. Screen-printing is commonly used for printing electrodes because it is a simple low-cost method for mass production of electrodes. Screen-printable ink formulations typically comprise of fillers, binders, solvents and additives. Fillers are the conductive component of ink and depending on the application, these conductive fillers could be silver or carbon particles or a combination of both [19], [20]. The different combinations of binders and fillers have opened up an avenue in the development of functional ink formulations depending on the application of the wearable sensor. For example, carbon fiber segments have been dispersed within ink matrices to increase the tensile strength of the printed electrode [21], while the elastomeric properties of polyurethane (PU) have been used as a binder to realize highly stretchable printed sensors [18]. Another example of a screen-printable formulation uses a stretchable elastic conductor ink comprised of silver flakes and fluorine rubber and reported an unimpaired functionality when stretched to 110 % [17]. This elastic conductor ink used fluorine rubber to enhance the stretchability of the polymer matrix while the use of fluorine surfactant increases the affinity between the fluorine copolymer and conductive Ag flakes to allow for high conductivity and demonstrated its potential as a wearable textile electromyogram sensor [17]. Bandodkar *et al*. have also presented an example of a screen-printable stretchable ink comprising of carbon nanotubes (CNTs) dispersed in mineral oil and PU for electrochemical sensing [18]. The group also use Ag/AgCl (dispersed in Ecoflex) printed in a serpentine pattern to incorporate a second degree of stretchability [18]. These inks were used to print serpentine electrodes with two contact pads for connection. These electrodes were characterised to determine the effect of applied strain on the resistance of the different iterations of the printed electrodes. It was observed that the non-stretchable (No CNT dispersed in PU) Ag/AgCl not dispersed in Ecoflex printed electrode could be stretched up to 200 % due to its serpentine design but additional stress led to fracturing.

However in the case for the Ag/AgCl/ CNT printed electrode it could be stretched by 500 % due to the presence of the CNT dispersed in PU and Ag/AgCl dispersed in Ecoflex [18]. They employed two degrees of stretchability into the Ag/AgCl/CNT printed electrode by using a combination of serpentine patterning to allow the electrodes to unwind and stretch and the PU binder which offered increased stretchability for the wearable platform. This innovative stretchable material showed promise as a glucose sensor when the CNT-based device was functionalized with GOx and displayed a linear response to glucose levels (0 – 10 mM) [18]. The development of these ink formulations have helped towards enhancing the stretchability of wearable platforms, which in turn helps towards improving adherence of these platforms to skin when subjected to mechanical stresses. These developments in ink formulation have been used as a means of inducing mechanical stability in wearables. This improvement in mechanical stability and adherence can help reduce motion induced noise from body movements or bending effects that can affect the response acquired by the skin-based wearables. Mechanical stability and good skin-electrode adherence methods are crucial in the development of skin-based wearable devices. In the case of wearable devices as a whole, each platform should be optimised for its specific application and the method of contact should be fit for purpose and the mechanical properties that relate to it.

This chapter assesses different approaches to enhance skin adherence of a wearable platform that can track electrical properties of skin. Firstly, it assesses the impact of elastomer in a silver ink formulation in terms of its influence on the electrical and mechanical characteristics of a screen-printed wearable platform. The mechanical and electrical properties the silver and silver-elastomer films were evaluated from a wearable perspective. Furthermore, this chapter investigates the incorporation of a conducting adhesive (CA) layer into the platform to induce consistent skin adherence while maintain electrical contact between the skin and the electrodes. The electrical and mechanical characteristics of this wearable platform after integrating the CA material were again evaluated. Finally, the functionality of the platform with the integrated CA material was evaluated by tracking the skin barrier condition of an individual after exposure to different irritants. A participant study was conducted to determine if this new platform correlated to Tissue Dielectric Constant (TDC) measurements from a commercial skin probe.

3.2 Materials and methods

3.2.1 Materials

Acheson Electrodag PF410 silver ink was purchased from Nor-Cote International Ltd, referred to as silver ink here. AG520 EI silver ink was purchased from Chimet® S.p.A. (Tuscany, Italy), referred to as silver-elastomer ink here. ARcare® 8881 electrically conductive adhesive was supplied by Adhesives Research Ireland Ltd. Temporary transfer tattoo paper substrates were purchased from Sports Ink™ (Dublin, Ireland). Strips boards were purchased from Maplin Electronics. Mill Max spring loaded contacts (Part. No. 0906-4-15-20-75-14-11-0) were purchased from Farnell Components (Ireland). 2.0 mm thick PMMA acrylic sheets and 1.5 mm diameter flat head probe tips (261-5109) were purchased from Radionics Ltd. (Ireland). Poly (ethylene glycol) diglycidyl ether (PEDGE, Avg. Mn 500) was purchased from Sigma-Aldrich. Acetone and ethanol were purchased from Brenntag UK Ltd. Jeffamine® EDR-148 polyetheramine was donated from Huntsman Chemical Company. Sodium lauryl sulfate (SLS) micropellets were purchased from Fischer BioReagents. Polyvinyl chloride (PVC) cloth was purchased from Home Focus, Hickey & Co Ltd. (Ireland).

3.2.2 Tattoo platform design, fabrication and application

The tattoo platform design, fabrication and application to a substrate has been described previously in Chapter 2, Section 2.2.2. This platform is referred to as the Direct Contact (DC) mode in this chapter.

3.2.3 Incorporation of Conducting Adhesive (CA)

ARcare® 8881 is a non-woven material with an electrically conductive acrylic adhesive on both sides, used to adhere the silver concentric electrodes to the skin. A Graphtec CE 6000 was used to machine the CA film according to the same two concentric electrode geometry used for the silver electrodes. The machined CA film was aligned and adhered on top of the silver electrodes before applying it to skin. When applied, the silver electrodes were face-up while the CA adhered to skin (Fig. 3.1b & c). This platform is referred to as the Conducting Adhesive Contact (CAC) mode in this chapter.

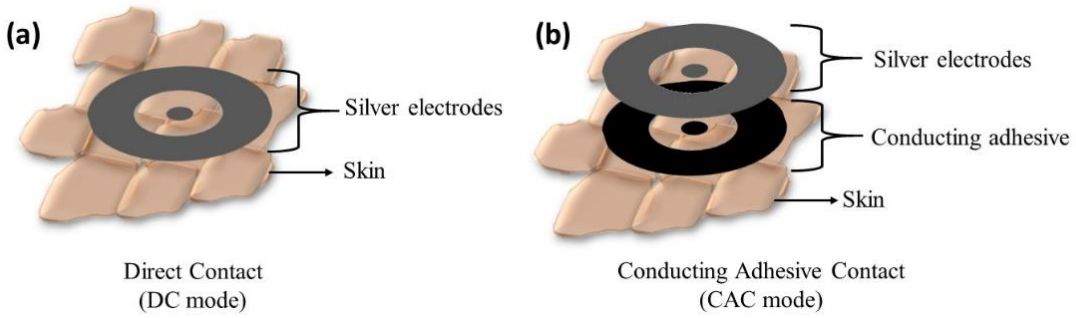

Figure 3.1 Schematic diagrams of skin the electrode interface in platforms using (a) DC mode and (b) CAC mode.

3.2.4 Physical characterisation of the tattoo platforms

3.2.4.1 Isolation of silver filler

The silver flake component of the inks were isolated via centrifugation. Approximately 1 g of ink was placed into a centrifuge tube and the ink was centrifuged at 7000 rpm for 1 h. This allowed for the silver particles to settle in the bottom of the centrifuge tube allowing the top layer of suspension to be removed. The remaining silver was washed with acetone (5 ml) and ethanol (2.5 ml). The silver precipitate was placed in the fumehood to allow the solvents to evaporate overnight.

3.2.4.2 Physical characterisation of printed electrode films

Two point probe resistance measurements were carried out on the screen-printed electrodes after curing using a Keithley 2420-C 3A SourceMeter®. The surface resistance of the silver films were measured by placing the probes 3 mm apart. The resistance of the CA was measured by placing the probes 10 mm apart. The Average Surface Height (ASH) of the materials were measured using a Bruker Dektak XT stylus profilometer. A Nikon D3300 camera was used for imaging during the on-body studies. A Keyence Digital Microscope (3D VHX-2000) was used to take high resolution images of the screen-printed electrodes to assess their conformability.

3.2.4.3 Mechanical characterisation

Three tattoo platforms were assessed using tensile testing: silver (DC mode), silver-elastomer (DC mode) and silver-elastomer (CAC mode). These platforms were assessed under tensile load applied using a Zwick Z5 (Zwick Roell, Germany) fitted with a 5kN load cell. Two rectangular plastic plates (2.0 mm thick PMMA) were clamped into tensile grips within the Zwick machine to adhere the tattoo platforms onto during testing. For all tests a tensile load was applied at a speed of 1 mm/min using the TestXpert software (Zwick Roell, Germany). These tattoo platforms were adhered to the plastic plates with a 2 mm starting displacement and tested to failure. The adhesive layers when assembled onto the electrodes, introduced a change in thickness and cross sectional area to the platforms. In order to calculate the cross-sectional area, the thickness used was 11.6 µm for the silver (DC mode) and silver-elastomer (DC mode) and 114.77 µm for silver-elastomer (CAC mode).

3.2.4.4 Electrical characterisation

Impedance spectroscopy was performed using an Autolab PGSTAT128N potentiostat. The frequency range scanned was 0.1 Hz to 1 MHz for all experiments, unless stated otherwise. Spectra collected on hydrogels were recorded at 0 V set potential and 0.01 V amplitude while spectra collected on skin were recorded at 0.1 V set potential and 0.03 V amplitude. Unless stated otherwise, skin was pre-treated with cotton wool soaked in deionised (DI) water for 1 min prior to application of tattoo platforms.

3.2.5 Hydrogel preparation

The hydrogels were prepared according to Section 2.2.5. Before impedimetric analysis the hydrogels were removed from the fridge and left to acclimatize to room temperature for 1 h. Tattoo platforms were applied to the surface of the hydrogels and an impedance spectra were recorded using the conditions in Section 3.2.4.4.

3.2.6 Participant study

Healthy participants aged 23-31 were recruited and instructed not to apply perfumes or cosmetics on their arms on the days of sample collection. Participants were informed of the aim and purpose of the study and asked to provide written informed consent. An example of the Plain language statement, Informed consent form and Questionnaire can be found in the Appendix, Section A3.A. The local ethics committee (Dublin City University Ethics Committee) approved the study and the study was performed according to the Declaration of Helsinki. The tattoo in CAC mode was applied on to the inner forearm and an impedance spectra was collected according to Section 3.2.4.4. The skin tissue dielectric constant (TDC) was taken on the inner forearm using a handheld Delfin MoistureMeterD probe (MMD) (Delfin Technologies, Finland).

3.2.6.1 Flexion-extension

Flexion-extension of the arm was performed by a single participant when wearing the tattoos in both DC and CAC modes. These were applied to the forearm of the participant and images of the platforms were taken with the arm extended and then again after flexing. This was repeated ten times in order to assess the mechanical stability and adherence of the platforms on the body.

3.2.6.2 Barrier disruption

DI water and 0.5% SDS in water were applied to two different, adjacent sites on the inner forearm of a single participant. Cotton wool soaked with the topical treatment were applied onto skin for 1 min. After 1 min, the cotton wool was removed and tattoos in CAC mode were applied to the sites and an impedance spectra were collected using the conditions in Section 3.2.4.3. A TDC measurement was taken before and after topical treatment of the skin at each site also.

3.3 Results and discussions

In the previous chapter, a tattoo platform based on a screen-printable, flexible silver ink was demonstrated to track electrical changes in skin. This platform allowed for good contact with the skin for single measurements, however it did not possess appropriate mechanical properties for continuous monitoring. In order to enhance the tattoo platforms' mechanical properties, an alternate silver-elastomer ink formulation was assessed for its suitability as a wearable platform. Films comprising the silver and silver-elastomer inks were compared electrically and mechanically in order to understand the impact of elastomer in ink formulations on a wearable tattoo platform. For the wearable being developed in this thesis, an ink formulation that is capable of stretching and moving with the skin without impeding the electrical measurements was investigated. In this section, two different commercial silver inks were investigated, one without elastomer and one with elastomer. These ink formulations were screen printed onto a temporary tattoo substrate as before in order to fabricate a skin-based wearable platform. The resulting platforms were subjected to tensile testing to understand their mechanical character and were characterised impedimetrically in order to understand which ink formulation might be more suitable for wearable electrodes interfaced with the skin.

3.3.1 Characterisation of inks for Direct Contact (DC) modes

The % silver content of the silver- and silver-elastomer inks were assessed using the method described in Section 3.2.4.1. The % silver found was 53.42 ± 1.57 % for the silver ink and 61.23 ± 2.01 % for the silver-elastomer ink (n=3). This higher loading in the silver-elastomer ink formulation may have been used to compensate for the presence of the insulating elastomer resin component of the ink, which is a PU thermoplastic in this case. Two-point probe resistance for the films comprising silver ink was measured to be 0.13 ± 0.01 Ω/mm and for the silver-elastomer ink, it was measured to be 0.15 ± 0.01 Ω/mm (n=5). This higher resistance value measured for the silver-elastomer films is again likely due to the presence of elastomer. Overall the thickness of the silver ink platform was measured to be 11.64 ± 1.55 µm and the silver-elastomer ink platforms was 11.20 ± 1.63 µm (n=4). From this initial physical characterisation, the silver-elastomer ink had a higher resistance compared to the silver ink and had reasonably comparable thicknesses when screen-printed under equivalent conditions.

The conformability and adherence of the different inks in DC mode to skin were compared via imaging of the materials when applied to textured surfaces and using on-body flexion-extension movements. One of the challenges of wearable sensors is good adherence to the skin. As the skin is a non-planar, dynamic surface, the wearable skin-based platform should be able to conform with skin mechanics while remaining adhered to the skin. To assess the conformability of the screen printed platforms, the DC mode platforms were applied to a PVC cloth substrate and imaged. The PVC cloth was used to emulate the non-planar surface of the skin [22]. From Fig. 3.2, it can be seen that the both inks adhere well to PVC. It can be seen that the silver ink platform sits over the surface (Fig. 3.2a), while the silver-elastomer ink platform conformed much better to the surface topology (Fig. 3.2b), demonstrating that the elastomeric properties of the latter ink allows for enhanced conformability.

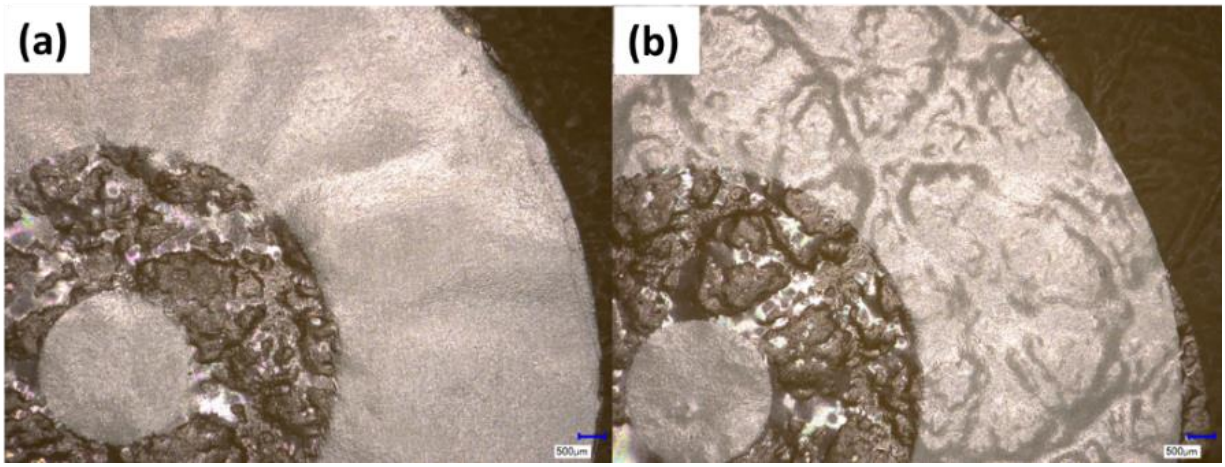

Figure 3.2 DC mode tattoo platforms comprising of (a) silver and (b) silver-elastomer applied to PVC substrate were imaged using a Keyence Microscope (Mag x30).

The platforms were applied to the skin of the forearm on a single participant to assess adherence to skin. The platforms were gently stretched to assess their durability under mechanical stress. The images in Fig. 3.3 shows that the DC mode platforms comprising the silver and silver-elastomer inks adhered well to skin (before stretching). However when mechanical stress in the form of stretching was applied, it was observed that the silver platform weakened to a point of fracture,

seen as in the image (Fig. 3.3, top right) on the outer electrode. On the other hand, the silver-elastomer platform did not fracture upon stretching but partial buckling did occur which was likely due to weak adherence (Fig. 3.3, bottom right). Buckling during stretching was observed for both platforms suggesting that consistent and stronger adherence to skin was still an issue which needed to be addressed. Consistent interfacial electrode contact with skin is important for this application in order to get reliable electrical measurements of the skin while being worn.

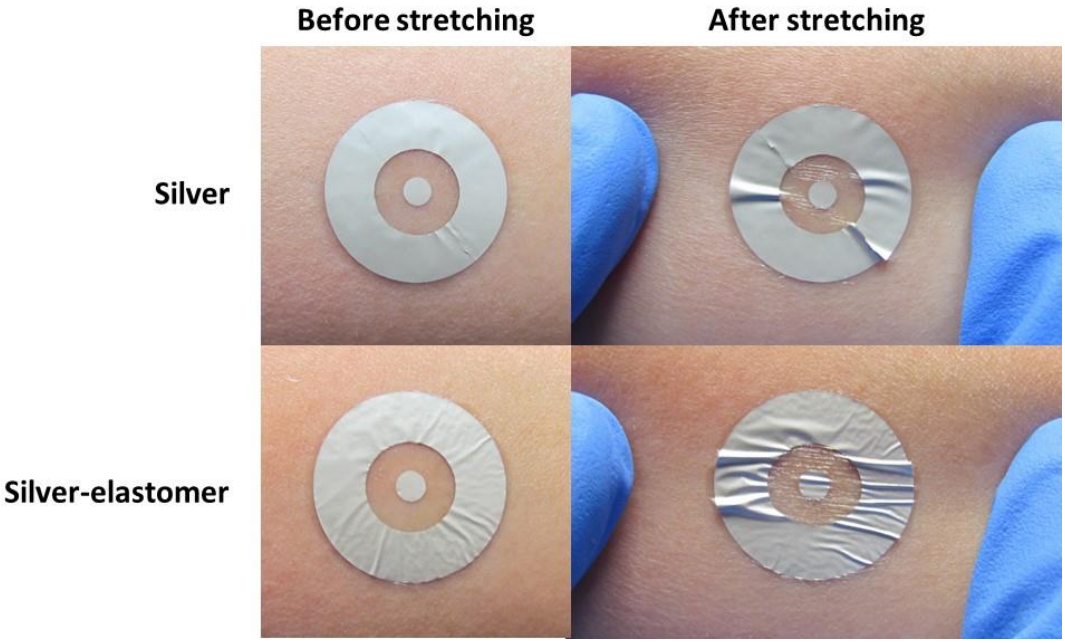

Figure 3.3 Images of silver DC mode and silver-elastomer DC mode platforms on skin before and after gentle stretching (tattoo electrode diameter: 20 mm). Images were taken using a Nikon D3300 camera.

The adherence and mechanical stability of the DC mode platforms during flexion and extension of the forearm of a single participant was also studied. Silver and silver-elastomer platforms were applied again on to the forearm in its relaxed position and the forearm was flexed and extended. This movement was repeated ten times in order to assess the stability of the platforms under this mechanical stress. From Fig. 3.4, the silver and silver-elastomer platforms adhered well to the skin initially, as expected. It was observed that the silver platform underwent severe delamination and

fracturing after several flexion/extensions compared to the silver-elastomer platform where delamination or fracturing did not occur. However, buckling effects were again observed with the silver-elastomer platform after movement. Despite the buckling effect the silver-elastomer platform remained intact, consistent adherence to skin was still an issue.

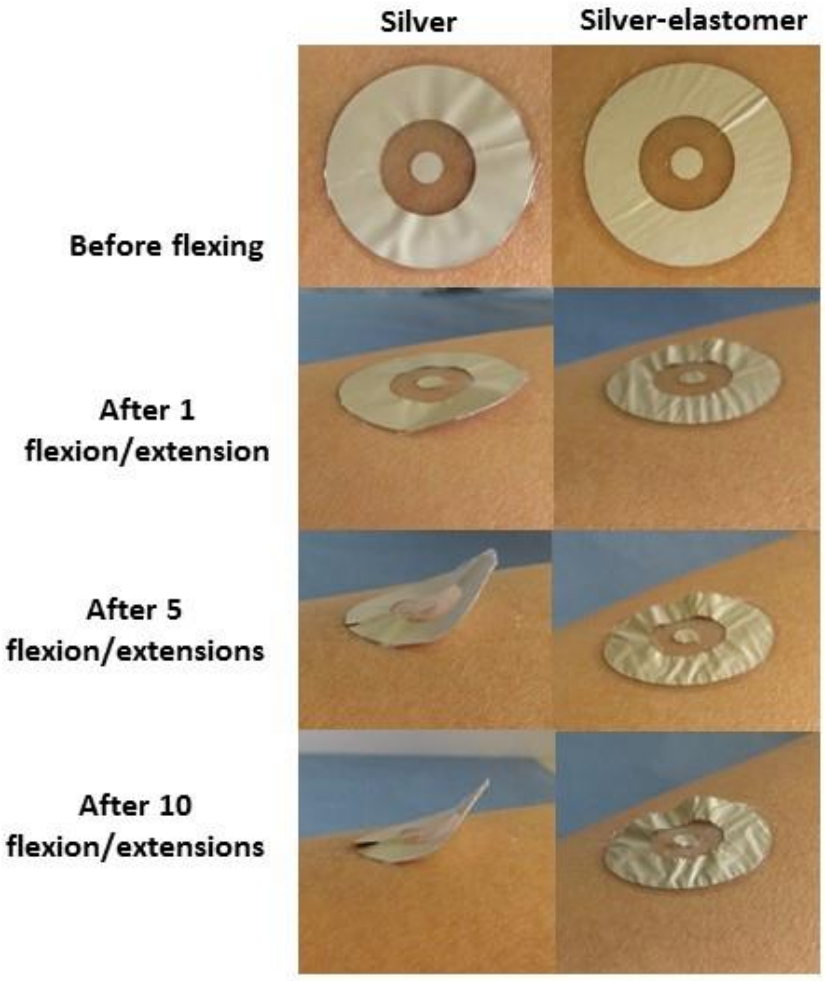

Figure 3.4 Images of the silver DC mode and silver-elastomer DC mode platforms on skin before and after flexion-extension movements of the forearm (tattoo electrode diameter: 20 mm). Images taken using a Nikon D3300 camera.

3.3.1.1 Electrical characterisation of tattoo platform

The silver and silver elastomer platforms were applied directly to the surface of bulk hydrogels and impedance spectra taken in order to compare the performance of the two different ink

formulations. Nyquist plots are displayed in Fig. 3.5 (a and b). The Nyquist plots for both inks show similar spectra with two well-defined regions: a semi-circle in the high frequency region and the opening of a larger second semi-circle at lower frequencies. The response in the higher frequency range is attributed to the bulk hydrogel while the response in the lower frequency range has been attributed to the highly capacitive electrode-hydrogel interface.

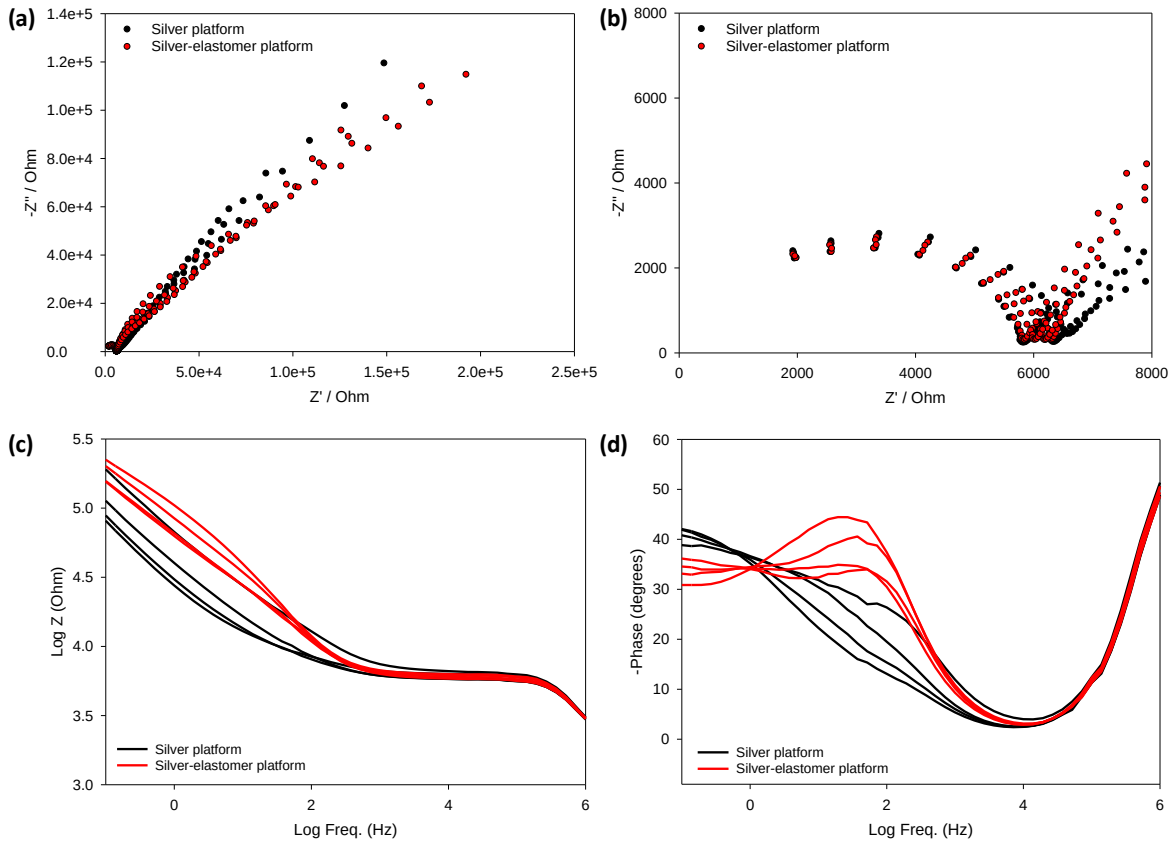

Figure 3.5 (a) Nyquist plots of the silver and silver-elastomer platforms on a PEDGE-Jeffamine® hydrogel. (b) Magnification of the high frequency region of the Nyquist plots in (a). Corresponding Bode plots for (c) Impedance and (d) Phase are also shown (n=4).

The spectra obtained for the silver and silver-elastomer platforms show similar consistent behaviours at high frequency, while the lower frequency range showed some differences (Fig. 3.5a). The spectra for the silver-elastomer platform at the lower frequency region shows a slightly higher impedance than that of the silver platform which could be attributed to the elastomer present in the ink formulation. The diameter of the semi-circle found in the high frequency region is taken

as the measure of bulk hydrogel resistance (R_{gel}). The Impedance plots (Fig. 3.5 c & d) show similar consistent behaviour in the higher frequency range which is attributed to the bulk hydrogel while the lower frequency range shows response differences which can be attributed to the variability in the electrode-hydrogel interface. R_{gel} values for the semi-circles in the Nyquist plots were 6223 ± 382 Ω, 6 % (n=4) for the silver platforms and 6195 ± 203 Ω, 3 % (n=4) for the silver-elastomer platforms showing that the measured R_{gel} values for the bulk hydrogel were equivalent using both platforms.

The silver and silver-elastomer DC mode platforms were further characterised electrically on human skin. Both platforms were applied to the inner forearm of a single participant. The Nyquist plots of skin showed single semi-circles with large diameters (Fig. 3.6). Using the silver platform resulted in a smaller semi-circular diameter compared to that using the silver-elastomer platform (Fig. 3.6a). The corresponding Bode plots in Appendix, Fig. A3.A also shows that the overall impedance for the silver-elastomer platform had a higher impedance compared to the silver platform, but shows that both platforms have similar profiles for the electrical signal of skin. This is likely due to differences in skin- electrode interfacial contact for the different materials. Both spectra show a large semi-circle for skin measurements, the response at high frequency region is typically dominated by the deeper skin tissue, while the response at the lower frequency region are typically dominated by the electrodes in contact with the SC layer of the skin. As discussed in the previous chapter, this semi-circle is understood to contain unresolved contributions from both the skin and the electrode-skin interface. A simplified model was selected to model the electrical properties of skin in this work [23], [24]. The circuit model comprises of a resistor, attributed to the viable tissue resistance (R_{vt}) in series with a second resistor, attributed to electrode-skin interface resistance ($R_{elec/skin}$) with a constant phase element (CPE) in parallel, attributed to capacitance of the electrode-skin interface. This simplified circuit model has been commonly used for modelling skin impedance data [14], [25]–[27].

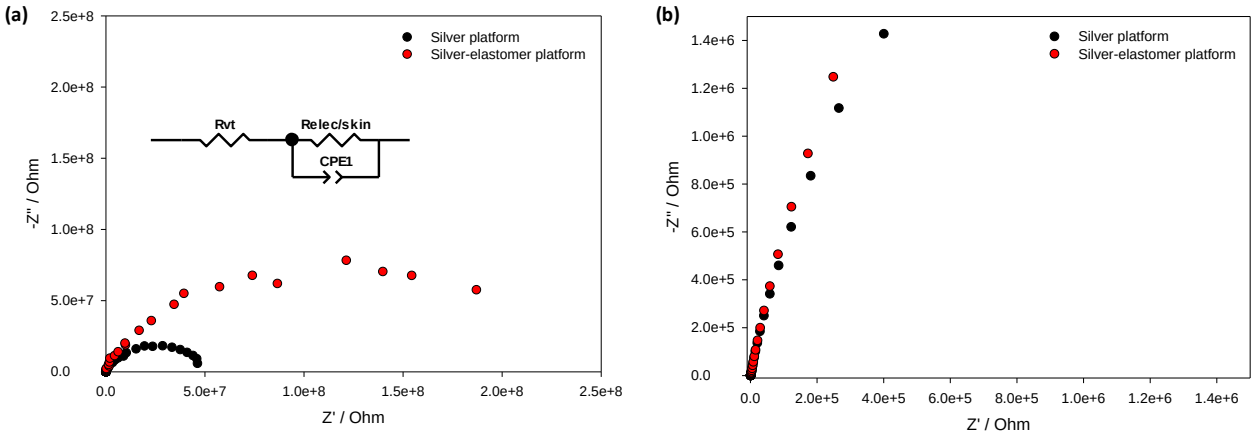

Figure 3.6 (a) Representative Nyquist plots of the inner forearm as measured by the silver platform and silver-elastomer platform. Inset shows the equivalent circuit used to model the data. (b) Magnification of the high frequency region in (a). Corresponding Bode plots in Appendix Fig. A3.A.

Using this circuit, the modelled contributions of the skin and the skin-electrode interface could be deconvoluted. The circuit element of interest was the resistance associated with the viable tissue (R_{vt}). Due to the presence of noise at frequencies below 100 Hz, circuit modelling was limited to the data collected between 1 MHz and 100 Hz. An example of the fitted spectra at the short frequency range can be seen in Fig. A3.D in the appendix. Based on this model, R_{vt} values were obtained for skin for both the silver and silver-elastomer platforms as paired repeated meaasurements (n=5) on a single participant. From the data, the silver platform had a lower average R_{vt} compared to that measured by the silver-elastomer platform. The measured R_{vt} for the silver platform was 455 ± 69 Ω, 15 % while the measured R_{vt} for the silver-elastomer platform was 518 ± 33 Ω, 6 %. Based on a paired t-test, a p-value of 0.07 (two-tailed) was returned indicating that there is no significant difference between the measured resistance data between the two platforms. However, it was observed that there was variability in the adherence of these electrodes on skin, it was noted that the silver platform partially buckles from the skin during meaurement, which is not ideal for a wearable sensor because this buckling would have an effect on the electrical signal measured from skin and could be a source of error during measurement. While the silver-eleastomer also shows minimal buckling, which is still not ideal therefore an adherence method should be consisdered to keep the electrodes consistentantly adhered to skin. The mechanical properties of these platforms will be further discussed in the next section.

3.3.1.2 Mechanical assessment of tattoo platform

The tensile strengths of the silver and silver-elastomer platforms were measured. The stress-strain curve gives information on the tensile properties of the silver and silver-elastomer DC mode platforms (Fig. 3.7). From tensile testing, the mechanical properties: Young's modulus (MPa), yield strength (N/mm^2) and yield strain (%) were measured and compared for each electrode platform (Table 3.1).

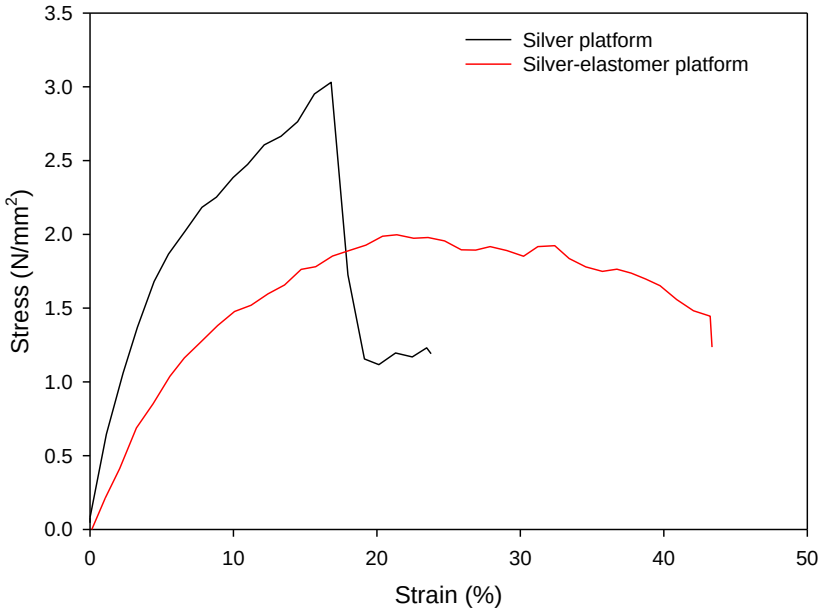

Figure 3.7 Stress-strain responses of the silver and silver-elastomer DC mode platforms.

Table 3.1 Comparison of the mechanical properties of the silver and silver-elastomer platforms (n=7).

Platform (DC mode)	**Young's Modulus (MPa)**	**Yield Strength (N/mm^2)**	**Yield Strain (%)**
Silver	0.27 ± 0.10	1.44 ± 0.67	3.83 ± 1.00
Silver-elastomer	0.16 ± 0.03	1.17 ± 0.16	6.27 ± 1.67

The Young's modulus (MPa), yield strength (N/mm^2) and yield strain (%) for each platform are tabulated in Table 3.1. The Young's modulus is also known as the modulus of elasticity and is used to describe the elasticity of the material. The Young's modulus of the epidermis is quite broad and can be between approx. 0.14 – 0.6 MPa [5]. It was observed that both silver and silver-elastomer DC mode platforms moduli lie within this broad range of the Young's modulus of the epidermis as seen in Table 3.1. However in this case, the silver-elastomer DC mode platform was almost half the Young's modulus of the silver DC mode platform. This suggests that the silver-elastomer DC mode platform is more elastic than the silver DC mode platform demonstrating the positive impact of the elastomeric properties present in the ink formulation. The yield strength of the different materials were assessed to determine at which point the elastic properties of the material have been exceeded and plastic deformation occurs. In this case, the yield strength for the silver DC mode platform was higher than the silver-elastomer DC mode platform indicating that the silver DC mode platform can withstand higher levels of stress before fracturing compared to that of the silver-elastomer DC mode platform. The yield strain gives an indication of how much the electrode material can be stretched prior to failure. In this case, the yield strain shows almost a two-fold increase for the silver-elastomer DC mode platform indicating that this was capable of withstanding higher strain than its silver DC mode counterpart. This suggests that the silver-elastomer DC mode platform is more pliable and so could withstand more stretching on the skin compared to the stiffer material. Overall these results indicate that the silver DC mode platform can withstand higher levels of stress however it can only withstand minimal strain and as such it fractures and delaminates from skin under mechanical stress. The results for the silver-elastomer DC mode platform show that despite it not handling high levels of stress, it is capable of greater strain demonstrating the positive impact of the elastomeric properties of the ink formulation. This suggests that the silver-elastomer DC mode platform has properties that would be suitable for an epidermal wearable. However, buckling effects observed earlier on skin remained an issue. Greater adherence to the skin is needed to overcome the buckling issue in order to reliably interface the platform to skin. An adherence strategy using a conductive adhesive (CA) to improve the adherence will be further discussed in the next sections.

3.3.2 Incorporation of CA into the tattoo platform

From the previous section, screen-printed silver and silver-elastomer platforms were characterised for their electrical and mechanical properties. From the investigation, the silver-elastomer platform showed improved mechanical properties that could potentially be used in this wearable platform for longer-term wear. However, consistent and stronger adherence to skin using the silver-elastomer platform is still an issue. In order to address the issue of adherence, a Conducting Adhesive (CA) was integrated with the silver-elastomer DC mode platform according to the method described in Section 3.2.3. The conductive nature of this adhesive was exploited here to allow propagation of the electrical signal between the electrodes and skin. In the next sections, the effect of this CA layer as a form of enhancing adherence with the skin is investigated.

3.3.2.1 Physical characterisation of CA contact mode (CAC)

The silver-elastomer ink was selected as the ink of choice for this study, whereby the DC and CAC modes were compared in order to assess the impact of the CA on the physical and mechanical properties of the tattoo platform. Two-point probe resistances were reported earlier for the DC mode as 0.15 ± 0.01 Ω/mm (n=5). The CA had a measured resistance of 1.53 ± 0.13 Ω/mm (n=5) which was an order of magnitude higher than the silver film.

The thickness of the DC mode platform was also compared to the thickness of the CA. As previously discussed the DC mode had a thickness of 11.20 ± 1.63 µm and the thickness of the CA on its own was measured to be 99.18 ± 1.32 µm, thus there was a 10-fold increase in platform thickness after integrating the CA into the silver-elastomer DC mode platform. The significant increase in overall thickness of the CAC mode had an effect on the overall conformability of the platform when adhered to a rough surface (Fig. 3.8). The DC mode had good conformability to the rough surface as observed previously, while the CAC mode had a reduced conformability when adhered to the PVC (Fig. 3.8b), due to the addition of the CA layer. Despite being a thicker platform, the use of the CA was investigated to enhance the mechanical properties of the platform due to its adhesive properties.

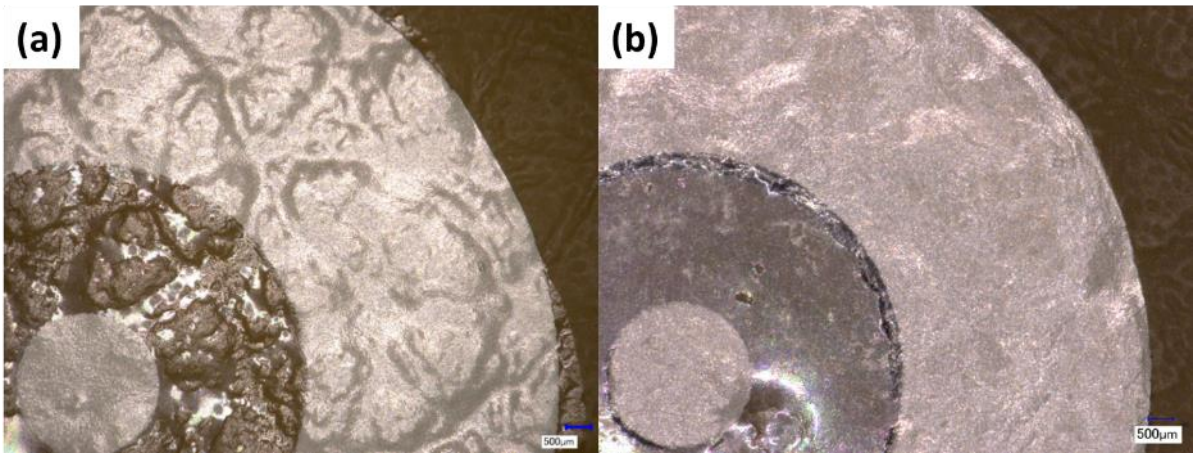

Figure 3.8 Images of the (a) silver-elastomer DC mode (as previously shown in Figure 3.2) and (b) silver-elastomer CAC mode adhered onto a PVC substrate and were imaged using a Keyence Microscope (Mag x30).

3.3.2.2 Investigation of the electrical properties of DC and CAC modes

The DC and CAC modes were then tested impedimetrically on both hydrogel and skin. These two platforms were initially applied to a hydrogel surface to investigate the impact of the CA on the electrical properties of the platform. The resulting Nyquist spectra in Fig. 3.9a shows two well-defined regions for the DC mode as before attributed to the bulk hydrogel (high frequency) and the electrode-hydrogel interface (low frequency). Interestingly, the Nyquist plot for the CAC mode shows three distinct regions comprising the openings of two semi-circles at high and mid frequency and a capacitive feature extending into low frequency region (Fig. 3.9a and b). The presence of this second semi-circle in the mid frequency region has been attributed to the CA. The CA material on its own was fabricated into the same configuration as the concentric electrodes. It was adhered onto the hydrogel surface and an impedance measurement was taken, results in Appendix Fig. A3.B. The results indicate that the CA material on its own has a high resistance and capacitance associated with it, which is not ideal. However, it may still be viable to use once its contribution to the impedance spectrum can be identified and isolated from that of the hydrogel. R_{gel} values from the circuit model attributed to the bulk hydrogel measurement were extracted to be 6856 ± 553 Ω, 8 % (n=3) for the DC mode platform while for the CAC mode platform it was measured to be 10283 ± 1646 Ω, 16 % (n=3). This indicated that the Z View software had difficulty

estimating the diameter attributed to the bulk hydrogel. This was likely due to the merging impedance contributions between the bulk hydrogel and CA layer (Fig. 3.9b). It was noted that the CAC mode platform had a higher variability compared to the DC mode platform, which can potentially be due to the electrical contribution of the CA layer merging with both the electrical contributions of the bulk hydrogel and electrode interface which makes it challenging to fully distinguish the CA layers electrical signal on its own.

The raw Z' values for both DC and CAC platforms were further investigated to deconvolute the contributions of the bulk hydrogel measurement for each platform. It was estimated that the DC mode platform had Z' values that measured 6737 ± 552 Ω, 8 % (n=3), while the CAC mode platform had Z' values of 6307 ± 724 Ω, 11 % (n=3). The results indicate that it is possible to resolve the different contributions on a hydrogel using the CAC mode platform. It is important to be able to resolve the different contributions, so the contribution associated with the CA does not interfere with the measurement of R_{vt} when the CAC mode platform is used on skin.

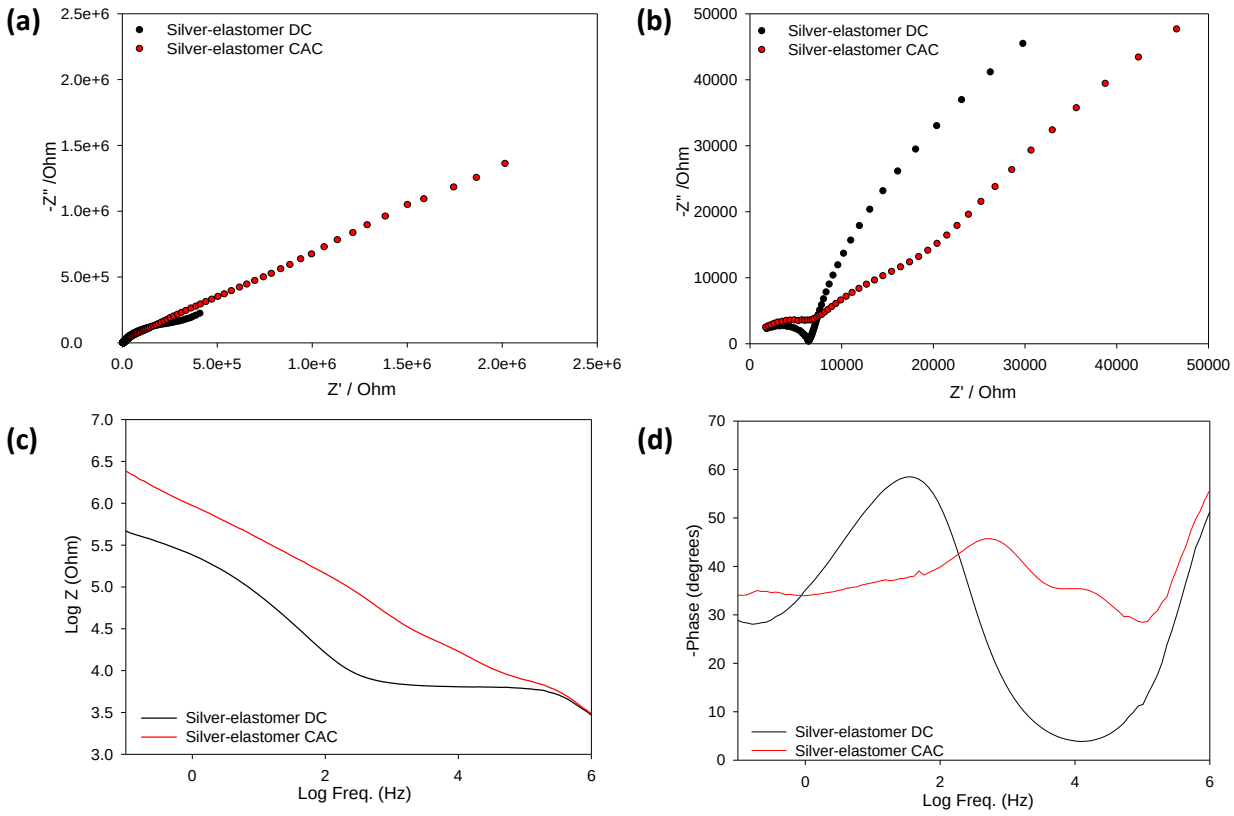

Figure 3.9 Representative (a) Nyquist plots comparing the silver-elastomer DC and CAC modes on a hydrogel, (b) magnification of higher frequency region of the Nyquist spectra attributed to bulk hydrogel and the corresponding (c) Impedance and (d) phase plots.

The DC and CAC modes were then applied onto human skin, on the inner forearm of a single participant, in order to assess the impact of the CA on the measured skin impedance. The Nyquist plots show single semi-circles in both instances (Fig. 3.10a) and it was observed that the CAC mode showed a higher overall impedance compared to the DC mode. It was also observed that the contribution associated with the CA was not fully resolved from other contributions for this skin measurement as was the case for the measurement on the hydrogel. This indicates that the additional resistance and capacitance contributed by the CA could have a significant impact on the skin measurement. The high frequency region is attributed to measurements of the deeper tissue, R_{vt} values modelled from the opening of the semi-circle at the high frequency were used to compare the DC and CAC modes measurements on human skin. The R_{vt} value from a single participant indicate that the silver-elastomer DC measured lower resistance values (432 ± 100 Ω,

23 % (n=3)) compared to the silver-elastomer CAC (688 ± 82 Ω, 12 % (n=4)). This suggests that the CA layer influenced the measured resistance, likely as a direct result of its high resistance which is not resolved from the time constant of skin, under the conditions tested.

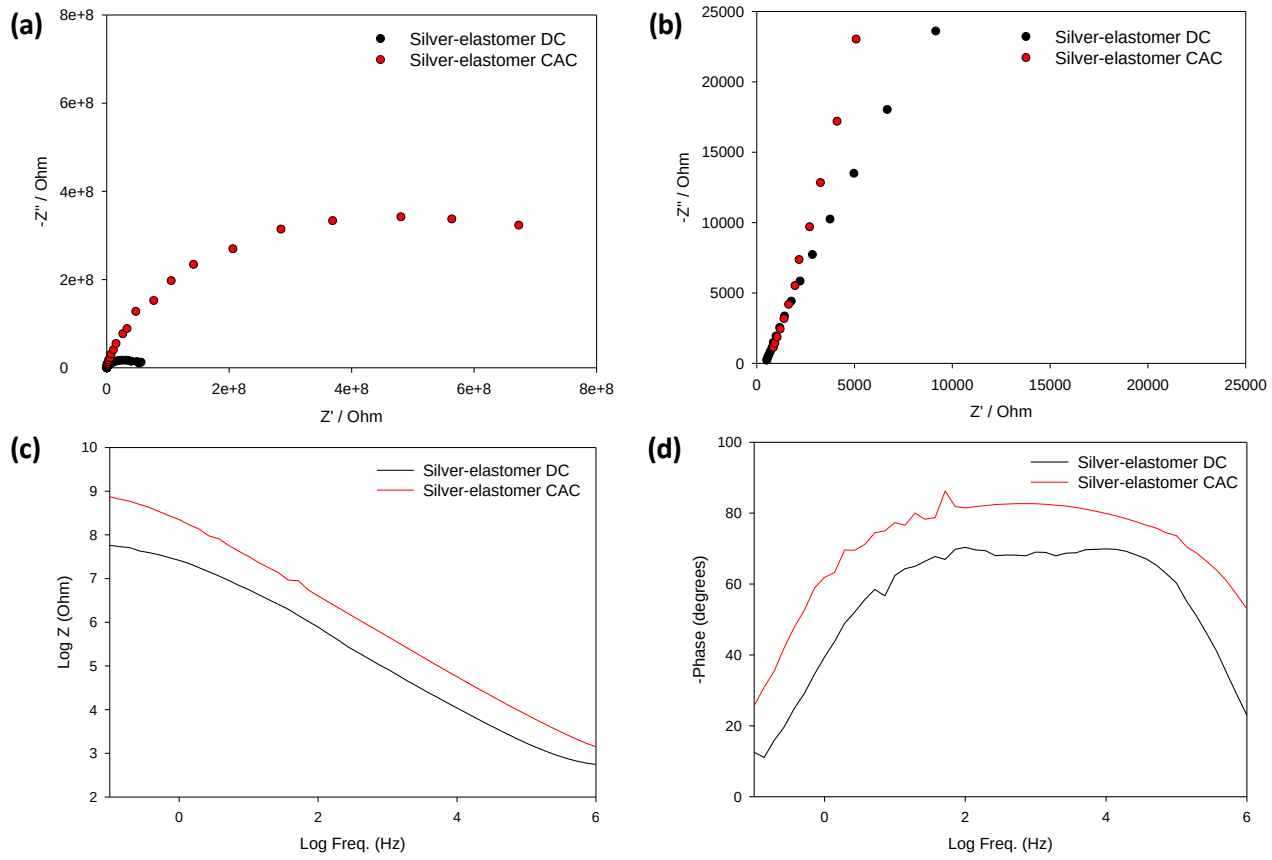

Figure 3.10 Representative (a) Nyquist plots of the inner forearm as measured by the silver-elastomer DC and CAC modes, (b) magnification of the higher frequency region of the Nyquist plots and corresponding (c) Impedance and (d) phase plots.

3.3.2.3 Mechanical comparison of DC and CAC modes

The tensile strength of the DC and CAC modes were measured. The stress-strain curves comparing the mechanical properties of the DC and CAC modes (using the silver-elastomer ink) are shown in Fig. 3.11. Using the stress-strain curve in Fig. 3.11, the data was processed and the Young's

modulus (MPa), yield strength (N/mm^2) and yield strain (%) for each platform and is tabulated below in Table 3.2

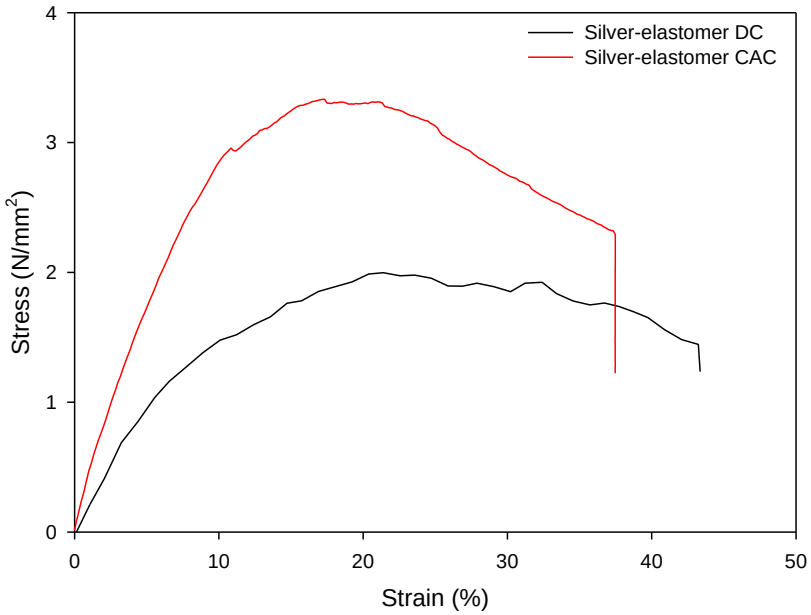

Figure 3.11 Stress-strain responses of the silver-elastomer DC and CAC modes.

Table 3.2 Mechanical properties of the silver-elastomer DC and silver-elastomer CAC (n=7).

Platform (Silver-elastomer)	**Young's Modulus (MPa)**	**Yield Strength (N/mm^2)**	**Yield Strain (%)**
Direct Contact (DC)	0.16 ± 0.03	1.17 ± 0.16	6.27 ± 1.67
Conducting Adhesive Contact (CAC)	0.34 ± 0.08	2.72 ± 0.69	8.12 ± 0.16

From Table 3.2, the Young's modulus of the CAC mode was greater than that of the DC mode. This suggests that the incorporation of the CA has made the overall platform less elastic, however it still broadly lies within the range of the Young's Modulus of the epidermis as previously discussed in Section 3.3.1.2. The yield strength indicates that the CAC mode is capable of withstanding stress two times more than its DC mode counterpart, suggesting that this CAC mode platform is more mechanically robust. While the yield strain suggests that the addition of the CA

has contributed to a 2 % increase in the strain the CAC mode can withstand. This indicates that it can stretch more than the DC mode before failure. Based on the results, the incorporation of the CA layer into the wearable platform has reduced its elasticity. However it can withstand higher levels of stress and strain suggesting it can withstand more mechanical stress compared to the DC mode.

The adherence and mechanical stability of the CAC mode was investigated during flexion and extension on the forearm of a single participant. This was also compared to the flexion and extension movements of the DC mode, previously observed in Fig. 3.4. The CAC mode was applied to the forearm in its relaxed position and the forearm was flexed and extended. This movement was repeated 10 times in order to assess the stability of the platforms under mechanical stress. From Fig. 3.12, both DC and CAC modes adhered well to the skin. However, buckling effects were observed with the DC mode after movement. The CAC mode did not show any visible buckling or fracturing, indicating that it had a robust adherence to skin after movement. As expected, the CA layer enhanced adherence of the overall tattoo platform to skin over the course of several flexion-extension movements. This shows that the CA layer had a positive impact on the CAC mode’s adherence and mechanical properties.

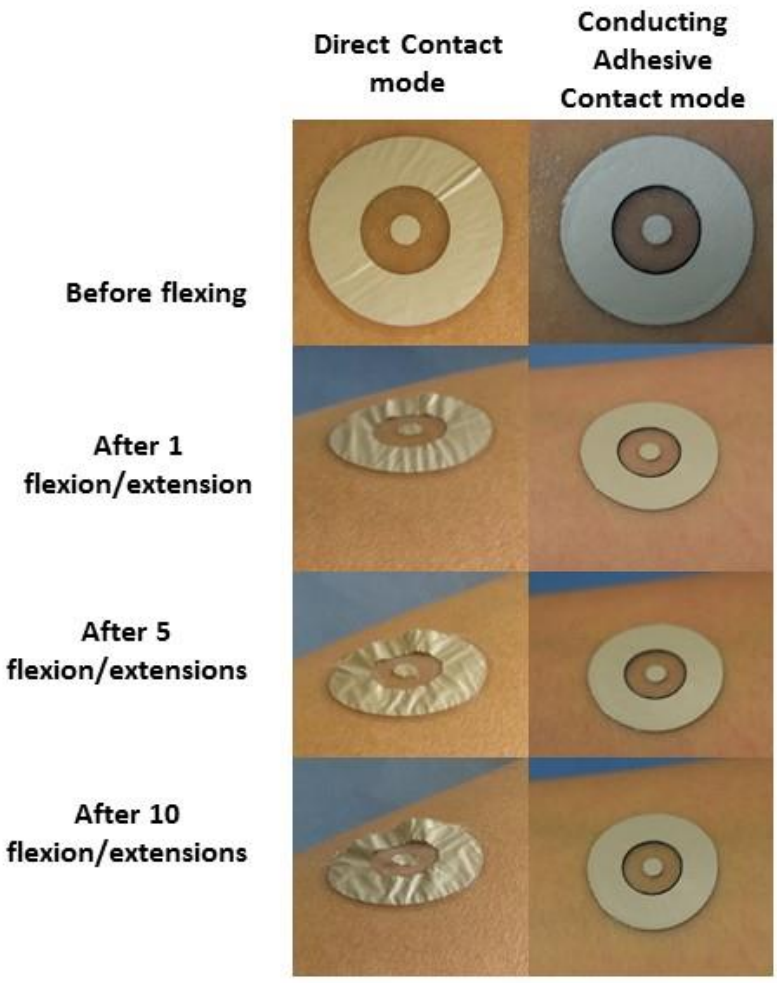

Figure 3.12 Images comparing the silver-elastomer DC (previously shown in Fig.3.4) and silver-elastomer CAC mode on skin before and after flexion-extension movements of the forearm (tattoo electrode diameter 20 mm). Images taken using a Nikon D3300 camera.

3.3.2.4 Tracking skin barrier properties upon exposure to topical treatments

A preliminary skin barrier disruption study was carried out on a single participant in order to test if the CAC mode was capable of tracking electrical changes after altering the skin barrier chemically. The skin barrier was exposed to DI water and 0.5% SDS in water for fixed periods of time in order to see if the tattoo could detect changes in the skins electrical properties after these treatments. Sodium dodecyl sulfate (SDS) has also been commonly used as an irritant in dermatological studies [28], [29] and skin exposure to SDS can lead to various degrees of skin

barrier damage. The CAC mode was used to track electrical changes of skin after these topical treatments. A narrow frequency range was used to mitigate the influence of noise as well as shorten the measurement (Fig. 3.13). A skin probe measurement was also taken to understand if it would be able to detect tissue dielectric constant changes in skin. The Nyquist plot shows a lower capacitive feature after exposure to 0.5 % SDS compared to water suggesting that the interface between the skin and electrode have been altered (Fig. 3.13). The corresponding Bode plots indicate that water applied on skin had a higher overall impedance while 0.5 % SDS on skin had a lower overall impedance, data shown in Appendix, Fig. A3.C. The Z' values at 1 MHz were collected before and after each type of exposure to investigate its effect on the viable tissue. The difference (delta values (Δ)) between the before and after measurements were calculated for the CAC mode and skin probe measurements (Table 3.4). The impedance was reduced after exposure to both topical treatments, which correlated to the increase in skin probe values measured tabulated in Table 3.3. It is interesting that the Δ values measured by the CAC mode platform for both exposures did not substantially differ. This suggests that the topical treatments had an effect on the skin surface, but it did not substantially affect the viable tissue associated to the high frequency measurement (Fig. 3.13b). However, the skin probe values indicate that the tissue dielectric constant after exposure to 0.5 % SDS was slightly higher compared to water. This suggests that the probe may be more sensitive to changes in tissue dielectric compared to the CAC mode platform. The difference after exposure to 0.5% SDS observed by the skin probe may likely be due to the partial disruption of the skin lipids [30]. Soltanipoor *et al*. has demonstrated on a small population that skin barrier impairment and the inflammatory response are specific to the irritants exposed to the skin [31]. They observed that the capacitance of the skin decreases 24 hours after exposure to 0.5% SDS [31], which was observed at the lower frequency region using the CAC mode platform after application of 0.5% SDS on skin. However another research group measured skin capacitance and observed that there was no statistical difference before and after immediate application of SDS [32]. The differences in results between the two research groups suggest that the effect ionic surfactant on human skin is still not fully understood and requires a standardized method of testing. Overall this study has shown that the CAC mode was capable of measuring a relative change before and after the different topical treatments. The data suggests that measurements from the CAC mode platform attributed to the deeper tissue layers after exposure to the two topical treatments could not be differentiated from each other. However, it was observed

that there was a decrease in capacitance at the lower frequency range after topical treatment of SDS indicating that the electrical properties have changed. Although it is difficult to know whether this was due to the addition of ions after treating the skin with SDS or the degradation of the lipids within the skin that has changed at the interfacial contact between the electrodes and skin. Further investigation using various topical treatments and concentrations would help towards understanding how the electrical properties of the skin surface and viable tissue can change and be affected by different types of chemical exposure.

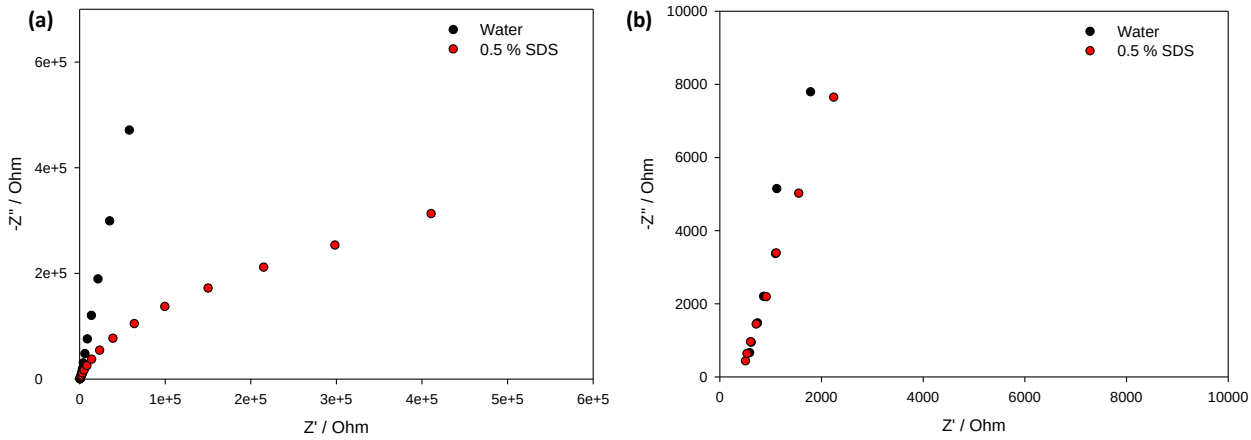

Figure 3.13 Representative (a) Nyquist plots of inner forearm after topical treatments of water and 0.5 % SDS in water collected using the silver-elastomer CAC platform and (b) magnification of the higher frequency region of the Nyquist plots. Corresponding Bode plots in Appendix Fig. A3.C.

Table 3.3 Comparison of measurements taken using the silver CAC mode and skin probe after different topical treatments (n=3).

Silver-elastomer CAC mode			
Topical treatment	**Before treatment Z/Ω**	**After treatment Z/Ω**	**Δ Z/Ω**
Water only	747 ± 27	572 ± 30	-175
0.5 % SDS	731 ± 39	540 ± 36	-190
Skin probe			
Topical treatment	**Before treatment**	**After treatment**	**Δ a.u.**

	a.u.	a.u.	
Water only	25.6 ± 1.2	30.1 ± 1.6	-4.5
0.5 % SDS	28.8 ± 0.7	35.9 ± 2.3	-7.1

3.3.2.5 Participant study using CAC mode

The CAC mode was applied onto the inner forearms of 8 healthy participants and impedance spectra were taken. As before, due to the presence of noise at frequencies below 100 Hz, modelling was carried out with data collected between 1 MHz and 100 Hz using the circuit model for skin described in Section 3.3.2. The measurements from the CAC mode were compared to skin probe measurements for the same participants using the Delfin skin probe (before pre-treatment of the skin). The Delfin skin probe used operates at a 300 MHz and can detect free and bound water in the tissue within the effective measurement depth of the probe [33], [34]. The skin probe used was had an effective depth measurement of 0.5 mm. Skin probe values (TDC) were compared to the R_{vt} values measured by the CAC mode by plotting them against each other and performing a regression analysis. A Pearson's correlation of 0.2533 was obtained indicating poor correlation between the R_{vt} and skin probe measurements in this participant study (Fig. 3.14).

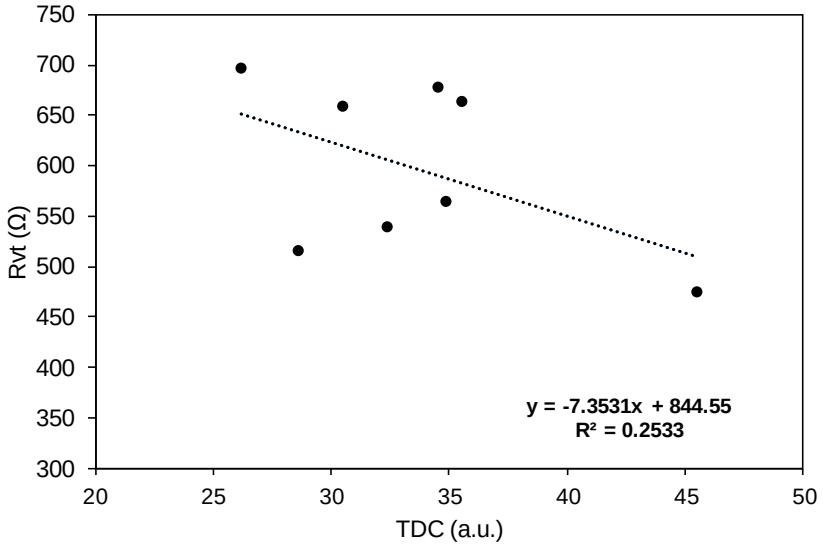

Figure 3.14 Regression analysis comparing the participant data from the tattoo platform (R_{vt} values) to that from the skin probe.

Further analysis of both Z'/Ohm values and R_{vt} from the wider frequency sweep (1 MHz to 0.1 Hz) were also compared to the skin probe measurements before and after pre-treatment, but these also showed poor correlation. This poor correlation between the silver-elastomer CAC mode measurements and skin probe measurements were likely as a result of not being able to deconvolute the R_{vt} measurement from that of the resistance of the CA. A reason for this could be the high resistance and capacitance contribution of the CA material on its own which makes it challenging to reliably differentiate the electrical contributions of the viable skin layer. Despite showing promising mechanical properties, the CAC mode was found not to be suitable for measuring the resistance values of viable tissue in a population. Future studies using this CAC mode might require the removal of the highly resistive SC barrier to reduce the contact impedance between the CA layer and the skin. Alternatively a thinner and more conducting adhesive could be used to adhere the electrodes onto the skin.

3.4 Conclusion

Initially, this chapter investigated the impact of elastomer in a silver ink formulation in relation to the wearability of a screen-printed tattoo platform. It was shown that the silver and silver-elastomer platforms had reasonably comparable physical and electrical characteristics. The silver-elastomer platform had a positive impact on the mechanical stability of the wearable platform as it did not fracture upon stretching and has improved the stretchability of the overall platform from 3.83 % to 6.27 %. However, delamination and buckling of both silver and silver-elastomer platforms on skin remained an issue. Therefore to further improve adherence to skin, a CA layer was incorporated into the silver-elastomer platform. The results from tensile testing indicated that the Young's modulus increased from 0.16 MPa to 0.34 MPa, while the yield stress increased from 1.17 N/mm^2 to 2.72 N/mm^2 suggesting that the CAC mode was more mechanically robust compared to the DC mode, which made it a promising platform for long-term monitoring. The impedance measurements indicated that the CA material had a high resistance and capacitance associated with it, which affected the impedance measurements of skin. This high impedance made it difficult to differentiate the electrical contributions of the viable skin from the CA, which was shown in the participant study. The participant study showed that the measurements from the CAC and TDC measurements from a skin probe poorly correlated (R^2 = 0.2533) with each other suggesting that values measured by this tattoo platform were not comparable to the TDC values measured across a large population. Nevertheless, the materials used to fabricate the CAC platform could potentially be used to measure relative changes in skin electrical properties as observed in the study for tracking barrier properties upon exposure to topical treatment. This would require further investigation into how the electrical properties of the skin surface and viable tissue can change and be affected by different types of chemical exposure. Future studies can also focus on alternative adhesive materials that are potentially more conducting than the CA material or another possible route could be developing a conductive ink formulation that has adhesive properties. However, this would require extensive knowledge in ink formulations in order to develop a formulation with adhesive properties that doesn't significantly affect the electrical performance of the electrodes.

Overall this chapter demonstrates that selection of ink formulations and adherence methodologies are important considerations in the fabrication and implementation of wearable based sensors. This work also demonstrates that a compromise between mechanical stability and acquisition of reliable

electrical measurements is required for wearable epidermal sensors of this type for long-term monitoring.

3.5 References

[1] J. Kim, R. Kumar, A. J. Bandodkar, and J. Wang, "Advanced Materials for Printed Wearable Electrochemical Devices: A Review," *Adv. Electron. Mater.*, vol. 3, p. 1600260, 2016.

[2] A. Martín, J. Kim, J. F. Kurniawan, J. R. Sempionatto, J. R. Moreto, G. Tang, A. S. Campbell, A. Shin, M. Y. Lee, X. Liu, and J. Wang, "Epidermal Microfluidic Electrochemical Detection System: Enhanced Sweat Sampling and Metabolite Detection," *ACS Sensors*, vol. 2, no. 12, pp. 1860–1868, 2017.

[3] A. Koh, D. Kang, Y. Xue, S. Lee, R. M. Pielak, J. Kim, T. Hwang, S. Min, A. Banks, P. Bastien, M. C. Manco, L. Wang, K. R. Ammann, K. I. Jang, P. Won, S. Han, R. Ghaffari, U. Paik, M. J. Slepian, G. Balooch, Y. Huang, and J. A. Rogers, "A soft, wearable microfluidic device for the capture, storage, and colorimetric sensing of sweat," *Sci. Transl. Med.*, vol. 8, no. 366, 2016.

[4] T. Guinovart, A. J. Bandodkar, J. R. Windmiller, F. J. Andrade, and J. Wang, "A potentiometric tattoo sensor for monitoring ammonium in sweat.," *Analyst*, vol. 138, no. 22, pp. 7031–8, 2013.

[5] D.-H. Kim, N. Lu, R. Ma, Y.-S. Kim, R.-H. Kim, S. Wang, J. Wu, S. M. Won, H. Tao, A. Islam, K. J. Yu, T. Kim, R. Chowdhury, M. Ying, L. Xu, M. Li, H.-J. Chung, H. Keum, M. McCormick, P. Liu, Y.-W. Zhang, F. Omenetto, Y. Huang, T. Coleman, and J. A. Rogers, "Epidermal Electronics," vol. 333, pp. 838–843, 2011.

[6] X. Huang, W.-H. Yeo, Y. Liu, and J. A. Rogers, "Epidermal differential impedance sensor for conformal skin hydration monitoring.," *Biointerphases*, vol. 7, no. 1–4, p. 52, Dec. 2012.

[7] S. Kabiri Ameri, R. Ho, H. Jang, L. Tao, Y. Wang, L. Wang, D. M. Schnyer, D. Akinwande, and N. Lu, "Graphene Electronic Tattoo Sensors," *ACS Nano*, vol. 11, no. 8, pp. 7634–7641, 2017.

[8] E. M. Ahmed, "Hydrogel: Preparation, characterization, and applications: A review," *J. Adv. Res.*, vol. 6, no. 2, pp. 105–121, 2015.

[9] L. Han, L. Yan, K. Wang, L. Fang, H. Zhang, Y. Tang, Y. Ding, L. T. Weng, J. Xu, J. Weng,

Y. Liu, F. Ren, and X. Lu, “Tough, self-healable and tissue-adhesive hydrogel with tunable multifunctionality,” *NPG Asia Mater.*, vol. 9, no. 4, 2017.

[10] H. Lee, S. M. Dellatore, W. M. Miller, and P. B. Messersmith, “Mussel-Inspired Surface Chemistry for Multifunctional Coatings,” *Science (80-.).*, vol. 318, no. 5849, pp. 426–430, 200AD.

[11] B. K. Ahn, D. W. Lee, J. N. Israelachvili, and J. H. Waite, “Surface-initiated self-healing of polymers in aqueous media,” *Nat. Mater.*, vol. 13, no. 9, pp. 867–872, 2014.

[12] Z. Wang, J. Chen, L. Wang, G. Gao, Y. Zhou, R. Wang, T. Xu, J. Yin, and J. Fu, “Flexible and wearable strain sensors based on tough and self-adhesive ion conducting hydrogels,” *J. Mater. Chem. B*, vol. 7, no. 1, pp. 24–29, 2019.

[13] S. H. Jeong, S. Zhang, K. Hjort, J. Hilborn, and Z. Wu, “Stretchable Electronic Devices: PDMS-Based Elastomer Tuned Soft, Stretchable, and Sticky for Epidermal Electronics (Adv. Mater. 28/2016),” *Adv. Mater.*, vol. 28, no. 28, p. 5765, 2016.

[14] S. Yao, A. Myers, A. Malhotra, F. Lin, A. Bozkurt, J. F. Muth, and Y. Zhu, “A Wearable Hydration Sensor with Conformal Nanowire Electrodes,” *Adv. Healthc. Mater.*, vol. 6, no. 6, pp. 1–8, 2017.

[15] J. a Fan, W.-H. Yeo, Y. Su, Y. Hattori, W. Lee, S.-Y. Jung, Y. Zhang, Z. Liu, H. Cheng, L. Falgout, M. Bajema, T. Coleman, D. Gregoire, R. J. Larsen, Y. Huang, and J. a Rogers, “Fractal design concepts for stretchable electronics.,” *Nat. Commun.*, vol. 5, p. 3266, 2014.

[16] Y. Liu, J. J. S. Norton, R. Qazi, Z. Zou, K. R. Ammann, H. Liu, L. Yan, P. L. Tran, K.-I. Jang, J. W. Lee, D. Zhang, K. A. Kilian, S. H. Jung, T. Bretl, J. Xiao, M. J. Slepian, Y. Huang, J.-W. Jeong, and J. A. Rogers, “Epidermal mechano-acoustic sensing electronics for cardiovascular diagnostics and human-machine interfaces,” *Sci. Adv.*, vol. 2, no. 11, pp. e1601185–e1601185, 2016.

[17] N. Matsuhisa, M. Kaltenbrunner, T. Yokota, H. Jinno, K. Kuribara, T. Sekitani, and T. Someya, “Printable elastic conductors with a high conductivity for electronic textile applications,” *Nat. Commun.*, vol. 6, no. May, p. 7461, 2015.

[18] A. J. Bandodkar, I. Jeerapan, J. M. You, R. Nuñez-Flores, and J. Wang, “Highly Stretchable

Fully-Printed CNT-Based Electrochemical Sensors and Biofuel Cells: Combining Intrinsic and Design-Induced Stretchability," *Nano Lett.*, vol. 16, no. 1, pp. 721–727, 2016.

[19] S. Yao and Y. Zhu, "Wearable multifunctional sensors using printed stretchable conductors made of silver nanowires," *Nanoscale*, vol. 6, no. 4, p. 2345, 2014.

[20] A. J. Bandodkar, W. Jia, C. Yardımcı, X. Wang, J. Ramirez, and J. Wang, "Tattoo-Based Noninvasive Glucose Monitoring: A Proof-of-Concept Study," 2014.

[21] A. J. Bandodkar, V. W. S. Hung, W. Jia, G. Valdés-Ramírez, J. R. Windmiller, A. G. Martinez, J. Ramírez, G. Chan, K. Kerman, and J. Wang, "Tattoo-based potentiometric ion-selective sensors for epidermal pH monitoring.," *Analyst*, vol. 138, pp. 123–128, Jan. 2013.

[22] A. K. Dąbrowska, G.-M. Rotaru, S. Derler, F. Spano, M. Camenzind, S. Annaheim, R. Stämpfli, M. Schmid, and R. M. Rossi, "Materials used to simulate physical properties of human skin," *Ski. Res. Technol.*, vol. 22, no. 1, pp. 3–14, 2016.

[23] T. Yamamoto and Y. Yamamoto, "Electrical properties of the epidermal stratum corneum," *Med. Biol. Eng. Comput.*, vol. 14, no. 2, pp. 151–158, 1976.

[24] E. A. White, M. E. Orazem, and A. L. Bunge, "Characterization of damaged skin by impedance spectroscopy: Mechanical damage," *Pharm. Res.*, vol. 30, no. 8, pp. 2036–2049, 2013.

[25] Y. Chen, W. Pei, S. Chen, X. Wu, S. Zhao, H. Wang, and H. Chen, "Poly(3,4-ethylenedioxythiophene) (PEDOT) as interface material for improving electrochemical performance of microneedles array-based dry electrode," *Sensors Actuators, B Chem.*, vol. 188, pp. 747–756, 2013.

[26] E. A. White, M. E. Orazem, and A. L. Bunge, "Characterization of damaged skin by impedance spectroscopy: Chemical damage by dimethyl sulfoxide," *Pharm. Res.*, vol. 30, no. 10, pp. 2607–2624, 2013.

[27] J. B. Simi??-Krsti??, A. J. Kalauzi, S. N. Ribar, L. R. Matija, and G. N. Misevic, "Electrical properties of human skin as aging biomarkers," *Exp. Gerontol.*, vol. 57, pp. 163–167, 2014.

[28] R. A. Tupker, C. Willis, E. Berardksca, C. H. Lee, M. Fartasch, T. Atinrat, and J. Serup,

"Guidelines on sodium lauryl sulfate (SLS) exposure tests," *Contact Dermatitis*, vol. 37, no. 2, pp. 53–69, 1997.

[29] I. Angelova-Fischer, I. Dapic, A. K. Hoek, I. Jakasa, T. W. Fischer, D. Zillikens, and S. Kezic, "Skin barrier integrity and natural moisturising factor levels after cumulative dermal exposure to alkaline agents in atopic dermatitis," *Acta Derm. Venereol.*, vol. 94, no. 6, pp. 640–644, 2014.

[30] C. Barba, C. Alonso, M. Martí, A. Manich, and L. Coderch, "Skin barrier modification with organic solvents," *Biochim. Biophys. Acta - Biomembr.*, vol. 1858, no. 8, pp. 1935–1943, 2016.

[31] M. Soltanipoor, T. Stilla, C. Riethmüller, J. P. Thyssen, J. K. Sluiter, T. Rustemeyer, T. W. Fischer, S. Kezic, and I. Angelova-Fischer, "Specific barrier response profiles after experimentally induced skin irritation in vivo," *Contact Dermatitis*, vol. 79, no. 2, pp. 59–66, 2018.

[32] K. De Paepe, D. Roseeuw, and V. Rogiers, "Repair of acetone- and sodium lauryl sulphate-damaged human skin barrier function using topically applied emulsions containing barrier lipids," *J. Eur. Acad. Dermatology Venereol.*, vol. 16, no. 6, pp. 587–594, 2002.

[33] H. N. Mayrovitz, A. Grammenos, K. Corbitt, and S. Bartos, "Young adult gender differences in forearm skin-to-fat tissue dielectric constant values measured at 300 MHz," *Ski. Res. Technol.*, vol. 22, no. 1, pp. 81–88, 2016.

[34] H. N. Mayrovitz and M. Luis, "Spatial variations in forearm skin tissue dielectric constant.," *Skin Res. Technol.*, vol. 16, no. 4, pp. 438–43, Nov. 2010.

Chapter 4

Porous Tattoo Platform For Skin Physiology Monitoring

4.1 Introduction

The development of wearable sensors aimed at personalised healthcare management has grown in recent years due to their potential value in continuous on-body monitoring [1]. Wearable sensing devices are growing in their capability around collecting real-time physical, chemical and even biochemical data [2]–[4]. The driver for the development of these devices is directly related to the big opportunity in healthcare whereby wearables have the potential to allow users or patients monitor their own health status aswell as disease progression, and inform on treatment compliance and efficacy outside the healthcare setting.

Skin-based wearable devices are an important subset of wearables, as directly adhering the sensor onto skin has clear advantages in terms of close proximity for accessing and monitoring skin physiology [5]–[7]. Skin-based wearable sensors have been applied recently in detecting physiological parameters such as skin temperature [8], transcutaneous oxygen pressure [9], and electromyography (EMG) [10]. The growing interest in this field has opened up opportunities for new developments in material engineering to meet the challenge of mechanical compliance and adherence of transducers on skin. Skin-based impedance measurements are used to measure electrophysiological properties including electrical activity of the heart and brain, and the electrical properties of skin tissue. When monitoring electrical activity in the body via the skin, understanding the electrode-skin interface is crucial as this can determine the quality of the signal. For example, in an electroencephalography (EEG) application, electrode formats were tested on scalp skin under different conditions in order to establish a stable and conductive pathway through the skin [11], [12]. The holy grail is to develop a wholly dry electrode system for this application, given the deletrious drying effects over time for wet electrodes [11], [13]. In the case of directly characterising the electrical properties of the skin tissue itself, dry electrodes are sufficient once electronic circuitry has the capability to measure the high impedances associated with the outer skin barrier. Dry electrodes have been used to track alterations in skin tissue, such as changes in water content [13], [14] and differentiating normal and cancerous tissue [15].

Human skin is a heterogeneous, anisotropic and non-linear visco-elastic material. Skin-based wearable sensors should ideally comprise materials that can conform to the topology of skin. Research groups such as that of Rogers have induced mechanical stability into epidermal devices through the design of stretchable periodic serpentine or fractal geometries for conducting tracks that can accommodate enhanced mechanical strain [16]. Another approach

reported by this group involves pre-stretching the substrate to produce buckling in the attached conductor [17].

Many other research groups have also been publishing methods and device prototypes for flexible and stretchable epidermal sensors that can acquire real-time, electrical measurements of skin using new materials and fabrication methods to also achieve mechanical compliance on skin [14], [18], [19]. For instance, Ameri *et al* reported a graphene-electronic tattoo using a 'wet transfer, dry patterning' method which resulted in a total thickness of just 463 ± 30 nm and a stretchability of more than 40% [18]. These resulting thin materials adhere well to the skin via just van der Waals forces. Adhesion could be further improved with liquid bandage coverage.

Screen-printing is a well-established technique for the fabrication of electrodes and has recently been used to fabricate epidermal sensing platforms. For instance, Wang's research group have shown the versatility of the screen-printing methodology by fabricating wearable electrochemical biosensors that can monitor ethanol [20] and sodium [21] via skin sweat using this technique. Screen-printing, as a thick film fabrication technology typically produces films with thicknesses between 0.1–100 mm. Temporary tattoo paper substrates can be used as substrate to print desired materials onto, which can be released and applied to skin via release liner. For example, Bandodkar *et al* reported a wearable solid state ion selective electrode (ISE) for the detection of sodium ions in sweat [21]. In this case, the sensing interface sits above the skin on adhesive and a fluidic channel was used to deliver induced sweat from the skin to the sensor. This platform was shown to withstand high strains without compromising its sensing properties. Imani *et al* also use a screen-printed electrochemical cell, this time for enzyme-based lactate detection. In this case, the sensing interface was separated from skin via a drop-coated polyvinyl chloride (PVC) membrane which the sweat-derived lactate could directly permeate [2].

Good resilience against the mechanical deformations of the epidermis is critical in all these types of devices. There is a need to improve the mechanical properties of these platforms above what can be realised using traditional formulations of screen-printable flexible inks for these epidermal applications. For example, the addition of carbon nanofibres into traditional screen-printable flexible inks has been used as a strategy to increase tensile strength [6]. Stretchability, a critical mechanical property for epidermal sensing, was induced into films by screen-printing a flexible silver particulate-based ink onto a thin polyurethane substrate. After curing, the ink-

based silver flakes became embedded in the substrate to form stretchable silver-polymer interconnects [22].

It should be noted that it can be difficult to compare platforms and approaches reported in the literature based on mechanical characterisations carried out since geometry, thickness, materials used etc. will all vary. Furthermore, tensile testing methods used will be different in many cases. However, what is important is that each platform should be optimised for its specific application and wearability requirements, e.g. retain the required contact with skin under the strain and tension needs for the given application, and be fit for purpose.

In many of the cases described above relating to screen-printed wearable and epidermal materials, adhesives among other approaches are used to mount electrodes onto skin. Adhesives serve primarily to induce strong adhesion between the sensor and the skin but can also have the consequence of isolating the sensing interface from the skin, which in many cases is required. Chapter 3 demonstrated that selection of ink formulations and adherence methodologies are important considerations in the fabrication and implimentation of skin-based wearable platforms. In this previous chapter, a conducting adhesive (CA) layer was incorporated into the screen-printed platform to improve adherence. Despite having robust mechanical properties, this CAC platform did not have the ideal electrical properties for a wearable hydration sensor because it was difficult to fully deconvolute the contributions from the viable tissue and CA layer. This chapter presents a new way to adhere screen-printed electrode materials that are both flexible and stretchable onto skin. This strategy incorporates the use of a porous adhesive layer between the screen-printed stretchable electrodes and the skin. The pores were machined into a thin non-conducting adhesive layer and the impact of these pores were investigated electrically on hydrogel and skin. The most promising porous adhesive layer platform was assessed for its mechanical robustness using tensile strength testing. Its potential as a wearable hydration sensor was investigated through a participant study and topical treament study.

4.2 Materials and methods

4.2.1 Materials

AG520 EI silver ink was purchased from Chimet® S.p.A. (Tuscany, Italy), referred to as silver-elastomer ink here. Temporary transfer tattoo paper and acrylic adhesive film substrates were purchased from Sports Ink™ (Dublin, Ireland). Strip boards were purchased from Maplin Electronics. Mill Max spring loaded contacts (Part. No. 0906-4-15-20-75-14-11-0) were purchased from Farnell Components (Ireland). 2.0 mm thick Poly(methyl methacrylate) (PMMA) sheetswere purchased from Radionics Ltd. (Ireland). Poly (ethylene glycol) diglycidyl ether (Avg. Mn 500) was purchased from Sigma-Aldrich (475696-500ML). Acetone and Ethanol were purchased from Brenntag UK Ltd. Jeffamine® EDR-148 polyetheramine (CAS No. 929-59-9) was donated from Huntsman Chemical Company. Silcocks Base and Vaseline® Intensive Care™ Advanced repair were bought from a local pharmacy. Porcine skin used for testing electrodes was bought from a local butcher. Polyvinyl chloride (PVC) cloth was purchased from Home Focus, Hickey & Co Ltd. (Ireland).

4.2.2 Tattoo platform design, fabrication and application

The tattoo platform design, fabrication and application to a substrate has been described previously in Chapter 2, Section 2.2.2. This platform is referred to as the Direct Contact (DC) mode in this chapter (Fig. 4.1a).

4.2.3 Assembly of adhesive layer: Adhesive Contact (AC) mode

A Graphtec CE 6000 knife cutter was used to cut arrays of defined pores (Table 4.1) into adhesive films. These porous adhesive layers were placed on top of the printed silver electrodes (Fig. 4.1b). When the tattoo was applied to substrate, the adhesive layer was sandwiched between the electrodes and the substrate surface. Various porous array designs were cut into the adhesive films (Fig. 4.2), all comprising a fixed centre pore surrounded by a set of outer pores whose pattern varied. These porous adhesives were applied onto the tattoo electrodes where the centre pore aligned with the centre of the inner electrode and the outer pores then overlaid the outer electrode. The number of outer pores varied in each design (Table 4.1). The pore diameter was maintained constant at 1.2 mm. The electrode areas reported in Table 4.1 and are based on geometrical surface areas.

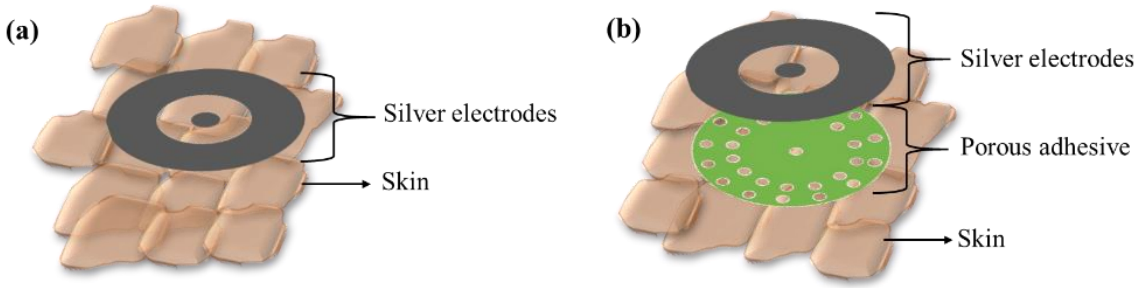

Figure 4.1 Schematic diagram of tattoo electrode platform on skin in (a) Direct Contact and (b) Adhesive Contact (Adhesive (27 pore)).

Table 4.1. Tattoo platform specifications with and without adhesive layers.

Tattoo design	**Inner pores**	**Exposed area of inner electrode (mm^2)**	**Outer pores**	**Exposed area of outer electrode (mm^2)**
Direct contact	-	7.07	-	250.54
Full adhesive	0	0	0	0
Adhesive (7 pore)	1	1.13	6	6.78
Adhesive (27 pore)	1	1.13	26	29.38
Adhesive (31 pore)	1	1.13	30	33.90
Adhesive (46 pore)	1	1.13	45	50.85

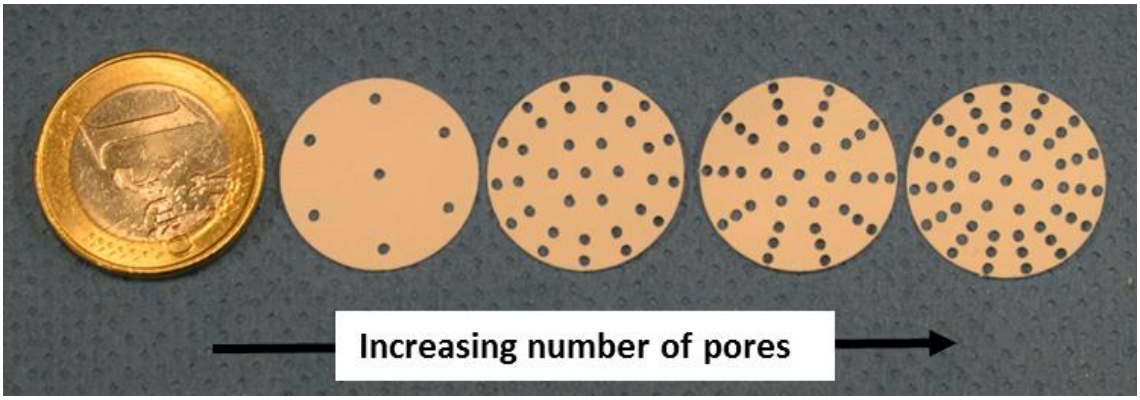

Figure 4.2 Image of the various porous adhesive film platforms.

4.2.4 Physical characterisation of DC and AC mode platforms

The electrode films were characterised by measuring resistance, thickness and imaging using the methods previously described in Section 3.2.4.2.

4.2.5 Hydrogel preparation

The hydrogels were prepared according to Section 2.2.5. Before impedimetric analysis the hydrogels were removed from the fridge and left to acclimatize to room temperature for 1 h. Tattoo platforms were applied to the surface of the hydrogels and an impedance spectra were recorded using the conditions in Section 3.2.4.4.

4.2.6 Mechanical characterisation

Tattoo platforms were assessed under tensile load using the method described in Section 3.2.4.3. For the screen printed silver-elastomer platforms, two different platforms were compared: Direct Contact and Adhesive (27 pore (referring to the number of pores in the platform). The tattoo platforms were adhered to the plastic plates with a 2 mm starting displacement. The adhesive layer when assembled onto the electrodes, introduces a change in thickness and cross sectional area to the platforms. The thickness used for the cross sectional area was 11.6 µm for the Direct Contact platform and 39.3 µm was used for the Adhesive (27 pore) platform.

4.2.7 Electrical characterisation

4.2.7.1 Impedance spectroscopy

Impedance spectroscopy was performed using an Autolab PGSTAT128N workstation. The frequency range scanned was 1 MHz to 0.1 Hz, unless stated otherwise. Spectra collected on the hydrogels were recorded at 0 V set potential and 0.01 V amplitude, while a set potential of 0.1 V and amplitude 0.03 V was used for skin. Unless stated otherwise, the skin was pre-treated with cotton wool soaked in deionised water for 1 min prior to application of tattoo electrodes. Spring loaded pins soldered to a strip board were used to contact the inner and outer electrodes of the platform in order to contact with the potentiostat (Fig. 4.3).

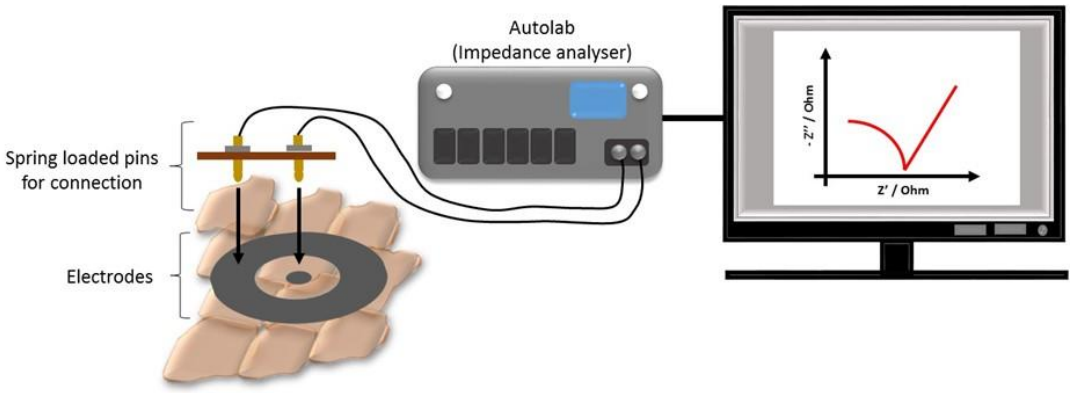

Figure 4.3 Schematic diagram of the experimental set-up when the tattoo electrodes are applied to skin and connected to the potentiostat.

4.2.7.2 Hydrogel study

Before impedimetric analysis, the hydrogels were removed from the fridge and left to acclimatize to room temperature for 1 hr. Tattoo electrodes were applied to the surface of the hydrogels and an impedance spectrum was recorded by contacting two spring loaded pins to the inner and outer electrodes of the platform.

4.2.7.3 Flexion-extension study

Flexion-extension of the arm was performed by a single participant when wearing the tattoos in both DC and Adhesive (27 pore) contact modes. These were applied to the forearm of the

participant and images of the platforms were taken with the arm extended and then again after flexing. This was repeated ten times in order to assess the mechanical stability and adherence of the platforms on the body. To assess the electrical performance of the different tattoo platforms before and after flexion-extension, the tattoo electrodes were applied onto the skin of a single participant (after pre-treatment) and an impedance spectrum was recorded using the parameters described in 4.2.7.1. An impedance measurement was recorded before flexion-extension and after each subsequent flexion-extension. A small frequency range (10,000 - 1,000 Hz) was used to reduce measurement time between flexion-extension.

4.2.7.4 Topical treatment study

DI water, water-based and oil-based moisturisers were applied to three adjacent sites on the inner forearm of a single participant. These topical treatments were applied and left on skin for 1 min. To monitor the change in electrical impedance of skin over time after application of a topical treatment, the tattoo platform (Adhesive (27 pore)) was applied to the inner forearm before any pre-treatment and the impedance was measured using a single frequency (100,000 Hz) and the parameters described in 4.2.7.1. Additional measurements were then taken at defined intervals over the following 30 min.

4.2.7.5 Participant study

Participants (3 males and 7 females, aged 19-32) were recruited and instructed not to apply perfumes or cosmetics on their arms on the days of sample collection. Participants were informed on the aim and purpose of the study and asked to provide written informed consent. An example of the Plain language statement, Informed consent form and Questionnaire can be found in the Appendix, Section A3.A. The local ethics committee (Dublin City University Research Ethics Committee) approved the study. Before application of the electrodes, tissue dielectric constants (TDC) measurements were taken on the inner forearm using a handheld Delfin MoistureMeterD (MMD) probe (Deflin Technologies, Finland) which had an effective measurement depth of 0.5 mm. Before impedance measurements, the inner forearm of the participant was pre-treated with cotton wool soaked in DI water for 1 min prior to application of tattoo electrodes. After application of the electrodes, an impedance spectra was collected using the conditions in Section 4.2.7.1.

4.3 Results and discussion

Chapter 3 has shown the use of a thick conductive adhesive as a means to adhere to the skin to improve skin-electrode adherence. The incorporation of the conducting adhesive material demonstrated robust mechanical properties for the potential of long-term monitoring. However, the electrical signal generated by conducting adhesive contact platform indicated that could not fully deconvolute the contributions from the viable tissue from the conducting adhesive layer. To enhance the wearability and improve the electrical contact of the platform, a screen-printed elastomeric silver ink formulation and non-conducting adhesive layer were used to improve skin adherence, whereby pores were designed into this layer to facilitate electrical contact between the electrodes and the skin as described in Section 4.2.3. Thus, the chapter reports the impact of these changes on the platform in order to demonstrate the applicability of our platform for wearable, continuous monitoring applications.

4.3.1 Physical characterisation of DC and AC tattoo modes

The conformability and adherence of the silver-elastomer Direct Contact (DC) and Adhesive Contact (AC) to skin were compared via imaging of the materials when applied to textured surfaces and using on-body flexion-extension movements. To assess the conformability of the screen printed platforms, the DC and AC mode platforms were applied to a PVC cloth substrate and imaged. The PVC cloth was used to emulate the non-planar surface of the skin [23]. From Fig. 4.4, it can be seen that both tattoos adhere well to the rough PVC surface. The electrodes comprising the silver-elastomer DC mode conform to the surface topology (Fig. 4.4a). An adhesive layer (film thickness: 25.82 ± 2.17 μm) was incorporated into this silver-elastomer platform to improve the electrodes adherence to skin. When this AC mode was adhered onto the PVC substrate it still maintains good conformability despite the additional thickness from the adhesive layer (Fig. 4.4b).

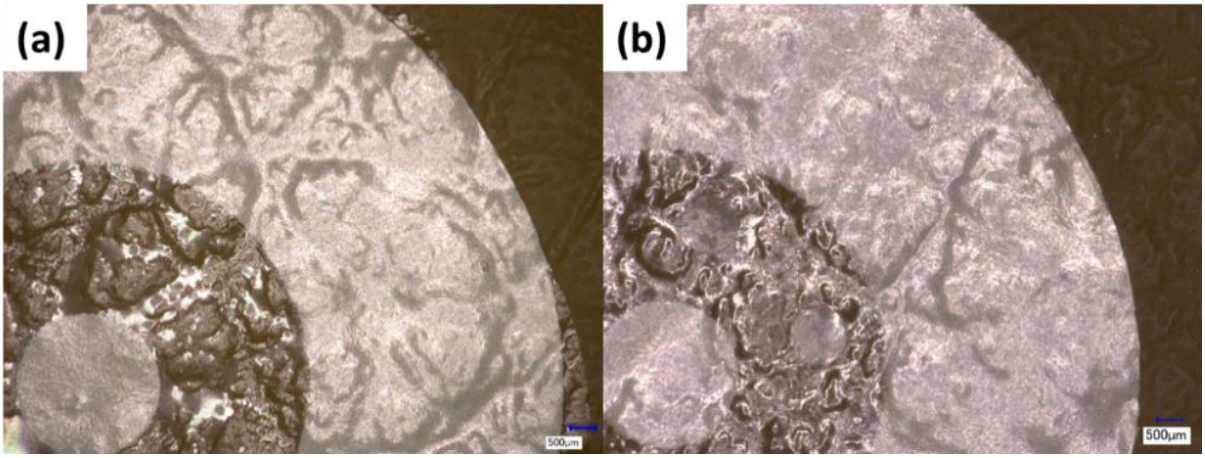

Figure 4.4 Screen-printed silver-elastomer tattoo electrodes in (a) DC mode (as previously shown in Figure 3.2) and (b) AC mode (Adhesive (27 pore)) applied to PVC substrate and were imaged using a Keyence microscope (Mag x30).

The platforms were applied to the skin of the forearm on a single participant to assess adherence to skin. The platforms were gently stretched to assess their durability under mechanical stress (Fig 4.5). It was observed that both DC and AC platforms adhere well to skin. However when mechanical stress in the form of stretching was applied, it was observed that the DC mode did not fracture upon stretching but partial buckling did occur which was likely due to weak adherence (Fig. 4.5, top right). In contrast, the AC mode remained adhered to skin to after stretching (4.5, bottom right). This indicates that the adherence of the platform has been enhanced after incorporation of this thin adhesive layer by minimising delamination and buckling during skin stretching. This indicates that the AC mode has potential in remaining adhered on skin during movement. The functionality and mechanical stability of these electrode platforms will be further investigated in Section 4.3.3.

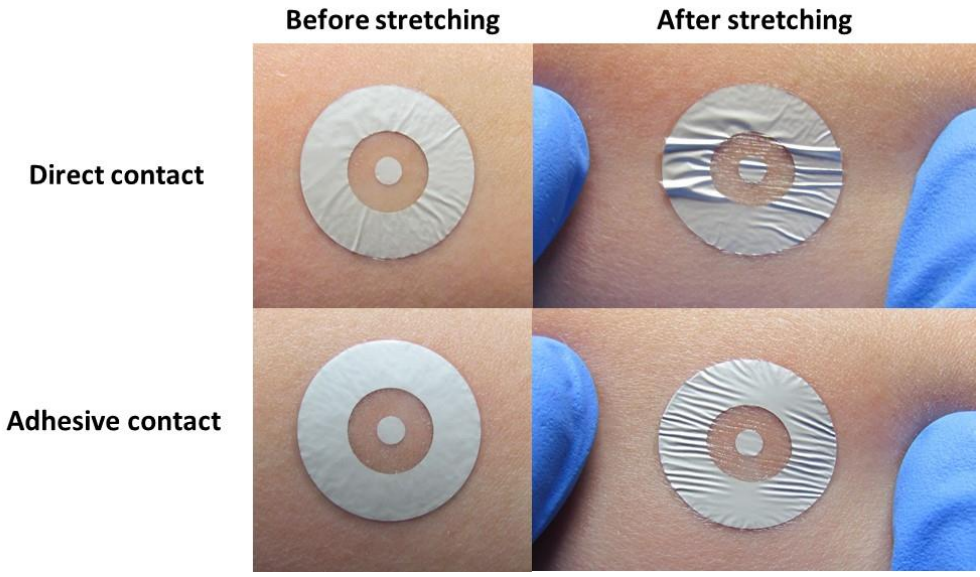

Figure 4.5 Images of the silver-elastomer based electrodes using DC (as previously shown in Figure 3.3) and AC (Adhesive (27 pore)) modes on skin before and after stretching (tattoo electrode diameter: 20 mm). Images were taken using a Nikon D3300 camera.

4.3.2 Impedance characterisation of DC and AC tattoo modes

In Chapter 3, thick conducting adhesive layer was used to adhere the electrodes to skin. However electrical measurements using this platform indicated that it was difficult to fully deconvolute the contributions from viable tissue and conducting adhesive layer. This section investigates the impact of using a thinner non-conducting adhesive layer to adhere the electrodes on to skin. The thinner adhesive would allow for closer skin-electrode contact while the porous arrays allowed propagation of the electrical signal between the electrodes. This porous adhesive, when assembled on top of the electrodes (Fig. 4.1b), served to decrease the surface area of electrode interfaced with the substrate (hydrogel or skin), compared to that without the adhesive. The number of outer pores, which refers to the number of pores on the outer electrode were varied. While a single inner pore, which refers to the pore on the inner electrode, remained fixed. The impact of the pore configuration on the impedimetric response was studied.

The DC and AC modes were initially assessed on a hydrogel to characterise the impact of the adhesive layer on the impedance response. The resulting Nyquist plots can be seen in Fig. 4.6a. Two well-defined regions attributed to the bulk hydrogel and electrode interface were observed for both platforms (Fig. 4.6b).

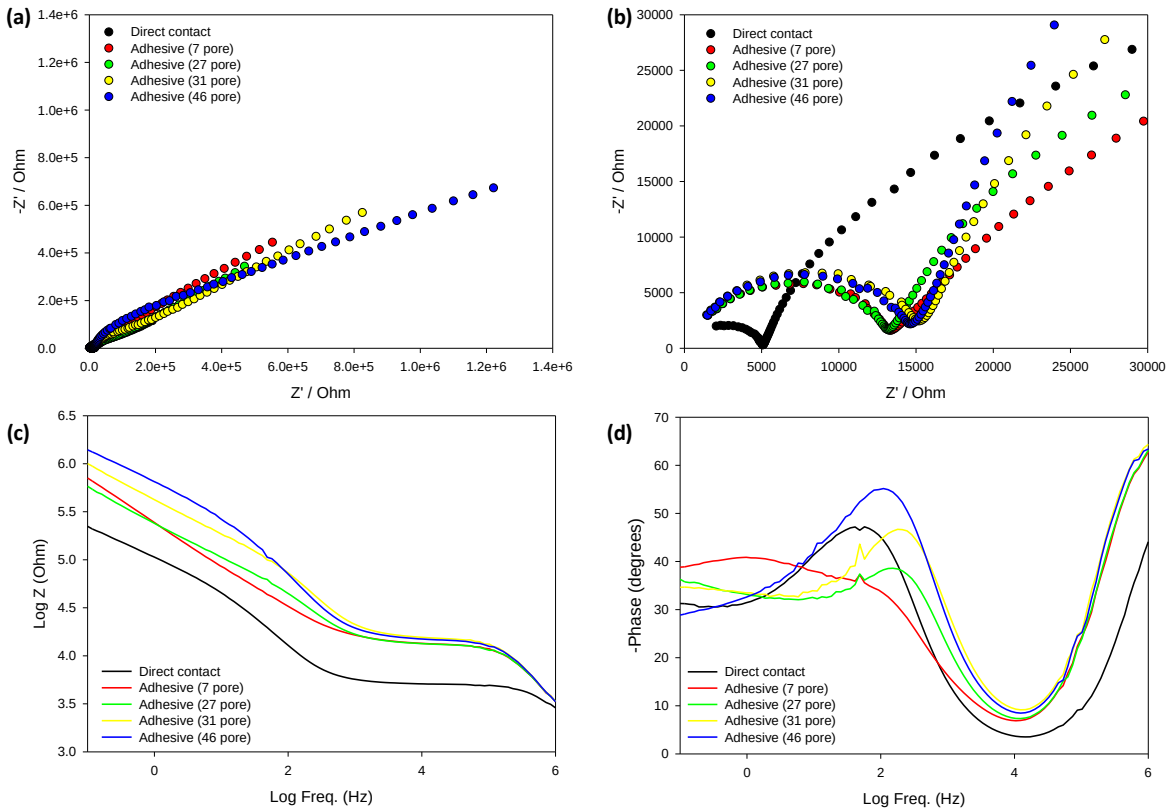

Figure 4.6 Representative (a) Nyquist plots for the PEDGE:Jeffamine hydrogel measured using the direct contact and adhesive contact platforms. (b) Magnification of the higher frequency region attributed to the bulk hydrogel. Corresponding (c) Impedance and (d) phase plots.

It was observed in the high frequency region of the Nyquist plots (Fig. 4.6b) a significant change in the diameter of the semi-circle for platforms with the porous adhesive. This region is the area of interest for the tattoo platform because the diameter of the semi-circle at the higher frequency has been attributed to the bulk hydrogel (R_{gel}) measurement. This region was modelled with a resistor and CPE in parallel seen in Fig. A4.A in the Appendix. The R_{gel} value of the DC platform was 5573 ± 495 Ω, 9 % (n=3) and increased when the porous adhesive layer was incorporated into the platform. The increase in diameter was likely due to the decrease in surface area of the electrodes in contact with the hydrogel. Therefore, the effect of the incorporation of the porous adhesive increased the total impedance of the system. It was noted that the number of pores on the outer electrode did not substantially change the R_{gel} measured: 7 pore (16887 ± 3074 Ω, 18

%), 27 pore (13944 ± 369 Ω, 3 %), 31 pore (14482 ± 2126 Ω, 15 %) and 46 pore (17301 ± 4430 Ω, 26 %) (n=3). This was likely due to the fact that the inner electrode pore was kept constant, and this limited the response. It is interesting to note that the 27 pore had the lowest %RSD compared to all the porous adhesive platforms. This indicates that the 27 pore platforms adherence and contact to the hydrogel was more repeatable compared to the other porous adhesive platforms. It was also observed that for some of the platforms with more pores on the outer electrode would be more fragile when adhered on to the hydrogel due to the smaller distances between the pores (i.e. pores would merge into one large pore). The lower frequency range attributed to the electrode-interface also had high variability and noise for the platforms with more pores on the outer electrode, indicating that the adherence of the electrodes to the hydrogel has been affected.

In order to assess the impact of the porous adhesive on the measurement of skin, the tattoo platform was applied to the inner forearm of a single participant after pre-treatment of the skin and the impedimetric response recorded. The resulting Nyquist plot of skin is shown in Fig. 4.7 and shows one semi-circle. This semi-circle has been understood as contributions from the skin and the electrode-skin interface. The R_{vt} values were extracted using the circuit model displayed in Fig. 4.7a. The corresponding Bode plots for the Direct Contact and Adhesive 27 pore are in Appendix, Fig. A4.B where it can be observed that the lower frequency range for the Adhesive 27 pore showed interfacial noise. This circuit element has been attributed to the resistance of the viable tissue at high frequency (Fig. 4.7b). Due to the presence of interfacial noise at frequencies below 100 Hz, circuit modelling was performed between 1 MHz and 100 Hz. A similar trend was observed for measurements on skin, where the DC contact platform had the lowest measured R_{vt} (518 ± 33 Ω, 6 %, n=5) while platforms with the porous adhesive layer had an increased impedance: 7 pore (641 ± 116 Ω, n=2), 27 pore (656 ± 63 Ω, 10 %, n=5), 31 pore (688 ± 60 Ω, 9 %, n=4) and 46 pore (687 ± 58 Ω, 8 %, n=4). This difference was attributed to the differences in exposed electrode surface areas as discussed above. It was noted that the platform with the lowest number of pores (7 pores) had the most noise and had the lowest repeatability (n=2), which was perhaps due to the difficulty of current passing through the resistive skin barrier and the reduced number of electrodes in contact with the skin. The impact of the number of pores on the structural integrity of the platform was also a significant consideration for choosing an appropriate adhesive contact platform for epidermal sensing. As

the number of pores increased in the adhesive layer, the reduced surface area of adhesive between the electrodes and the substrate results in a weakening of adhesion strength which would not be ideal for the epidermal sensor. Therefore, the platform chosen for the impedimetric studies in the next sections was the AC mode that utilised 27 pores on the outer electrode. It should be noted that the precision for the adhesive contact mode was lower than that for the direct contact mode. This was attributed to the presence of the porous adhesive, the thickness of which results in a more variable skin-electrode interfacial contact. For the next studies, Adhesive contact mode will be referred to as Adhesive (27 pore) mode.

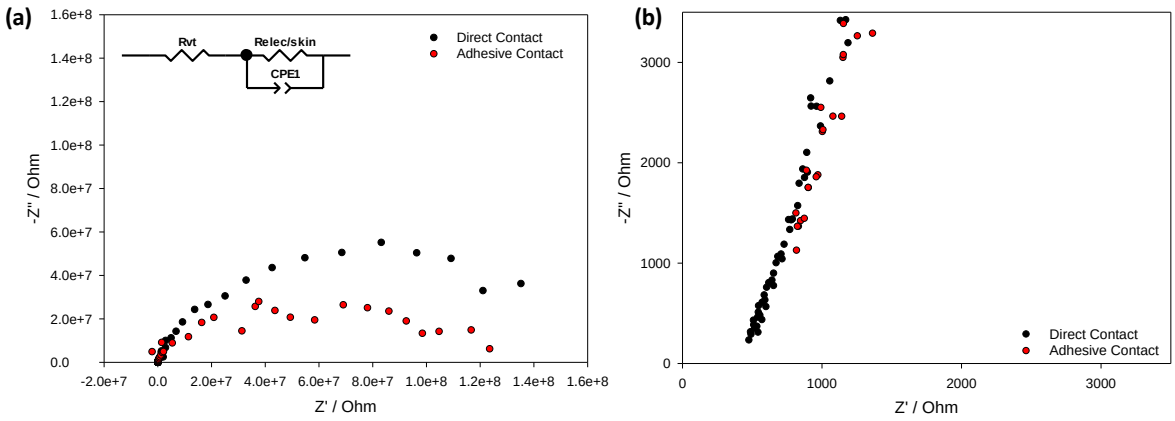

Figure 4.7 Representative (a) Nyquist plot of human skin (single participant) measured by DC and AC mode platforms and circuit model for skin (Left inset) and (b) magnification of the high frequency region. Corresponding Bode plots in Appendix, Fig. A4.B.

4.3.3 Mechanical characterisation of DC and AC tattoo modes

As discussed in Section 4.3.1, incorporation of the adhesive layer improves adherence and prevents delamination of the electrodes. The adherence and mechanical stability of the DC and Adhesive (27 pore) modes during flexion and extension of the forearm of a single participant were studied. The Adhesive (27 pore) mode was applied on to the forearm in its relaxed position and the forearm was flexed and extended and compared to the previous DC and Conducting Adhesive Contact (CAC) platform. This movement was repeated ten times in order to assess the stability of the platforms under this mechanical stress (Fig. 4.8). It can be observed that the platform that utilises DC resulted in poor skin contact causing delamination and buckling of the

platform even after a single flexion. However, the delamination effect was significantly lower in the cases of the CAC and Adhesive (27 pore) mode. Incorporation of an adhesive layer, whether it was conducting or non-conducting dramatically enhances adherence to the skin, even after a number of flexion and extensions.

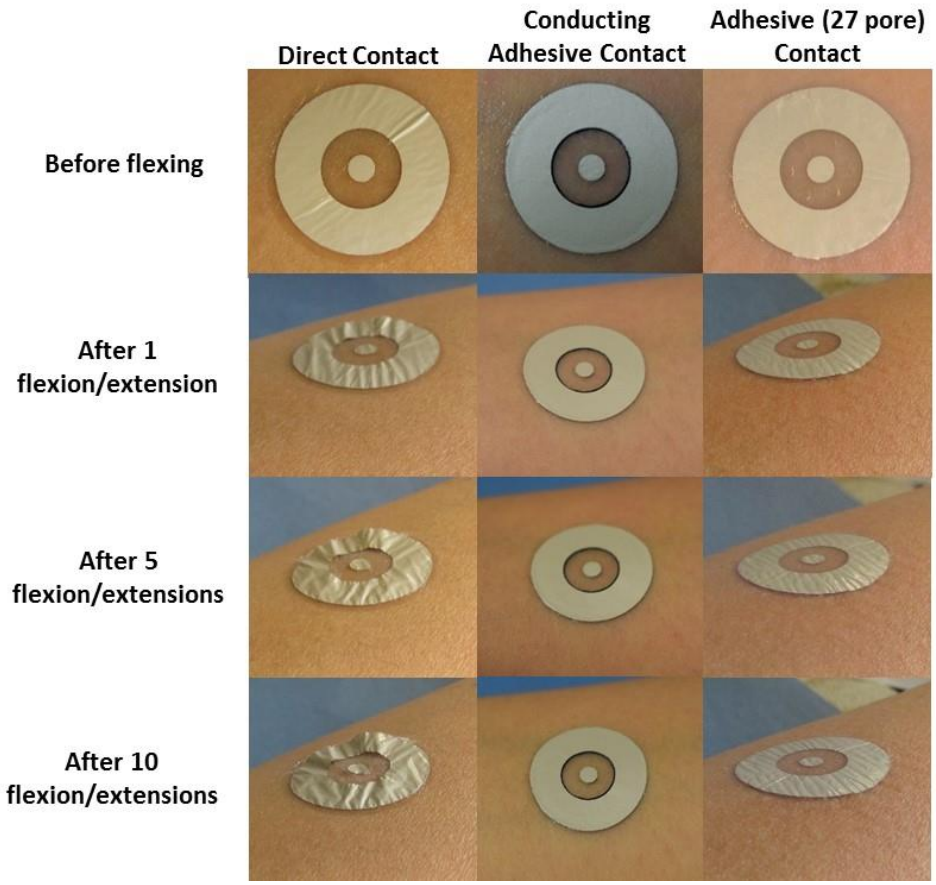

Figure 4.8 Images of the silver-elastomer electrodes comparing Direct Contact (previously shown in Fig.3.4), Conducting Adhesive Contact (previously shown in Fig.3.12) and Adhesive (27 pore) Contact on skin before and after different numbers of forearm flexion/extension movements (tattoo electrode diameter 20 mm). Images taken using a Nikon D3300 camera.

These platforms were subjected to further mechanical and electrical testing to investigate the functionality of these platforms after flexion-extension movements. In this study, the impedance response of skin was measured with the DC and Adhesive (27 pore) modes after each flexion-extension movement. The % change in the impedance response after each flex was measured using a short frequency range (Fig 4.9) and was repeated three times (n=3) for each platform. It

can be seen that the impedance response using the DC mode had large and inconsistent % changes after each flex (black dots and lines), due to inconsistent contact between the electrode and the SC, with the highest % change in response at 414 % in between flexes. The Adhesive (27 pore) mode (green dots and lines) response was < 105 % and under 8 % after 5 flexes. This demonstrates that the Adhesive (27 pore) mode, not only improves the mechanical properties of the tattoo, but also potentially improves the reliability of the electrical signal on the skin during movement. The use of the porous adhesive layer shows promising results towards a more mechanically stable skin-electrode interface. However further understanding of this porous adhesive skin-electrode interface such as other mechanical movements on different anatomical sites or during angular movements would be required to understand the mechanical and electrical capabilities or limitations of this adherence method.

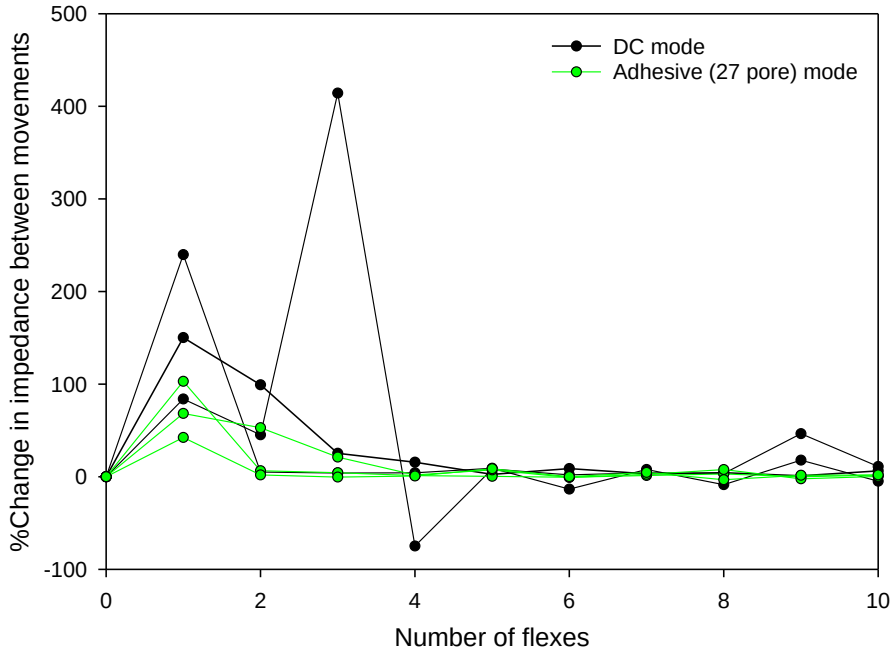

Figure 4.9. Percentage change in impedance response between flexes comparing DC and Adhesive (27 pore) modes (n=3). The DC platform (black dots and lines) show inconsistent % changes while the Adhesive (27 pore) mode (green dots and lines) shows the largest % change in impedance after the initial flex but becomes consistent after the subsequent flexes.

The DC and Adhesive (27 pore) modes were further subjected to mechanical tensile testing and the results shown in Fig. 4.10. The Young's modulus (MPa), yield strength (N/mm^2) and yield strain (%) for each of the platforms were tabulated in Table 4.2. It was observed that the Young's modulus of the Adhesive (27 pore) was five times lower than that of the DC mode. This suggests that the incorporation of a thinner porous adhesive has made the overall platform more elastic. The yield strength indicates that the DC mode is capable of withstanding higher stress compared to the Adhesive (27 pore) mode, suggesting that the pores were a point of weakness in the platform. While the yield strain suggests that incorporation of the porous adhesive layer has contributed to a 2% increase in the strain it can withstand. This indicates that the Adhesive (27 pore) can stretch more than the DC mode before failure because the porous adhesive layer is acting as a support. Based on the results, the incorporation of the porous adhesive layer in to the platform has reduced the amount of stress it can endure before fracture. However, the thinner adhesive shows enhanced elasticity and strain indicating that the platform is stretchable which would be promising for wearable sensing.

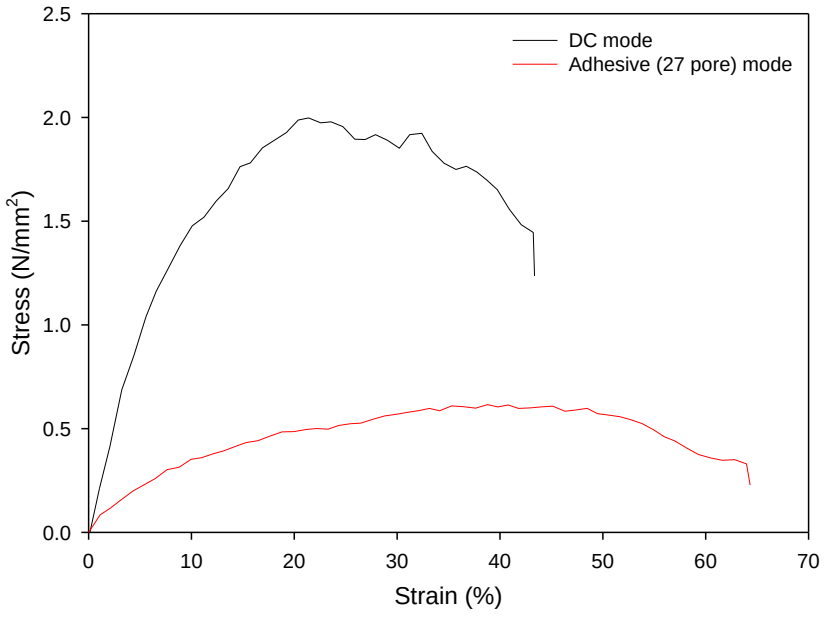

Figure 4.10 Stress-strain curves comparing the DC and Adhesive (27 pore) modes.

This Adhesive (27 pore) mode platform has a measured moduli smaller than that of the epidermis, whose modulus is taken broadly to be between 0.14 MPa – 0.6 MPa [24] but is known to be highly variable [25]. Roger's research group reports a very different electrophysiological epidermal platform. In this case, it incorporates Cu serpentine interconnects and chip components encapsulated in an elastomeric core. It was reported to have an effective moduli of 0.0318 MPa (x-direction) and 0.0311 MPa (y-direction) were reported for this device [26] which were comparable to the stiffness values of the Adhesive (27 pore) mode platform reported. The yield strength and strain values were determined using the 0.2% offset from the stress-strain curves (Table 4.2). This Adhesive (27 pore) mode platform was capable of withstanding 8% strain. However, other devices with greater yield strain values have been reported [26], [27], where these devices were typically based on serpentine designs of conductive thin films. For instance, other screen printed electrodes utilise chopped carbon fibers dispersed into the carbon and silver ink in order to add mechanical robustness into their platform, allowing the platforms to be stable under 10 % [28] and 26 % [21] strain. It should be noted that it is difficult to compare platforms based on these values since electrode configuration, device/sensor thickness, materials used and tensile testing method will be very different in all instances. However, what is important is that each platform should be optimised for its specific application and wearability requirements, e.g., retain the required contact with the skin under the strain and tension needs for the given application

Compared to all previous iterations from the previous chapter, the Adhesive (27 pore) mode platform shows promise towards a low-modulus flexible wearable sensor. Although this Adhesive (27 pore) mode platform shows excellent mechanical properties in relation to normal extension-flexion movements (Fig. 4.10), there is still opportunity to further improve the strain capability in future platforms.

Table 4.2. Summary of the mechanical properties comparing the DC and Adhesive (27 pore) modes (n=7).

Platform (Silver-elastomer)	**Young's Modulus (MPa)**	**Yield Strength (N/mm^2)**	**Yield Strain (%)**
Direct contact (DC) mode	0.16 ± 0.03	1.17 ± 0.16	6.27 ± 1.67
Adhesive (27 pore) contact mode	0.034 ± 0.005	0.32 ± 0.03	7.99 ± 1.07

4.3.4 Validation study

The Adhesive (27 pore) mode platform was applied onto the inner forearms of 11 healthy participants (between 19-32) and an impedance spectra taken according to Section 4.2.7.1. R_{vt} values obtained from the Adhesive (27 pore) mode platform were compared to TDC values measured by a skin probe (before pre-treatment). Data for one of the participants was classified as an outlier based on a regression analysis of the standardised residuals and so was omitted from further analysis. In order to compare the R_{vt} participant values with the TDC values, a regression analysis was performed (Fig. 4.11). Strong correlation (Pearson's correlation coefficient (R^2): 0.93) was observed in participants where the water content of the skin tissue was measured to be high (TDC > 27.5) (Fig. 4.13, closed circles). When the tissue dielectric constant for skin was measured to be low (TDC < 27.5), R_{vt} values no longer correlated with TDC (Fig. 4.11, open circles). This is likely due to the higher resistances of the SC in these cases, which prevented reliable R_{vt} measurements being taken with the Adhesive (27 pore) mode platform. Nonetheless, this data shows that when skin TDC values were greater than a critical value, R_{vt} correlated strongly to skin TDC.

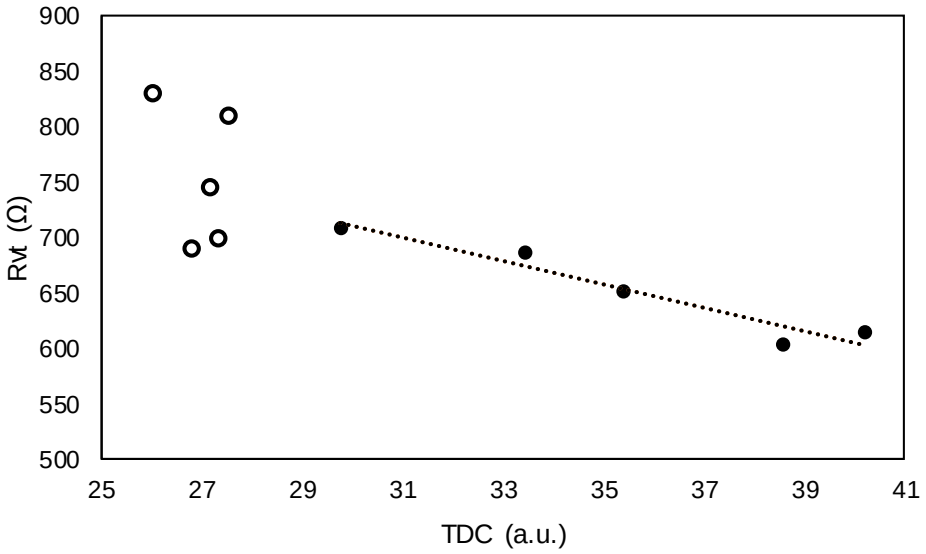

Figure 4.11 Regression analysis comparing the participant data from the tattoo platform (R_{vt} values) to that from the skin probe (black dots). Data points with TDC values <27.5 were excluded from the regression analysis (open circles).

Other works [13],[29],[30] reporting wearable skin hydration sensors, have also used skin probes to compare with their sensor responses. The group of Rogers for example, demonstrate strong correlation of their epidermal sensing approach with commercial skin probes [30]. However, to our knowledge, this is the first report of a wearable hydration sensor showing direct correlation of the individual participant responses with a TDC measurement related to the combination of skin and the deeper tissue. The result demonstrates the potential of the tattoo platform for monitoring differences in the viable tissue impedance across individuals in a population using an epidermal wearable sensing approach. Future work can potentially use the tattoo platform to measure the viable tissue water content and understand its relationship with gender, skin condition, lifestyle or age. This can potentially help with further understanding of skin physiology and its link to human health.

4.3.5 Tracking hydration uptake in skin

A study investigating the diffusion of moisturisers through skin was carried out on a single participant in order to test if the Adhesive (27 pore) mode was capable of tracking electrical changes after application of various topical treatments. The skin was exposed to three different topical treatments: DI water, water-based moisturiser and oil-based moisturiser and this was applied to three adjacent sites on the forearm. The Adhesive (27 pore) mode platform was used for tracking changes in the electrical properties of skin over time after application of different topical treatments: DI water, water based moisturiser and oil based moisturiser. After application of the treatment, the Adhesive (27 pore) mode was applied to the skin and single frequency measurements (100,000 Hz) and were taken regularly for 30 min. This data was plotted and used to track the uptake of the different topical treatments into skin over time (Fig. 4.12). After application of topical treatment, the measured impedance increased over time, indicating absorption of the topical treatment into the skin. The rate of change in the impedance response for the water treatment is greatest, indicating that the water was absorbed/diffused away into the deeper layers of the skin most rapidly. Both the water- and oil based moisturisers were taken up more slowly by the skin as indicated by the slower rate of increase in the impedance response.

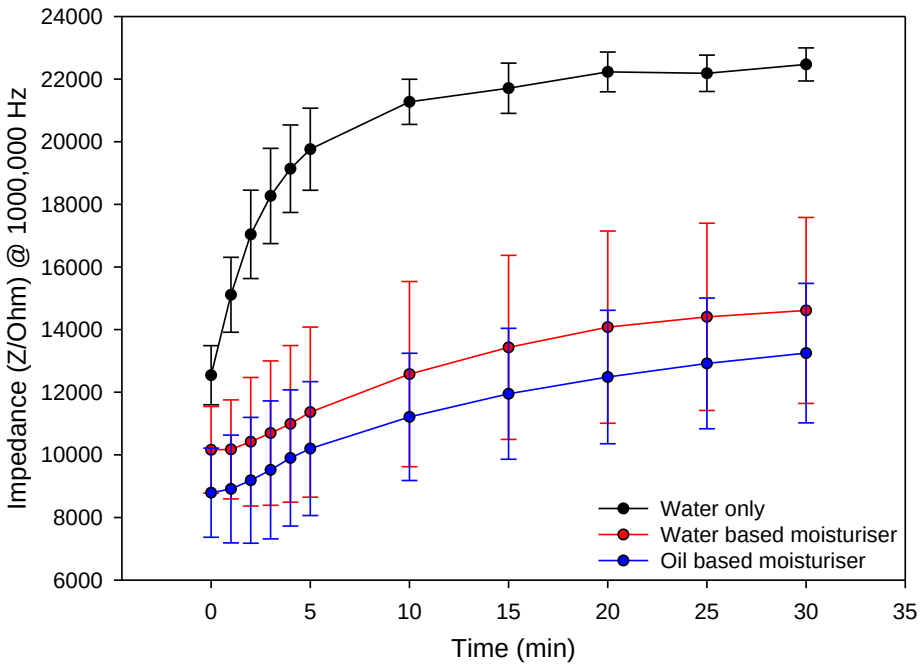

Figure 4.12 Graph showing the impedance response of Adhesive (27 pore) mode on the inner forearm after application of water, water based and oil based moisturiser overtime using single frequency measurements (100,000 Hz) (n=3).

While the skin probe was able to track the hydration changes overtime, however it did not differentiate between the different topical treatments, data shown in Appendix Fig. A4.C. It could be due to the various components present in the moisturiser formulation and the probe is only selective to changes in water content. Similar trends were also observed for other wearable skin hydration sensors reported [13], [29], [31], i.e. high impedance measured by the wearable sensor, low hydration measured by the commercial probe and vice versa. The results indicate that the Adhesive (27 pore) mode platform was capable of tracking the uptake of the water and moisturisers over time. It also demonstrates the potential use of isolating a single frequency in order to reduce measurement time of skin. This would prove advantageous for rapid analysis or measurement of skin using a wearable platform in a larger clinical setting in future. Another potential study could look at individuals with and without a known skin condition and understand the changes in electrical properties over a few days or months as an initial investigation towards understanding the differences in individuals with and without skin barrier integrity. Future work using this platform could also investigate the diffusion rate of burn gels

on skin overtime to determine the occlusive properties of such a gel and its impact on preserving skin barrier integrity.

4.4 Conclusion

This chapter presents a new way to adhere screen-printed flexible and stretchable conducting materials onto skin using an elastomeric ink formulation with a thin non-conducting adhesive material. The use of elastomeric inks give the advantage of enhanced strain while the incorporation of a thinner porous adhesive reduces stiffness and improves adherance and importantly, permits electrical field propagation into the skin. Mechanical testing indictes that this porous adhesive platform had the lowest Young's Modulus (0.03 MPa) compared to all the previous iterations, making it an ideal epidermal platform. Its mechanical and electrical stability during movment was enhanced because the highest measured change in impedance between flexes was 103 % for the porous adhesive platfrom compared to its direct contact counterpart without adhesive which had the highest change at 414 %. This indicates that the porous adhesive layer has reduced the effect of buckling and delamination of the tattoo platform on skin without substantially changing the measured electrical signal. The viable tissue resistances measured by the tattoo platform were validated against TDC measurements taken by a commercial skin probe in a participant study and has shown promsing correlation that indicates that the porous adhesive platform can function reliably when individuals have high water content (> 27.5). This indicates that the porous adhesive plaform can function reliably in an analytical window and it has also shown promising results tracking the rate of change in impedance overtime after application of different topical treatments. Overall this work has culminated in an epidermal sensing platform that will be potentially advantageous for long-term monitoring.

Future research could potentially focus on assessing mechanical and electrical properties across larger numbers of participants to further validate the platform. Another potential population study could look at individuals with and without a known skin conditions over a long period of time to start developing an understanding of the electrical properties of individuals with a healthy and disrupted skin barrier. Perhaps a thinner adhesive material could potentially be assessed and compared to this platform in order to mitigate the noise observed at the frequency range attributed to the electrode interface. This could potentially help further understand the electrode interface and contact impedance of the tattoo platform. The integration of responsive materials into the wearable platform for tracking chemical- and bio-chemical changes in skin will also be explored.

The results between Chapters 2-4 indicate that the selection of conducting ink formulation and adherence methodologies are important considerations in the fabrication and implementation of wearable skin-based sensors. Acquiring high fidelity electrical measurement in conjunction with obtaining good mechanical stability is indeed challenging and requires continued innovations in materials science aswell as a comprehensive understanding of the mechanics and conformability needs of wearable sensors on the highly textured surface of skin. Addressing these challenges using our approaches as described allows us to move towards the successful realization of a skin-based wearable device capable of collecting electrophysiological data in the skin.

4.5 References

[1] T. Glennon, C. O'Quigley, M. McCaul, G. Matzeu, S. Beirne, G. G. Wallace, F. Stroiescu, N. O'Mahoney, P. White, and D. Diamond, "SWEATCH : A Wearable Platform for Harvesting and Analysing Sweat Sodium Content," *Electroanalysis*, vol. 28, no. 6, pp. 1283–1289, 2016.

[2] S. Imani, A. J. Bandodkar, A. M. V. Mohan, R. Kumar, S. Yu, J. Wang, and P. P. Mercier, "A wearable chemical-electrophysiological hybrid biosensing system for real-time health and fitness monitoring," *Nat. Commun.*, vol. 7, no. May, pp. 1–7, 2016.

[3] A. Alizadeh, A. Burns, R. Lenigk, R. Gettings, J. Ashe, A. Porter, M. McCaul, R. Barrett, D. Diamond, P. White, P. Skeath, and M. Tomczak, "A wearable patch for continuous monitoring of sweat electrolytes during exertion," *Lab Chip*, vol. 18, no. 17, pp. 2632–2641, Aug. 2018.

[4] M. Markina, N. Stozhko, V. Krylov, M. Vidrevich, and K. Brainina, "Nanoparticle-based paper sensor for thiols evaluation in human skin," *Talanta*, vol. 165, pp. 563–569, Apr. 2017.

[5] A. J. Bandodkar and J. Wang, "Non-invasive wearable electrochemical sensors: A review," *Trends in Biotechnology*, vol. 32. pp. 363–371, 2014.

[6] A. J. Bandodkar, W. Jia, and J. Wang, "Tattoo-Based Wearable Electrochemical Devices: A Review," *Electroanalysis*, vol. 27, no. 3, pp. 562–572, 2015.

[7] H. Jin, Y. S. Abu-Raya, and H. Haick, "Advanced Materials for Health Monitoring with Skin-Based Wearable Devices," *Adv. Healthc. Mater.*, 2017.

[8] Y. Chen, B. Lu, Y. Chen, and X. Feng, "Breathable and Stretchable Temperature Sensors Inspired by Skin," *Sci. Rep.*, vol. 5, no. 1, p. 11505, 2015.

[9] C.-J. Lim, S. Lee, J.-H. Kim, H.-J. Kil, Y.-C. Kim, and J.-W. Park, "Wearable, Luminescent Oxygen Sensor for Transcutaneous Oxygen Monitoring," *ACS Appl. Mater. Interfaces*, vol. 10, p. acsami.8b13276, 2018.

[10] L. M. Ferrari, S. Sudha, S. Tarantino, R. Esposti, F. Bolzoni, P. Cavallari, C. Cipriani, V. Mattoli, and F. Greco, "Ultraconformable Temporary Tattoo Electrodes for Electrophysiology," *Adv. Sci.*, vol. 5, no. 3, p. 1700771, 2018.

[11] G. Li, S. Wang, and Y. Y. Duan, “Sensors and Actuators B : Chemical Towards conductive-gel-free electrodes : Understanding the wet electrode , semi-dry electrode and dry electrode-skin interface impedance using electrochemical impedance spectroscopy fitting,” *Sensors Actuators B. Chem.*, vol. 277, no. April, pp. 250–260, 2018.

[12] G. Li, S. Wang, and Y. Y. Duan, “Towards gel-free electrodes: A systematic study of electrode-skin impedance,” *Sensors Actuators, B Chem.*, vol. 241, no. October 2016, pp. 1244–1255, 2017.

[13] S. Yao, A. Myers, A. Malhotra, F. Lin, A. Bozkurt, J. F. Muth, and Y. Zhu, “A Wearable Hydration Sensor with Conformal Nanowire Electrodes,” *Adv. Healthc. Mater.*, vol. 6, no. 6, pp. 1–8, 2017.

[14] K. De Guzman and A. Morrin, “Screen-printed Tattoo Sensor towards the Non-invasive Assessment of the Skin Barrier,” *Electroanalysis*, vol. 29, no. 1, pp. 188–196, 2017.

[15] S. Laufer, A. Ivorra, V. E. Reuter, B. Rubinsky, and S. B. Solomon, “Electrical impedance characterization of normal and cancerous human hepatic tissue,” *Physiol. Meas.*, vol. 31, no. 7, pp. 995–1009, 2010.

[16] J. A. Fan, W.-H. Yeo, Y. Su, Y. Hattori, W. Lee, S.-Y. Jung, Y. Zhang, Z. Liu, H. Cheng, L. Falgout, M. Bajema, T. Coleman, D. Gregoire, R. J. Larsen, Y. Huang, and J. A. Rogers, “Fractal design concepts for stretchable electronics,” *Nat. Commun.*, vol. 5, p. 3266, 2014.

[17] Y. Sun, W. M. Choi, H. Jiang, Y. Y. Huang, and J. A. Rogers, “Controlled buckling of semiconductor nanoribbons for stretchable electronics,” *Nat. Nanotechnol.*, vol. 1, no. 3, pp. 201–207, Dec. 2006.

[18] S. Kabiri Ameri, R. Ho, H. Jang, L. Tao, Y. Wang, L. Wang, D. M. Schnyer, D. Akinwande, and N. Lu, “Graphene Electronic Tattoo Sensors,” *ACS Nano*, vol. 11, no. 8, pp. 7634–7641, 2017.

[19] Y. Wang, Y. Qiu, S. K. Ameri, H. Jang, Z. Dai, Y. Huang, and N. Lu, “Low-cost, μm-thick, tape-free electronic tattoo sensors with minimized motion and sweat artifacts,” *npj Flex. Electron.*, vol. 2, no. 1, p. 6, Feb. 2018.

[20] J. Kim, I. Jeerapan, S. Imani, T. N. Cho, A. Bandodkar, S. Cinti, P. P. Mercier, and J. Wang, "Noninvasive Alcohol Monitoring Using a Wearable Tattoo-Based Iontophoretic-Biosensing System," *ACS Sensors*, vol. 1, no. 8, pp. 1011–1019, 2016.

[21] A. J. Bandodkar, D. Molinnus, O. Mirza, T. Guinovart, J. R. Windmiller, G. Valdés-Ramírez, F. J. Andrade, M. J. Schöning, and J. Wang, "Epidermal tattoo potentiometric sodium sensors with wireless signal transduction for continuous non-invasive sweat monitoring," *Biosens. Bioelectron.*, vol. 54, pp. 603–609, 2014.

[22] J. Suikkola, T. Björninen, M. Mosallaei, T. Kankkunen, P. Iso-Ketola, L. Ukkonen, J. Vanhala, and M. Mäntysalo, "Screen-Printing Fabrication and Characterization of Stretchable Electronics," *Sci. Rep.*, vol. 6, p. 25784, May 2016.

[23] A. K. Dąbrowska, G.-M. Rotaru, S. Derler, F. Spano, M. Camenzind, S. Annaheim, R. Stämpfli, M. Schmid, and R. M. Rossi, "Materials used to simulate physical properties of human skin," *Ski. Res. Technol.*, vol. 22, no. 1, pp. 3–14, 2016.

[24] D.-H. Kim, N. Lu, R. Ma, Y.-S. Kim, R.-H. Kim, S. Wang, J. Wu, S. M. Won, H. Tao, A. Islam, K. J. Yu, T. Kim, R. Chowdhury, M. Ying, L. Xu, M. Li, H.-J. Chung, H. Keum, M. McCormick, P. Liu, Y.-W. Zhang, F. Omenetto, Y. Huang, T. Coleman, and J. A. Rogers, "Epidermal Electronics," vol. 333, pp. 838–843, 2011.

[25] K. A and L. A, "Mechanical Behaviour of Skin: A Review," *J. Mater. Sci. Eng.*, vol. 5, no. 4, 2016.

[26] Y. Liu, J. J. S. Norton, R. Qazi, Z. Zou, K. R. Ammann, H. Liu, L. Yan, P. L. Tran, K.-I. Jang, J. W. Lee, D. Zhang, K. A. Kilian, S. H. Jung, T. Bretl, J. Xiao, M. J. Slepian, Y. Huang, J.-W. Jeong, and J. A. Rogers, "Epidermal mechano-acoustic sensing electronics for cardiovascular diagnostics and human-machine interfaces," *Sci. Adv.*, vol. 2, no. 11, pp. e1601185–e1601185, 2016.

[27] R. C. Webb, A. P. Bonifas, A. Behnaz, Y. Zhang, K. J. Yu, H. Cheng, M. Shi, Z. Bian, Z. Liu, Y.-S. Kim, W.-H. Yeo, J. S. Park, J. Song, Y. Li, Y. Huang, A. M. Gorbach, and J. a Rogers, "Ultrathin conformal devices for precise and continuous thermal characterization of human skin.," *Nat. Mater.*, vol. 12, no. 10, pp. 938–44, Oct. 2013.

[28] A. J. Bandodkar, V. W. S. Hung, W. Jia, G. Valdés-Ramírez, J. R. Windmiller, A. G.

Martinez, J. Ramírez, G. Chan, K. Kerman, and J. Wang, “Tattoo-based potentiometric ion-selective sensors for epidermal pH monitoring.,” *Analyst*, vol. 138, pp. 123–128, Jan. 2013.

[29] X. Huang, W.-H. Yeo, Y. Liu, and J. A. Rogers, “Epidermal differential impedance sensor for conformal skin hydration monitoring.,” *Biointerphases*, vol. 7, no. 1–4, p. 52, Dec. 2012.

[30] “Multimodal epidermal devices for hydration monitoring | Microsystems & Nanoengineering.” .

[31] S. Krishnan, Y. Shi, R. C. Webb, Y. Ma, P. Bastien, K. E. Crawford, A. Wang, X. Feng, M. Manco, J. Kurniawan, E. Tir, Y. Huang, G. Balooch, R. M. Pielak, and J. A. Rogers, “Multimodal epidermal devices for hydration monitoring,” *Microsystems Nanoeng.*, vol. 3, no. October 2016, p. 17014, 2017.

Chapter 5

Towards Using Chemically Responsive Hydrogels in Epidermal Sensing

5.1 Introduction

In the previous chapters, an epidermal tattoo platform has been developed and has demonstrated great potential as a wearable sensing platform for monitoring electrical changes in skin. In this chapter, a strategy towards developing a chemical sensing interface using this platform was investigated. As previously discussed, the skin and its associated matrices offer a rich biochemistry where specific analytes such as glucose [1], [2] and lactate [3], [4] can be targeted and monitored. For example, glucose would be a target of interest as this analyte is a marker for diabetes and can potentially be monitored in sweat [2] and interstitial fluid (ISF) [1]. Its concentration range is between 10 µM – 1 mM [2] in sweat, while glucose ISF has a concentration range of 10 - 100 µM [1]. Blood glucose levels can vary between 3 - 8 mM healthy people and 2 – 40 mM in diabetics [5]. Given the low concentration of glucose present in these matrices, highly sensitive sensing materials and approaches are required.

Lactate is known to be part of the skins natural moisturising factors (NMF) and it is known that individuals that suffer from mild atopic dermatitis have reduced levels of lactate, indicating that this analyte could potentially be used to track skin barrier changes [6]. Sweat constitutes several natural moisturising factors (NMF) such as lactate and urea as well as amino acids and their derivatives such as urocanic acid [7], [8]. By absorbing atmospheric water, hygroscopic NMF components act as humectants which help preserve the hydration state of the SC layer [7] and it has been used in emollient formulations to reduce the severity of dry skin [6], [9]. Lactate levels in sweat are also commonly used to evaluate anaerobic/aerobic status and assess physical fitness [4], where concentration levels can vary between 1 and 60 mM [2], [10], [11]. However, a limitation of using sweat as a sampling matrix would be generating a sweat volume output large enough to be able to analyse.

AA is another analyte also present in skin and has been widely used in cosmetic formulations due to its antioxidant properties and ability to increase collagen synthesis [12]. UV radiation damages skin through the production of reactive oxygen species, which can damage the extracellular matrix components and affect both the structure and function of cells. AA is a potent antioxidant that can donate electrons and neutralize free radicals present in the intra and extracellular matrix, repairing the damage caused by oxidative stress [12], [13]. There is a wide range of reported skin AA levels indicating that the concentration of this particular analyte is highly variable. Pullar and co-workers have published a review on the other potential roles of AA in skin health and summarises the in vitro and in vivo research to date [14]. In terms of skin

sensing, AA could be an analyte of interest for monitoring UV damage of skin. Modifying the tattoo platform with responsive chemistries that potentially target analytes such as these by way of soft responsive hydrogel materials is an exciting prospect.

Hydrogels are 3D crosslinked hydrophilic polymer networks that are capable of swelling and retaining large quantities of water whilst maintaining structural stability. Hydrogels are commonly synthesised with functional groups that respond to a variety physical and chemical stimuli such as temperature and pH [15]. They can be formed by physical or chemical crosslinks of homo-polymer or co-polymers which can be used to tune 3D hydrogel structures with the desired mechanical and chemical characteristics required for a specific application [16]. They can be classified into different groups based on their: physical structure (amorphous or semicrystalline), electric charge (ionic or neutral), crosslinking (physically or chemically crosslinked), their responses to external stimuli and their source (synthetic or natural) [16]. Throughout the last few years, research has shown the potential applications of hydrogel materials in biomedical research such as tissue engineering [17], [18], wound dressings [19] and biochemical sensing [20], [21]. Due to their unique properties such as high hydrophobicity, softness and biocompatibility, they have been used to resemble living tissue both compositionally and mechanically for biomedical applications [22], [23]. Hydrogels can be rendered as sensing materials that can be tailored to respond to specific targets, as well as be designed to have tissue-like mechanical properties that are necessary to aid with mechanical stability and adherence on the body for epidermal sensing applications.

The progress in hydrogel development has enabled researchers to develop these soft materials for applications such as controlled drug release applications and targeting biomarkers relevant to human health. Therefore these hydrogels could potentially be used in wearable [24] or even implantable [25] sensors. One of the interesting applications for hydrogels is drug delivery; where the hydrogels act as a drug carrier, retaining and releasing the loaded drug based on the environmental stimuli. For example, Ma *et al*. reported the characterisation and modification of a hybrid hydrogel composed of poly(N-isopropyl acrylamide) (PNIPAm) and polyethyleneimine (PEI) for controlled drug release [26]. PNIPAm is a thermoresponsive hydrogel that is limited by poor mechanical character and lack of ability for sustained release. PEI was incorporated to modify the structure and pore size within the hydrogel but also to enable tunable release of a drug wrapped in the hydrogel network [26]. The chemical integration of PEI transforms the neutral PNIPAm hydrogel to ionized PNIPAm realizing the feasibility of tuning

its swelling ratio for controlled drug release. To demonstrate this interaction, negatively charged folic acid was used as a drug model to investigate its controlled release property as it undergoes electrostatic attraction with PEI. It was observed that the release rate from this hydrogel is dependent on the interactions between the loaded drug and the PEI, including electrostatic repulsion or attraction, i.e. when the amount of PEI is increased, the water retaining effect dramatically slows down the rate of release [26].

Hydrogels have also been tailored for biosensing applications also. These hydrogels typically require a recognition element that initiates its responsive behaviour by introducing selective enzymes such as glucose oxidase (GOx) into the hydrogel matrix [27] or by tailoring the hydrogel chemistry to selectively respond to a target analyte [28]. For example, Brahim *et al*. reported the development of a hydrogel matrix composed of poly(2-hydroxyethyl methacrylate, (pHEMA) combined with polypyrrole (PPy) and GOx for glucose biosensing [27]. They observed that addition of the polypyrrole had an effect on the diffusion properties of the hydrogel, therefore they could tailor the monomer formulation using hydroxyethylmethacrylate (HEMA), tetraethyleneglycol diacrylate (TEGDA) as a crosslinker and pyrrole (Py) in order to get the desired response needed for this glucose sensor. For example, a monomer formulation ratio of 85:10:05 vol% (HEMA:TEGDA:PPy) as this had response time of 70 s. This enzyme-based working electrode was fabricated using platinum foil where the hydrogel mixture containing the GOx was applied to the surface of the platinum electrode and then irradiated with UV light under argon to polymerise the hydrogel [27]. The optimised sensor was used in a 3-electrode electrochemical cell where platinum was used as a counter electrode and Ag/AgCl was used as a reference electrode. This set-up was capable of amperometrically detecting glucose over the range of 5.0×10^{-5} - 2.0×10^{-2} M [27] which is within range for glucose concentration in sweat [2] and also ocular fluid [29]. However, there was a 30 % decline in hydrogel response after several months of storage indicating that long term storage of this biosensor would be challenging. An alternative hydrogel-based approach for glucose sensing is through the introduction of a boronic acid (BA) functionality into the polymer chain to induce diol sensitivity. BA can form esters, most frequently with 1,2- and 1,3-diols, allowing boronate ester formation with a number of biological species such as saccharides, glycoproteins, and dopamine opening up the applicability of BA to a wide range of biomedical sensing applications [30]–[32]. Phenyl boronic acid (PBA) moieties are commonly used for both electrochemical and optical sensing [30]. Various substituents can be attached to the phenyl ring of the BA,

altering the pKa of the BA allowing it to be used over a specific pH range depending on its application [30], [33]. For example, Daikuzono *et al*. have demonstrated the fabrication of a paper-based carbon interdigitated electrode modified with a PBA polymer for sugar sensing [28]. This hydrogel system consisted of acrylamide co-polymerised with 3-(acrylamido)phenyl boronic acid cured using UV light [28]. This PBA-modified paper electrode was capable of impedimetrically responding to both fructose and glucose, where the impedance measured at a specified frequency decreased with increasing sugar concentration. The interaction between the sugar and the PBA induces capacitive changes in the hydrogel film, whereby the different concentrations of sugar in solution induced hydrogel swelling, leading to increased diffusion of ion species and thus increased current flow that can be measured through impedance changes [28]. The modified paper electrode responded to sugar concentrations of up to 5 mM [28]. Lin *et al*. as a proof of concept have presented a 3-aminophenyl boronic acid based hydroxyethyl methacrylate (HEMA) contact lens sensor for diabetes patients [34]. The PBA-based HEMA contact lens could function as a sensitive glucose sensor changing thickness in the presence of different glucose concentrations [34]. These changes were monitored with images taken using a smartphone. These images were captured by a photosensitive sensor that uses a light emitting diode (LED) to focus on red light emission. The observed difference from a designated red reference point (edge of the contact lens) was compared to the red light area from the centre of the lens which changes based on the lens either converging or diverging light that changes the thickness of the contact lens due to a change in glucose concentration [34]. This group has shown the potential of using a PBA-based contact lens for glucose sensing. However in-vivo testing is still required to fully understand the capabilities and limitations of this sensor. Another example of a BA-based contact lens was by Badugu and co-workers, however in this case a fluorescent component was attached to the BA [35]. The use of a fluorescence component allows the response of glucose to be monitored using a simple approach of excitation and emission detection and in this case the change in the electronic properties and geometry at the boron atom induces the fluorescence changes [35]. With this fluorescence-based BA contact lens, a decrease in the fluorescence intensity was observed with increasing sugar concentration. The sensing mechanism of this fluorescence-based BA contact lens was based on fluorescence quenching via a charge neutralisation-stabilisation mechanism where the anionic boronate ester formed on glucose binding was stabilised by a positively charged nitrogen atom in the quinoline structure, which consequently quenched the fluorescence of the BA sensor [35]. Continued innovations

of these PBA functionalized hydrogels to serve as smart responsive materials for detecting specific biomarkers shows promise towards the development of chemically selective sensors for health monitoring.

This chapter investigates the use of PBA-based hydrogels for chemical sensing. The previous examples of polymeric BA hydrogels, based on neutral PBA monomers with short tethers, the two PBA hydrogels used in this study contain a quaternised nitrogen atom along the monomer chain attached to the phenyl group. The viability of these PBA based hydrogels as a chemical sensing interface were investigated by integrating these hydrogels into two different sensor platforms: a 3-electrode Au-paper based platform and a 2-electrode planar epidermal tattoo platform. Impedance spectroscopy was used to characterise and track the electrical response of these hydrogel systems. The electrical responses of these hydrogel systems were investigated under different pH conditions and its applicability for detecting different analytes such as glucose, lactate and ascorbic acid was also examined to understand its potential as an epidermal chemical sensing interface.

5.2 Materials and methods

5.2.1 Materials

AG520 EI silver elastomer ink was purchased from Chimet® S.p.A. (Tuscany, Italy). Temporary transfer tattoo paper and acrylic adhesive film substrates were purchased from Sports Ink™ (Dublin, Ireland). Strip boards were purchased from Maplin Electronics. Mill Max spring loaded contacts (Part. No. 0906-4-15-20-75-14-11-0) were purchased from Farnell Components (Ireland). Polyethylene terephthalate (PET, 175 µm) sheets purchased from HiFi Industrial Film®. Poly(methyl methacrylate) (PMMA) sheets were purchased from Radionics Ltd. (Ireland). VWR 413 filter paper was purchased from VWR International Ltd. (Ireland). 2-bromomethyl phenyl boronic acid (2B-PBA) and 4-bromomethylphenyl boronic acid (4B-PBA) were purchased from Fluorochem Ltd. (UK). N-[3-(dimethylamino)propyl] methacrylamide, N-N'-methylenebisacrylamide and hydroxyl-2-methylpropiophenone, dichloromethane (DCM), dimethyl sulfoxide (DMSO), potassium dihydrogen phosphate, sodium hydroxide, sodium bicarbonate, acetic acid, sodium acetate, methanol, D-(+)-glucose, sodium lactate and ascorbic acid were purchased from Sigma Aldrich. Filter pads (3 cm diameter and 1 mm thickness) composed of rubber, viscose polyester and silicone were obtained from EnviroDerm Service UK Ltd. The dimethyl(amino)propyl-2-boronic acid (DMAP-2BA) monomer was provided by Prof. D. Diamond's research group.

5.2.2 Synthesis of dimethyl(amino)propyl-2-boronic acid (DMAP-2BA)

For the Au-paper working electrode, the dimethylamino propyl-2-boronic acid monomer (DMAP-2BA) was synthesized and donated by Prof. D. Diamond research group. Quaternization reactions with PBA have been described in literature [36], [37]. 1 g of 2-bromomethyl phenyl boronic acid (2B-PBA) was dissolved in 30 mL DCM. To this, a solution of N-[3-dimethyl(amino)propyl]methacrylamide (1.58 g, 9.3 mmol) in 10 mL DCM was added dropwise, and the reaction mixture stirred vigorously at room temperature overnight. Solvent was then decanted off and the solvent was dried under vacuum. Structure of the 2B-PBA starting material and DMAP-2BA monomer can be seen in Fig. 5.1a and b.

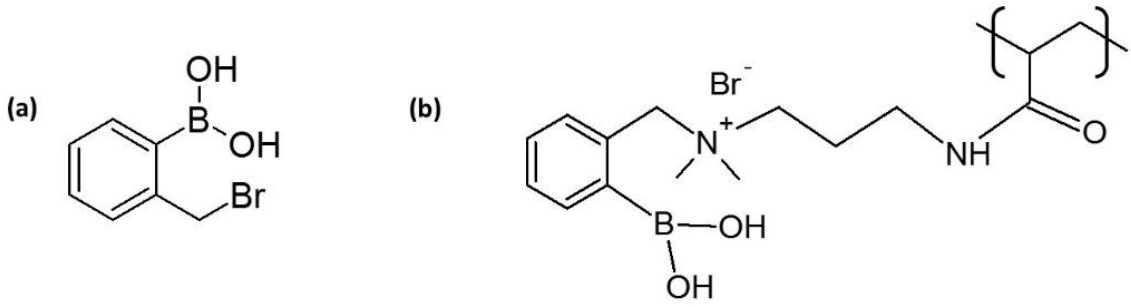

Figure 5.1 Chemical structures of (a) 2-bromomethyl phenyl boronic acid (2B-PBA) starting material and (b) its corresponding monomer (DMAP-2BA).

5.2.3 Fabrication of Au-paper working electrode & its modification with DMAP-2BA

The Au-working electrodes were fabricated by the research group using a similar technique described in a paper by A. Murphy *et al* [38]. Briefly, hydrophobic wax frames were printed on VWR413 filter paper (18 x 18 mm). A mask containing the design for the conducting track was positioned on top of the wax barrier and secured with tape. This mask was placed into a gold sputter coater (Quorum Q150T S, current 45 mA, time 60 s) with the design facing up to produce a gold track (35 x 8 mm) (Fig. 5.2a). The hydrophobic wax was melted at 110 °C for 10 min until the wax had visibly permeated through the filter paper.

The drop casting and curing method used was similar to Daikuzono *et al*. [28]. To prepare the monomer for deposition and curing, 0.3 g of the prepared 2B-PBA monomer was dissolved in 250 µL 50:50 DMSO/DI water mixture. To this, 1.2 mg N,N′-methylenebisacrylamide and 1 µL 2-hydroxy-2-methylpropiophenone photoinitiator were added. 4 µL DMAP-2BA monomer was drop cast on a designated area of the conducting gold track (9 x 8 mm) surrounded by the hydrophobic wax barrier (Fig. 5.2b). The monomer solution was allowed to absorb into the surface for approx. 30s and polymerized under UV light (CL-1000 Ultraviolet Crosslinker) for 15 min.

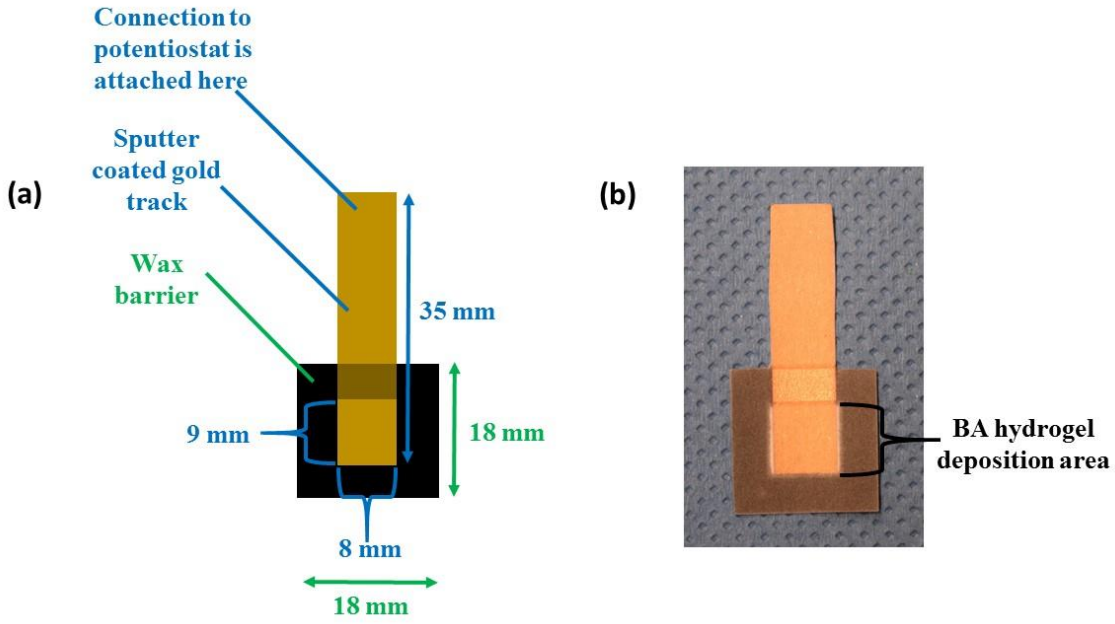

Figure 5.2 (a) Dimensions of the sputter coated gold track (in blue) and hydrophobic wax barriers (in green) (b) Image of the Au-paper working electrode and deposition area of the monomer mixture.

5.2.4 Synthesis of dimethyl(amino)propyl-4-boronic acid (DMAP-4BA)

500 mg of 4-bromomethyl phenyl boronic acid (4B-PBA) was dissolved in 1 mL methanol and 1 mL N-[3-(dimethylamino)propyl] methacrylamide in a 25 mL round bottom flask and was left to stir overnight. 20 mL of diethyl ether was used to wash the mixture and was left to stir for 10 min. The excess solvent was decanted from the round bottom flask and the washing step was repeated with another 20 mL of diethyl ether. After washing, the solution had a honey like consistency and was placed under vacuum overnight to remove as much excess solvent as possible. Structure of the 4B-PBA starting material and corresponding monomer can be seen in Fig. 5.3a and b.

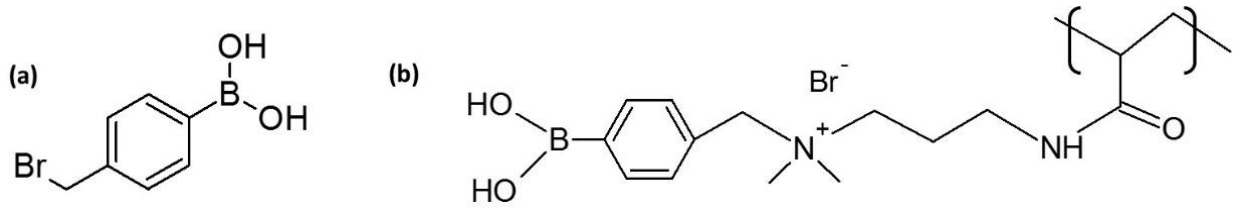

Figure 5.3 Chemical structures of (a) 4-bromomethyl phenyl boronic acid (4B-PBA) starting material and (b) its corresponding monomer (DMAP-4BA).

5.2.5 Fabrication of the tattoo & its modification with DMAP-4BA hydrogel

The tattoo sensor design and fabrication has been described in Chapter 2, Section 2.2.2. This platform was further modified with DMAP-4BA monomer using the following method. The screen printed platform was modified using double-sided adhesive material were adhered together as a spacer (approx. 0.2 mm thick). These spacers (Fig. 5.4a) were placed on either side of the electrodes and a piece of PMMA (approx. 40 x 25 mm) (Fig. 5.4b) was placed onto the spacers over the tattoo to define the depth of the space above the electrodes to be approx. 0.2 mm in depth. 270 mg of DMAP-4BA monomer solution was fully dissolved in 460 µL 50:50 DMSO/DI water. 2 mg N-N'-mmethylenebisacrylamide and 2 µL 2- hydroxyl-2-methylpropiophenone, were added into the solution and was placed onto a vortex to homogenise. The DMAP-4BA monomer solution was dispensed adjacent to the gap between the PMMA and the substrate allowing the solution to fill the void gap over the electrodes via capillary action (Fig. 5.4c). Once the gap was fully covered with the DMAP-4BA solution, it was cured under UV light for 30 min and the PMMA sheet gently removed to reveal the DMAP-4BA modified hydrogel tattoo (Fig. 5.4d). These modified electrodes were then applied to the desired substrate (PET disc) by placing the cured DMAP-4BA modified side face down on the substrate and wetting the tattoo backing paper with DI water for approx. 1 min, which was gently removed to expose the silver electrodes.

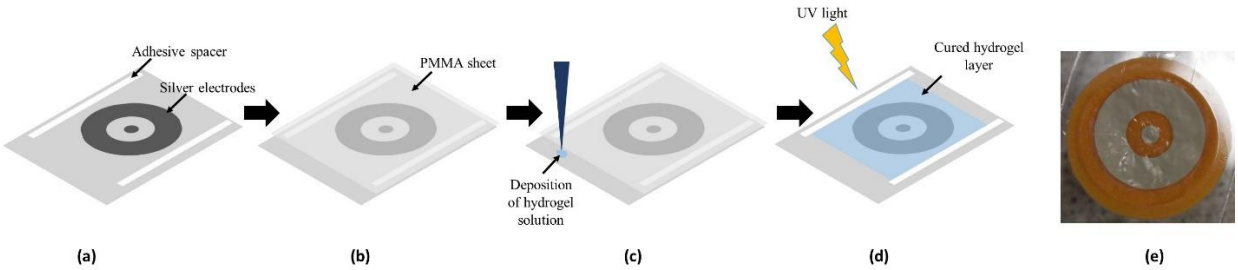

Figure 5.4 Schematic diagram of DMAP-4BA modified tattoo platform: (a) Adhesive spacers on either side of the electrodes, (b) PMMA sheet overlaying the electrodes (c) deposition of monomer solution on the side opening of the substrate near the electrodes (d) cured hydrogel layer on the tattoo and (e) image of the DMAP-4BA modified tattoo adhered on to a filter pad (tattoo electrode diameter: 20 mm).

5.2.6 Buffer preparation

For studies carried out on the hydrogel modified electrodes, the following pH buffers were prepared: pH 3 (0.1 M sodium acetate and 0.1 M acetic acid), pH 7.4 (0.1 M potassium dihydrogen phosphate and 0.1 M sodium hydroxide) and pH 12 (0.05 M sodium hydrogen phosphate dibasic and 0.1 M sodium hydroxide).

5.2.7 Impedance study of DMAP modified electrodes

5.2.7.1 Impedance characterisation of DMAP-2BA Au-paper working electrodes

Electrical impedance spectroscopy of the DMAP-2BA modified Au-paper working electrode was performed using a 3-electrode set-up in buffer (pH 3, 7.4 and 12) using a CHI 660C impedance analyser. A 0 V set potential and 0.01 V amplitude was used and the frequency range scanned was 100,000 Hz to 0.1 Hz, unless stated otherwise. An Ag/AgCl electrode was used as a reference electrode and a platinum wire mesh electrode was used as a counter electrode.

To investigate the glucose response of the DMAP-2BA modified Au-paper working electrode, 1 M glucose solution in DI water and was added in aliquots into the 3-electrode cell containing 20 mL of buffer. After glucose aliquot additions, the solution was allowed to stir for 10 min at which point an impedance measurement was taken.

5.2.7.2 Impedance characterisation of DMAP-4BA tattoo electrodes

Electrical impedance spectroscopy of the DMAP-4BA modified tattoo was performed using an Autolab PGSTAT128N workstation. Spectra collected on the hydrogels were recorded at 0 V set potential and 0.01 V amplitude and the frequency range scanned was 1 MHz to 0.1 Hz, unless stated otherwise.

For the studies carried out to determine the stability in buffer only, the DMAP-4BA modified tattoo were adhered to PET disc (25 mm diameter, Fig. 5.5a) and an impedance measurement recorded before being fully immersed in buffer. The PET immobilised DMAP-4BA modified tattoo were then fully immersed in buffer for 10 min (Fig. 5.5b). It was subsequently removed from solution, excess solution was wiped away and a second impedance measurement was again recorded

For studies to investigate the response of the DMAP-4BA modified tattoo electrodes, the platform was exposed to a range of analytes: glucose, lactate, ascorbic acid and sodium chloride in buffer (pH 7.4) at different concentrations (10, 30, 50, 75 and 100 mM). The DMAP-4BA modified tattoo were immersed in buffer for 30 min and then measured using impedance. This step was repeated at 60 and 90 min to ensure the hydrogel system reached equilibrium. The DMAP-4BA modified tattoo was then fully submerged into the lowest analyte concentration (10 mM) for 1 hr. It was then removed from solution and any excess solution was removed before an impedance spectra was recorded. This procedure was repeated for subsequent concentrations for each analyte investigated.

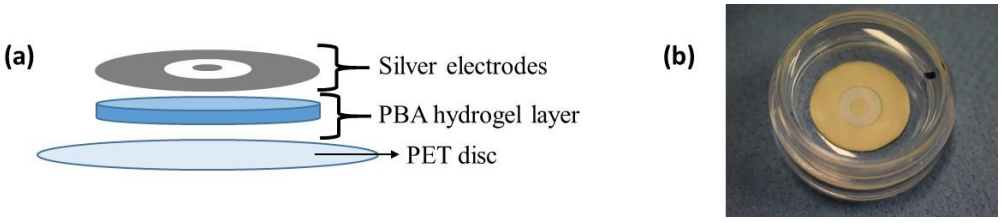

Figure 5.5 (a) Schematic diagram of DMAP-4BA modified tattoo (diameter: 20 mm) with PET disc for support and (b) image of DMAP-4BA modified tattoo submerged in buffer (pH 7.4).

5.3 Results and discussion

Boronic acids (BA) bind favourably to diols and polysaccharides containing diols such as glucose, fructose and mannose. This reversible covalent interaction of BA with a diol group forms five- or six- membered cyclic esters [39]. BA can either form neutral or anionic esters depending on the pH (Fig. 5.6). Stable BA-diol binding is favoured at basic pH, while these boronate esters are completely cleaved under acidic pH ranges [40]. In DMAP-2BA, there is an electron deficient boron atom and two hydroxyl groups (Fig. 5.6, (1)) at high pH, it forms an anionic tetrahedral boronate (Fig. 5.6, (2)) [5], [41]. Both forms may covalently bind to diols Fig. 5.6 ((3) and (4)). With phenyl boronic acid (PBA), functional groups present on the phenyl ring can alter the pKa of the molecule (range between 4.2 – 9.0). For example, 2-fluoro-5-nitrophenyl boronic acid has a pKa of 6 and its optimal pH for stable BA-diol binding occurs at pH 5, while 2-methoxyphenyl boronic acid has a pKa of 9 and its optimal pH for BA-diol binding occurs at pH 7.5 [33]. Therefore depending on the type of functional group present on the PBA, the formation of the anionic tetrahedral boronate is pH dependent. This study looks to characterise the BA-based hydrogel materials, a DMAP-2BA and DMAP-4BA based on the hypothesis that the generation of charged boronate species may change the electrical properties of the modified hydrogels. DMAP-2BA contains a quaternised nitrogen in close proximity to the BA unit, where the BA is at the ortho position on the phenyl ring. It has been postulated that electron withdrawing groups could potentially lower the pKa of the BA because an electron withdrawing group decreases the electron density on the boron atom and renders the boron to be more acidic [42]–[44].

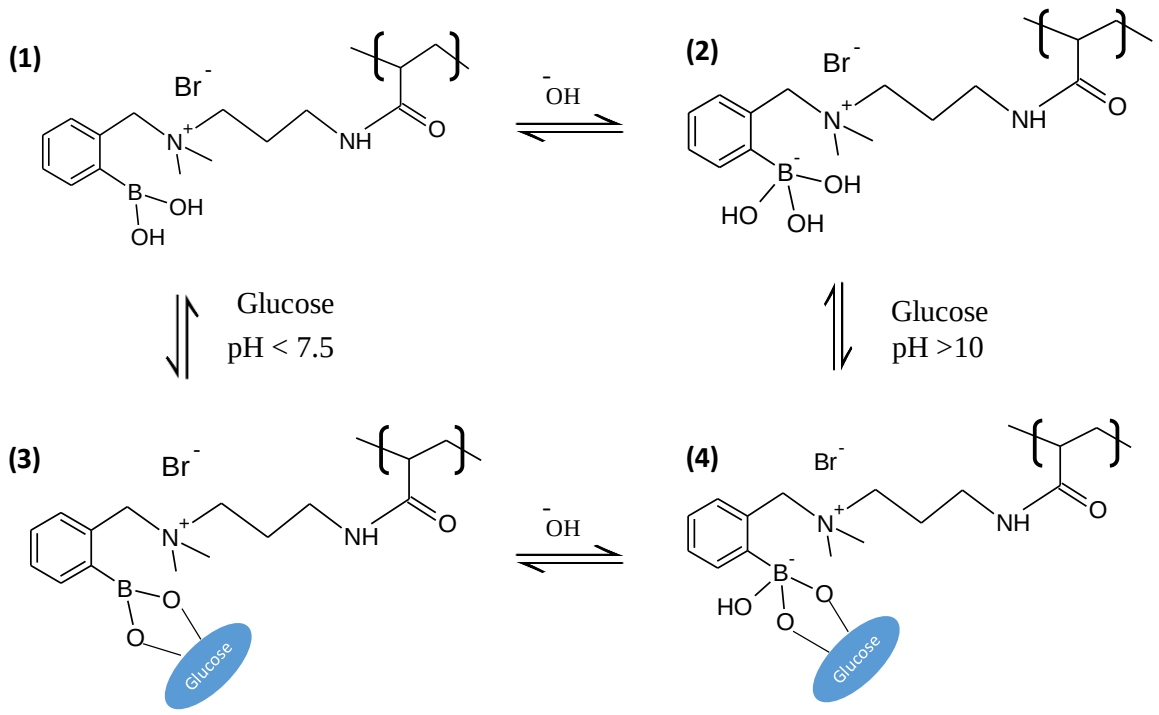

Figure 5.6 Schematic of the DMAP-2BA binding to glucose under different pH conditions. Similar diol exchange with phenylboronic acid [40].

5.3.1 pH dependence of the electrical response of DMAP-2BA Au-paper working electrodes

In this study, a Au-paper working electrode was constructed from gold-sputtered filter paper. It was modified with the hydrogel and then characterised impedimetrically under various pH conditions. This was used as the working electrode in a 3-electrode cell for non-faradaic impedance measurements. The Nyquist plots of the DMAP-2BA Au-paper electrode at different pH condition are shown in Fig. 5.7. It was observed that the impedance measured at pH 3 using the Au-paper electrode had a higher resistance compared to the impedance measured at pH 7.4 and 12, this trend can be clearly seen in the Nyquist plots below and Bode plots in the Appendix, Fig. A5.A.

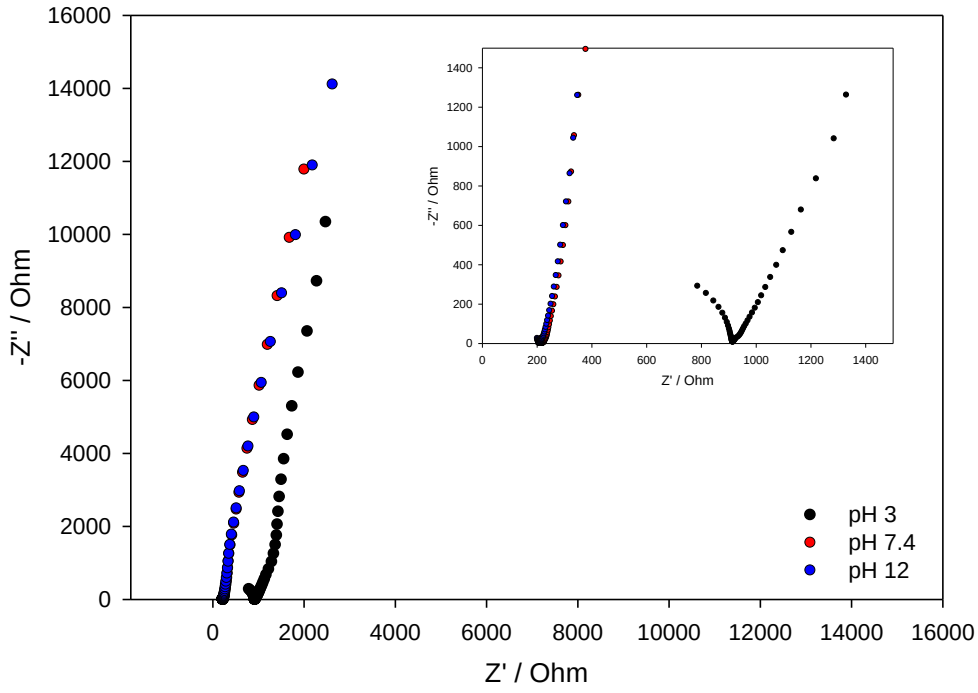

Figure 5.7 Representative Nyquist plots of DMAP-2BA on Au-paper working electrode in buffer (pH 3, 7.4 and 12). Inset: magnification of the high frequency range for the Nyquist plots. Corresponding Bode plots in Appendix Fig. A5.A.

The high frequency regions of the Nyquist plots comprises of partially formed semi-circular arcs that are attributed to the time constant of the bulk hydrogel. The diameter of this semi-circle was taken as the point at which it intersected with the x-axis which was attributed to bulk hydrogel resistance, which will be referred to as $R_{gel.}$ The capacitive feature at lower frequencies was attributed to the hydrogel-paper electrode interface. It was observed that in the high frequency region, the highest R_{gel} value observed for the hydrogel modified Au-paper electrode was at pH 3 (approx. 900 Ω), while R_{gel} values were significantly lower at pH 7.4 and 12 (approx. between 205-217 Ω). The increased resistance observed at pH 3 could potentially be due to the neutral charge on the boron groups along the polymer chains under acidic conditions reducing the conductivity of the hydrogel, while at basic pH R_{gel} decreased potentially due to the generation of the negatively charged boron. At pH 3, it has been expected that BA would exist mostly in its neutral trigonal form, while at pH 7.4, an equilibrium exists between the anionic tetrahedral and neutral trigonal form and at pH 12, BA would exist solely in its anionic form.

In order to further understand the electrical response of the DMAP-2BA modified Au-paper electrode, the electrode stability under each pH condition was studied over time. Impedance spectra were taken at 5 min intervals for 35 min. R_{gel} values were extracted and plotted against time (Fig. 5.8) linear regression was applied and the slope values were compared. The slopes were -1.4847 (pH 3), 0.018 (pH 7.4) and -0.0062 Ω/min (pH 12). At pH 3, the large slope of the regression line indicates that in acidic conditions, there is a process causing significant reduction in resistance over time, which may be due to a degradation process of the Au-paper electrode in this acidic pH although no visual degradation was observed on the surface of the Au-paper electrode in the cell. It was observed that at pH 7.4 and 12 the DMAP-2BA modified Au-paper electrode was stable on due to their low slope values

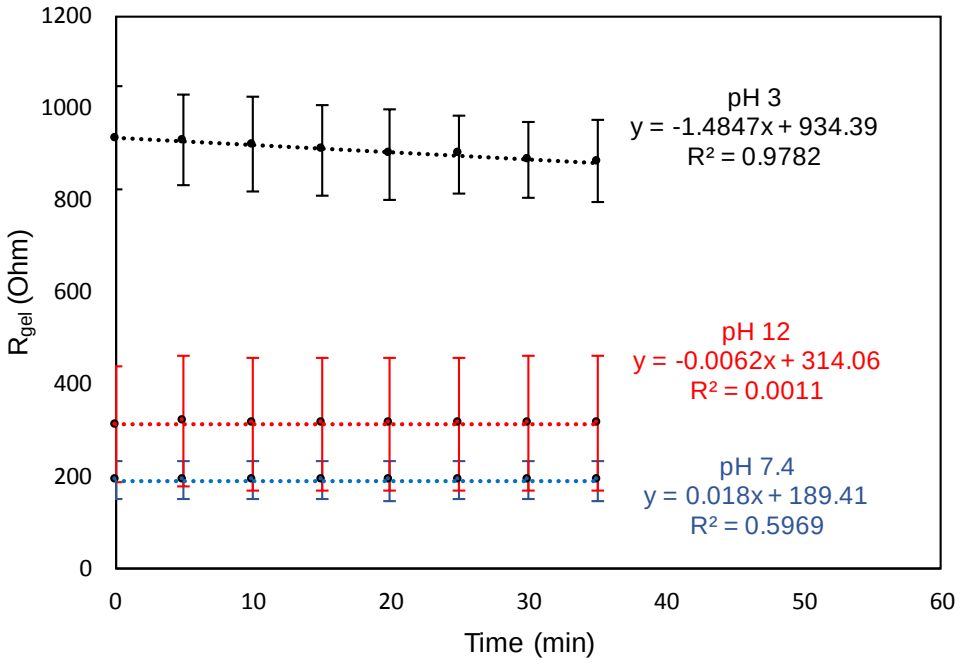

Figure 5.8 Time-base study of DMAP-2BA Au-paper electrodes at different pH conditions pH 3 (n=4) pH 7.4 (n=3) and 12 (n=3) over time.

5.3.2 Glucose dependence of DMAP-2BA Au-paper working electrodes

The electrical response of the DMAP-2BA Au-paper electrode after exposure to glucose was studied. Increasing glucose concentrations were introduced to the electrochemical cell at pH 7.4 (Fig. 5.9a). Initially, the DMAP-2BA Au-paper electrode was placed into buffer (pH 7.4) and

an impedance spectrum collected. Upon increasing glucose concentrations, a decrease in R_{gel} was observed as seen in the Nyquist plots (Fig. 5.9b). This indicates that the glucose introduced into the solution diffuses into the hydrogel and likely binds with DMAP-2BA resulting in the negative shift in pKa of the BA and consequently a shift in the equilibrium between the charged and uncharged boron states. This binding interaction may induce change in the electrical state of the hydrogel which can be attributed to the increased anionic boronates. However, no visible swelling was observed when glucose was introduced into the cell indicating that the electrostatic repulsive interactions between the charged borons was not strong. In order to fully understand if swelling occurs, a gravimetric study of the DMAP-2BA hydrogel in response to buffer only compared to glucose should be considered for future investigations.

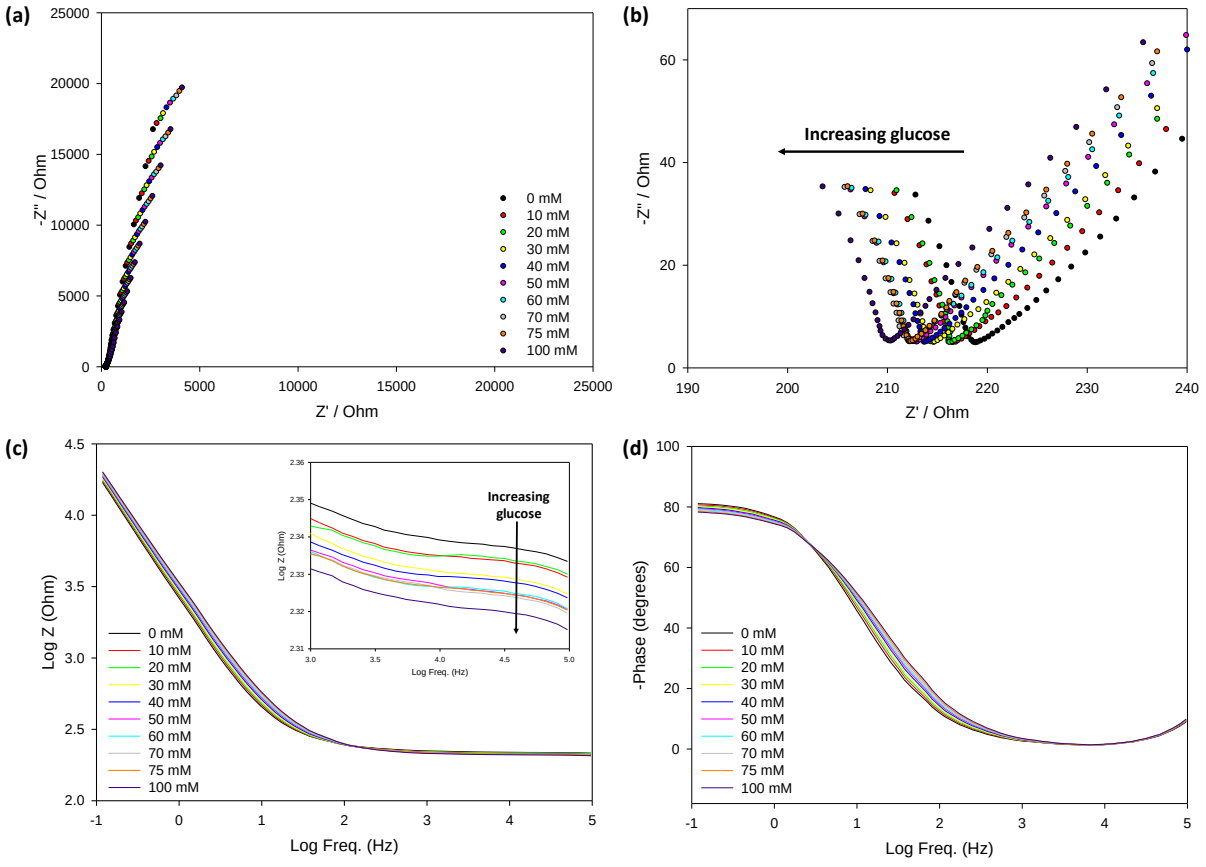

Figure 5.9 Representative (a) Nyquist plots of DMAP-2BA Au-paper electrode in buffer (pH 7.4) and its response to glucose additions (b) magnification of the higher frequency attributed to the bulk hydrogel and corresponding (c) Impedance and (d) phase plots.

In order to study the impact of pH on this response, R_{gel} values were extracted after each glucose addition at the different pH conditions. Aliquots of glucose added to the cell were allowed to stir for 10 min in order for the system to reach equilibrium, before the impedance measurement was taken. Measured R_{gel} values were normalised to the R_{gel} value in buffer. Normalised resistance values were then plotted against glucose concentration (Fig. 5.10). From the results, it was observed that responses in both pH 7.4 (n=3) and 12 (n=2) buffers had low sensitivities compared to the responses in pH 3 buffer (n=4). It was also observed that from 50 mM onwards, R_{gel} values obtained at both pH 7.4 and pH 12 start to plateau, which implies that diffusion may become inhibited as the amount of glucose increases inside the DMAP-2BA. A linear regression was performed and slope values based on R_{gel} before and after glucose was plotted and compared.

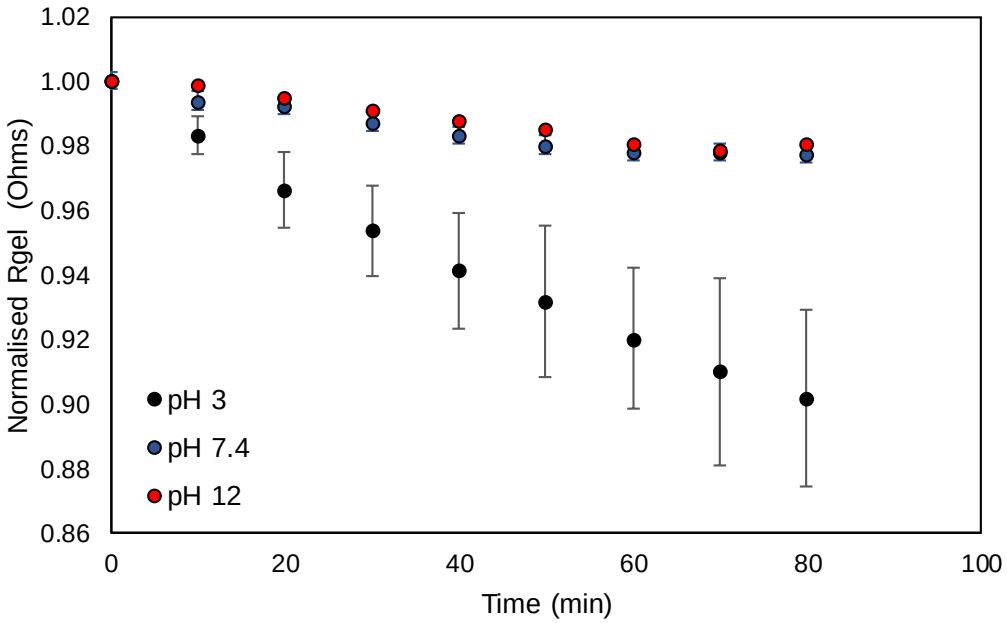

Figure 5.10 Normalised resistance values of DMAP-2BA Au-paper electrodes upon increasing glucose in buffer (pH 3, 7.4 and 12).

These normalised R_{gel} values were then plotted against time for each pH condition (Fig. 5.11a) and was compared to a matched set of timed glucose additions (Fig. 5.11b). All data was fitted

with linear regression lines (plateau in the glucose data was excluded). The slope values for each pH condition (no glucose) was compared to a matched set of timed glucose additions taken under the same conditions which have been tabulated in Table 5.1.

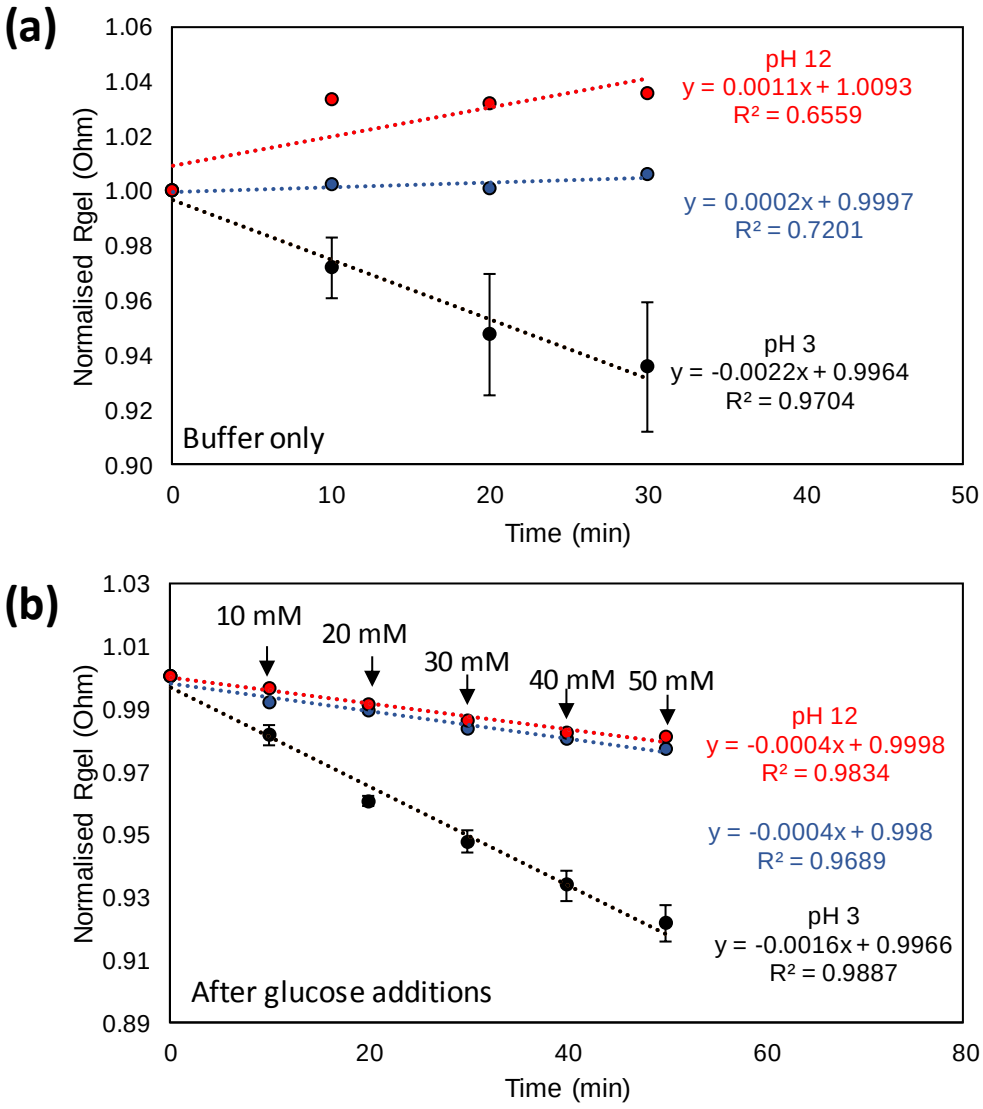

Figure 5.11 Normalised resistance values plotted against time (min) (a) before and (b) after glucose additions at pH 3, 7.4 and 12 using the DMAP-2BA Au-paper electrode.

Table 5.1 Comparison of slope values in the absence and presence of glucose measured using the DMAP-2BA Au-paper electrode.

Buffer Conditions	**Buffer only (Ω/ min)**	**Buffer/Glucose (Ω /min)**
pH 3 (n=3)	-0.00217 ± 0.00074	-0.00157 ± 0.00032
pH 7.4 (n=2)	+0.00020	-0.00045
pH 12 (n=2)	+0.00105	-0.00040

At pH 3, the slope shows a decrease in R_{gel} in the absence and presence of glucose in the electrochemical cell. It was also observed that the slope after glucose at pH 3 (Table 5.1) had reduced but was still negative indicating that the electrical response of the DMAP-2BA Au-paper electrode at this pH would be challenging to differentiate between the absence and presence of glucose. It may have been that the DMAP-2BA modified Au-paper electrode becomes degraded in acidic conditions as observed earlier. It is expected for binding would occur to form a neutral trigonal boronate ester at this acidic pH but it has been suggested that the boronate ester could also be cleaved under strong acidic conditions [40]. Therefore, the significant decrease in R_{gel} could be due to instability arising from both binding and cleaving of glucose from BA as well as potential degradation of the paper electrode over time. The BA-diol binding interaction in acidic pH has been studied by Chen and co-workers and they have observed that acidic conditions (pH 4.0) can be used to remove the diol from BA [45], [46].

At pHs 7.4 and 12, it was observed that there was a small change in slope values after glucose additions suggesting that glucose binding to DMAP-2BA Au-paper electrode could potentially be detected electrically based on the change in slope in the presence of glucose (Fig. 5.11b). At pH 7.4, there should be an equilibrium between the boronic acid in its anionic tetrahedral form and neutral trigonal form. Binding of glucose to BA is preferential when the boron is in its anionic tetrahedral form and once bound to glucose, the pKa of the BA is lowered and the anionic form becomes stable again [39]. At pH 12, it has been postulated that BA would exist solely in its anionic form, therefore glucose binding should not result in a change in charge. However, the data from the study indicates that there was a change in R_{gel} after glucose additions. The R_{gel} data from both pH 7.4 and pH 12 suggests that there is potential binding occurring between glucose and PBA. It may be that there is some binding occurring but it is limited due to the substituent present on the phenyl ring and its position relative to the BA

moiety. The BA moiety is in the ortho position relative to the quaternised nitrogen atom of the polymer backbone which could possibly be limiting the availability of BA for binding (Fig. 5.1b). It has been previously discussed that the presence of a quaternised nitrogen atom can lower pKa of the BA, which could be likely due to its electron withdrawing nature [47]. The BA group in the ortho position is adjacent to the N^+ on the polymer chain, which allows for N^+-B^- interaction. This close proximity of the BA moiety to the N^+ moiety enhances the charge neutralization stabilization in the BA and glucose binding can also be limited by steric hinderance of the methyl groups attached to the adjacent N^+ moiety [37]. Therefore, the low electrical responses of BA glucose binding (0 - 50 mM) with the DMAP-2BA could potentially be due to steric and electrostatic hindrance. This is supported by Brooks *et al*., where they observed that BA with functional groups directly attached or adjacent to boron would have binding constants were much lower, likely due to steric hindrance at the boron centre compared to BA with functional groups in the meta- or para- position [48]. Further investigation would be required to fully understand the electrical response of the DMAP-2BA modified Au-paper electrode to glucose as there was potential degradation occurring in acidic pH, low sensitivity detecting glucose and a limited number of replicates, which limits the conclusions that can be drawn. Future studies could potentially look at smaller pH increments to fully understand the impact of pH on the electrical signals generated by the BA binding with the hydrogel. This would help potentially narrow down an optimised pH range where the Au-paper electrode platform can function reliably.

5.3.3 Study on the electrical response of DMAP-4BA tattoo electrodes

The electrical response of a DMAP-4BA modified in a different set-up was also investigated. This structure has a BA moiety in para-position from the polymer backbone as opposed to the ortho-position (Fig. 5.3b) and has been referred to as DMAP-4BA. In this case, the BA moiety is in the para-position from the polymer backbone which could potentially reduce the effect of steric and electrostatic hindrance in contrast to the ortho-position of the BA in DMAP-2BA in the previous studies. In the following studies, the DMAP-4BA polymer was used as a modification layer of the 2-electrode tattoo platform. This approach was used to investigate if impedance changes could be observed for the DMAP4BA in this format for the hydrogel material in the presence of the analytes glucose, lactate and ascorbic acid (AA).

The 2-electrode tattoo platform was used to investigate the potential of DMAP-4BA as a more appropriate set-up for skin sensing in place of the 3-electrode cell. In this format, the polymer could interface directly with the SC and the concentric electrodes overlay the polymer for tracking impedance changes in the polymer as a result of a chemical response. In order to perform the studies, the DMAP-4BA modified tattoo was released onto the desired substrate, in this case a PET disc. Once released on to the PET disc, an impedance measurement was taken. Following this, it was immersed in buffer (pH 7.4) and subsequently measured. The initial Nyquist plot of the DMAP-4BA modified tattoo showed two distinct regions (Fig. 5.12). The high frequency range shows a semi-circle that was attributed to the bulk hydrogel which will be referred to as R_{gel}, while the capacitive feature seen at the lower frequency range has been attributed to the electrode interface. It was noted that prior to immersion in buffer there was high variability in the impedance spectra, which can be clearly seen in the Nyquist plots below and the Bode plots in the Appendix, Fig. A5.B. This is likely linked to differences in the water content of these DMAP-4BA hydrogels as they were stored for different lengths of time before being tested. A significant reduction in R_{gel} was observed after immersion in buffer which is likely as a result of the uptake of water and ions to increase the osmotic pressure of the gel resulting in swelling. The swelling of this mentioned platform was also noted by the observation of folding on the edges of the film on the outer electrodes after being imbibed with buffer.

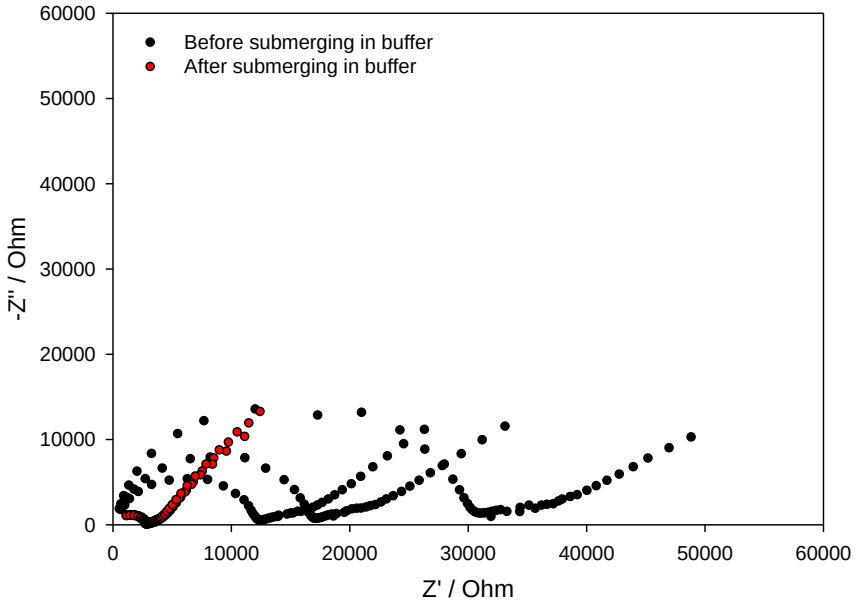

Figure 5.12 Nyquist plots of DMAP-4BA modified tattoo before and after being immersed in buffer (pH 7.4) (n=3). Corresponding Bode plots in Fig. A5.2.

A stability study was then performed on the DMAP-4BA modified tattoo to investigate electrical changes over time to establish the time required for the hydrogel to reach equilibrium in buffer. For this study, the DMAP-4BA modified tattoo was submerged in buffer (pH 7.4) and an impedance measurement was taken at 10 min intervals over 1 h. The Nyquist plots (Fig. 5.13a) show a significant reduction in R_{gel} after the initial 10 min and a more gradual decrease was then observed up to 1 hr. These R_{gel} values were plotted against time (Fig. 5.13b). The results indicate that the DMAP-4BA decreased over time and suggests at 60 min the DMAP-4BA modified tattoo was at equilibrium. The corresponding Bode plots are shown in the Appendix, Fig. A5.C which shows the same trend of decreasing impedance.

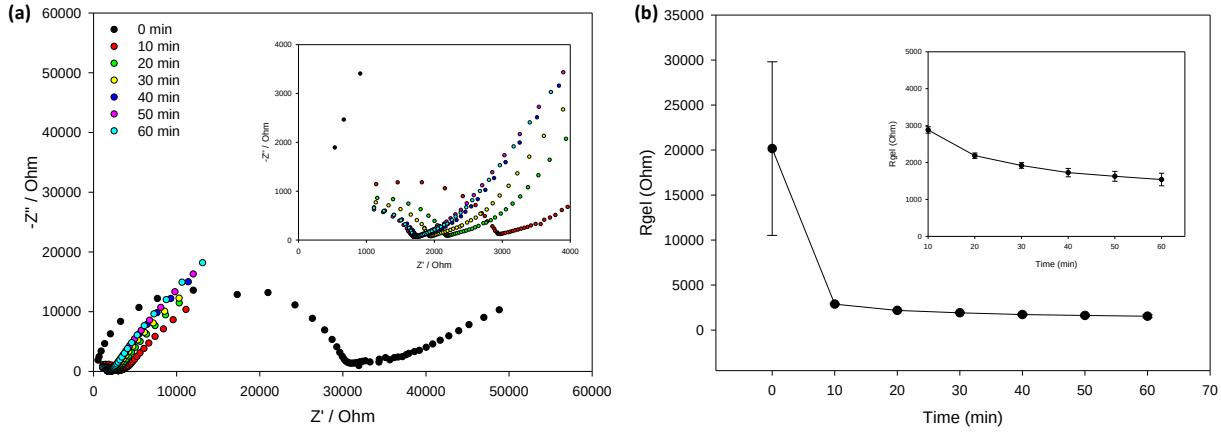

Figure 5.13 Representative (a) Nyquist plots of DMAP-4BA modified tattoo over time in buffer (pH 7.4), magnification of the high frequency region inset top right and (b) extracted R_{gel} values plotted against time (n=3). Corresponding Bode plots in Fig. A5.3.

To further study the DMAP-4BA modified tattoo behaviour, different concentrations of NaCl was used for uptake into the DMAP-4BA to study the impact of changing ionic strength on the electrical characteristics of the hydrogel. The DMAP-4BA modified tattoo was initially immersed in buffer and was monitored to establish equilibrium. The DMAP-4BA was in buffer for a total of 90 min before it was immersed in the lowest concentration of the NaCl (10 mM) for 1 h before an impedance measurement was taken. The DMAP-4BA was immersed in increasing NaCl concentrations and impedance spectra was taken (Fig. 5.14a). Fig. 5.14b shows a decrease in R_{gel} values as the concentration of NaCl increased. This decrease can be explained

by a resulting increase in ionic conductivity due to an influx of ions into the hydrogel. It was also observed that there was no further decrease in R_{gel} after 50 mM, which suggests that the hydrogel has reached a maximum resistance at this point.

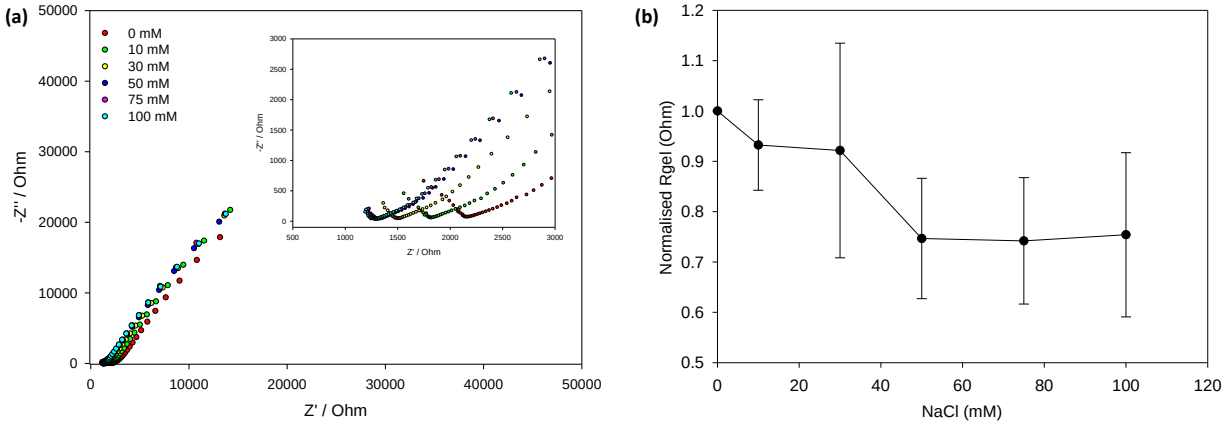

Figure 5.14 Representative (a) Nyquist plots of DMAP-4BA modified tattoo in increasing ionic strength of buffer (pH 7.4) and magnification of high frequency region inset top right and (b) extracted R_{gel} values plotted against NaCl concentration (n=3).

5.3.4 Investigation of the electrical response of DMAP-4BA tattoo to diols and α-hydroxy acid functional groups

As previously discussed, PBA has an affinity to diols such as glucose and AA as well as the α-hydroxy acid, lactate [39], [49]. These analytes were selected based on their diol functional groups, α-hydroxy acid and their relevance to skin physiology. As previously discussed earlier in the chapter, glucose has been a common target of interest as this analyte is a marker for diabetes and has a glucose concentration range of 10 µM – 1mM in sweat [2]. However this concentration range is low and thus challenging to obtain. Lactate is another potential analyte of interest as it is present in the skin NMF and could potentially be used to track skin barrier changes that could be related to atopic dermatitis. This analyte has also been used to monitor anaerobic levels for fitness applications for its concentration range can vary between 1 and 60 mM in sweat [2], [10], [11] which makes it a promising analyte to detect in sweat in contrast to glucose. AA is another analyte present in skin.

In this initial study, the impedance response of the DMAP-4BA modified tattoo in the presence of glucose, AA and lactate were investigated. The DMAP-4BA platforms were exposed to increasing concentrations of the analyte and the impedimetric response for each analyte concentration was recorded (Section 5.2.7.2). Initially, increasing glucose and AA concentrations were monitored. Impedance spectra were taken and the R_{gel} values attributed to the bulk hydrogel were extracted and plotted against time. When the DMAP-4BA modified tattoo was exposed to increasing glucose concentrations a gradual increase in R_{gel} was observed (Fig. 5.15a and b).

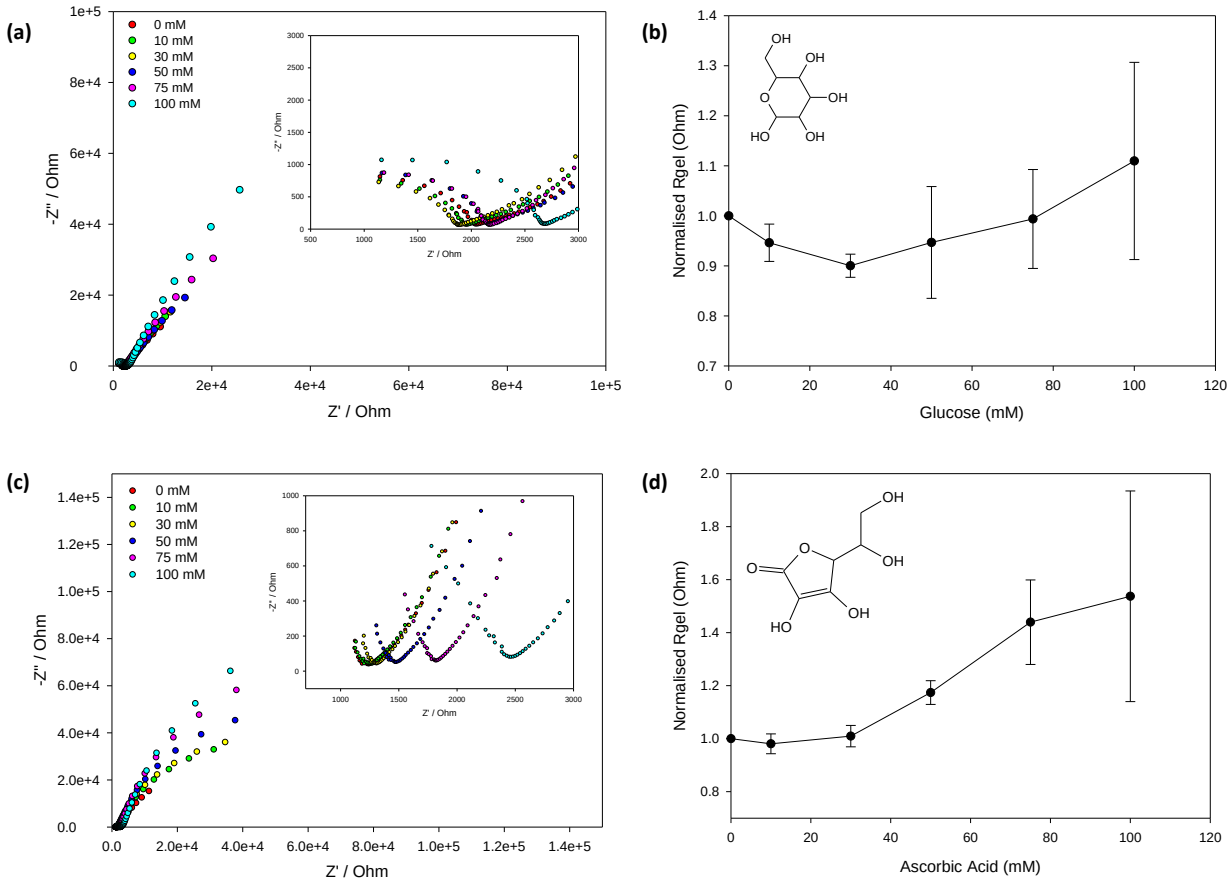

Figure 5.15 Representative (a) Nyquist plots of DMAP-4BA modified tattoo in buffer (pH 7.4) in the presence of glucose (0-100 mM) with magnification of the high frequency range inset (top right), (b) corresponding calibration data, (c) Nyquist plots of ascorbic acid (0-100 mM) and magnification of the high frequency region inset (top right) and (d) corresponding calibration data. (n=3).

Interestingly, this was the opposite of what was expected based on the experiments using DMAP-2BA in the 3-electrode system, where a decrease in resistance was observed as glucose concentration increased. The difference in response could be attributed to the different set-ups or to the positions of the polymer chain on the phenyl ring relative to the boron. When the polymer chain was in the ortho-position, small responses were observed. In this case, with the polymer chain in the para-position, larger shifts in R_{gel} values were observed. Glucose is distinct from other sugars because it has two sets of planar diols within its structure that are available to bind with BA. Therefore, a single glucose molecule can bind with BA moieties on separate polymer chains, forming inter-functional group bridges [42], [49], [50], which could induce additional crosslinking within the hydrogel matrix. This could potentially be a consequence of altering the position of the boron on the phenyl ring from ortho-position to para-position, allowing these glucose bridges to form more readily, condensing the hydrogel network which could account for the increase in resistance. The same trend was observed with AA, which also binds with PBA through its diols (Fig. 5.15b and d) [51]. AA also contains two sets of diols, where one is a planar enediol [52]. It is possible for one molecule of AA to also form these bridges between different PBA moieties on separate polymer chains, again condensing the hydrogel network and so resulting in an increasing R_{gel}. It is important to note that no significant swelling and deswelling of these electrode films was observed in these experiments implying that there were no significant repulsive interactions occurring across the network on account of binding. However, further research would be required, such as performing gravimetric studies to confirm this hypothesis.

Lactic acid is an α-hydroxyl acid which can also to bind to BA through its α-hydroxyl and carboxyl anion [51], [53] to form boronate esters. In a similar manner to before, the DMAP-4BA modified tattoo was studied in the presence of lactate (Fig. 5.16a). When increasing amounts of lactate were introduced to the DMAP-4BA modified matrix, a negative shift in resistance was observed (Fig. 5.16b). This is in contrast to the negative shift observed for glucose and AA. Interestingly it was noted that there was swelling of the hydrogel in the presence of lactate (not shown). It is known that glucose preferably binds to the anionic tetrahedral form at alkaline pH, however lactate is believed to generate a stronger complex with the neutral trigonal form at weakly acidic pH [54].

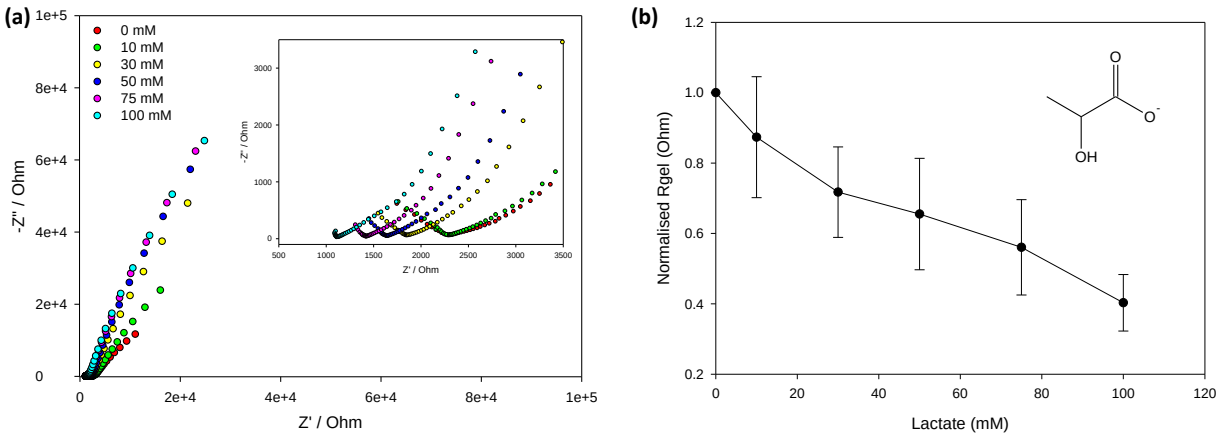

Figure 5.16 Representative (a) Nyquist plots of DMAP-4BA modified tattoo (pH 7.4) in the presence of lactate (0-100 mM) and magnification of the high frequency range inset (top right) (b) corresponding calibration data. (n=3).

In aqueous conditions, an equilibrium between the trigonal and tetrahedral BA species is established [51]. It was proposed that the trigonal boron was attacked by the carboxylic anion and converted into the tetrahedral configuration, followed by binding of the α-hydroxyl group forms an ester bond [54]. Lactate generates a complex with the trigonal form of the boronate and a reaction with the tetrahedral form occurs at a slower rate, however it is not possible to determine which step takes place first, but both are necessary for the complex formation [51], [54] (Fig. 5.17). This complexation generates charge on the boron which leads to an influx of ions in the presence of lactate which potentially could cause the decrease observed in R_{gel}.

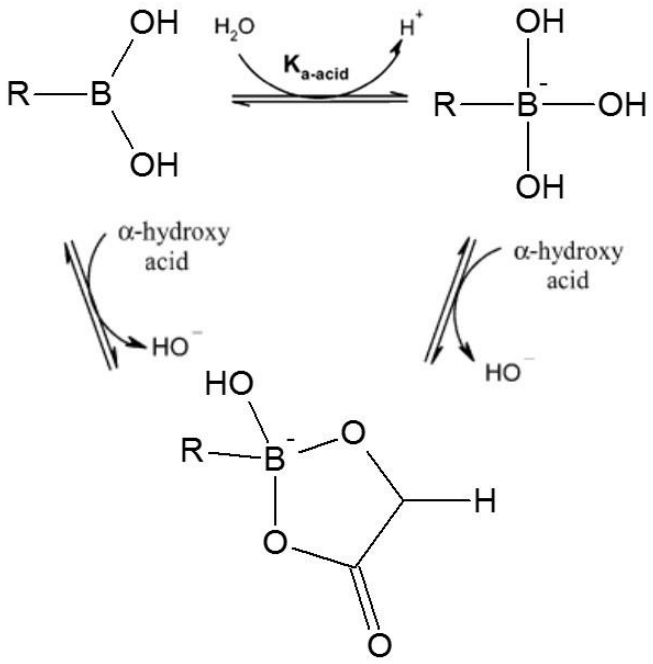

Figure 5.17 The equilibrium between a boronic acid and its boronate ester on reaction with α-hydroxy acid [51].

Overall these experiments demonstrate initial evidence to support the integration of chemically responsive material interfaces into the tattoo platform. The DMAP-4BA modified tattoo can respond electrically to the presence of glucose, AA and lactate between 10 – 100 mM at pH 7.4. The results also show that glucose, AA and lactate were within similar R_{gel} value ranges when exposed to the same concentrations, therefore the issue of interference between all three analytes is a possibility which would not be ideal when applied to a complex matrix such as skin. The studies carried out using the DMAP-4BA modified tattoo and its exposure to various analytes were carried out in solution, therefore the real challenge would be translating the DMAP-4BA modified tattoo into an epidermal sensing platform on skin to date, it has shown promising adherence and mechanical stability on human skin (Fig. 5.18) however its sensing response remains to be studied. This platform shows an exciting approach to epidermal sensing and could potentially be tailored to selectively detect analytes in skin because these results have shown that the material is capable of responding across a physiologically relevant range, in particular to lactate.

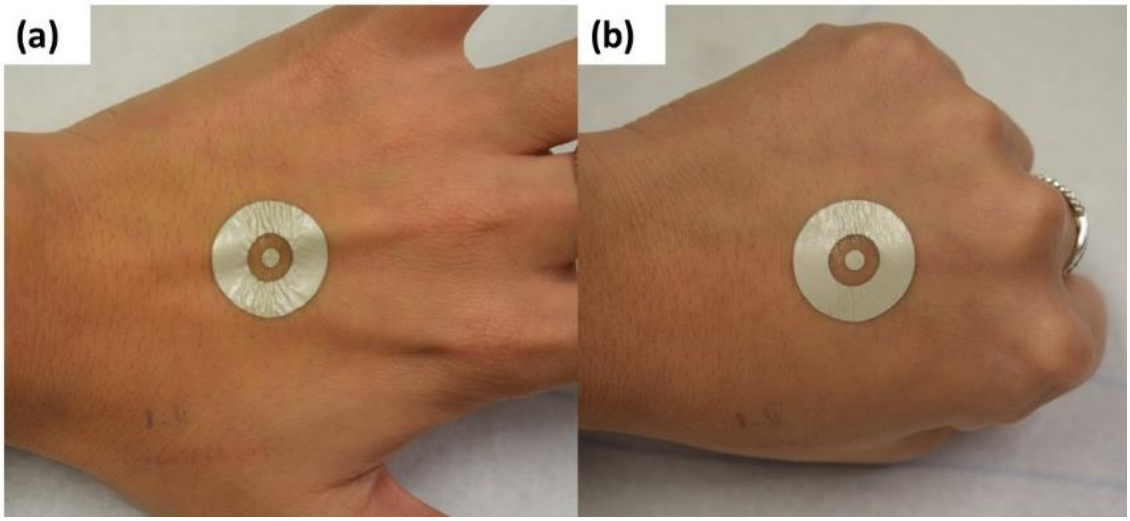

Figure 5.18 Images of DMAP-4BA modified tattoo on the back of (a) open fist and (b) closed fist to show adherence and conformability of the DMAP-4BA modified tattoo on skin (tattoo electrode diameter: 20 mm).

Overall the studies have shown that the PBA-based hydrogels used as a chemical interface show great potential in detecting analytes such as glucose, lactate and AA. Further investigation is required to fully understand the electrical response of the DMAP-4BA modified tattoo to these analytes at different pHs and outside of buffered conditions because sweat pH can vary between pH 5-7 [55], while SC barrier pH is acidic and can be between pH 4-5 [56]. Addressing the issue of selectivity towards one analyte can be challenging because factors such as pH and molecular geometry play a role in PBA binding affinity as observed in the results. However, the main challenge of using the DMAP-4BA as an epidermal sensing platform would be applying this material to skin and detecting analytes in a complex matrix such as skin. This would require further optimisation of the hydrogel matrix in order for the material to respond in an efficient manner in this dynamic environment. Gravimetric swelling experiments should be considered to validate and quantify swelling responses upon exposure to target diols or α-hydroxy acid. Mechanical studies of the DMAP-4BA modified tattoo should also be considered to determine its mechanical stability under drying effects when worn for long periods of time as drying effects would have an impact on the overall adherence and performance of the platform. Therefore, thorough understanding of these parameters are key steps for developing a BA-based selective hydrogel that can ultimately be integrated into an epidermal platform in the future.

5.4 Conclusions

This chapter demonstrates the concept of utilising PBA-based hydrogels as a smart chemically responsive material for the potential of chemical epidermal sensing. The tracked impedance changes of the hydrogel systems investigated shows promising results in detecting analytes such as glucose, lactate, and AA using particular formats and materials. The initial results from the Au-paper electrode indicate that pH and the position of the BA moiety and the charged polymer backbone have an effect on the binding of BA with glucose. The pH studies indicate that the Au-paper electrode seems to suffer from a degradation effect at pH 3 suggesting that the electrode might not function reliably in acidic conditions. While at pH 7.4 and 12, indicate minimal binding suggesting that binding of the BA with glucose has been limited due to the position of the BA from the charged N^+ on the polymer backbone. This indicates that further studies such as investigating smaller pH increments are required to understand the impact of pH on binding on the electrical properties of the hydrogel. While another investigation on the effect of changing the relative position of the BA moiety from the charged polymer backbone can potentially help understand its impact on optimal binding with target analytes.

The DMAP-4BA modified tattoo has shown promising initial results indicating that it can potentially be used to track between 10 – 100 mM concentrations of glucose, lactate and AA at pH 7.4. This platform represents a novel conformable epidermal sensor that can potentially be used on skin to respond electrically to glucose, AA and lactate. However other challenges need to be addressed such as investigating an optimal pH range for this epidermal platform because sweat pH can vary between pH 5-7 [55], while SC barrier pH is acidic and can be between pH 4-5 [56]. Interestingly, all these analytes are hydrophilic, low molecular compounds that depending on the porosity and diffusion properties of the hydrogel, these analytes could diffuse from the SC directly into the adhered hydrogel material. However, this would require the concentration of the analytes can be high enough to be detected. The next real challenge is on-body testing of the hydrogel material to determine its viability as an epidermal sensor. In the first instance, hydrogel chemistry may need to be further optimised to tailor the hydrogel matrix for selective binding because other constituents present in skin may interfere with measurements. A selective hydrogel could serve as a sensor to quantify glucose, lactate or AA in the skin. Therefore the next step would be understanding analyte diffusion from the SC into the hydrogel material since diffusion of analytes into the hydrogel governs the response. However, extraction of analytes from skin into the hydrogel may be challenging and depend on

the concentration of analyte present in the matrix. If these concentrations are too low for detection, techniques such as reverse iontophoresis or pilocarpine delivery could be considered to generate high volumes of skin fluids so that access to analytes maybe more facile. The mechanical properties of the hydrogel material also require testing in order to understand the mechanical stability and adherence on skin as drying effects could potentially restrict the long-term wearablity of these types of epidermal sensor. Once these factors are thoroughly understood and addressed, the rational design of a selective PBA-based hydrogel platform can be achieved. Overall, these PBA-based hydrogels and their integration in to a tattoo platform has shown initial promise towards introducing a chemical sensing interface into this epidermal sensor.

5.5 References

[1] A. J. Bandodkar, W. Jia, C. Yardımcı, X. Wang, J. Ramirez, and J. Wang, "Tattoo-Based Noninvasive Glucose Monitoring: A Proof-of-Concept Study," 2014.

[2] H. Lee, C. Song, Y. S. Hong, M. S. Kim, H. R. Cho, T. Kang, K. Shin, S. H. Choi, T. Hyeon, and D. H. Kim, "Wearable/disposable sweat-based glucose monitoring device with multistage transdermal drug delivery module," *Sci. Adv.*, vol. 3, no. 3, p. e1601314, 2017.

[3] M. Onor, S. Gufoni, T. Lomonaco, S. Ghimenti, P. Salvo, F. Sorrentino, and E. Bramanti, "Potentiometric sensor for non invasive lactate determination in human sweat," *Anal. Chim. Acta*, vol. 989, pp. 80–87, 2017.

[4] W. Jia, A. J. Bandodkar, G. Valdés-Ramírez, J. R. Windmiller, Z. Yang, J. Ramírez, G. Chan, and J. Wang, "Electrochemical tattoo biosensors for real-time noninvasive lactate monitoring in human perspiration," *Anal. Chem.*, vol. 85, no. 14, pp. 6553–6560, 2013.

[5] R. Badugu, J. R. Lakowicz, and C. D. Geddes, "Noninvasive Continuous Monitoring of Physiological Glucose Using a Monosaccharide-Sensing Contact Lens," *Anal. Chem.*, vol. 76, pp. 610–618, 2004.

[6] T. Sugawara, K. Kikuchi, H. Tagami, S. Aiba, and S. Sakai, "Decreased lactate and potassium levels in natural moisturizing factor from the stratum corneum of mild atopic dermatitis patients are involved with the reduced hydration state," *J. Dermatol. Sci.*, vol. 66, pp. 154–159, 2012.

[7] A. Watabe, T. Sugawara, K. Kikuchi, K. Yamasaki, S. Sakai, and S. Aiba, "Sweat constitutes several natural moisturizing factors, lactate, urea, sodium, and potassium," *J. Dermatol. Sci.*, vol. 72, pp. 177–182, 2013.

[8] T. Oranges, V. Dini, and M. Romanelli, "Skin Physiology of the Neonate and Infant: Clinical Implications," *Adv. Wound Care*, vol. 4, no. 10, pp. 587–595, 2015.

[9] M. Jennings, D. Alfieri, K. Ward, and C. Lesczczynski, "Comparison of salicylic acid and urea versus ammonium lactate for the treatment of foot xerosis. A randomized, double-blind, clinical study," *J. Am. Podiatr. Med. Assoc.*, vol. 88, no. 7, pp. 332–336, 1998.

[10] M. A. Abrar, Y. Dong, P. K. Lee, and W. S. Kim, "Bendable Electro-chemical Lactate Sensor Printed with Silver Nano-particles," *Sci. Rep.*, vol. 6, no. July, pp. 1–9, 2016.

[11] D. A. Sakharov, M. U. Shkurnikov, M. Y. Vagin, E. I. Yashina, A. A. Karyakin, and A. G. Tonevitsky, "Relationship between lactate concentrations in active muscle sweat and whole blood," *Bull. Exp. Biol. Med.*, vol. 150, no. 1, pp. 83–85, 2010.

[12] L. Maione-Silva, E. G. de Castro, T. L. Nascimento, E. R. Cintra, L. C. Moreira, B. A. S. Cintra, M. C. Valadares, and E. M. Lima, "Ascorbic acid encapsulated into negatively charged liposomes exhibits increased skin permeation, retention and enhances collagen synthesis by fibroblasts," *Sci. Rep.*, vol. 9, no. 522, pp. 1–14, 2019.

[13] F. Al-Niami and N. Y. Z. Chiang, "Topical Vitamin C and the Skin: Mechanisms of Action and Clinical Applications," *J. Clin. Aesthet. Dermatol.*, vol. 10, no. 7, pp. 14–17, 2017.

[14] J. M. Pullar, A. C. Carr, and M. C. M. Vissers, "The roles of vitamin C in skin health," *Nutrients*, vol. 9, no. 8, p. 866, 2017.

[15] E. M. Ahmed, "Hydrogel: Preparation, characterization, and applications: A review," *J. Adv. Res.*, vol. 6, no. 2, pp. 105–121, 2015.

[16] K. Deligkaris, T. S. Tadele, W. Olthuis, and A. van den Berg, "Hydrogel-based devices for biomedical applications," *Sensors Actuators, B Chem.*, vol. 147, no. 2, pp. 765–774, 2010.

[17] L. Zhang, K. Li, W. Xiao, L. Zheng, Y. Xiao, H. Fan, and X. Zhang, "Preparation of collagen-chondroitin sulfate-hyaluronic acid hybrid hydrogel scaffolds and cell compatibility in vitro," *Carbohydr. Polym.*, vol. 84, no. 1, pp. 118–125, 2011.

[18] E. Shirzaei Sani, R. Portillo-Lara, A. Spencer, W. Yu, B. M. Geilich, I. Noshadi, T. J. Webster, and N. Annabi, "Engineering Adhesive and Antimicrobial Hyaluronic Acid/Elastin-like Polypeptide Hybrid Hydrogels for Tissue Engineering Applications," *ACS Biomater. Sci. Eng.*, vol. 4, no. 7, pp. 2528–2540, 2018.

[19] J. Qu, X. Zhao, Y. Liang, T. Zhang, P. X. Ma, and B. Guo, "Antibacterial adhesive injectable hydrogels with rapid self-healing, extensibility and compressibility as wound dressing for joints skin wound healing," *Biomaterials*, vol. 183, no. August, pp. 185–199, 2018.

[20] X. Zhang, S. Wang, M. Hu, and Y. Xiao, "An immunosensor for ferritin based on agarose hydrogel," *Biosens. Bioelectron.*, vol. 21, no. 11, pp. 2180–2183, 2006.

[21] Q. Li, Y. Guan, and Y. Zhang, "Thin hydrogel films based on lectin-saccharide biospecific interaction for label-free optical glucose sensing," *Sensors Actuators, B Chem.*, vol. 272, no. May, pp. 243–251, 2018.

[22] A. S. Hoffman, "Hydrogels for biomedical applications," *Adv. Drug Deliv. Rev.*, vol. 54, pp. 3–12, 2002.

[23] E. Caló and V. V. Khutoryanskiy, "Biomedical applications of hydrogels: A review of patents and commercial products," *Eur. Polym. J.*, vol. 65, pp. 252–267, 2015.

[24] Z. Lei, Q. Wang, S. Sun, W. Zhu, and P. Wu, “A Bioinspired Mineral Hydrogel as a Self-Healable, Mechanically Adaptable Ionic Skin for Highly Sensitive Pressure Sensing,” *Adv. Mater.*, vol. 29, no. 22, p. 1700321, 2017.

[25] G. Justin, S. Finley, A. R. Abdur Rahman, and A. Guiseppi-Elie, “Biomimetic hydrogels for biosensor implant biocompatibility: Electrochemical characterization using micro-disc electrode arrays (MDEAs),” *Biomed. Microdevices*, vol. 11, no. 1, pp. 103–115, 2009.

[26] C. Ma, Y. Shi, D. A. Pena, L. Peng, and G. Yu, “Thermally Responsive Hydrogel Blends: A General Drug Carrier Model for Controlled Drug Release,” *Angew. Chemie - Int. Ed.*, vol. 54, no. 25, pp. 7376–7380, 2015.

[27] S. Brahim, D. Narinesingh, and A. Guiseppi-Elie, “Polypyrrole-hydrogel composites for the construction of clinically important biosensors,” *Biosens. Bioelectron.*, vol. 17, no. 1–2, pp. 53–59, 2002.

[28] C. M. Daikuzono, C. Delaney, H. Tesfay, L. Florea, O. N. Oliveira, A. Morrin, and D. Diamond, “Impedance spectroscopy for monosaccharides detection using responsive hydrogel modified paper-based electrodes,” *Analyst*, vol. 142, no. 7, pp. 1133–1139, 2017.

[29] R. Badugu, J. R. Lakowicz, and C. D. Geddes, “Fluorescence sensors for monosaccharides based on the 6-methylquinolinium nucleus and boronic acid moiety:potential application to ophthalmic diagnostics,” *Talanta*, vol. 65, no. 3, pp. 762–768, 2005.

[30] W. L. A. Brooks and B. S. Sumerlin, “Synthesis and Applications of Boronic Acid-Containing Polymers: From Materials to Medicine,” *Chem. Rev.*, vol. 116, no. 3, pp. 1375–1397, 2015.

[31] Y. Guan and Y. Zhang, “Boronic acid-containing hydrogels: Synthesis and their applications,” *Chem. Soc. Rev.*, vol. 42, no. 20, pp. 8106–8121, 2013.

[32] G. Springsteen and B. Wang, “A detailed examination of boronic acid - diol complexation,” *Tetrahedron*, vol. 58, pp. 5291–5300, 2002.

[33] J. Yan, G. Springsteen, S. Deeter, and B. Wang, “The relationship among pKa, pH, and binding constants in the interactions between boronic acids and diols - It is not as simple as it appears,” *Tetrahedron*, vol. 60, no. 49, pp. 11205–11209, 2004.

[34] Y. R. Lin, C. C. Hung, H. Y. Chiu, B. H. Chang, B. R. Li, S. J. Cheng, J. W. Yang, S. F. Lin, and G. Y. Chen, “Noninvasive glucose monitoring with a contact lens and smartphone,” *Sensors (Switzerland)*, vol. 18, no. 10, pp. 1–12, 2018.

[35] R. Badugu, J. R. Lakowicz, and C. D. Geddes, “Ophthalmic Glucose Monitoring using

Disposable Contact Lenses-A Review," *J. Fluoresc.*, vol. 14, no. 5, pp. 617–633, 2004.

[36] D. Bruen, C. Delaney, D. Diamond, and L. Florea, "Fluorescent Probes for Sugar Detection," *ACS Appl. Mater. Interfaces*, vol. 10, pp. 38431–38437, 2018.

[37] D. Bruen, P. P. Campos, M. Ferreira, D. Diamond, C. Delaney, and L. Florea, "Boronic Acid Homopolymers as Effective Polycations for Sugar-Responsive Layer-by-Layer Assemblies," *ACS Appl. Polym. Mater.*, vol. 1, pp. 990–996, 2019.

[38] A. Murphy, B. Gorey, K. De Guzman, N. Kelly, E. P. Nesterenko, and A. Morrin, "Microfluidic paper analytical device for the chromatographic separation of ascorbic acid and dopamine," *RSC Adv.*, vol. 5, no. 113, pp. 93162–93169, 2015.

[39] X. Wu, Z. Li, X. X. Chen, J. S. Fossey, T. D. James, and Y. B. Jiang, "Selective sensing of saccharides using simple boronic acids and their aggregates," *Chem. Soc. Rev.*, vol. 42, no. 20, pp. 8032–8048, 2013.

[40] B. Pappin, M. J., and T. A., "Boron-Carbohydrate Interactions," in *Carbohydrates - Comprehensive Studies on Glycobiology and Glycotechnology*, 2012.

[41] H. Fang, G. Kaur, and B. Wang, "Progress in boronic acid-based fluorescent glucose sensors," *J. Fluoresc.*, vol. 14, no. 5, pp. 481–489, 2004.

[42] C. Ancla, V. Lapeyre, I. Gosse, B. Catargi, and V. Ravaine, "Designed glucose-responsive microgels with selective shrinking behavior," *Langmuir*, vol. 27, pp. 12693–12701, 2011.

[43] C. Zhang, M. D. Losego, and P. V. Braun, "Hydrogel-based glucose sensors: Effects of phenylboronic acid chemical structure on response," *Chem. Mater.*, vol. 25, pp. 3239–3250, 2013.

[44] A. Matsumoto, R. Yoshida, and K. Kataoka, "Glucose-responsive polymer gel bearing phenylborate derivative as a glucose-sensing moiety operating at the physiological pH," *Biomacromolecules*, vol. 5, pp. 1038–1045, 2004.

[45] S. Liu, B. Miller, and A. Chen, "Phenylboronic acid self-assembled layer on glassy carbon electrode for recognition of glycoprotein peroxidase," *Electrochem. commun.*, vol. 7, pp. 1232–1236, 2005.

[46] S. Liu, L. Bakovic, and A. Chen, "Specific binding of glycoproteins with poly(aniline boronic acid) thin film," *J. Electroanal. Chem.*, vol. 591, pp. 210–216, 2006.

[47] M. Takeuchi, K. Koumoto, M. Goto, and S. Shinkai, "Efficient glucoside extraction mediated

by a boronic acid with an intramolecular quaternary ammonium ion," *Tetrahedron*, vol. 52, no. 40, pp. 12931–12940, 1996.

[48] W. L. A. Brooks, C. C. Deng, and B. S. Sumerlin, "Structure-Reactivity Relationships in Boronic Acid-Diol Complexation," *ACS Omega*, vol. 3, no. 12, pp. 17863–17870, 2018.

[49] A. M. Horgan, A. J. Marshall, S. J. Kew, K. E. S. Dean, C. D. Creasey, and S. Kabilan, "Crosslinking of phenylboronic acid receptors as a means of glucose selective holographic detection," *Biosens. Bioelectron.*, vol. 21, no. 9, pp. 1838–1845, 2006.

[50] A. Kim, S. Mujumdar, and R. Siegel, "Swelling Properties of Hydrogels Containing Phenylboronic Acids," *Chemosensors*, vol. 2, no. 1, pp. 1–12, 2013.

[51] F. K. Sartain, X. Yang, and C. R. Lowe, "Holographic lactate sensor," *Anal. Chem.*, vol. 78, no. 16, pp. 5664–5670, 2006.

[52] S. R. Ali, R. R. Parajuli, Y. Ma, Y. Balogun, and H. He, "Interference of ascorbic acid in the sensitive detection of dopamine by a nonoxidative sensing approach," *J. Phys. Chem. B*, vol. 111, no. 42, pp. 12275–12281, 2007.

[53] S. Kabilan, A. J. Marshall, F. K. Sartain, M. C. Lee, A. Hussain, X. Yang, J. Blyth, N. Karangu, K. James, J. Zeng, D. Smith, A. Domschke, and C. R. Lowe, "Holographic glucose sensors," *Biosens. Bioelectron.*, vol. 20, no. 8 SPEC. ISS., pp. 1602–1610, 2005.

[54] X. Yang, X. Pan, J. Blyth, and C. R. Lowe, "Towards the real-time monitoring of glucose in tear fluid: Holographic glucose sensors with reduced interference from lactate and pH," *Biosens. Bioelectron.*, vol. 23, no. 6, pp. 899–905, 2008.

[55] V. F. Curto, C. Fay, S. Coyle, R. Byrne, C. O'Toole, C. Barry, S. Hughes, N. Moyna, D. Diamond, and F. Benito-Lopez, "Real-time sweat pH monitoring based on a wearable chemical barcode micro-fluidic platform incorporating ionic liquids," *Sensors Actuators, B Chem.*, vol. 171–172, pp. 1327–1334, 2012.

[56] M. H. Schmid-Wendtner and H. C. Korting, "The pH of the skin surface and its impact on the barrier function," *Skin Pharmacol. Physiol.*, vol. 19, pp. 296–302, 2006.

Chapter 6

Conclusions & Future Work

6.1 Conclusions and Future Work

As reviewed in Chapter 1, there has been a substantial growth in the field of epidermal sensors which is partly due to the skins accessibility and role in human physiology. Researchers have demonstrated the potential of these epidermal sensors for sampling and detecting analytes from matrices, such as sweat and interstitial fluid (ISF). As a result of monitoring specific analytes from these matrices, researchers can potentially gain insight into metabolic processes within the body. Challenges such as extracting the analytes from skin as well as electrical and mechanical suitability of these epidermal sensors has limited these sensors from reaching their full potential. However, on-going research towards innovative materials and sensor designs will open up new avenues towards the realization of greater numbers of successful epidermal sensors for health diagnostics.

This thesis shows the evolution of a screen-printed epidermal sensor for monitoring physiological activity related to skin barrier function to biomarker analysis. The thesis proposed a planar concentric electrode design based on soft and flexible materials that can be adhered directly onto skin as the epidermal sensor. The transduction method of choice was non-faradaic impedance spectroscopy in order to interrogate the skin. In this work, the first iterations of the epidermal sensor focused on enhancing electrical and mechanical stability from its first iteration as a single-use flexible sensor to an improved stretchable sensor with robust adherence to skin and enhanced mechanical durability. The final aspect focused on strategies to modify the sensor with responsive hydrogel materials to enable chemical sensing of analytes relevant to skin.

The main conclusions of each chapter have been outlined in the bullet points below:

- Chapter 2 demonstrated the fabrication and development of the first iteration of the screen-printed silver tattoo platform. With this first iteration, water content changes were tracked in a hydrogel, porcine skin as well as human skin using impedance, which demonstrated the potential of the sensor for monitoring stratum corneum (SC) hydration. However, this iteration did not fully conform or adhere to skin for a long period of time and was more suited for single measurement.
- Chapter 3 presented the investigation of ink formulations and has demonstrated the positive impact of using an elastomeric silver ink formulation to enhance mechanical properties. It also explored the use of a conducting adhesive (CA) layer to enhance adherence to skin. This CAC platform showed robust mechanical properties compared

to the previous platform. However, its electrical properties were not fully ideal for an epidermal sensor.

- Chapter 4 considered an alternative adherence approach in an effort towards improving the electrical interface with skin. A thinner, non-conducting adhesive with pores were incorporated into the platform. It showed enhanced electrical and mechanical properties of the sensor compared to the previous platforms. Overall, these chapters demonstrated that selection of ink formulations and adherence methodologies were important considerations in the fabrication and implementation of epidermal sensors.
- Chapter 5 investigated the use of phenyl boronic acid (PBA) functionalized hydrogels for chemical sensing ultimately for application in chemical epidermal sensing. The initial results indicate that PBA functionalized hydrogels are a promising smart material for the detection of monosaccharides and α-hydroxyls, glucose, lactate and ascorbic acid. Further modifications are required to fabricate an analyte selective sensor that can target specific analytes related to skin or health conditions.

Overall the Chapters 2-4 has demonstrated that a compromise between mechanical stability and acquisition of reliable electrical measurements were important considerations for fabricating epidermal sensors. While the work from Chapter 5 showed promising results towards integrating a chemical interface that can potentially target analytes specific to skin or health conditions. However, there are still electrical and mechanical challenges that still need to be addressed before realizing their full potential. One of the major challenges that was addressed was establishing a robust platform that can reliably measure the skin. The approach investigated in Chapter 4 was a step in the direction towards the realization of an epidermal sensor that was mechanically robust as well as being capable of collecting good electrical signal from the SC.

The following sections outline possible areas of improvement that could be made to the work described in Chapters 2-5. Future work can look at further understanding the capabilities of this platform would prove advantageous towards optimising the overall epidermal platform, such as a larger population study that look at the impedance signals generated by healthy and diseased skin states on various anatomical sites. This type of investigation can improve the understanding of the electrical properties of healthy and diseased individuals as well as the impact of anatomical site. Another potential route for future work could investigate the electrical signals generated at skin-electrode interface during motion. Motion artefacts arise from the interface

due to relative motion of electrodes on skin which in turn can affect signal quality [1]. This can be potentially reduced by exploring other robust and reliable adherence methods between the skin and electrodes. Further understanding of the noise generated at skin-electrode interface could potentially help improve data processing or circuit modelling to reduce the effect of noise as well as improve reproducibility of the epidermal sensor.

To optimise the sensing methodology using the epidermal sensor, a single frequency measurement or isolation of a small frequency range dominated by the target skin layer would simplify the method and reduce sampling time. Miniaturisation of the electronics should also be considered to lower costs and incorporate portability by moving away from bench top settings. An impedance chip such as an AD5933 chip (Analog Devices, Ireland) can be used as a portable impedance unit that can potentially be used for single frequency measurements as seen in Fig. 6.1a and b. Initial steps towards moving from a bench top potentiostat to a portable system with impedance chip has indicated a promising correlation between as seen in Fig. 6.1c. Due to the human skin barriers highly resistive nature and variability between individuals, the next step would be on extensive calibration studies on a large population. This would also require further electronic modifications of the device. Once these technological challenges have been addressed, a low-cost portable impedance system coupled with the epidermal sensor could potentially be used in clinical studies in a hospital setting to investigate and understand skin barrier properties of healthy and damaged skin across a large population. Technological advances using the impedance chip would also help towards the next step of integrating wireless data transmission into the epidermal sensor to enable individuals to receive data to their mobile phones or computer for real-time monitoring.

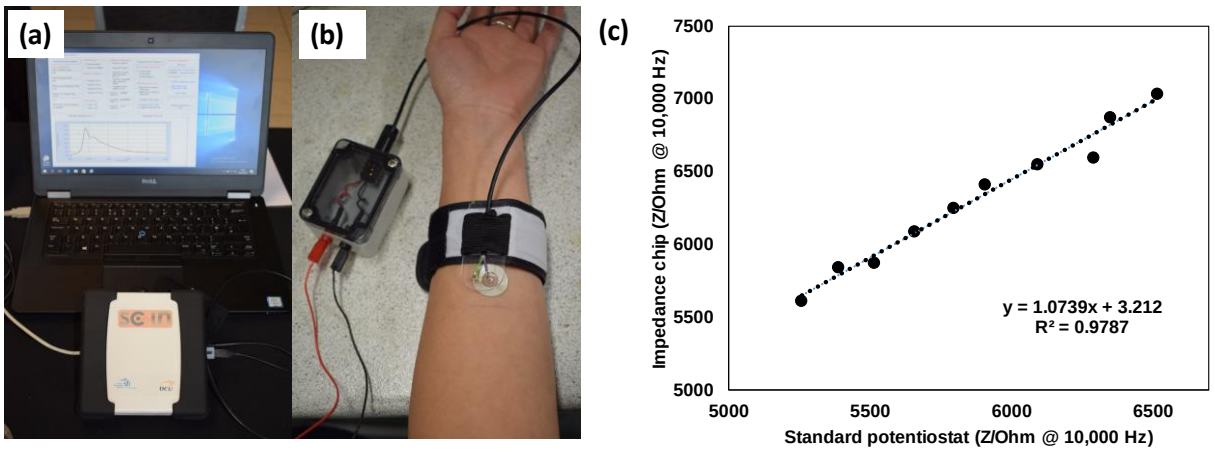

Figure 6.1 An example of (a) the integrated impedance chip in a portable housing unit with measuring software on the laptop, (b) wristband used to connect the epidermal sensor to the portable impedance unit and (c) regression analysis comparing data measured on a hydrogel skin mimic by the epidermal sensor using a standard potentiostat versus an impedance chip.

The skin adherence approach relating to the use of a CA in Chapter 3 was limited by the difficulty of differentiating the electrical signals from viable skin and the CA layer. This was due to the combination of the high resistance and capacitance associated with the CA layer as well as measuring a highly resistive SC barrier. However, there is potential for this adhesive approach to be used in a different application where the tissue investigated is more conducting and doesn't have a resistive barrier. Based on this, the sensor can potentially be used as a platform to measure intrinsic resistance of knee ligaments for a surgical application to gauge ligament tautness. The knee, is a complex joint where its mobility and stability are supported by the surrounding ligament system. A torn or damaged ligament due to high impact physical activity or illness (i.e. osteoarthritis) affects an individuals' mobility [2], [3] and require surgical operation to repair the damage, therefore a method to quantify tautness of knee ligaments during surgery would be advantageous. A potential electrode platform can be comprised of two CA-silver electrodes as seen in Fig. 6.2a where the electrodes are small enough it can be applied to a porcine knee ligament. These electrodes can potentially monitor the changes in impedance due to changes in ligament tension as seen in Fig. 6.2b. Future work using this electrode platform to monitor ligament tension can potentially look at performing tests on excised human ligament tissue. The impact of drying effects on ligament-electrode adherence should also need to be

considered as these effects could potentially have an effect on the reliability of the electrical signals measured.

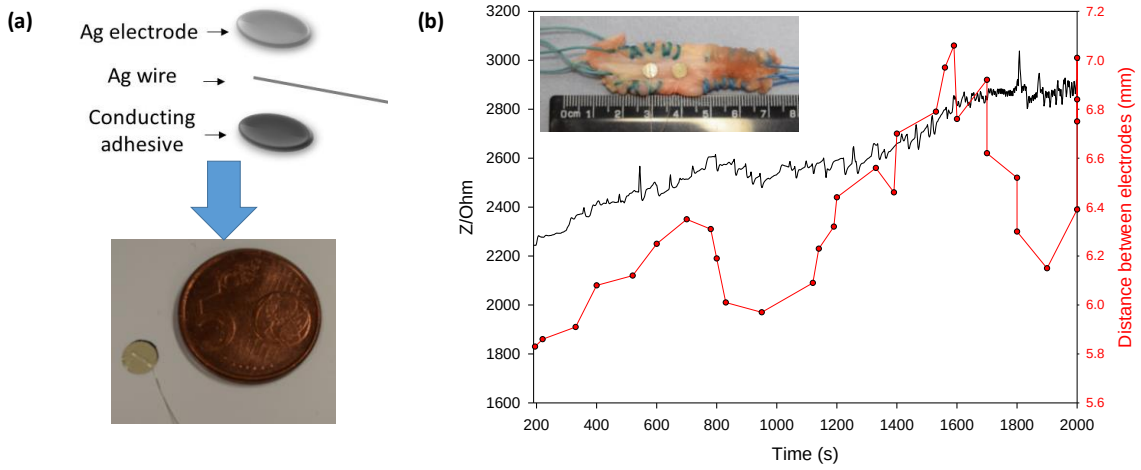

Figure 6.2 (a) Schematic diagram and image of the CA-silver electrodes (2 x 5 mm diameter electrodes) and (b) Graphs comparing the impedance measured by the electrodes with the change in electrode distance (mm) during stretching and relaxation of a ligament. Inset (top left) is the image of the electrode platform on a porcine ligament.

The initial experimental results for the PBA-modified electrodes in Chapter 5 have shown that PBA-based hydrogels integrated into an epidermal sensor as a chemical interface show great potential in detecting biomarkers. These results suggested that the electrical response of these hydrogels to analytes were influenced by pH and the relative position of the boronic acid (BA) moiety with regards to the charged polymer chain. Further investigation is required to fully understand the specific electrical responses that was observed by this modified sensor to analytes such as glucose and lactate. This can be done by investigating the effect of changing the position of the BA relative to the N^+ moiety on the polymer chain in order to understand the charge neutralisation effect and BA binding. Another consideration would be investigating a broader pH range because this would help tailor the PBA-modified electrodes to work at a pH range relevant to skin. The next challenge for the hydrogel modified epidermal sensors will be in applying them to skin for detecting analytes. This will require further optimisation of the hydrogel matrix in order for the material to respond in an efficient manner in this dynamic

environment. Hydrogel chemistry could also be further optimised to tailor greater binding selectivity. Ideally, a selective hydrogel could serve as a sensor to quantify glucose or lactate in skin (Fig. 6.3). Mechanical studies of the hydrogel modified epidermal sensor also need to be considered to determine mechanical and chemical stability when worn for long periods of time as factors such as drying effects would have an impact on the adherence and performance of the platform. Addressing these challenges are key towards developing a PBA-based selective hydrogel that can ultimately be integrated into an epidermal platform in the future.

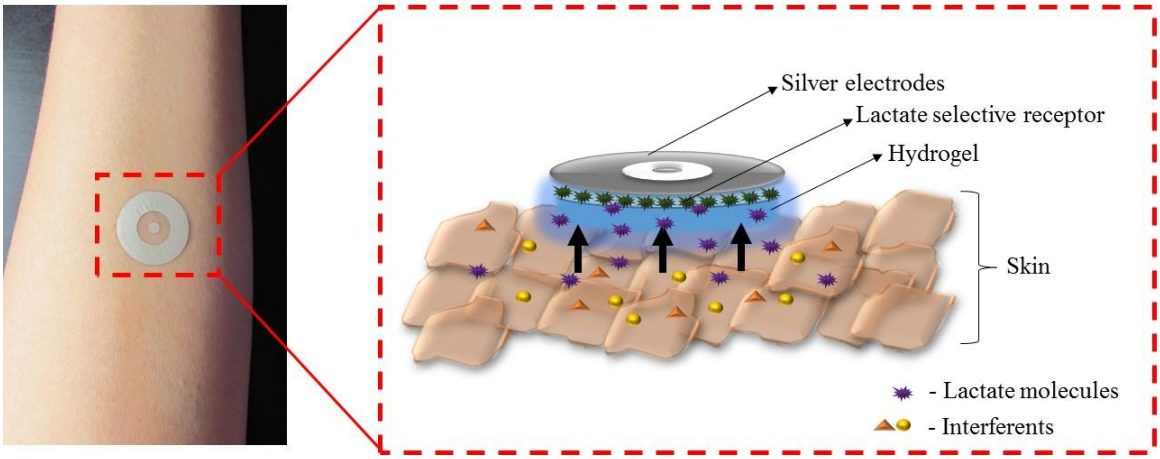

Figure. 6.3 Schematic diagram of a smart responsive hydrogel for selective lactate sensing in skin using the tattoo platform.

An alternative approach for chemical sensing using hydrogel chemistry would be the development of a biocompatible pH sensitive hydrogel that can be coupled with the epidermal platform. Healthy skin has an acidic pH between 4-5 in healthy adults [4]. In contrast, individuals who suffer from skin conditions have elevated skin pH (pH > 6) where an alkaline environment may impair healing by allowing invasive bacteria or fungi to thrive [5], [6]. This pH difference could be exploited by tailoring the swelling properties of pH sensitive hydrogels. Hydrogels based on hydroxyethyl cellulose/hyaluronic acid have shown desirable biocompatibility and pH sensitivity [7] and could potentially be tailored into an epidermal sensor. Swelling properties in response to analytes would need to be understood and characterised electrically as the swelling rate is primarily diffusion controlled, reducing the

diffusion path by producing thinner films could be a simple method of controlling swelling rate to prevent the electrodes from fracturing due to over swelling.

The continued research into developing smart chemically responsive materials for epidermal sensing will help towards improving its electrical, mechanical and chemical modalities. These developments can lead towards the realization of successful epidermal devices that can potentially fuse chemical, physical and electrophysiological sensors into one epidermal platform for health diagnostics. Innovative wearable point-of-care devices for health diagnostics such as these proposed here hold great potential to comprehensively and continuously monitor an individuals' health. The development of these epidermal sensors still face multiple challenges as outlined in this thesis. However, the continued progress in the fabrication of soft conformable materials and development of innovative responsive chemistries coupled with technological advancements such as wireless transmission of data, presents exciting opportunities for epidermal sensors to collect vital real-time health information bringing us a step closer towards realising personalised healthcare.

6.2 References

[1] J. Heikenfeld, A. Jajack, J. Rogers, P. Gutruf, L. Tian, T. Pan, R. Li, M. Khine, J. Kim, J. Wang, and J. Kim, "Wearable sensors: Modalities, challenges, and prospects," *Lab Chip*, vol. 18, no. 2, pp. 217–248, 2018.

[2] J. Melrose, "The Importance of the Knee Joint Meniscal Fibrocartilages as Stabilizing Weight Bearing Structures Providing Global Protection to Human Knee-Joint Tissues," *Cells*, vol. 8, p. 324, 2019.

[3] M. Sommerfeldt, A. Raheem, J. Whittaker, C. Hui, and D. Otto, "Recurrent Instability Episodes and Meniscal or Cartilage Damage After Anterior Cruciate Ligament Injury: A Systematic Review," *Orthop. J. Sport. Med.*, vol. 6, no. 7, pp. 1–9, 2018.

[4] S. Luebberding, N. Krueger, and M. Kerscher, "Skin physiology in men and women: In vivo evaluation of 300 people including TEWL, SC hydration, sebum content and skin surface pH," *Int. J. Cosmet. Sci.*, vol. 35, pp. 477–483, 2013.

[5] C. R. Kruse, K. Nuutila, C. C. Y. Lee, E. Kiwanuka, M. Singh, E. J. Caterson, E. Eriksson, and J. A. Sørensen, "The external microenvironment of healing skin wounds," *Wound Repair Regen.*, vol. 23, no. 4, pp. 456–464, 2015.

[6] L. A. Schneider, A. Korber, S. Grabbe, and J. Dissemond, "Influence of pH on wound-healing: A new perspective for wound-therapy?," *Arch. Dermatol. Res.*, vol. 298, no. 9, pp. 413–420, 2007.

[7] S. S. Kwon, B. J. Kong, and S. N. Park, "Physicochemical properties of pH-sensitive hydrogels based on hydroxyethyl cellulose-hyaluronic acid and for applications as transdermal delivery systems for skin lesions," *Eur. J. Pharm. Biopharm.*, vol. 92, pp. 146–154, 2015.

Appendix

Appendix Figures for Chapter 2

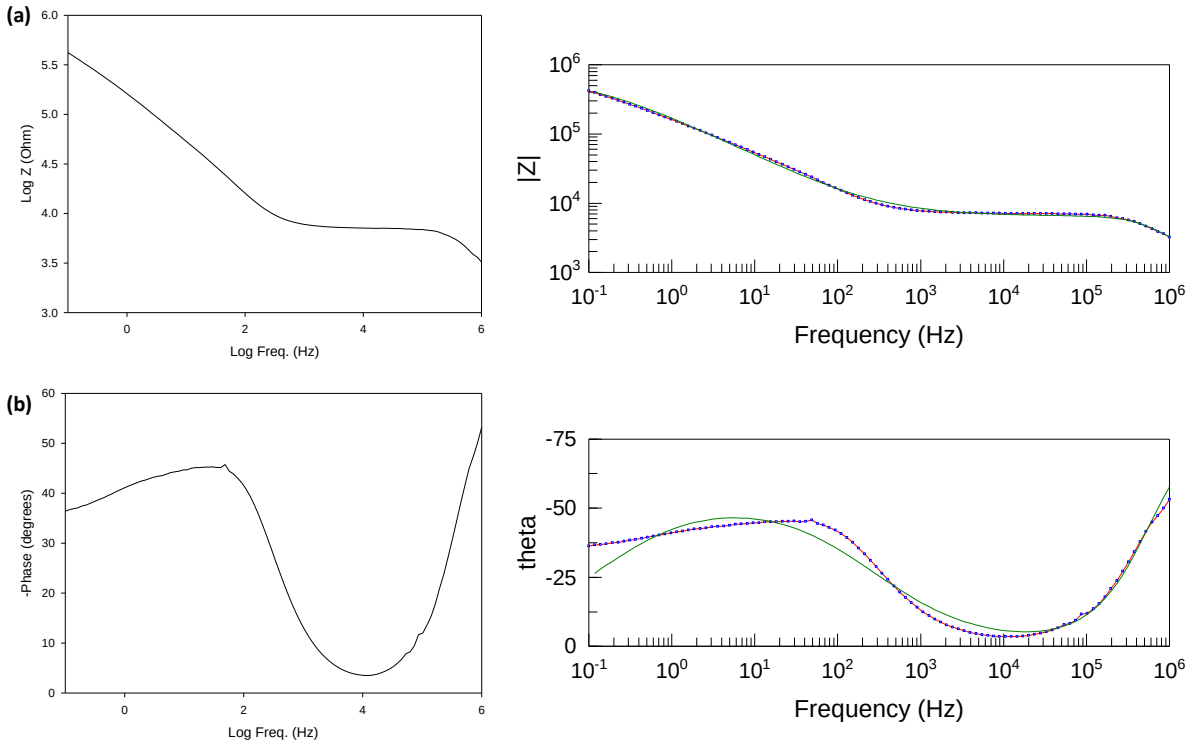

Figure. A2.A Example of (a) Impedance and (b) phase plots with corresponding fitted data of the screen printed electrode (PF410 silver ink) on a hydrogel using ZView. (Data points are in blue, interconnected with a red line, and the fits are shown in green).

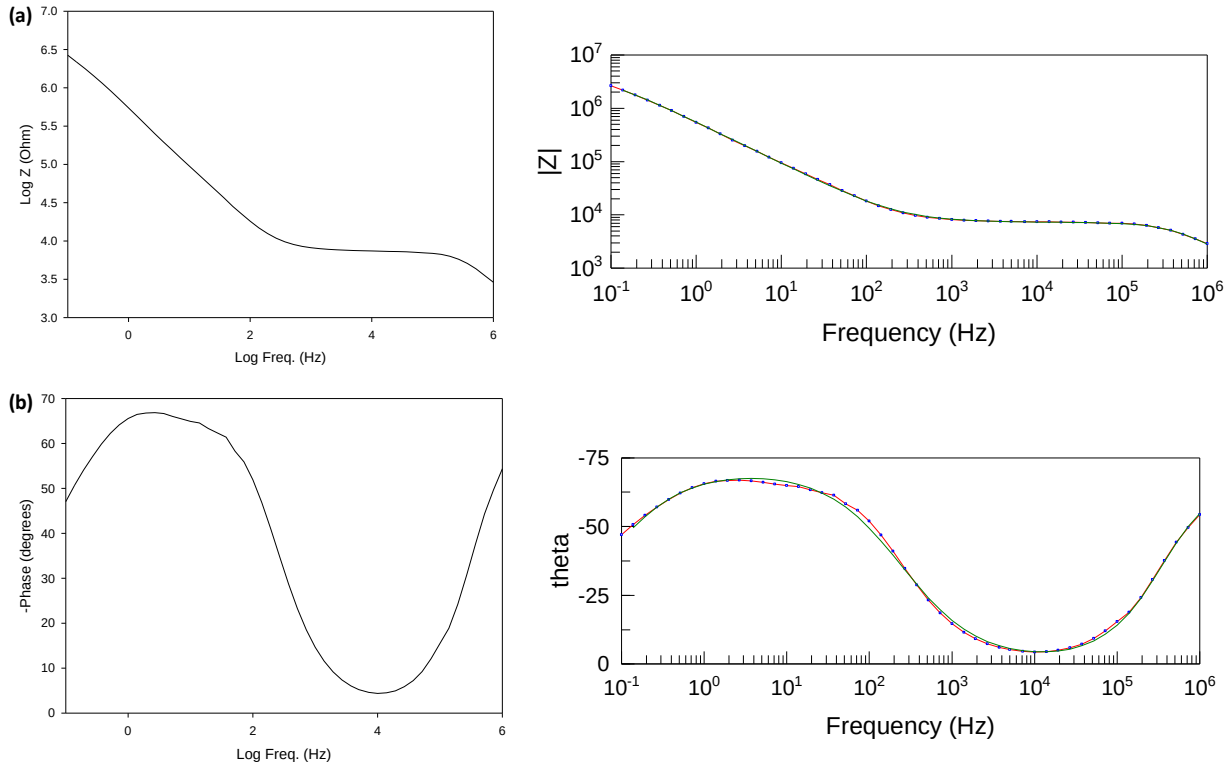

Figure A2.B Example of (a) Impedance and (b) phase plots with corresponding fitted data of the screen printed electrode (PF410 silver ink) on porcine skin using ZView. (Data points are in blue, interconnected with a red line, and the fits are shown in green).

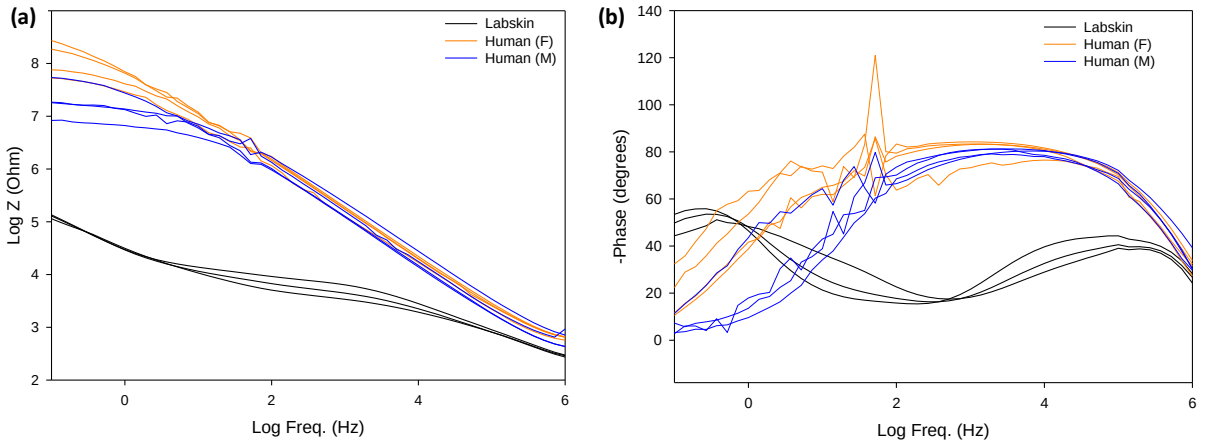

Figure A2.C (a) Impedance and (b) phase plots comparing the electrical signals from a human skin equivalent and human skin.

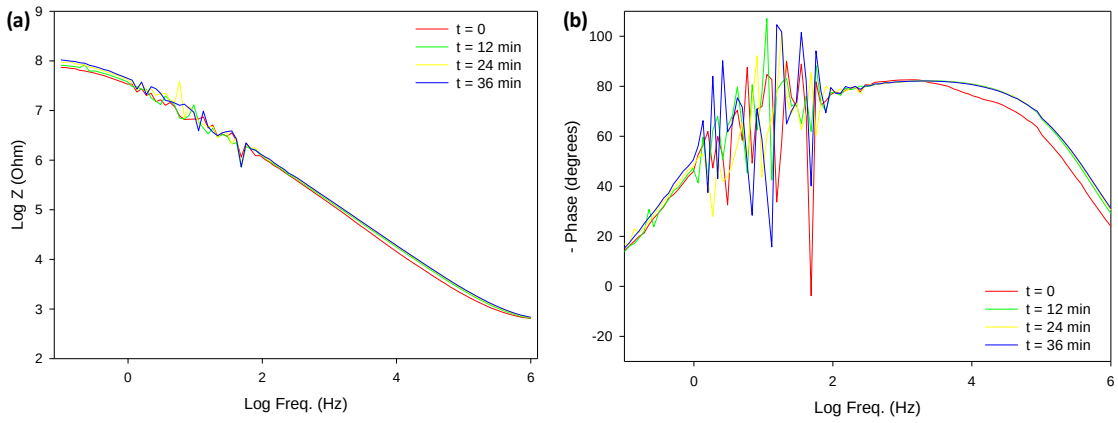

Figure A2.D (a) Impedance and (b) phase plots of the screen printed electrodes on human skin during dehydration.

The skin was soaked with water by a topical application (according to Section 2.7) and a tattoo electrode was applied. Impedance measurements were taken at 6 min intervals. After 42 min, the tattoo was removed and a topical application of water was done again to rehydrate the skin. A fresh tattoo was applied and measurements were taken for a further 32 min. Impedance values (Z) were isolated at 1 kHz and plotted over time. This was then validated by the MMD probe. The impedance measurements with the TDC measurements show that the tattoo electrodes were able to track changes in hydration levels of skin, suggesting that the tattoo electrodes are a promising means to assess the hydration state of the skin but addressing adherence to the skin would be an important issue to address.

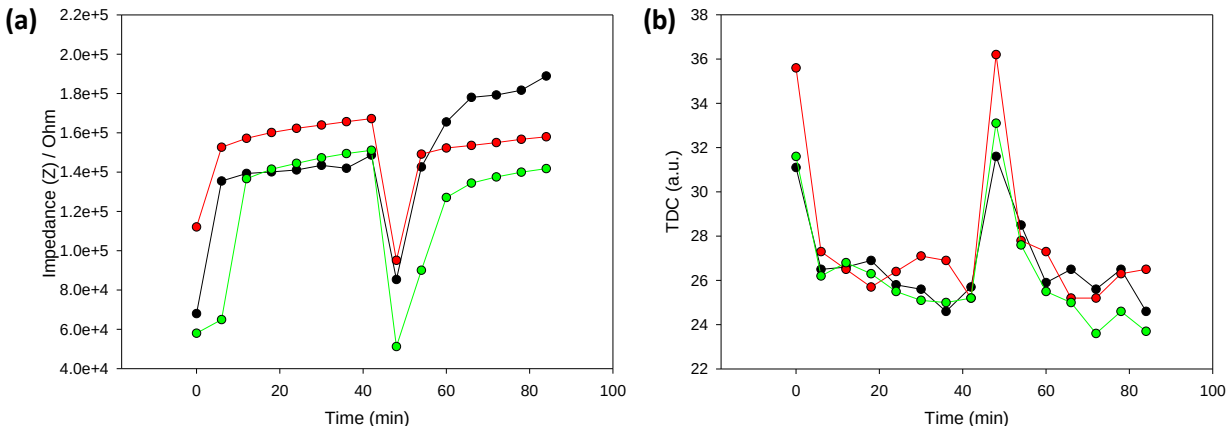

Figure A2.E Response of (a) tattoo electrodes on human skin during dehydration and rehydration (b) corresponding TDC measurements using the MMD probe.

Appendix Figures for Chapter 3

Section A3.A Example of Plain Language Statement, Informed Consent form and Questionnaire

DUBLIN CITY UNIVERSITY

Plain Language Statement

I. *Understanding Skin Barrier Function to aid the Development of Skin Electrodes for Healthcare is a Science Foundation Ireland (SFI) funded research study led by Dr Aoife Morrin within the National Centre for Sensor Research and the School of Chemical Sciences at Dublin City University. Ms Keana De Guzman is the researcher investigating the development of wearable skin electrodes for healthcare and diagnostics. The group needs to collect data on skin that will be vital to the development of these skin electrodes.*

II. *We ask that you do not wear perfumes/cosmetics on your arm on the day you participate in this Research Study, as they could interfere with the outcome. Upon meeting the researcher, you will be shown the hand held commercial skin hydration probe and skin electrodes to be used in the study.*

The first non-invasive measurement will measure the hydration levels of your skin before and after washing the arm using the commercial skin hydration probe (Delfin MoistureMeterD). This will be done by placing the flat bottom probe on the surface of the inner forearm for 15 seconds. These measurements will be repeated 3 times to make sure the data is reliable.

The second measurement will measure hydration of skin using a temporary press-on tattoo approach. This approach uses skin electrodes which are applied in a similar manner to that of temporary press-on tattoos where upon application the skin electrodes sit on the skin surface. The skin electrodes are comprised of 2 electrodes in a format that is 2 cm in diameter overall. These skin electrodes are supplied on backing paper and has an adhesive on top that is used to adhere the skin electrodes to the skin surface. The electrodes are based on a flexible silver thin films. The skin electrodes will be applied to the skin in the same manner as temporary press-on tattoos where the electrodes sit on the skin surface. It will be applied onto the skin surface by placing the adhesive side-down onto the skin and then wetting the backing paper with water. The backing paper then releases the adhesive and skin electrodes onto the surface of the skin. After application to the skin, the skin electrodes will be electrically connected with a custom armband in order to generate an electric field in the skin using the skin electrodes. This electrical measurement will take a maximum of 10 minutes. Once the measurement is done, the researcher will carefully remove the armband and you can remove the skin electrodes by peeling it off the skin and washing your arm with water and soap to remove any residue. The skin electrodes can then be disposed.

After all measurements are taken, you will be asked to complete a questionnaire about your skin care habits/lifestyle which should take 5-10 minutes. After completion of the questionnaire, you should seal it in the envelope provided and submit them before you leave. The researchers will not open the envelope until all data collection for the Research study has been completed.

III. *There is a risk that the skin electrodes with adhesive can cause itching and irritation, and if this occurs you should discontinue your participation in the study. The skin electrodes generates an electric field across a small 3 mm region of skin on your inner forearm. The current level that will pass through the skin during the measurement is very low that no sensation should be felt during this time. In the event that you do experience a slight tingling sensation under the skin electrodes, you should discontinue your participation in the study. There is a risk that you may feel uncomfortable*

providing information on skin care habits or lifestyle. If this occurs, you may discontinue participating in the study.

IV. *Potential benefits of participating in this research study include increased awareness of skincare and the effects of lifestyle on the skin's condition. You will have the opportunity to learn about the role of science and technology in skin care and skin research during the measurement of your skin's properties using new sensor technology.*

There are also some indirect benefits from your involvement in the study. The data collected from the study will help advance the development of non-invasive diagnostics in human healthcare. This technology has the potential to provide a safer and more comfortable experience for patients by reducing the need for blood tests and skin biopsies, which could speed up hospital workflows and personalize healthcare.

V. *All data collected in this study will remain anonymous and will be treated with the highest standards of security and confidentiality. It will not be linked to your identity. The measurements made on your skin will be assigned a random 8-digit number for the purpose of this research study. Data generated will be encrypted and stored securely stored at DCU until the end of the research project in 2019, which time it will be destroyed. At this time, all digital data will be deleted with subsequent hard drive secure deletion to ensure the files can't be recovered. The confidentiality of information provided by this study is subjected to legal limitations, i.e. data collected during this study can be subject to subpoena, freedom of information claim or mandated reporting.*

VI. *Data collected from this study will be analysed and compared within the group of participants. It is important for the research team to understand what similarities and differences exist between different skin and its links with lifestyle or environmental factors. This data is important in establishing a baseline profile for the development of skin electrodes to allow us to distinguish between normal and other skin types.*

VII. *Your involvement in the research study is voluntary. You may change your mind and withdraw from the study at any point in time without providing any reason for doing so. I am aware that once the research study is completed, the data will be anonymised and it will no longer be possible to withdraw from the study.*

VIII. *If you would like to receive an update on the progress and outcomes of this study please send your request via e-mail to dcuskinstudy@gmail.com.*

Contact Details for further information:
You can contact the research team for further information by e-mailing dcuskinstudy@gmail.com or phoning 01-700-5791.

If participants have concerns about this study and wish to contact an independent person, please contact:
The Secretary, Dublin City University Research Ethics Committee, c/o Research and Innovation Support, Dublin City University, Dublin 9. Tel 01-7008000, e-mail **rec@dcu.ie**

DUBLIN CITY UNIVERSITY
Informed Consent Form

I. Understanding Skin Barrier Function to aid the Development of Skin Electrodes for Healthcare

This Science Foundation Ireland funded research is led by Dr Aoife Morrin and is currently underway within the National Centre of Sensor Research and the School of Chemical Sciences, DCU. Ms Keana De Guzman will be collecting important data that will advance the development of skin electrodes in healthcare and diagnostics

II. Why is this research being carried out?

Our research group is developing non-invasive skin electrodes that could be used to gain important information about a person's health in place of using more invasive approaches like taking a blood sample or a biopsy. We first need to understand human skin in the general population to ensure the successful development of the skin electrodes. In this Research Study, we hope to find out how the properties of different skin can vary and if lifestyle and environmental factors play a role in these differences. We are interested in studying the hydration/electrical properties of the skin. The data collected will help us establish baseline trends for the skin to ensure that the skin electrodes developed can distinguish between different skin types.

III. What do I have to do?

I will be asked to attend one meeting with the research team, on the day of which I should not apply perfume or cosmetics to my arms/hands as this could interfere with the outcome of the study. Upon meeting the researchers and discussing the research carried out and signing this Informed Consent Form, the researcher will collect the form and the measurements will be taken.

A hydration measurement using a commercial hydration probe (Delfin MoistureMeterD, MMD) will be the first non-invasive measurement taken from my skin before and after washing my skin with water. I am aware the measurements are non-invasive will be repeated 3 times.

The second measurement will measure hydration of skin using a temporary press-on tattoo approach. This approach uses skin electrodes which are applied in a similar manner to that of temporary press-on tattoos where upon application the skin electrodes sit on the skin surface. These skin electrodes are comprised of 2 electrodes in a format that is 2 cm in diameter overall. These skin electrodes are supplied on backing paper and has an adhesive on top that is used to adhere the skin electrodes to the skin surface. The skin electrodes are based on a flexible silver thin film. The skin electrodes will be applied to the skin in the same manner as temporary press-on tattoos. It will be applied onto skin by placing the adhesive side-down onto the skin and then wetting the backing paper with water. The backing paper then releases the adhesive and electrodes onto the surface of the skin. After application to the skin, the skin electrodes will be electrically connected with a custom armband in order to generate an electric field in the skin. The maximum voltage used for this is 0.1 volts. This electrical measurement will take a maximum of 10 minutes. Once the measurement is done, the researcher will carefully remove the armband and I can remove the skin electrodes by peeling it off the skin and washing my arm with water and soap to remove any residue. After this time I will spend 5-10 minutes completing the questionnaire. I will seal my questionnaire in the envelope provided and submit it to the researcher before leaving. I am aware that the researcher will not open this envelope immediately afterwards, but that it will be opened when all data collection for the study has been completed.

When the measurements and questionnaire have been collected, I am finished participating in the Research study.

<u>Participant – please complete the following (Circle Yes or No for each question)</u>
I have read the Plain Language Statement (or had it read to me) *Yes/No*

I understand the information provided *Yes/No*
I have had an opportunity to ask questions and discuss this study *Yes/No*
I have received satisfactory answers to all my questions *Yes/No*

IV. *I am aware that my participation in the Research Study is voluntary and that I may withdraw from the study at any time without having to provide any reason for doing so. I am aware that when I have finished participating in the research study, the data will be anonymised and it will no longer be possible to withdraw from the study.*

V. *I am aware that my identity will not be linked to any data collected during this study, and that the confidentiality of information provided during the study can only be protected within the limitations of the law. I am aware that it is possible for the information to be subjected to subpoena, freedom of information claim or mandated reporting.*

VI. *If I have any contact allergies or very sensitive skin it may be best to discontinue my participation in the study as there is the potential for the skin electrodes with adhesive to irritate my skin. If I proceed with the study and encounter skin irritation or discomfort (i.e. tingling sensation) while wearing the skin electrodes, I should discontinue my participation in the study. If this occurs, I will remove the skin electrodes and wash my skin with water and soap. I understand that contact can be made on my behalf or a phone can be provided to me to make contact with Student Health Services (In CG13, Ph: 01 700 5143) or the Healthy Living Centre (School of Nursing & Human Sciences, Ph: 01 700 7171) to seek medical attention if necessary.*

VII. *If I would like to receive any update on the findings or outcomes of this Research Study I should send an email requesting this information to dcuskinstudy@gmail.com.*

VIII. *I have read and understood the information in this form. My questions and concerns have been answered by the researchers, and I have a copy of this consent form. Therefore, I consent to take part in this research project.*

Participants Signature: _____

Name in Block Capitals: _____

Witness: _____

Date: _____

Age: _____

Gender: ☐ Male ☐ Female

How would you classify your skin type?

☐ Very Dry

☐ Dry

☐ Normal

☐ Oily

☐ Very oily

☐ Not sure

☐ Other (please specify below)

_____

Do you have an existing skin condition?

☐ Yes

☐ No

If YES, can you specify what the skin condition is?

_____

Do you moisturise your skin (specifically arms) regularly?

□ Yes

□ No

If YES, how often do you moisturise?

□ Daily

□ Weekly

□ Monthly

□ Other (please specify below)

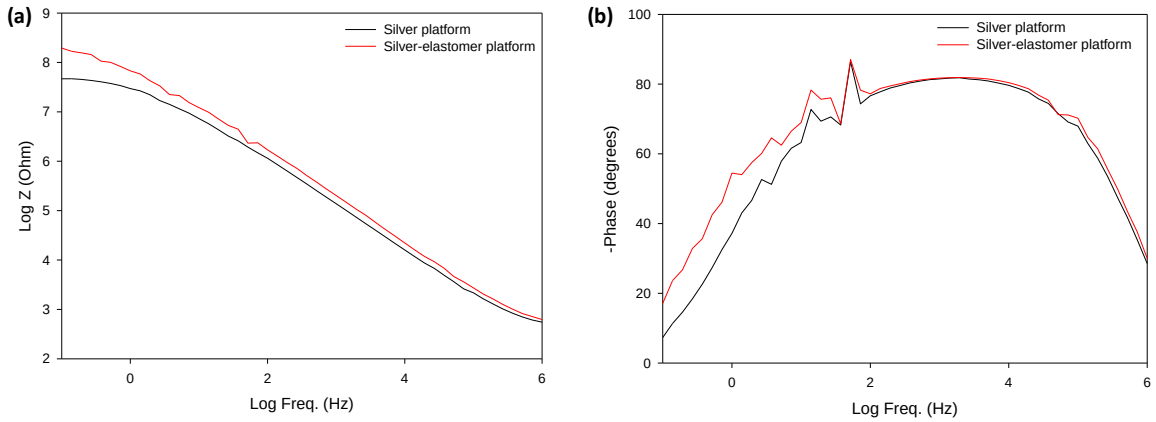

Figure A3.A Representative (a) Impedance and (b) phase plots as measured by the silver and silver-elastomer DC modes of the inner forearm.

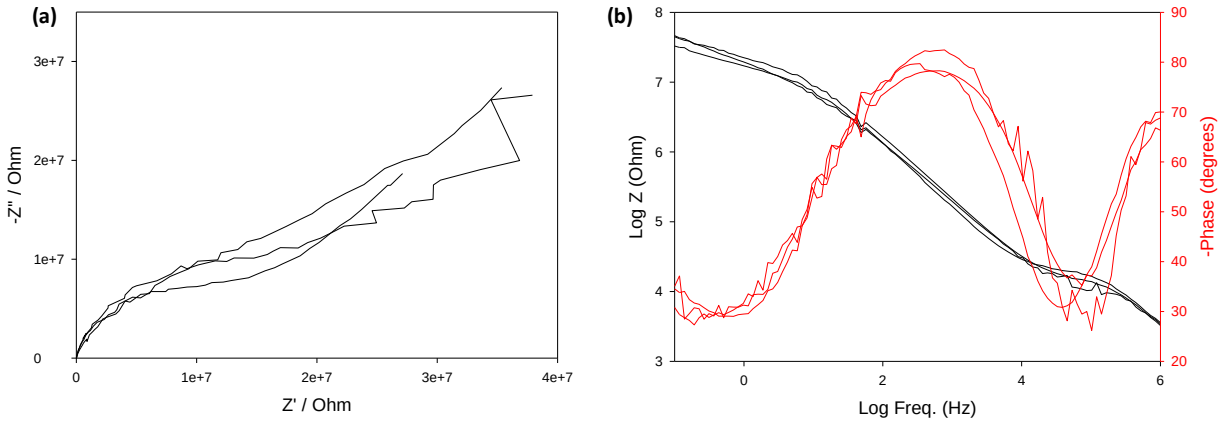

Figure A3.B (a) Nyquist and (b) Bode plots of the conducting adhesive material only on a hydrogel.

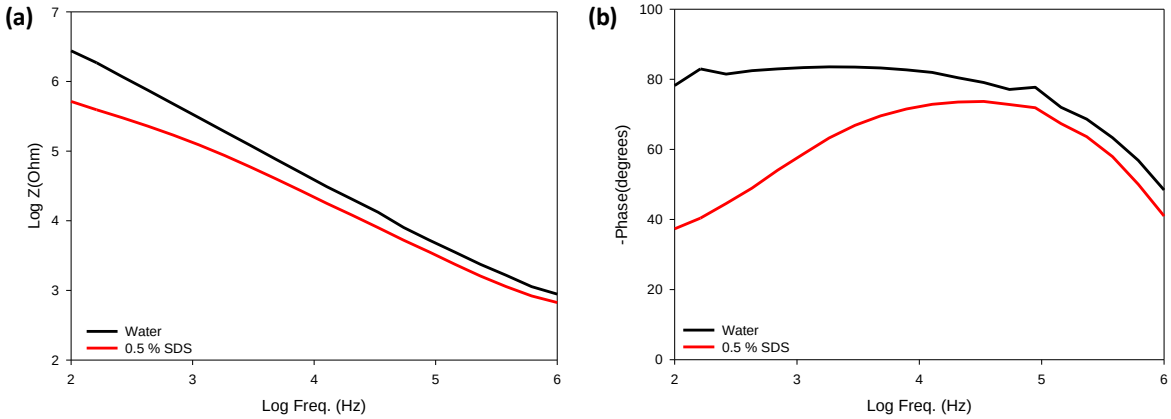

Figure A3.C (a) Impedance and (b) phase plots of the inner forearm as measured by the silver-elastomer CAC mode after altering the barrier properties with different topical treatments.

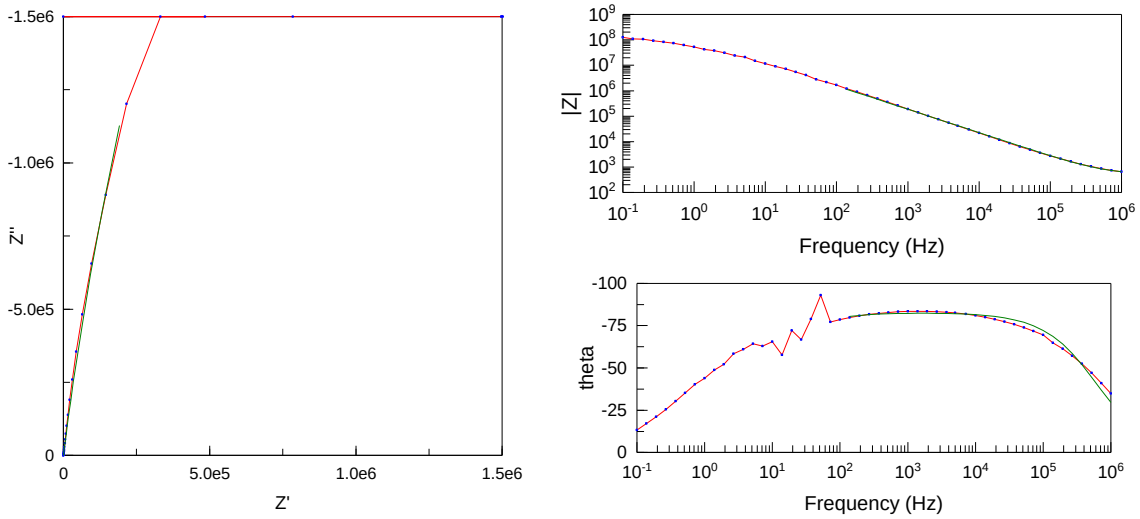

Figure A3.D Example of fitted impedance spectra of human skin during a short frequency measurement (1 MHz to 100 Hz) using the DC platform.

Appendix Figures for Chapter 4

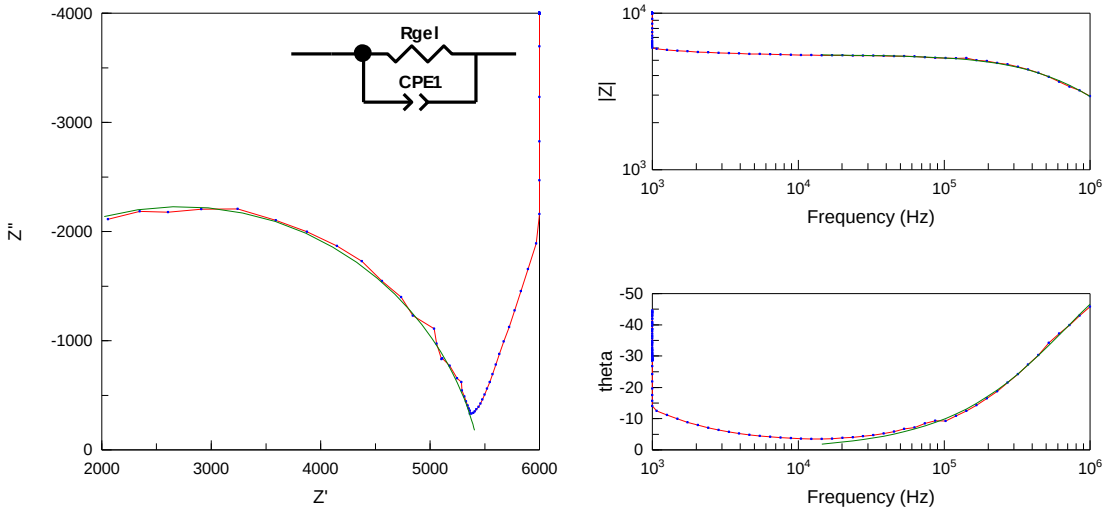

Figure A4.A Example of fitted impedance spectra at the high frequency region of a hydrogel using ZView. (Data points are in blue, interconnected with a red line, and the fits are shown in green).

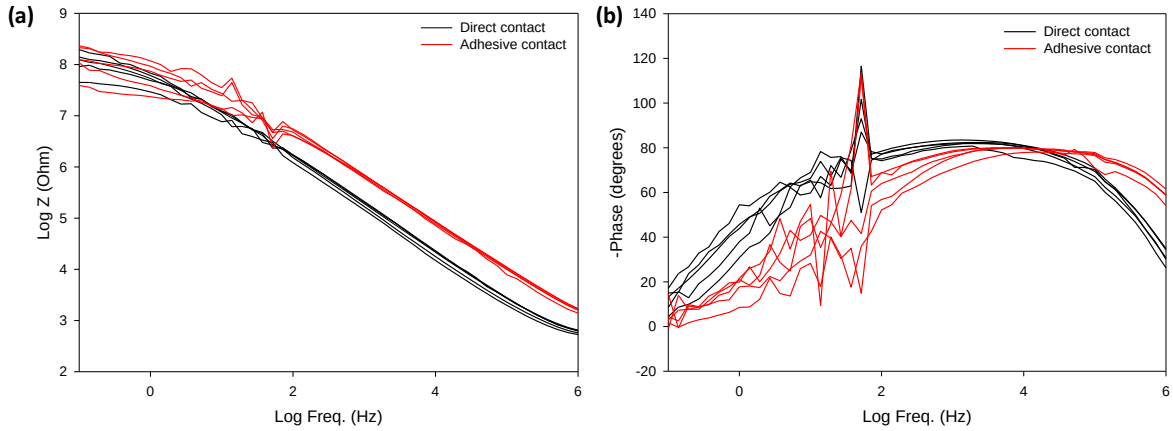

Figure A4.B (a) Impedance and (b) phase plots of human skin (single participant) measured by the Direct contact and adhesive contact (Adhesive (27 pore)) platforms.

A Delfin MoistureMeterD (MMD) probe was used for validation of the moisturisers on skin. Based on the Tissue Dielectric Constants measured by the probe, a decrease in hydration properties were seen overtime which indicates the uptake of the different types of moisturisers.

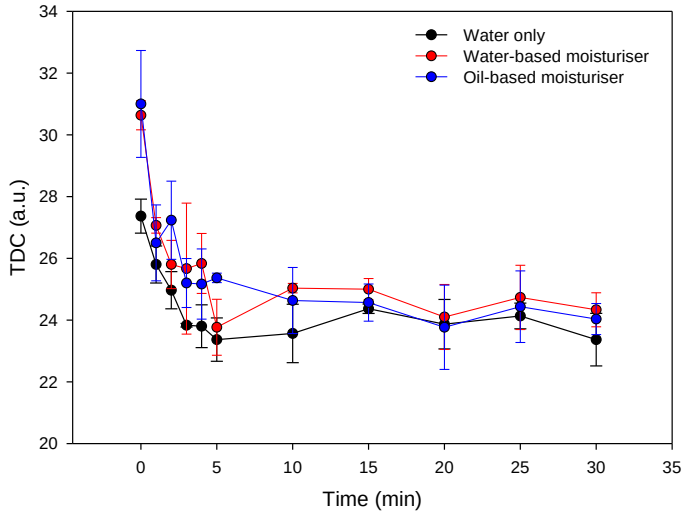

Figure A4.C Tracking water, water-based and oil-based moisturiser uptake through the skin (single participant) using the Delfin MoistureMeter D probe. (one day, three measurements on the forearm).

Appendix Figures for Chapter 5

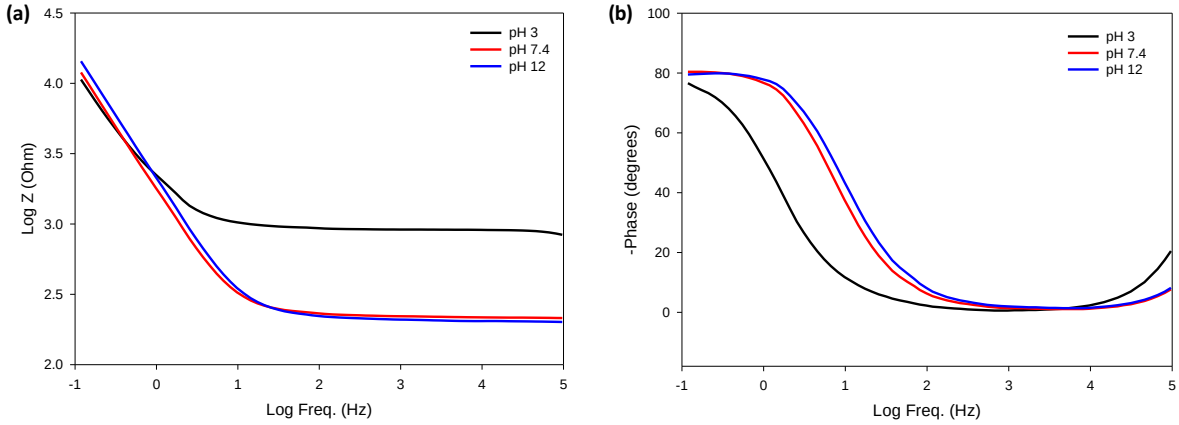

Figure A5.A (a) Impedance and (b) phase plots of the DMAP-2BA hydrogel Au-paper working electrode at different pH conditions.

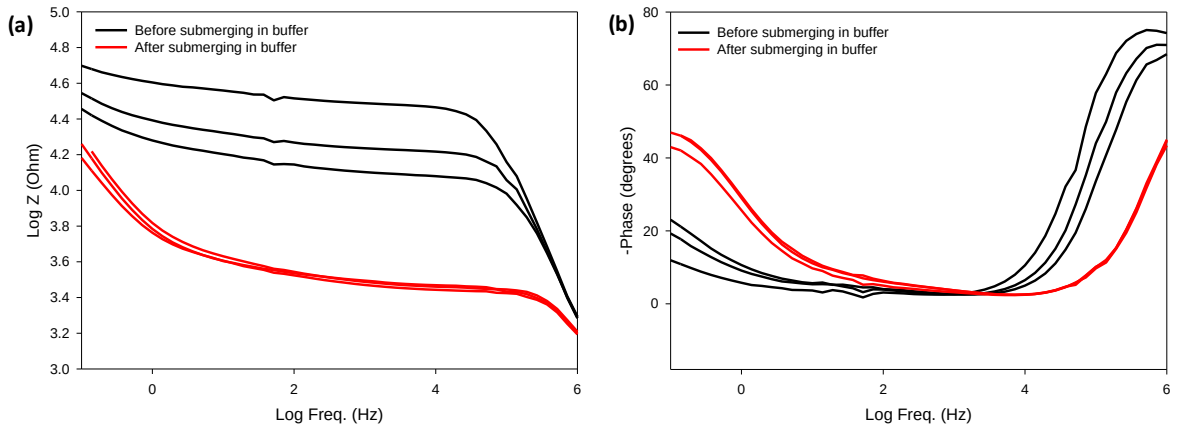

Figure A5.B (a) Impedance and (b) phase plots of the DMAP-4BA hydrogel tattoo electrodes before and after submerging in pH 7.4 buffer.

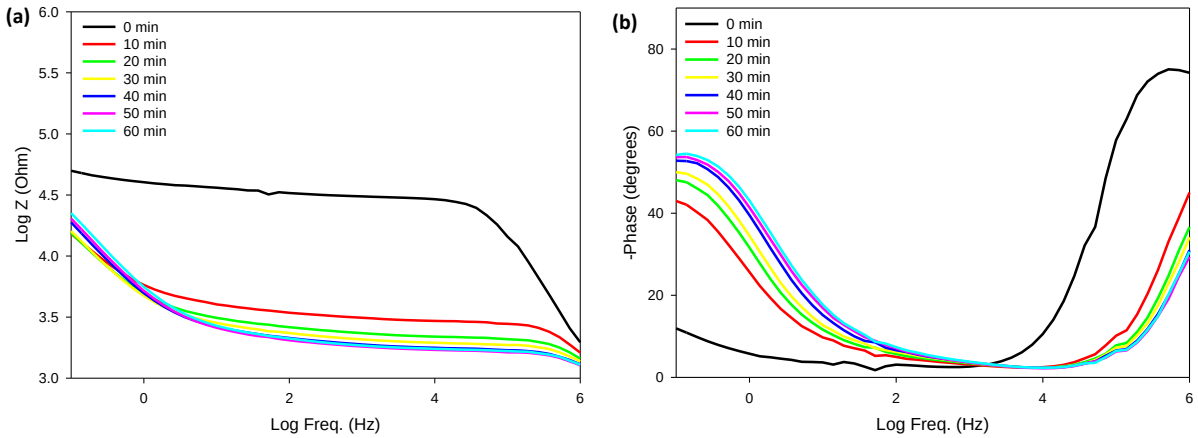

Figure A5.C (a) Impedance and (b) phase plots of the DMAP-4BA hydrogel tattoo electrodes over time to monitor stability.